Critical Dimension Control: Influencing Factors and Measurement

Thesis submitted by

Iona B. Binnie

for the degree of

Doctor of Philosophy

Edinburgh Microfabrication Facility,
Department of Electrical Engineering,
University of Edinburgh,
Scotland.

May 1991

EX BIBL. UNIV. EDINBURGH

Abstract

Advanced Lithography continues to be the limiting factor in the drive for higher levels of microcircuit integration. The key to the successful management of a lithography process is the integration of full measurement and instrumentation functions with the process, and the adoption of effective process control strategies. The aim of this research is to improve the understanding of critical dimension (CD) control by an investigation of the sources of variations in linewidth dimensions. Having identified the key factors, it should be possible to characterize and control their influence.

Experimental analysis suggests that film thickness and photoresist thickness have a profound effect on linewidth dimensions. Simulation techniques are used to establish a theory which uses standing wave patterns within film stacks to predict reflectance and exposure threshold, as well as the dimensions of the developed resist images. This theory is later corroborated by measurements on test wafers.

Having established the need to monitor film thickness variations, a novel metrology technique which incorporates both film thickness and linewidth uniformity measurements is introduced. The technique is based on the optical characteristics of a "chequerboard" test pattern, consisting of clear and opaque squares. The chequerboard effectively enhances deviations in CD by translating changes in linewidth into an area change on the chequerboard.

The technique was originally based on the measurement of light transmitted through glass wafers. The implementation of the technique using reflectance from silicon wafers is described, and possible future developments of the system are discussed.

Acknowledgements

I would like to thank my supervisor Dr Robert Holwill for his energy and enthusiasm, and his positive attitude to tackling problems. I am also indebted to Prof. John Robertson for his continued interest in this project and his tireless persual of reports and deadlines.

I have received invaluable help from the EMF staff; Dr Tom Stevenson contributed many painstaking hours printing and measuring wafers - all the Nanolab data was produced by Tom's expert driving of the SEM; and Mr Alan Gundlach proved a reliable fountain of knowledge for all areas of processing. Thanks are due to the EMF technicians for their helpful and cheerful advice, in particular Joe Gow, Catherine McGuigan, Iain Rutherford and Ross King.

Financial assistance was received from SERC and from Plessey Semiconductors PLC. I am grateful to my industrial supervisor Mr Jon Burnie for providing me with a valuable insight into commercial semiconductor manufacturing, and to the staff in the Process Development Group, in particular Neil Harper, Dave Martin and Kevin Stribley.

My fellow PhD students have over the years proved an endless source of help and humour. Deserving of special mention are Robin Smith and Gerry Allan who advised on computers and word-processing, Derek Ward who had an answer to every question, Robbie Hannah who organised the ski trips and Stewart Robertson who contributed many ideas, some of them quite bright.

Finally, and most importantly, I would like to thank my parents, family and friends without whose support this thesis could not have been achieved.

1. Overview of Semiconductor Industry **1**

1.1 Introduction 1

1.2 Economics of Processing 3

1.3 Technology Trends 5

1.3.1 Minimum Feature Size 5

1.3.2 Larger Chip Size 6

1.3.3 Larger Diameter Wafers 6

1.3.4 Innovations 8

1.3.5 Automation 9

1.4 Lithography: Control and Verification 10

1.4.1 Process Control 10

1.4.2 Yield 10

1.4.3 Metrology 12

1.5 CD as Lithographic Performance Monitor 17

1.5.1 Transistor Characteristics 17

1.5.2 CD Control 18

1.6 Aim of Project 18

1.7 Thesis Structure and Chapter Headings 20

Bibliography 22

2. Lithography **25**

2.1 Introduction 25

2.2 Exposure Methods 28

2.2.1 Contact Printing 28

2.2.2 Proximity Printing 28

2.2.3 Projection Printing 29

2.2.4 Direct-Step-on-the-Wafer (DSW) 29

2.3 Imaging Characteristics of a Projection System 31

2.3.1 Numerical Aperture (NA) 31

2.3.2 Illumination Coherence (σ) 33

2.3.3 Modulation Transfer Function (MTF) 33

2.3.4 Rayleigh Limits 33

2.3.5 Choice of Wavelength 34

2.4 Photoresist 36

2.4.1 Introduction 36

2.4.2 Optical Characteristics 39

2.4.3 Physical Characteristics 41

2.4.4 Exposure 42

2.4.5 Development 47

2.5 Process Simulation 50

2.5.1 Introduction 50

2.5.2 EMF Simulation Programs 50

2.5.3 Simulation of Exposure 53

2.5.4 Simulation of Development 55

2.6 Lithography Control 56

Bibliography 58

3. Metrology **67**

3.1 Introduction 67

3.1.1 CD Measurement 68

3.2 Optical Techniques 69
3.2.1 Determination of Threshold 69
3.2.2 Measurement Systems 71
3.3 Scanning Electron Microscope 74
3.4 Electrical Techniques 77
3.5 Reliability 79
3.5.1 Error Sources 79
3.5.2 Photoresist 80
3.6 Linewidth Measurements at the EMF 82
3.6.1 Nanolab SEM 82
3.6.2 Nanolab Repeatability Tests 83
3.6.3 Quaestor 85
3.6.4 Quaestor/Nanolab Correlation 87
3.7 The Plessey Metrology System 91
3.8 Quaestor/Prometrix Correlation 96
3.8.1 Test Pattern 96
3.8.2 Test Procedure 96
3.8.3 Comparison of Quaestor Before and After Etch 97
3.8.4 Comparison of Prometrix and Quaestor 102
3.8.5 Comparison of Prometrix Statistics and Full Data Set 107
3.8.6 Preliminary Conclusions 109
3.9 System Limitations 112
3.9.1 Nanolab 112
3.9.2 Quaestor 112

3.9.3 Lithomap 113

3.10 Conclusions 113

Bibliography 115

4. Film Thickness Effects on CD **124**

4.1 Introduction 124

4.2 Simulation: Single Layer Films 124

4.2.1 Choice of Film Thickness 125

4.2.2 Standing Wave Profiles 126

4.2.3 Standing Wave Intensity 130

4.2.4 Reflectance 131

4.2.5 Threshold Exposure 133

4.2.6 Linewidth 133

4.2.7 Summary: Single Layer Films 136

4.3 Simulation: Double Layer Films 138

4.3.1 Standing Wave Profiles 140

4.3.2 Reflectance 147

4.3.3 Threshold Exposure 149

4.3.4 Linewidth 149

4.3.5 Summary: Double Layer Films 152

4.4 Experimentation 153

4.4.1 Results 154

4.4.2 Discussion 154

4.4.3 Linewidth Control 158

4.4.4 Reducing Standing Waves 158

4.5 Conclusions 159

Bibliography 161

5. Film Thickness Measurements **162**

5.1 Introduction 162

5.2 Spectral Analysis 163

5.2.1 Interferometry (3000 A - 2μm) 163

5.2.2 Thin Films (100 - 3000 A) 164

5.3 Ellipsometry 167

5.4 Film Thickness Measurements at the EMF 169

5.4.1 Nanospec 169

5.4.2 EllipsometerII 170

5.4.3 Monolight Spectrum Analyser 170

5.4.4 Preliminary Conclusions 173

5.5 Optical Multichannel Analyser 173

5.5.1 Introduction 173

5.5.2 System Controller 174

5.5.3 Wafer Prober 175

5.5.4 Microscope 177

5.5.5 Spectrograph 177

5.5.6 Photodiode Array Detector 178

5.6 Software 178

5.6.1 Reflectivity Curve 178

5.6.2 Turning values 179

5.6.3 Film Thickness Algorithm 179

5.7 Testing 183
5.7.1 Silicon Dioxide Thickness Tests 183
5.7.2 Resist Thickness Tests 189
5.7.3 Repeatability 189
5.7.4 Discussion 193
5.8 Conclusions 194
Bibliography 195

6. A Novel Metrology Technique **199**

6.1 Introduction 199
6.2 Design Considerations 199
6.3 Chequerboards in Transmission 202
6.3.1 Glass Wafer 1 202
6.3.2 Glass Wafer 2 206
6.3.3 Spray versus Ultrasonic Develop 209
6.3.4 Conclusions 211
6.4 Chequerboards in Reflection 211
6.4.1 Preliminary Testing 212
6.5 Experimental Assessment of Chequerboard Reflectance and CD . . 216
6.5.1 Procedure 216
6.5.2 CD versus Film Thickness 218
6.5.3 Reflectance versus Thickness 222
6.5.4 Discussion 226
6.6 Conclusions 228
Bibliography 229

7. Conclusions **231**

7.1 Metrology: No Longer an Afterthought 231

7.2 Thesis Summary 232

Appendix 235

Chapter 1

Overview of the Semiconductor Industry

1.1 Introduction

The first integrated circuits (ICs) were produced in 1959, and since that date, progress in the design and fabrication of memory and logic chips has proceeded at an astonishing rate. In the last few years, the number of bits in advanced memory chips has been doubling almost every year, while the minimum circuit linewidth has been shrinking continuously to the present half-micron level. (See Fig. 1–1).

This trend to higher packing densities has placed an enormous strain on lithography and the processes to manufacture ICs.

Optical lithography was the method originally employed by the semiconductor industry, and it is still by far the most widely used technique for pattern transfer. Although alternative techniques for exposure of resist materials using X-rays, electrons or ions are being explored, which have greater resolution, the limit of optical lithography has not yet been reached. [1]

1M bit DRAM's with minimum linewidth of 1μm have been manufactured for the last three years using primarily optical g-line steppers (436 nm wavelength) and positive NOVOLAC-based photoresists. In order to obtain smaller linewidths, i-line steppers are being built, operating at 365 nm, at which wavelength excessive

	Year				
	85	89	93	97	2000
DRAM size	256K	1M	4M	16M	64M
Wafer diam (in)	6	6	6	8	8
CD (μm)	1.25	1.0	0.7	0.5	0.3
Wafers/year (k)	100	80	70	50	20
Factory cost (M$)	100	250	720	1320	2500
Price/wafer (k$)	1.2	3.75	12.3	31.7	150
Die size (mm^2)	40	70	120	280	600
Yield (%)	90	85	80	70	70
Good die/wafer	400	215	118	78	36
Cost/die ($)	3	17.5	105	406	4200
Cost/bit (mc)	1	1.75	2.6	2.5	6.5

Figure 1–1: Trends in DRAM Dimensions [4]

absorption of conventional resists is already a problem. More aggressive designs of steppers using novel materials for lenses and new UV sources (excimer lasers at 248nm) are already on the market and experimental designs of 16M bit DRAM's at 0.5μm linewidths are being built by some IC manufacturers. Furthermore, the phase-shift mask concept promises an extension of deep UV lithography to below 0.3μm rules.

Yet only a few years ago, the general belief was that optical lithography could never achieve half-micron design rules in the manufacturing environment. If the present trend continues, and all indications are that it will, quarter-micron design rules could be reached by the mid-nineties. [2] Certainly, the economic motivation to continue using a proven technology will ensure that optical lithography remains the mainstay for the next five years. [3]

1.2 Economics of Processing

To date, the growth of IC sales has kept pace with the rate of technological advance of the semiconductor industry. Fig. 1–2 shows the sales of ICs and electronic equipment in the USA. [4] Other countries, notably Japan, show an even more rapid rate of growth, and the whole process has been driven by the ability to create increasingly complex electronic functions on a single chip of silicon. The market has continued to expand since increasing the packing densities of ICs has resulted in a reduced cost per function. [5] However this trend can no longer be sustained. The economic basis of wafer processing is under threat due to the combined effects of the following factors: [6]

1. The capital cost of an IC fabrication plant is rising faster than the sales revenue [7]

2. Packaging of devices is becoming increasingly complex and expensive

3. IC design remains a labour-intensive process and is becoming increasingly significant in terms of overall production cost.

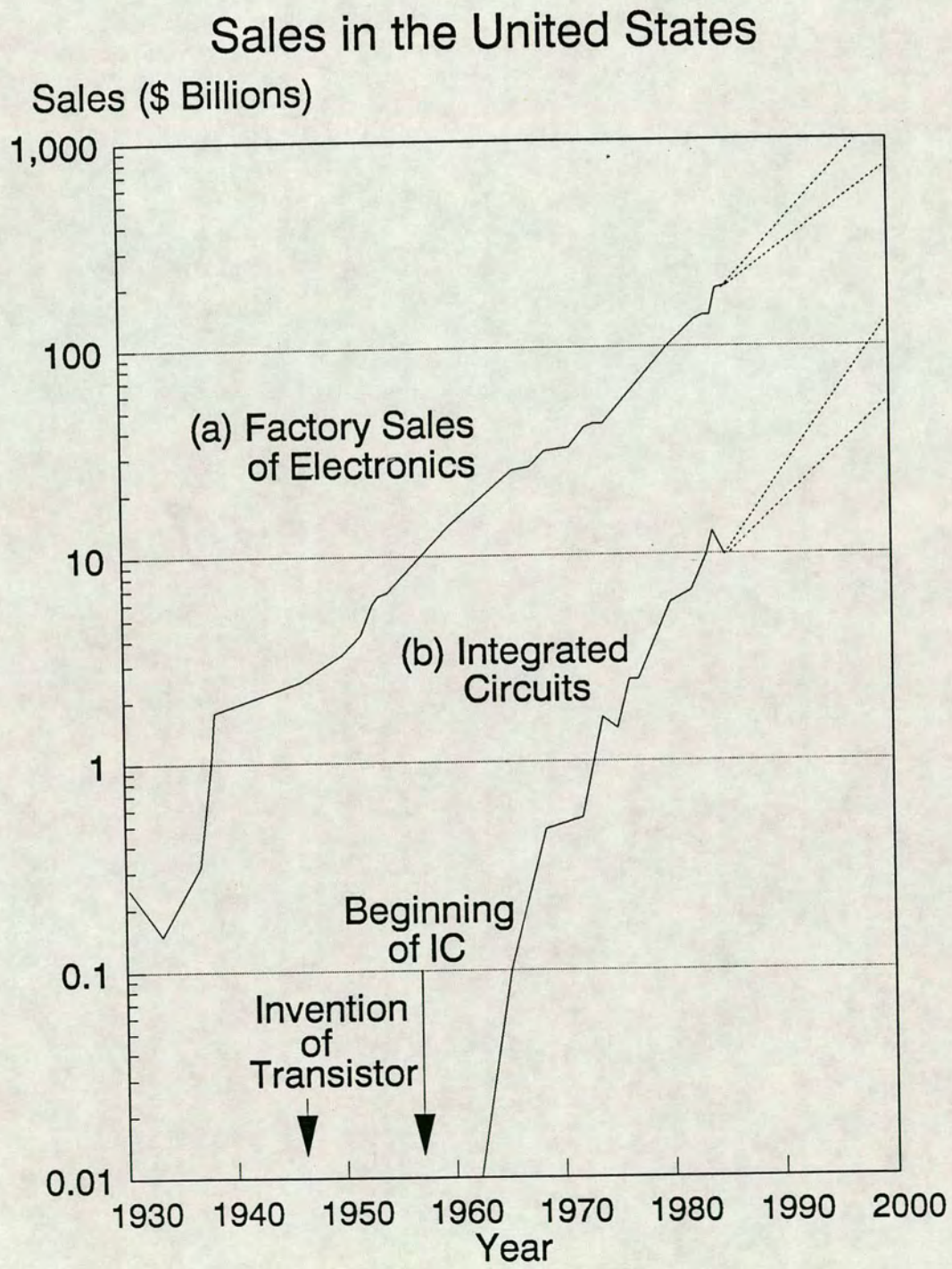

Figure 1–2: USA Sales Figures for ICs [6]

These factors have been recognised by the semiconductor industry, and it is generally accepted that if processing is to remain financially viable there must be an increase in engineering yield and a corresponding decrease in production costs. These conditions will necessarily impose more stringent demands on the tolerances designed into the fabrication process. There is therefore a need for a better understanding of the process so that the key issues in terms of process control may be addressed.

1.3 Technology Trends

A study by Donofrio [8] into the factors which drive improvements in the productivity of semiconductor production has identified four major categories:

- Smaller feature size
- Larger chip size
- Larger diameter wafers
- Innovations

Historical trends indicate that each category contributes about the same amount to the overall increase in productivity.

1.3.1 Minimum Feature Size

Several significant advantages are realised when reducing linewidth geometries. Circuit densities can be increased, and die area correspondingly decreased, so that more ICs can be produced per wafer. Also, decreasing IC geometries minimizes stray circuit capacitances and resistances, which have an adverse effect upon speed and performance. (See Fig. 1–3)

As an example, consider shrinking the minimum feature size of a circuit by a factor "s". The following condition then apply: [8]
Device delay time decreases by factor $\frac{1}{s}$
Packing density increases by factor s^2
Power-Delay product decreases by factor $\frac{1}{s^3}$

However scaling down dimensions is not a simple matter. Practical limitations are reached well before achieving quantum dimensions. For example, current density in wiring may increase substantially as dimensions are made smaller. This can cause electromigration problems to arise.

1.3.2 Larger Chip Size

It is easy to see that increasing the size of the chip provides another attractive path to higher productivity. Larger chips offer the opportunity for increased functionality and hence have a higher intrinsic value. As chip sizes increase however, the lithography engineer is challenged to maintain image fidelity, critical dimension (CD) control and registration over a larger field. Today the industry is using lens fields as large as a state-of-the-art stepper can provide, yet there is still a demand for larger chips.

1.3.3 Larger Diameter Wafers

The trend to increased wafer size has produced enormous economic benefits. (See Fig. 1–4) The number of chips increases as the square of the diameter, whereas the fabrication cost increase is roughly linear. [5]

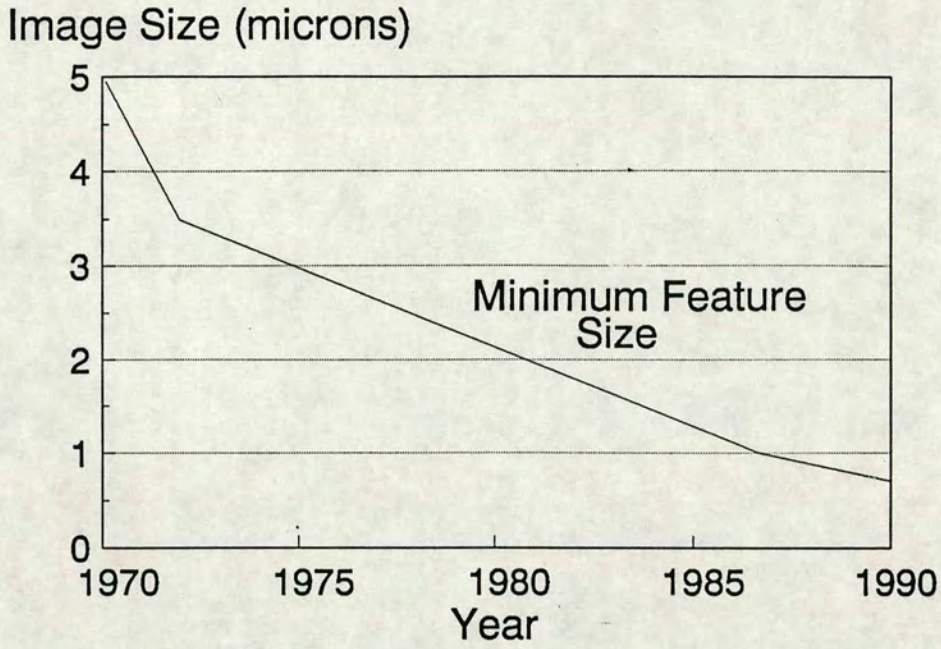

Figure 1–3: Lithography Evolution [8]

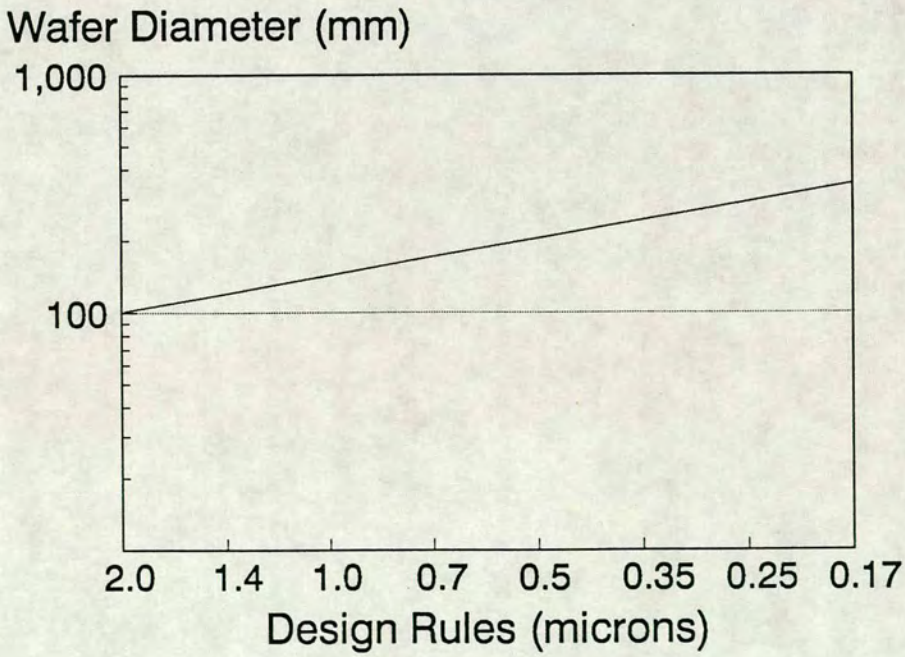

Figure 1–4: Lithography Trends for DRAMS [10]

Consider the difference between 150 mm and 200 mm wafers. Although the increase in area is around 78%, the available sites for large die increases this difference to over 90%, assuming a die area of approximately 200 mm^2 (c.f. 4 Mbit DRAM). Also, improved handling efficiencies reduce total stepper time by 10%. With other factors unchanged, the combined effect is an approximate doubling of productivity with 200 mm wafers. [9]

1.3.4 Innovations

In this context, innovation usually relates to circuit design breakthroughs and process invention. However innovation is also to be found in the lithographic processes. Consider for example, the production of ASICs (Application Specific Integrated Circuits).

The ASIC market is currently the fastest growing sector of the IC market. Commonly, ASICs are designed using a semi-custom technique, in which standard logic blocks are connected by a final unique interconnection layer. [10] The main features of ASIC production are: [6]

1. fast and flexible system for fabricating a wide range of circuits [11]

2. low volume production of chip designs is made feasible

3. customers specify the tolerances on final circuit performance

The high cost of this customisation of products is reflected in the price. The production of ASICS offers lucrative returns, and manufacturers compete aggresively to lead the market in terms of circuit speed and packing density. [12] [13]

Lithography has a key contribution to make towards this goal. For example, if processes are developed that are not disturbed by adjacent and underlying structures, then more flexible design rules may be applied and the silicon area used more efficiently. Packing densities can be increased if the borders required

around contacts are minimized. This requires a tightly controlled and innovative lithography process.

1.3.5 Automation

An analysis of the historical trends shown throughout the development of the semiconductor industry reveals an increased use of automated equipment and processes. As wafer fabrication becomes increasingly complex there will be a need to further automate the process line. [14]

Factory management software systems such as COMETS are the first evolutionary stage towards full automation. COMETS is a Computerized On-line Manufacturing and Engineering Tracking System which tracks each batch of wafers along the process line. Operators provide the interface between the fabrication line and the central computer control by inputting test data generated from the wafers. If the data is within specifications the process continues according to a sequence of batch-recipe cards. If however the data is outside the tolerances set by the system, then production of that batch halts until a process engineer decides whether the wafers are to be passed on, reworked or scrapped.

The next generation of process control system will remove the human interface. The first stage will remove the need for operator-input, by creating automatic feedback of information. The second, and much more complex stage, is to build decision-making into the system to replace engineer-input. This would allow for feed-forward compensation to offset tolerances and to achieve tighter product specifications. (See Fig. 1–5). A massive increase in the engineering database available to the decision-making control system will be required to implement this function.

The widespread use of automation and feed-forward control will only become feasible once there is a much greater understanding of wafer processing. It will depend on identifying and measuring the key processing parameters in terms of process control.

The same conclusion can be drawn from all the processing trends mentioned above. The evidence is that tighter tolerances on process parameters are inevitable for the continued economic success of the semiconductor industry.

1.4 Lithography: Control and Verification

1.4.1 Process Control

Advanced lithography continues to be the limiting factor in the drive for higher levels of microcircuit integration. [15] An analysis of megabit technologies shows that greater than 50% of the length or complexity of the process is due to lithography steps. [16] (See Fig. 1–6). The longer the process, the more handling, delays and contamination are end results. The key to a successful management of a lithography process is the integration of full measurement and instrumentation functions with the process and the adoption of effective process control strategies. Without sensitive, fast and accurate measurement techniques, process trends will remain undetected, corrective action will be delayed, the process will be unstable and the overall result will be wide process spreads and reduced engineering yield.

It is important to realise that the level of integration of semiconductor chips in the 1990's is likely to be limited by the requirements of low defect levels and improved process control. [17]

1.4.2 Yield

Concern about the degradation of yield due to defects incorporated into the semiconductor device structures during fabrication has always been a major preoccupation of the semiconductor industry. [18] Each lithography stage will introduce defects into the pattern, for example, pinholes in dark areas or opaque debris in clear areas, and these may reduce yield.

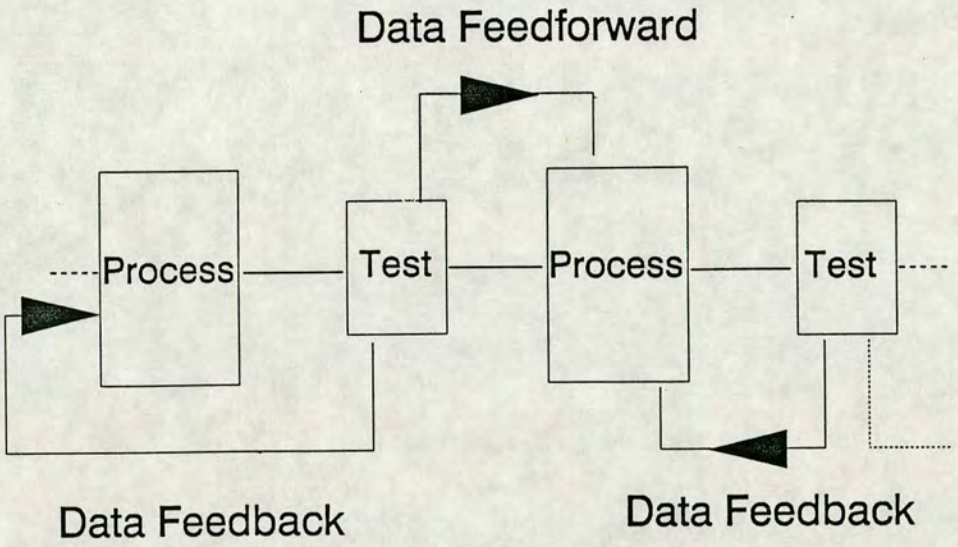

Figure 1–5: Automated Lithography Sequence

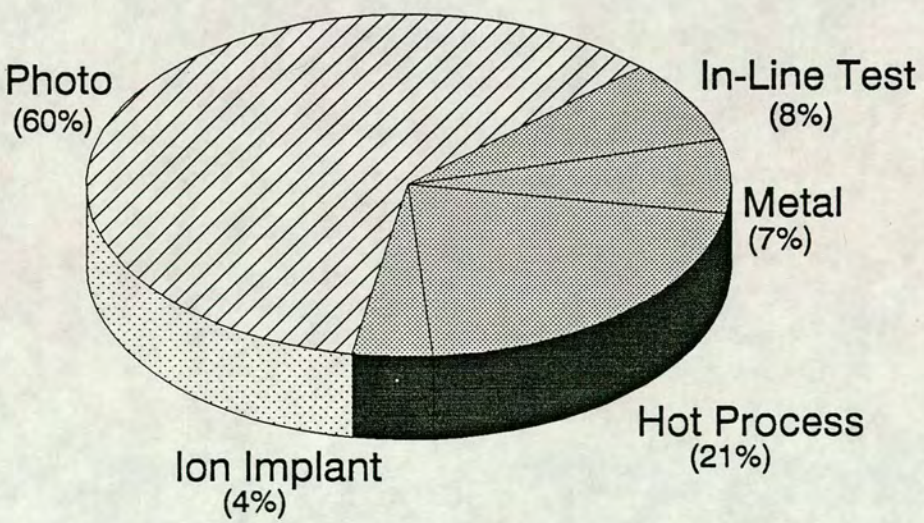

Figure 1–6: Pie Chart of the Major Processes in Wafer Fabrication Reveals that Lithography Processes Represent 60% of the Total Fabrication Time [10]

Fortunately, every defect does not necessarily lead to the failure of the device, depending on its size and where it occurs in the pattern. Any defect which is larger than about one quarter of the minimum feature size on the pattern could cause a failure due to a break in a track or a bridge between two tracks.

To illustrate the seriousness of the problem, consider a simple yield model given by the equation: [8]

$$Y = Y_0 \left(1 + \frac{\lambda}{\alpha}\right)^{-\alpha} \tag{1.1}$$

where Y_0 is the gross yield, λ is the average number of faults and α is a cluster parameter.

This model is used to calculate the relative yield loss from a given distribution of defects as circuit complexity and chip size is increased. In Fig. 1–7 yield is plotted using the model above. The model assumes that the chip's area is increased by a factor "n" and that defect distribution remains constant. It is evident on the logarithmic scale that without improvement in defect control, the yield drops sharply as area increases.

An estimate of the defect detection that will be required for submicron lithography is given in Fig. 1–8.

1.4.3 Metrology

Throughout the lithographic process there are many potential error sources. The objective of the process engineer is to manage the net errors and keep them from exceeding IC device design margins. [19] Lithography errors can be categorized into two principal types: registration errors and linewidth errors.

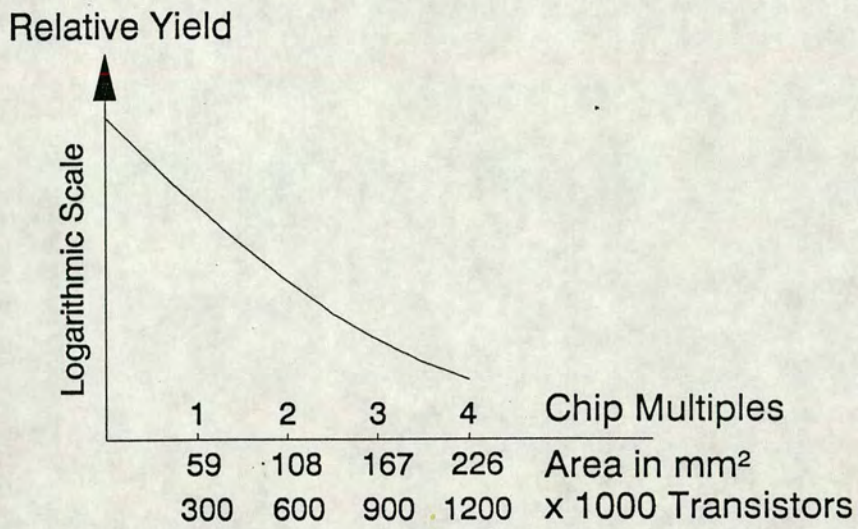

Figure 1–7: Yield as a Function of Chip Multiples [8]

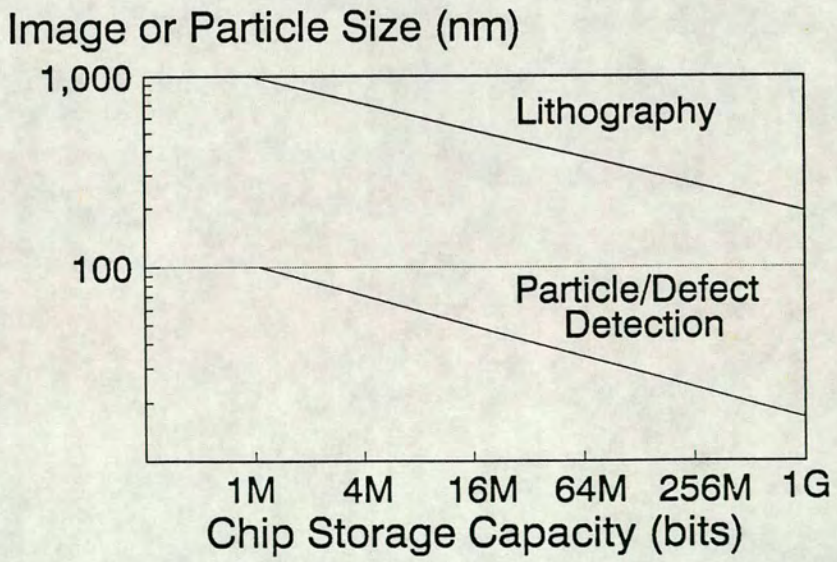

Figure 1–8: Particle Size and Defect Measurement Trends [8]

Registration

Wafer registration measures how well printed layers match each other at the wafer level. It is the most comprehensive measure of geometric positioning effects on wafer fabrication. [20] Registration errors include overlay errors in the mask, errors in aligning the pattern to the wafer, and repeatability errors of the wafer printing tool. Whenever any part of the circuit exceeds the registration design margin, the topology of the pattern changes and the circuit may fail. It is generally accepted that the total budget for registration errors, including all sources, should be no greater than on third of minimum feature size. (See Fig. 1–9).

Linewidth

The prime lithographic production requirement is to maintain the size of all etched features on all devices within acceptable limits. Linewidth error is the deviation of feature size (edge to edge) from a nominal value. Linewidths are measured over small regions and are independent of feature location. Linewidth metrics include an average value and a uniformity value (standard deviation) characterizing linewidth fluctuation over different regions on the substrate. Since they have a first-order influence on device parameters, linewidth error tolerances are typically less than registration design margins. As a general rule, linewidth variations are usually kept to within $\pm 10\%$ of nominal values. (See Fig. 1–10). [21]

Error Budgets

Error budgeting is a technique for predicting the net effects of accumulated errors. [22] The technique is extremely useful to designers and process engineers for optimizing wafer fabrication productivity. For example, the correct estimation of linewidth performance will determine the optimum circuit size by trading die density in a wafer against yield loss from variations in CD. This method depends

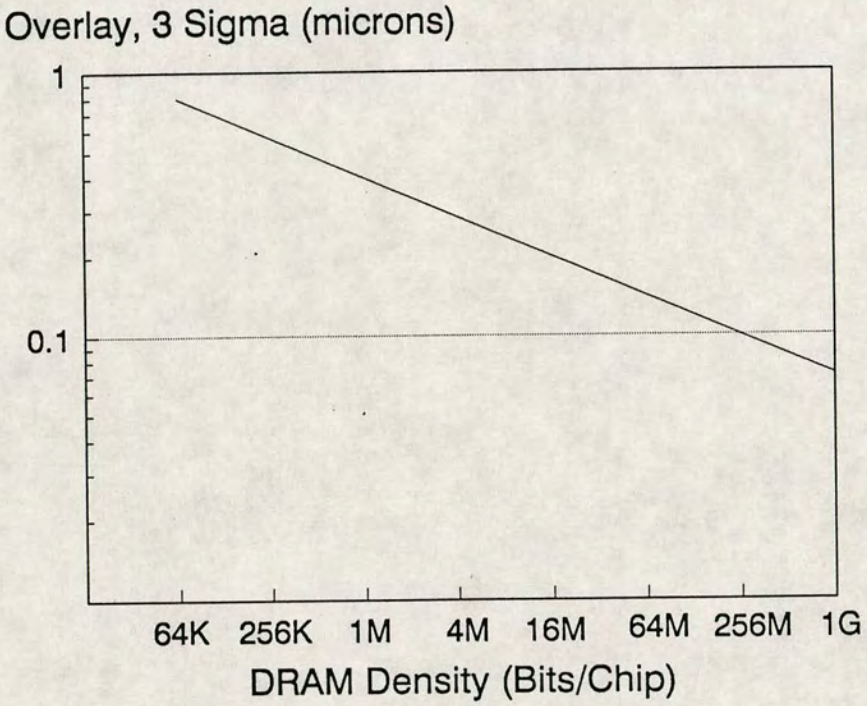

Figure 1–9: Lithography Trends for Overlay [10]

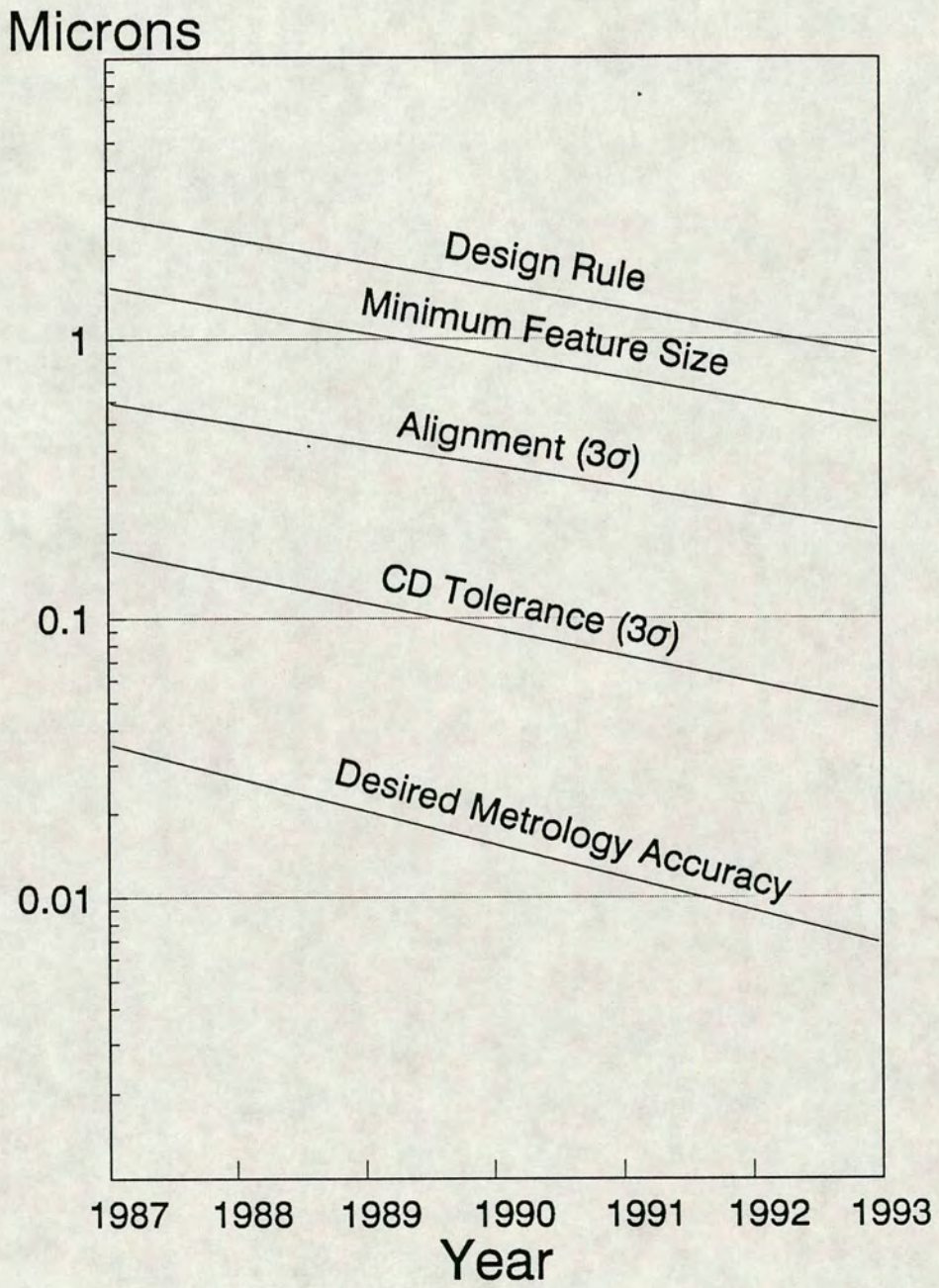

Figure 1–10: Forecast of Leading-Edge CMOS Production Dimension and Control Budgets [9]

on characterizing error behaviour in terms of a common set of parameters, usually the statistical measurement of range, mean and standard deviation.

During the next decade, many high density microelectronic circuits will have design rules in the half-micron range. If a 10% error budget for linewidth control is allowed on any given layer, it will be necessary to control dimensions to accuracies of a few hundredths of a micron. [23]

1.5 CD as Lithographic Performance Monitor

1.5.1 Transistor Characteristics

Linewidth is of fundamental importance in terms of device characteristics. A change in CD will affect the drain current I_D and transconductance g_m of a transistor as shown by the simple equations: [24]

Drain Current

$$I_{D,sat} \approx \frac{\frac{W}{L}\mu_N C_o (V_G - V_T)^2}{2} \tag{1.2}$$

Transconductance

$$g_{m,sat} = \frac{\partial I_{D,sat}}{\partial V_G} \tag{1.3}$$

$$= \frac{W}{L}\mu_N C_o (V_G - V_T) \tag{1.4}$$

where μ_N is the average drift mobility of channel electrons and C_o is the insulator capacitance per unit area. Both equations contain the area-dependent term $\frac{W}{L}$ where W is the gate width and L is channel length. Small differences in channel length affect device turn-on characteristics. [25] Variations in transistor operation across the chip result in timing problems for the logic circuit. Circuit speed must therefore be reduced to allow devices to track together, and thus is lost some of the benefits obtained by producing smaller images.

1.5.2 CD Control

CD control must be stable in three separate ways. First, feature size across any given exposure field must be centered in specification and have an acceptable distribution. (See Fig. 1–11). Second, feature size variations from field to field on one wafer must not exceed acceptable limits. Third, long term stability is required. (See Fig. 1–12).

It must be emphasized that uniformity of CD is more important than absolute dimensions. [26] It is relatively easy to offset linewidths to match a target, but only if the process is stable. Thus any measurement instrument must exhibit good resolution but not necessarily be calibrated to an absolute standard. It is essential however that all CD systems within a plant should be consistent. [27]

1.6 Aim of Project

To preserve device yield it is essential to maintain the correct width of feature not only over the entire wafer but for all wafers in a batch, and from batch to batch. The ability to control linewidth (or critical dimension CD) is usually the factor that determines the limiting feature size. [28] The aim of this project is to improve the understanding of CD control by an investigation of the sources of variations in linewidth dimensions. If these key factors can be identified, then it should be possible to characterize and control their influence. The following Chapter describes the main components of the lithographic process, in terms of the exposure and development of photoresist.

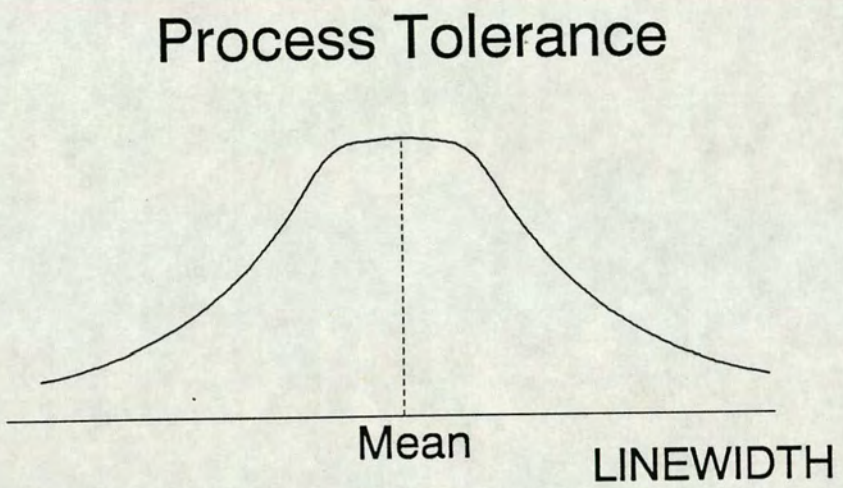

Figure 1–11: The Distribution of Linewidth Dimensions May be Used to Specify Process Tolerances

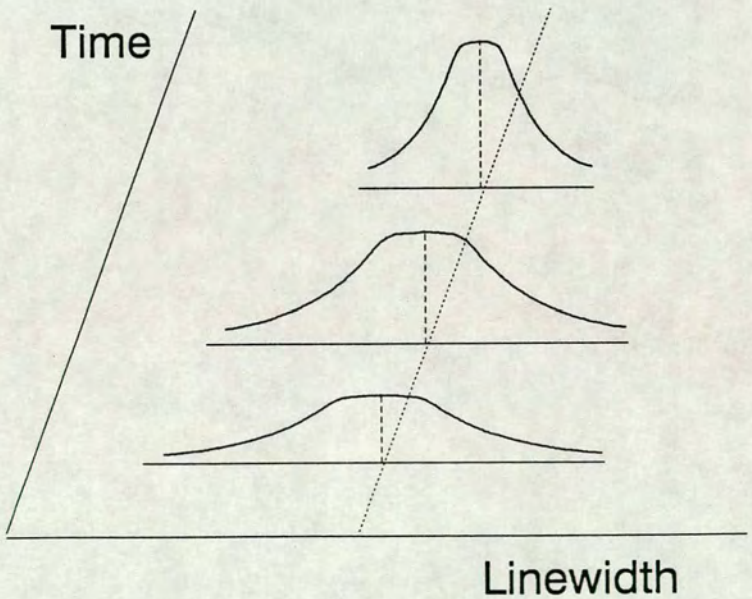

Figure 1–12: Over a Period of Time, the Mean Linewidths Should Remain Centered on Target, and the Distributions Become Narrower

1.7 Thesis Structure and Chapter Headings

Chapter 1: Introduction. This chapter examines the technological trends demonstrated by the semiconductor industry, and the significance of these trends in terms of future processing requirements. It establishes the central role played by lithography in achieving these goals. The final section concludes that CD uniformity is the key parameter for measuring and controlling lithography.

Chapter 2: Lithography. This chapter describes the lithographic process in detail in order to determine the principal causes of variations in CD. The conclusions drawn from this chapter are that film thickness and photoresist thickness are the most significant lithographic factors in terms of CD control.

Chapter 3: Metrology. This chapter reviews the main techniques for measuring linewidth dimensions. It includes a comparison of the "Quaestor" optical measurement system with the Prometrix "Lithomap", which measures linewidths by probing electrical test structures. It is concluded that there is a need for a fast CD scanning system, based on an optical technique, and suitable for automation.

Chapter 4: Film Thickness Effects on CD. This chapter describes the tests carried out to measure the effect of film thickness variations on CD. The tests show that the thickness uniformity of both photoresist and underlying films are significant in terms of CD control. Experimental results are confirmed by simulation.

Chapter 5: Film Thickness Measurements. This chapter reviews film thickness measurement systems in common use, and concludes that the EMF has need of a fast scanning system for measuring and mapping film thickness uniformity on-line. The second half of the chapter describes the design and construction of a prototype thickness scanning system based on an Optical Multichannel Analyser (OMA). Test wafers are measured on the OMA, Nanospec and Ellipsometer. The results confirm that the OMA system merits further development.

Chapter 6: A Novel Metrology Technique. This chapter introduces a novel CD uniformity technique based on the optical characteristics of a chequerboard test pattern. The development of the technique is described from working in transmission through glass test wafers, to working in reflection from product wafers.

Chapter 7: Conclusions. This Chapter summarizes the thesis and examines its final conclusions with regard to its original aims. Areas of research requiring further work are outlined for future development.

Bibliography

[1] J.Greeneich and B.Katz. i-line stepper technology for 16 Mbit DRAMs. *Solid State Technology*, (3):63–68, 1990.

[2] P.Burggraaf. Approach to lithography in 1990's. *Semiconductor International*, (3):22, 1990.

[3] H.L.Stover. Frontiers of optical lithography. *Solid State Technology*, (1):53, 1987.

[4] J.Robertson and R.Holwill. Information management in VLSI technology. Technical report, Edinburgh Microfabrication Facility, University of Edinburgh, 1989.

[5] SERC School on Microfabrication, Edinburgh Microfabrication Facility, University of Edinburgh. *CAM, Yield and Information Management*, June 1990.

[6] SERC School on Microfabrication, Edinburgh Microfabrication Facility, University of Edinburgh. *The Business of Semiconductor Technology*, June 1990.

[7] G.Burns, J.Grenier, and R.McGeary. Wafer fabrication equipment five-year forecast. *Solid State Technology*, (1):35–38, 1989.

[8] N.M.Donofrio. The real challenge in lithography. In *INTERFACE 86*, pages 4–16. Kodak Microelectronics Seminar, 1986.

[9] R.J.Kopp. What's ahead in wafer processing and materials. *Semiconductor International*, (1):54–58, 1989.

[10] K.Skidmore. Fabricate ASICs feasibly. *Semiconductor International*, (2):84–88, 1989.

[11] J.Gee. European Silicon Structures: An old world idea, updated. *Semiconductor International*, (2):132–135, 1989.

[12] K.M.Kearney. Choosing the path to the right ASIC vendor. *Semiconductor International*, (2):62–67, 1989.

[13] K.Skidmore. Semicon/Europa 89 features processing. *Semiconductor International*, (2):110–111, 1989.

[14] C.R.Clare. On-line process control using a tree-structured computer network. In *Proceedings of Microelectronics Measurement Technology Seminar*, pages 215–218, 1979.

[15] J.H.McCoy, W.Lee, and G.L.Varnell. Optical lithography requirements in the early 1990s. *Solid State Technology*, (3):87–92, 1989.

[16] A.S.Oberai. Lithography - challenges of the future. *Solid State Technology*, (9):123–128, 1987.

[17] R.Carlson. Manufacturing one micron. *Solid State Technology*, (1):141–144, 1985.

[18] SERC School on Microfabrication, Edinburgh Microfabrication Facility, University of Edinburgh. *Statistics of Defects*, June 1990.

[19] L.Liauw, A.Murray, and M.Chen. Impact of wafer flatness on submicron optical lithography. In *Proc. SPIE*, volume 772, pages 232–238, 1987.

[20] M.G.Buehler. VLSI process monitoring: Current practice/ future trends. In *Microelectronics Measurement Technology Seminar*, pages 309–312, 1979.

[21] B.Dance. Don't count the Europeans out. *Semiconductor International*, (2):116–124, 1989.

[22] M.L.Rieger and J.A.Schoeffel. Managing lithography errors. *Solid State Technology*, (4):151–155, 1989.

[23] D.W.Widmann and H.Binder. Linewidth variations in photoresist on profiled surfaces. *IEEE Transactions on Electron Devices*, ED-22(7):467–471, 1975.

[24] J.Mavor, M.A.Jack, and P.B.Denyer. *Introduction to MOS LSI Design*, chapter 2. Addison-Wesley, 1983.

[25] W.Murakami. VLSI process monitoring: Current practice/ future trends. In *Microelectronics Measurement Technology Seminar*, pages 313–320, 1979.

[26] D.S.Perloff, L.V.Lybeck, and L.A.Lane. Using personal computers for process control. *Microelectronic Manufacture and Testing*, (8):51–54, 1986.

[27] W.E.Ham. VLSI process monitoring: Current practice/ future trends. In *Microelectronics Measurement Technology Seminar*, pages 306–308, 1979.

[28] D.S.Perloff. VLSI process monitoring: Current practice/ future trends. In *Microelectronics Measurement Technology Seminar*, pages 300–305, 1979.

Chapter 2

Lithography

2.1 Introduction

The previous chapter outlined the fundamental aim of this project: to improve CD control. In order to assess the likely sources of influence on linewidth dimensions, it is necessary to have a detailed understanding of the lithographic process. This chapter will describe the major chemical and physical mechanisms involved in pattern transfer via the exposure and development of photoresist. The final section will examine the lithographic factors which are most significant in terms of CD control.

Microcircuits are multilayer devices; each process layer has to be deposited and then patterned with all the patterns aligned to each other. The completed device may have between 5 and 15 layers, as shown in Fig. 2–1. [1]

Optical lithography is based on the use of photoresists - light sensitive paints which can be applied as thin-film coatings on surfaces where a pattern is to be delineated. The photoresist film is exposed to an optical pattern printed on a glass or chrome mask, using ultra violet light, creating exposed and unexposed areas. Development selectively removes the resist according to its exposure state. The remaining pattern of resist protects the unexposed material allowing the exposed areas to be removed by etching. [2] (See Fig. 2–2)

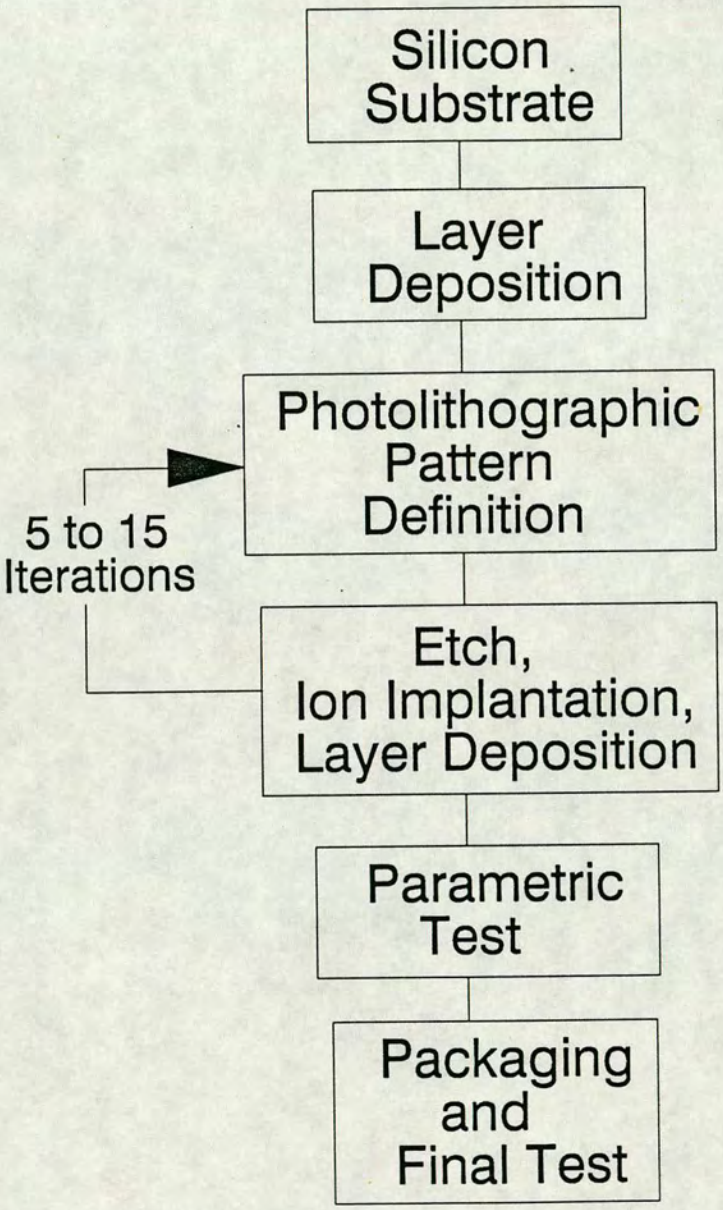

Figure 2–1: Microelectronic Device Process Fabrication Sequence [1]

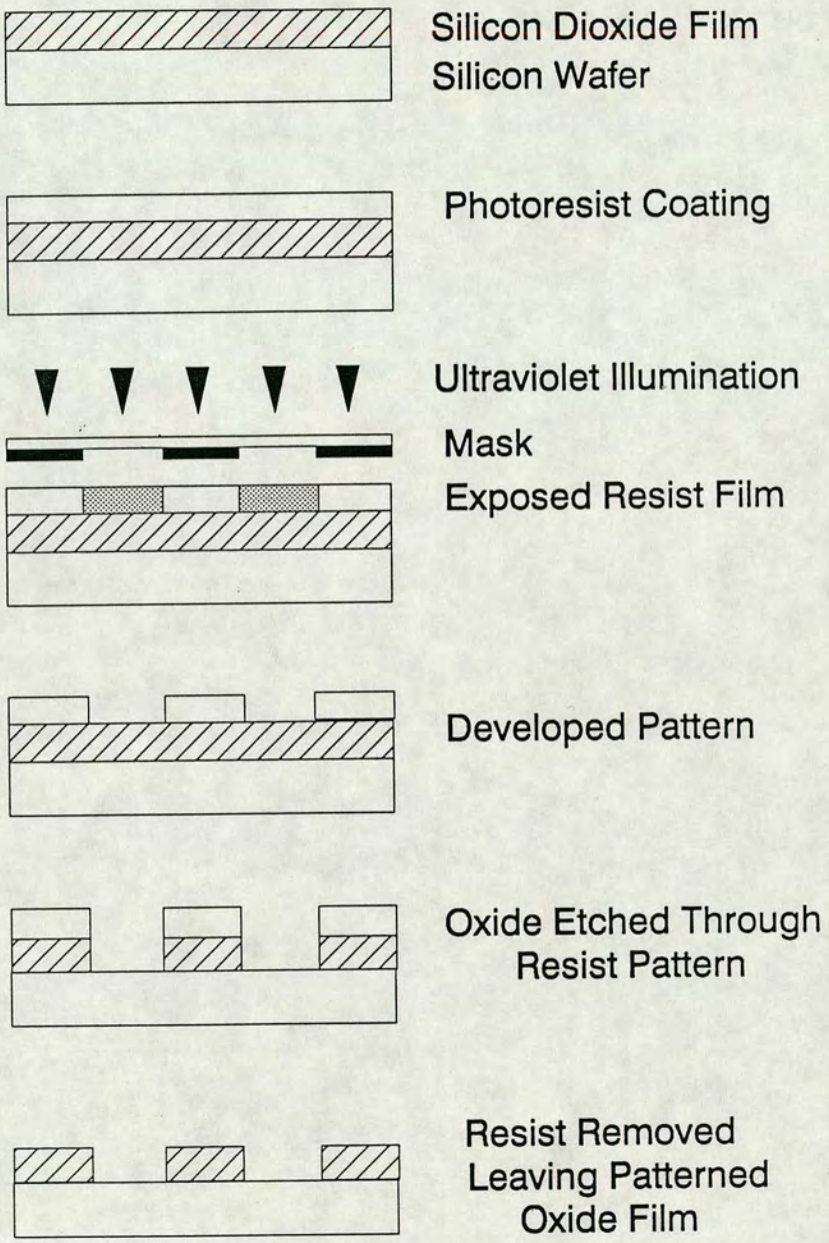

Figure 2–2: Lithographic Definition of Pattern in Film Using Positive Resist [1]

2.2 Exposure Methods

2.2.1 Contact Printing

Exposure systems vary widely in terms of complexity and cost. The simplest method of exposure is contact printing, in which the mask and the surface of the wafer are brought into contact once they have been aligned. Resolution of less than one micron linewidth is possible, but because of spatial non-uniformity of the contact, resolution may vary considerably across the wafer. The major drawback of contact printing is a steady increase in the defect level from one wafer to the next. The contact produces defects in both the mask and the wafer, so that the mask must be scrubbed or discarded after a short period of use. Contact printing continues nevertheless to be widely used at coarse geometries.

2.2.2 Proximity Printing

Proximity printing has the advantage of longer mask life because there is no contact between mask and wafer. Typical separations between mask and wafer are in the range 20 to 50 μm. Resolution is not as good as in contact printing. The minimum dimension d_{min} which can be reliably printed by shadow printing across a finite gap is:

$$d_{min} \approx (g\lambda)^{\frac{1}{2}} \tag{2.1}$$

where g is the gap between mask and wafer and λ is the wavelength of the exposure source. [3]

(Taking λ = 365nm and g = 20μm gives a d_{min} of 2.7μm.)

2.2.3 Projection Printing

Proximity printing solves some of the problems of contact printing but suffers from severe limitations due to diffraction effects. These limitations can be overcome by not using shadow casting techniques and instead projecting an image of the mask onto the wafer using a system of lenses. [4]

Projection printing offers higher resolution than proximity printing, and with no contact between mask and wafer, these systems do not have the yield problems of contact printing. The earliest design of projection printers produced a 1:1 image of the mask on the wafer by scanning the mask and wafer smoothly past the optical system with uniform velocity. However, systems which expose the whole wafer at 1:1 are unable to cope with in-plane wafer distortions which arise during processing. This results in a mismatch between mask and wafer known as run-out which may amount to 1 or 2 μm across a 4 inch wafer. [5] Therefore to meet the requirements of VLSI circuits with resolution below 1.5μm and registration to better than 0.5μm, direct-step-on-the-wafer (DSW) machines were developed. [6]

2.2.4 Direct-Step-on-the-Wafer (DSW)

These are basically step-and -repeat cameras in which a mask pattern is imaged directly onto the wafer surface with a reduction ratio of 5X or 10X. The image field is restricted to less than 20 mm square and the wafer is stepped and repeated on an XY stage to expose the whole surface. [7] Misalignment between mask and wafer can be overcome as only a small area of the wafer is exposed at a time, and alignment and focus corrections can be made at each exposure site. [8] [9] The numerical aperture is much higher than in the whole-wafer projection systems, usually $NA > 0.3$ giving improved resolution but with reduced depth of focus. [10] [11]

Unfortunately, fine control of CD is achieved at the cost of throughput. Unlike the contact printing or 1:1 projection systems, step-and-repeat systems are inherently slow. The use of DSW machines can only be justified on a cost basis

	Wafer Stepper 10X	1:1 Projection	Proximity	Contact
Resolution	1.0 um	2-3 um	3-5 um	1.0 um
Alignment	±0.14 μm	±0.7 μm	±1.0 μm	±1.0 μm
Overlay	±0.3 μm	±1.2 μm	±1.5 μm	±1.5 μm
Throughput	10-40 w/hr	60 w/hr	100 w/hr	100 w/hr
Mask Induced Defects	0	3 per Square inch	10 per Square inch	
Sensitivity To Soft Defects	5 um	0.5 um	0.5 um	0.5 um
CD on Oxide	±0.1 μm	±0.25 μm	±0.5 μm	±0.5 μm
Yield	Best	Fair	Poor	Worst
Mask Life	Infinite	Infinite	Infinite	Short
Mask Cleaning	Infre-quent	= 3-4 hrs	2 hrs	10 Expo-sures
Wafer Size Capability	2-6 inch	3-4 inch	3-4 inch	2-4 inch
Price (1982)	$650K	$300K	$50K	$50K

Figure 2–3: Lithography Comparisons [3]

for small geometries. [12] The yield from 1:1 projection aligners becomes unacceptable below about 2μm. [13](See Fig.2–3).

2.3 Imaging Characteristics of a Projection System

Fig. 2–4 shows a typical projection exposure environment. The entire optical system is optimised for its intended purpose of highest possible resolution over a given field size. This means that the light source and its condenser come as close as possible to uniformly filling the entrance pupil of the projection lens. [14] Modern projection printers are designed to provide uniform illumination over the entire mask object, and employ optics which are essentially diffraction-limited. This implies that the resolution of the lens is determined by its aperture, not by imperfections of design or manufacture. [1] [15] [16]

It is useful to recall the definitions of several parameters to specify an imaging system.

2.3.1 Numerical Aperture (NA)

Numerical Aperture is given by:

$$NA = n \sin \alpha \tag{2.2}$$

where n is the refractive index (usually unity) in image space, and 2α is the maximum cone angle of rays reaching an image point on the optics axis of the projection system. [17] [18] (See Fig. 2–5)

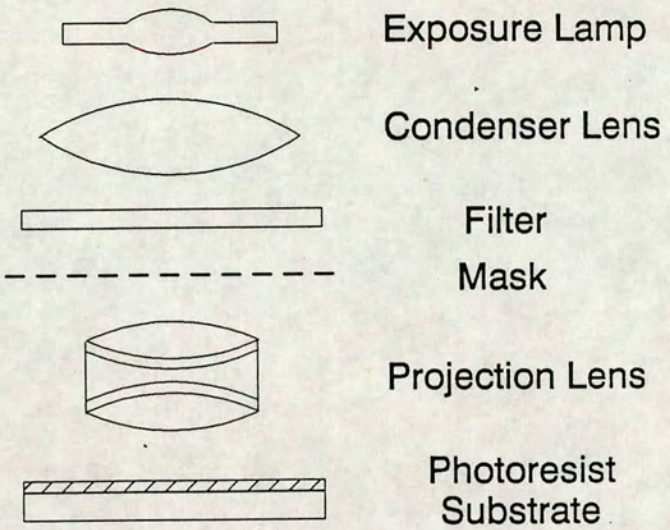

Figure 2–4: Typical Projection Exposure Environment [67]

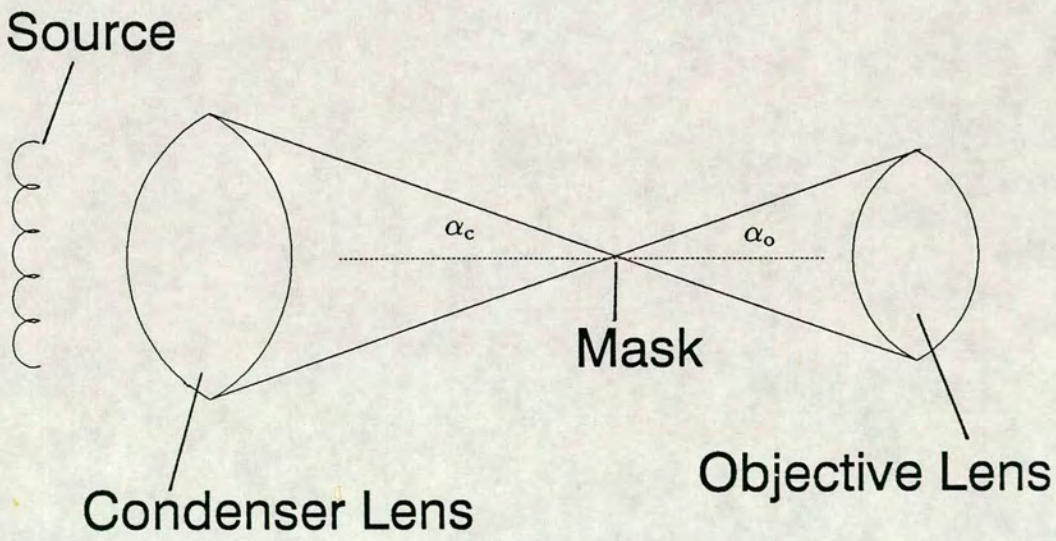

Figure 2–5: Lens Projection System

2.3.2 Illumination Coherence (σ)

Illumination Coherence is defined by the ratio: [19]

$$\sigma = \frac{\text{NA of Condenser Lens}}{\text{NA of Objective Lens}} \tag{2.3}$$

The parameter σ describes the degree of filling of the entrance pupil of the imaging lens by the source. Most projection system operate in the range $0.1 < \sigma < 0.8$. [20]

2.3.3 Modulation Transfer Function (MTF)

The Modulation Transfer Function MTF can be used to describe the resolution characteristics of the projection system. In principle, the MTF curve is obtained by imaging gratings placed in the object plane. Each grating is characterized by a frequency (measured in lines per mm) and a modulation: [3]

$$M_0 = \frac{I_{max} - I_{min}}{I_{max} + I_{min}} \tag{2.4}$$

where I_{max} and I_{min} are the local maximum and minimum light intensities emerging from the spaces and lines. The ratio $\left(\frac{I_{max}}{I_{min}}\right)$ is called the **Contrast** (C). The corresponding modulation $M_i(v)$ in the image plane can be measured by scanning a very small photodetector across the image of the grating. The MTF at frequency v is given by:

$$MTF(v) = \frac{M_i(v)}{M_0} \tag{2.5}$$

2.3.4 Rayleigh Limits

The **Resolution** of a lens is specified by plotting its MTF against spatial frequency. [21] A common rule of thumb is that an MTF of more than 50% is required for reliable imaging in positive photoresist. [22] The MTF of a perfect lens falls to zero at a value of spatial frequency v_0 given by: [23]

$$v_0 = \frac{2NA}{\lambda} \tag{2.6}$$

where NA is the numerical aperture of the lens and λ is the wavelength of illumination. (See Fig. 2–6). The minimum feature size d_{min} which a lens will resolve is given by:

$$d_{min} = \frac{k\lambda}{NA} \tag{2.7}$$

where k is a constant of proportionality.[24] The traditional values for k are k = 0.5 for "theoretical" resolution and k = 0.8 for "production" resolution. Recent trends seen in specifications from major stepper manufacturers show that the most advanced lenses are being guaranteed for resolution performance beyond that given by the traditional k = 0.8 and tending towards k = 0.5. [25]

If k = 0.5 and λ = 193nm, then $d_{min} = 0.25\mu$m. The feasibility of printing quarter-micron dimensions with optics would not have been entertained five years ago. [26]

From Equation 2.7 it can be seen that the ability to resolve smaller features can be achieved by either reducing the wavelength used for exposure or increasing the numerical aperture. However, since an increase in NA would result in a reduced **Depth of Focus** (Δs), the former option has been favoured as a long-term means of improving resolution. [27]

$$\Delta s = \pm\frac{\lambda}{2(NA)^2} \tag{2.8}$$

New lenses must therefore be designed to operate at lower wavelengths. [28]

2.3.5 Choice of Wavelength

Virtually all lithographic equipment in IC production uses mercury-vapour lamps for a light source. Consider the emission spectrum of a mercury-vapour lamp illustrated in Fig. 2–7. In the wavelength range between 350 and 450 nm there are three strong spectral lines, designated g, h and i lines. [29]

Traditionally, steppers were designed to operate using the 436 nm emission line of mercury (g-line) for exposure. [30] [31] Developments in lens design and

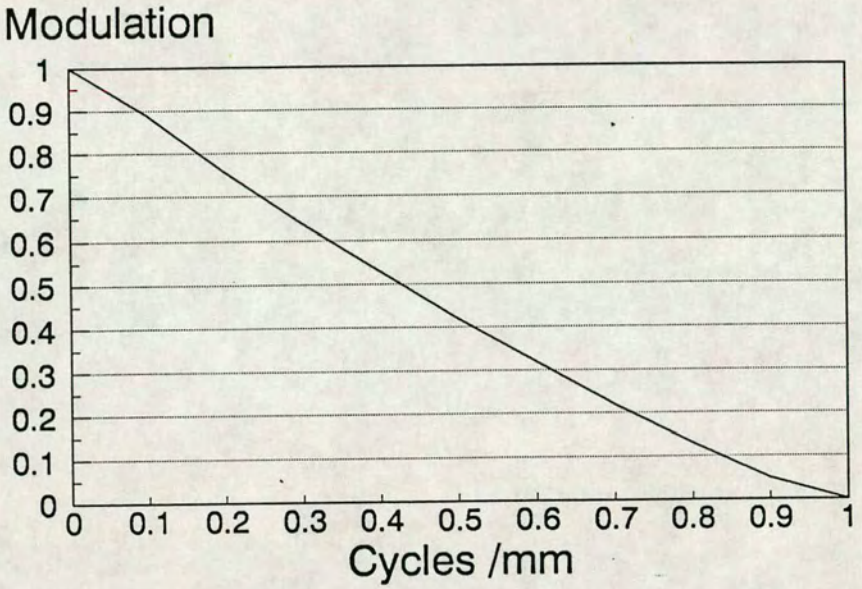

Figure 2–6: MTF of a Perfect Lens [3]

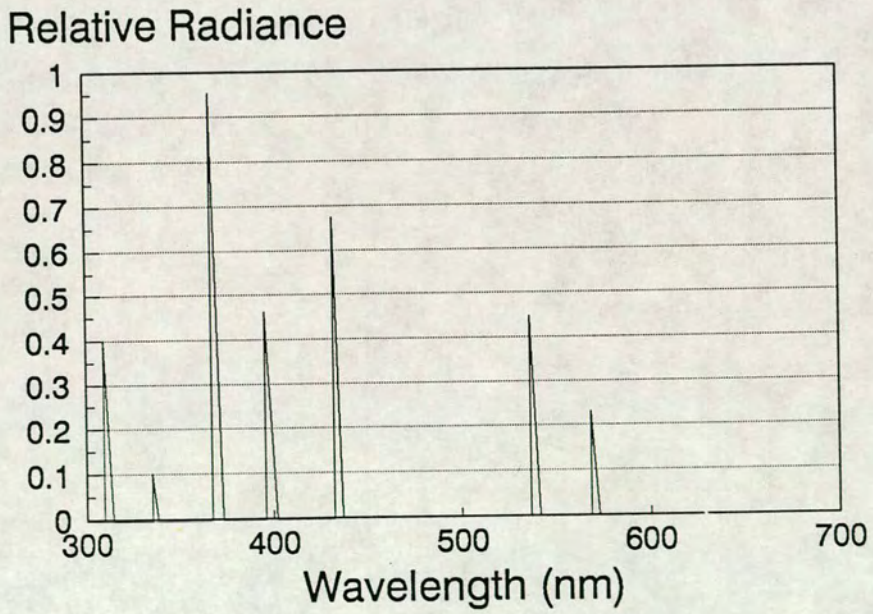

Figure 2–7: Mercury-Vapour Spectrum [20]

resist processes enabled the conversion to h-line (405 nm) and then i-line (365 nm). [32] [33] [34] In 1987, the first steppers operating in the deep ultra-violet (DUV) region of the spectrum were developed. [35] [36] These used excimer lasers with a wavelength of 248 nm as their light source.

DUV lithography requires a higly transparent resist, and this can cause problems in controlling CD over topography, due to substrate reflections. Problems are also encountered with resist stability and adhesion. However, although as yet no DUV resist process is commercially available, and several years of research are required before high volume production is possible, it is predicted that DUV lithography will be firmly established by the mid 1990's. [37] [38]

The ultimate move to even shorter wavelengths, especially 193 nm has been contemplated by many authors. [39] [40] [41] It is not easy to project the development path or time-scale for practical applications of wavelengths below 200 nm. However, research is undoubtedly proceeding in several laboratories internationally. [42] [43]

2.4 Photoresist

2.4.1 Introduction

The basic Photolithography sequence is shown in simplified form in Fig. 2–8. To perform successfully in the microfabrication process, the resist must have certain properties which are well defined and consistent from batch to batch. Photoresists may be negative or positive working. With positive resists, exposure to light increases the solubility of the film in developer, whilst with negative resist the converse is true. Positive photoresist has inherently superior resolution characteristics and is usually preferred for high resolution applications. [44]

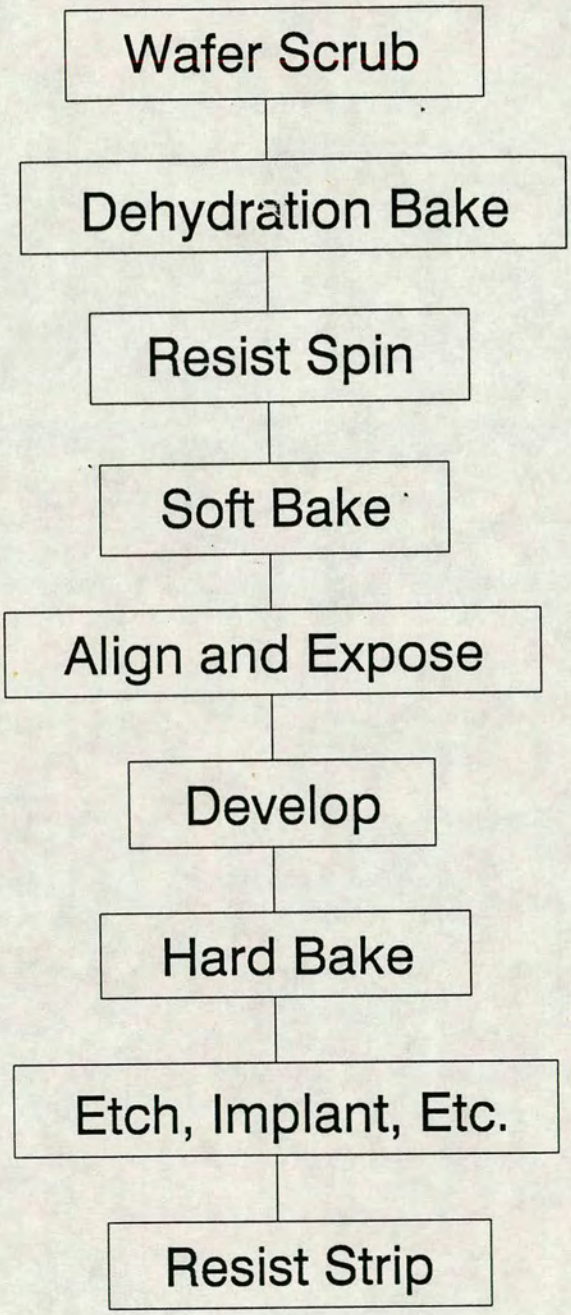

Figure 2–8: Photolithography Sequence [22]

Positive photoresist has three principal components: a resin that gives the resist its coating and chemical resistance properties, a volatile carrier solvent, and a photoactive compound (PAC) which inhibits dissolution of the resist in aqueous solutions. The photoactive compound reacts in exposure to light to form a carboxylic acid, losing its inhibitor properties and allowing for the dissolution of the resist in aqueous alkaline solutions. [45]

The first positive resists widely used for semiconductor processing were based on phenol-formaldehyde (NOVOLAC) resins and diazo napthaquinone sensitizers. [46] This technology remains the standard of the resist industry, and is adequate down to one micron linewidths, in terms of resolution, adhesion to any substrate, and resistance to pattern transferring process. [47]

UltraViolet Resists

However these resists are too absorbing for UV wavelengths below 400 nm with the result that it is difficult to obtain vertical resist sidewalls at shorter wavelengths, thereby limiting resolution. For this reason new resists had to be found, based on different principles and using materials that are less absorbing down to 248 nm. [48]

Some of the polymers that are acceptable in terms of thermal stability, resistance to chemicals, and reactive ion etching, are based on polystyrenes that owe their stability to the benzene ring. Purified forms of styrenes can be fairly transparent to UV down to 248 nm. [49]

Using these new polymers many new deep UV resists are being developed by the resist manufacturers. These resists provide not only higher transparency, but also higher sensitivity than conventional resists by almost one order of magnitude. [50]

Multi-Layer Resists

One problem associated with new high numerical aperture steppers is the limited depth of focus, a problem that is especially severe when exposing thick resist layers on wafers with topographic features of depth higher than 0.5μm. [51] A possible solution to this problem is provided by the use of multilayer resist systems. These systems can be divided into two main categories: [52]

1. Tri-layer in which three or more layers of material are required. The initial material acts as a planarizing layer, the second as a barrier layer for image transfer, and the top layer is the imaging layer.

2. Bi-layer in which both layers are photo-active, or where the functions of image formation and etch barrier are combined in the top layer. [53]

Multilayer resists solve the problems of depth of focus, increase resolution, and reduce standing wave effect, but at the same time increase complexity and cost.[54] Their use has not been widespread.

2.4.2 Optical Characteristics

The main parameters of interest are the sensitivity, contrast and useable resolution. **Characteristic Curves** are generated by measuring the percentage of remaining resist after development as a function of the logarithm of exposure. Fig. 2–9 is a typical curve for positive resist with the main features labelled.

Region A of the curve represents low exposures, showing some loss of resist thickness due to the solubility of resist in developer. At this stage of exposure the inhibitor concentration has not been sufficiently modified to induce significant resist solubility.

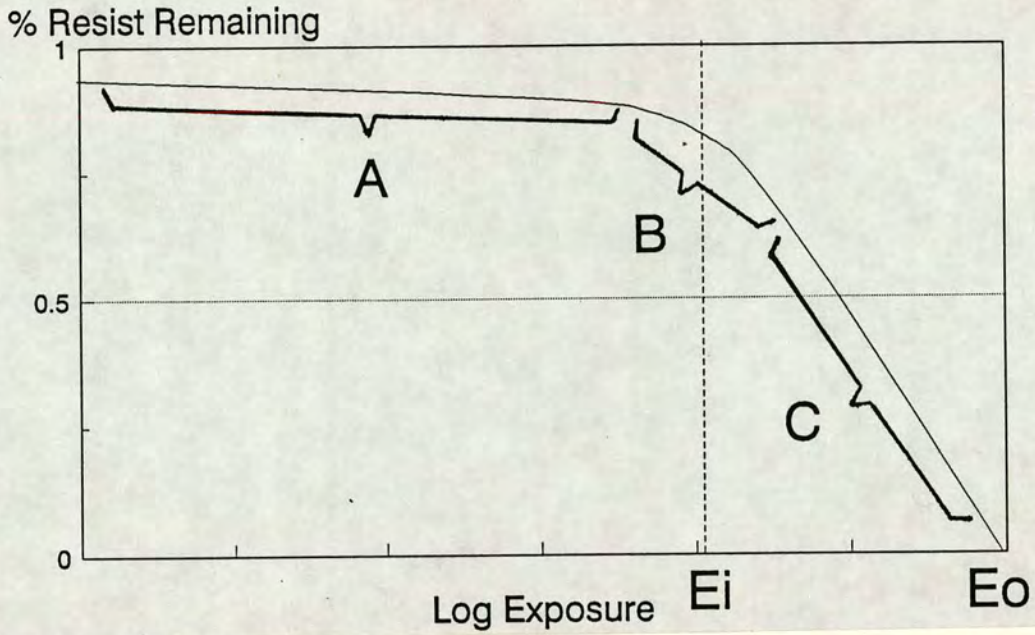

Figure 2–9: Characteristic Curve for a Positive Resist. [63] Region A Represents Low Exposures, where Thickness is Lost Due to the Solubility of Unexposed Resist in Developer. In Region B the Inhibitor Concentration Starts to Respond Significantly to Exposure. In Region C the Curve Becomes Linear to the Point of Complete Resist Removal

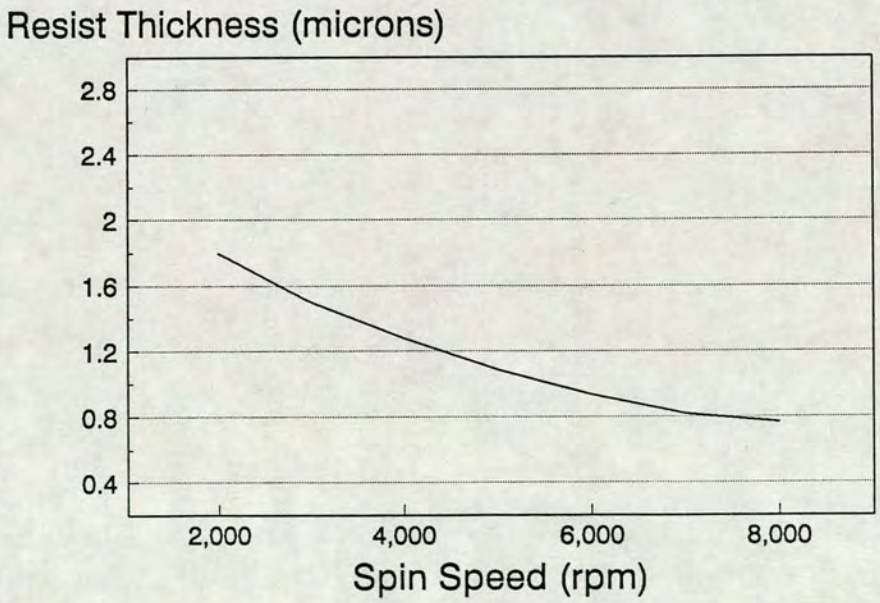

Figure 2–10: Spin Speed Curve for a Typical Positive Resist.[22] The Final Spin Speed of the Coating Track is the Major Parameter Affecting Resist Thickness. Spin Speed Curves are Generated by IC Manufacturers to Characterize the Coating Properties of Each Resist

In region B, the inhibitor concentration starts to respond significantly to exposure and the resist solubility is altered. The width of this region is important. If it is too wide, a weak response of resist solubility is indicated, giving inferior contrast characteristics. In Region C the curve becomes linear to the point of complete resist removal.

E_0, the **Exposure Threshold** for complete resist removal is an important parameter of a process. It is useful for measuring relative photospeed and as a process control parameter. A tangent is drawn at E_0 and extrapolated to the ordinate at 100% resist thickness, to define E_i. E_i is sometimes described as the exposure threshold for first significant resist removal.

The **Contrast** (γ) is the slope of this tangent line: [55]

$$\gamma = log_{10}\left(\frac{E_0}{E_i}\right)^{-1} \tag{2.9}$$

King [56] has shown theoretically that high gamma values lead to increased edge-wall angles and improved linewidth control over steps.

2.4.3 Physical Characteristics

Thickness

A small quantity of resist (between 1 and 10 ml depending on wafer diameter) is dispensed as a puddle on the stationary wafer surface and after a short time to permit spreading, is spun off to leave the film coating. The final thickness and uniformity of the film is a function of dispensed quantity, spreading time, acceleration spin time, exhaust extract flow rate and final spin speed. The last of these is the major parameter affecting thickness, whilst the remainder control radial uniformity. Fig. 2–10 indicates thickness as a function of spin speed for typical resists used in IC manufacture.

Adhesion

Reliable adhesion of the resist to the underlying material is essential. In the MOS process the materials to be patterned will be nitride, oxide, polysilicon and aluminium. To ensure adhesion the wafer surface must be absolutely dry. The wafers are given a de-hydration bake and adhesion promoter, commonly hexamethyldisilazane (HMDS), is applied prior to resist coating.

Resist adhesion is further improved by "soft-baking" the film immediately after spinning to remove solvent. This is usually done on a hotplate at around 100 degrees Centigrade for about 60 seconds.

Etch Resistance

The etching operation may subject the developed resist to severe chemical and physical attack depending on the process. Wet etching may involve immersion in concentrated acids at temperatures up to 150 degrees Centigrade for several minutes, whereas plasma or reactive ion etching may cause significant mechanical abrasion of the resist. To improve etch resistance, the resist film is usually "hard-baked" at about 130 degrees Centigrade after development and before etching. If further hardening of the film is necessary it can be given a flood exposure with deep uv after development.

2.4.4 Exposure

Standing Wave Effects

In order to predict the effect of lithographic exposure upon a film of photoresist, there must be an understanding of the "thin film physics" involved. A photoresist film comprises a complex optical environment with wavelength dependent properties.

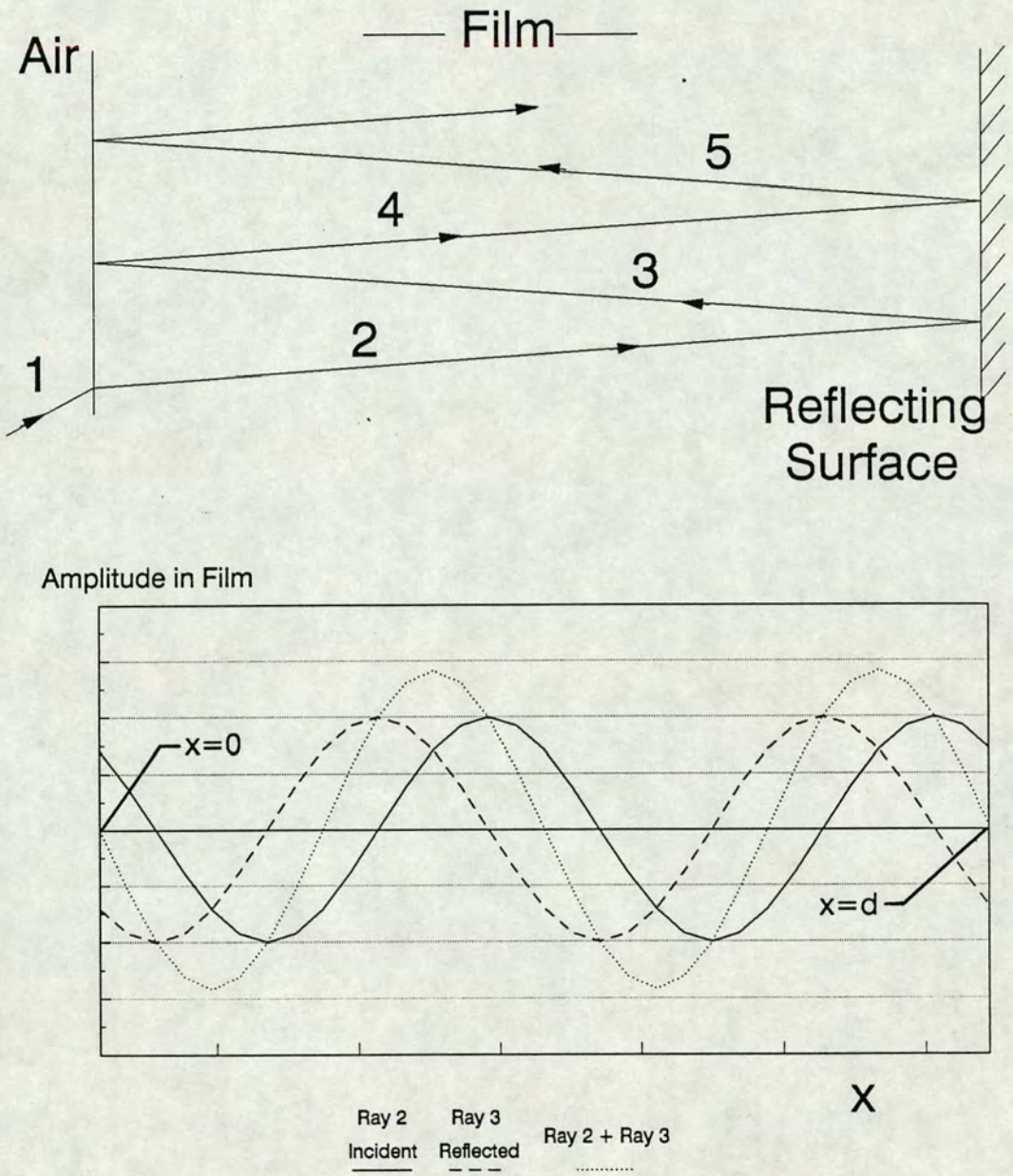

Figure 2–11: Standing Wave Effects [57] The Top Digram Represents the Major Internal Reflections which Occur within a Thin Film when Exposed to Light. The Bottom Diagram Represents the Amplitude of the Rays within the Film, and Demonstrates that Interference Between Incident and Reflected Rays Results in a Standing Wave

Weakly Absorbing Film

Consider the approximation of a weakly absorbing resist film of thickness d on a perfectly reflecting substrate with monochromatic illumination. Although this is a special case it does approximate some printing situations. Later on the effect of resist absorption will be taken into consideration. If the incident light wave "1" as shown in Fig.2–11 has unit amplitude, the light wave "2" in the film can be represented by :

$$E_2(x) = E_2 \sin(wt - kx + \phi) \tag{2.10}$$

where $E_2 = (1 - r^2)^{\frac{1}{2}}$ and absorption effects are neglected. $r = \frac{n-1}{n+1}$ is the reflection coefficient at the air/film interface, $k = \frac{2\pi n}{\lambda}$ and n is the real part of the resist dielectric constant $\tilde{n} = n - jK$. [57]

The amplitude of the reflected wave "3" is:

$$E_3(x) = E_2 \sin[wt - k(2d - x) + \phi + \pi] \tag{2.11}$$

A phase change of π is assumed during reflection. As illustrated in Fig. 2–11 these add to give a standing wave $E_{23}(x)$ given by:

$$E_{23}(x) = 2E_2 \sin k(d - x) \cos(wt - kd + \phi) \tag{2.12}$$

The location of the maxima (antinodes) and minima (nodes) are clearly independent of the arbitrary phase constant ($wt + \phi$) of the incoming wave. [58] Measured from the reflector, the location of the intensity extrema are given by the following conditions, where $N_1 = 0, 1, 2 \ldots$ [59]

For antinodes (maxima):

$$n(d - x) = \frac{\lambda}{4}, \frac{3\lambda}{4} \ldots (2N_1 + 1)\frac{\lambda}{4} \tag{2.13}$$

For nodes (minima):

$$n(d - x) = \frac{\lambda}{2}, \lambda \ldots N_1 \frac{\lambda}{2} \tag{2.14}$$

The air/film interface at the plane x=0 will generate waves 4 and 5 in Fig. 2–11. These waves are represented by:

$$E_4 = rE_2 \sin[wt - k(2d + x) + \phi + \pi] \tag{2.15}$$

$$E_5 = rE_2 \sin[wt - k(4d - x) + \phi + \pi] \tag{2.16}$$

Note that there is no phase change for internal reflections at the air/film interface. [60] Waves 4 and 5 combine to give a second standing wave:

$$E_{45} = -2rE_2 \sin k(d-x) \cos(wt - 3kd + \phi) \tag{2.17}$$

Additional pairs of waves are treated similarly. The resulting standing waves can be summed to give:

$$E(x,d) = 2E_2 \sin k(d-x) \sum_{N=0}^{\infty} (-r)^N \cos\left[wt - (2N+1)kd + \phi\right] \tag{2.18}$$

This equation shows that the location of the nodes and antinodes in the film are given by Equations 2.13 and 2.14. [61]

Effect of Resist Absorption

Now consider the effect of the optical absorption of the resist film. The locations of the intensity nodes and antinodes relative to the substrate are unaffected by absorption in the resist and are still given by Equations 2.13 and 2.14. However, the modulation M_{sw} of the standing waves is, in general, dependent on resist absorption and is therefore time dependent.

Fig. 2–12 shows the optical intensity within the resist film at the start of exposure. At this stage the absorption constant is relatively high, which causes the decrease in average intensity from the surface to the substrate. The modulation M_{sw} is depressed and standing waves effects minimized.

Exposure of photoresist under this condition destroys more inhibitor at the intensity maxima than the minima. The increased transparency of the resist results in an increased modulation M_{sw}. Standing wave effects therefore become more pronounced. The distribution of inhibitor within the film after exposure is shown in Fig. 2–13.

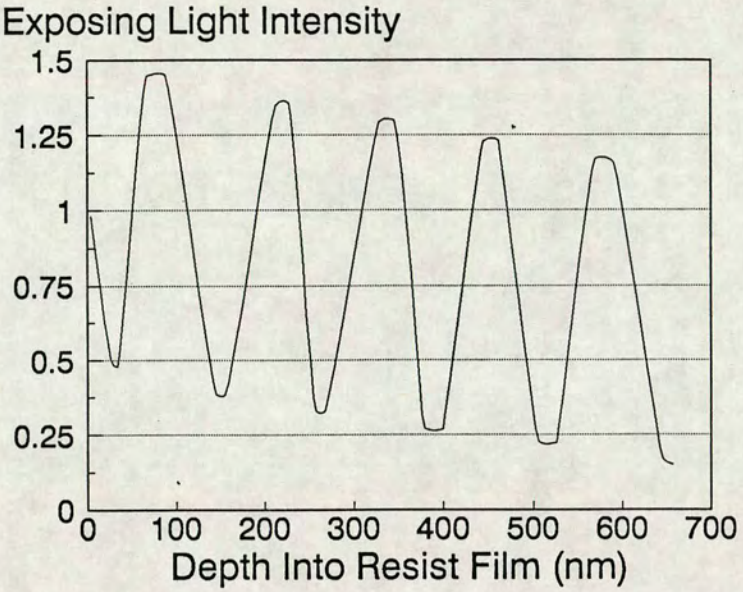

Figure 2–12: Start of Exposure: Intensity versus Depth into Resist Film [80]

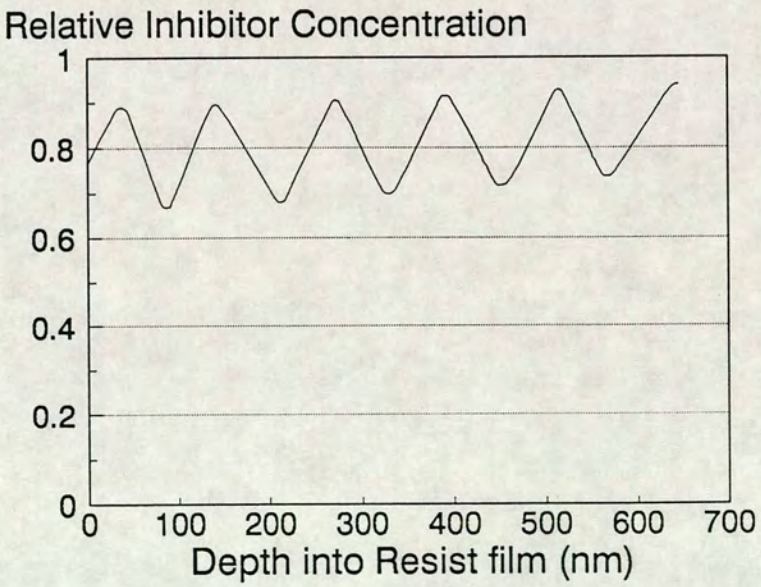

Figure 2–13: End of Exposure: Inhibitor Concentration versus Depth into Resist Film [80]

2.4.5 Development

Development of positive photoresist can be considered a surface-controlled etching reaction which is simply determined by the relative photoactive compound density and the developer chemistry at the surface of the resist. [62] The physical phenomena involved in resist removal include: i) the transport of developer molecules to the resist surface ii) chemical reactions taking place at the resist-developer interface iii) the transport of dissolution products away from the reacting surface. [63]

Fig. 2–14 shows a typical development rate R(M) curve for AZ 1350 J resist in 1:1 AZ developer: H_2O at 20 degrees Centigrade. This curve can be used to obtain a development rate profile R(z) for the inhibitor distribution shown in Fig. 2–13. This is shown in Fig. 2–15.

The time to develop from the surface (z=0) to any depth w in a "uniformly exposed" resist film can be calculated from:

$$t(w) = \int_0^w \frac{dz}{R(z)} \tag{2.19}$$

where R(z) is a rate profile like that shown in Fig. 2–15.

This result is shown plotted as the thickness of a developing photoresist film as a function of development time in Fig. 2–16. The staircase shape is evidence of the interference effects in photoresist exposure. Since the development rate varies throughout the film, it will obviously take a relatively long time to etch through regions of low development rate compared to those with high development rate. This can cause problems developing through the exposure minimum nearest the substrate.

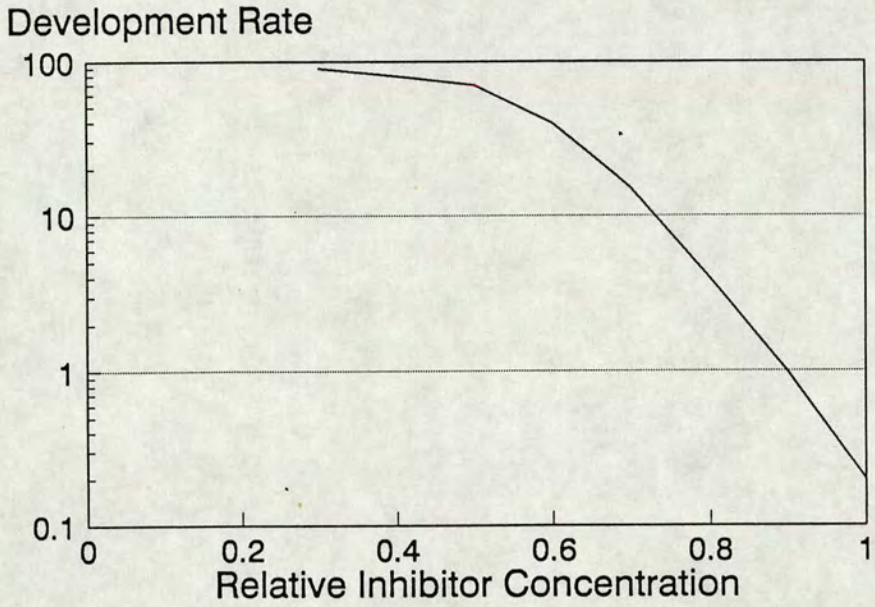

Figure 2–14: Development Rate as a Function of Inhibitor Concentration [80]

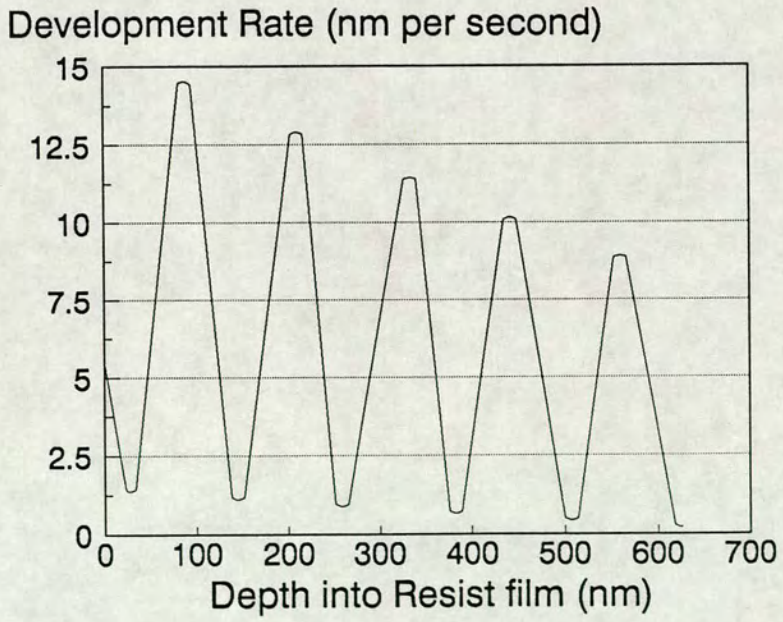

Figure 2–15: Development Rate as a Function of Depth into Film [80]

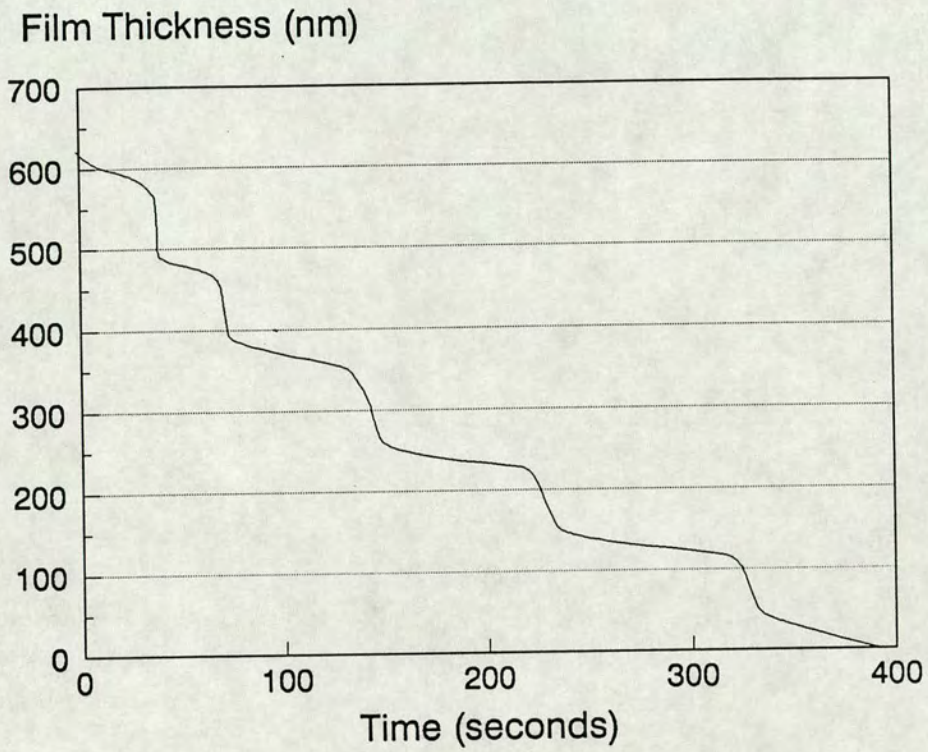

Figure 2–16: Resist Thickness as a Function of Time [80]

2.5 Process Simulation

2.5.1 Introduction

The lithographic process model represents a powerful tool for studying projection exposure. Simulation programs enable the changes in resist parameters and processing conditions to be studied in terms of image profiles and profile sensitivities. [64]

The theoretical aspects of partially coherent imaging in microfabrication have been quantitatively studied by Lin [65] who plotted the intensity profiles of the aerial image to show the effect of de-focus and partial coherence on the projected linewidth, independent of the properties of the substrate and the photoresist.

Prediction of the developed resist profile must also take account of the optical properties of the substrate and the response of the resist and developer to the intensity profiles in the aerial image. [66]

The photoresist process separates conveniently into two distinct parts: exposure and development. The parameters used to characterize exposure and development have a strong physical basis and only a weak link to the chemistry of the process. [67]

2.5.2 EMF Simulation Programs

The Edinburgh Microfabrication Facility (EMF) has access to three lithography simulation packages:

1. DEPICT was developed by Technology Modeling Associates (TMA) Inc. It models deposition, lithography and etching processes. Version 8716 is installed on the VMS operating system for access throughout the department.[68]

2. SAMPLE (Simulation And Modeling of Profiles for Lithography and Etching) was developed at the University of California, Berkley under the direc-

tion of Profs. W.G.Oldham and A.R.Neureuther.[69] [70] Version 1.7 a is installed on machines within the EMF.[71]

3. PROLITH (Positive Resist Optical Lithography) was developed at the National Security Agency largely through the efforts of Chris Mack. It calculates resist profiles for all three major printing methods in use today: projection, contact and proximity.

The optical simulations carried out by these programs model one-dimensional objects, namely periodic patterns of lines and spaces of finite width but assumed to be of infinite length. When projected onto the resist film, the resulting images are described in two dimensions. The principal projection lithography outputs produced by these programs are:

- The illumination intensity distribution (aerial image)
- The illumination intensity distribution within the photoresist film (standing wave)
- The photoactive compound (PAC) concentration distribution within the resist film (latent image)
- The resulting resist thickness as a function of horizontal location after development (edge profile)

The advantage of having three different simulation packages is the ability to compare results. [72] Although different mathematical models are built into each simulator, it is possible to duplicate the intensity profiles from any of the software packages. The main features of the SAMPLE program are shown in Fig.2–17. [73]

EX BIBL UNIV. EDINBURGEN.

Inputs	Outputs
Image Simulator	
Lens Numerical Aperture (NA)	Image Profile
Illumination Coherence	Contrast
Focus Error	Slope
Mask Line and Space Width	
Exposure Simulator	
Substrate Properties	2-D Array of Resist Exposure Against Position and Depth
Thin Film Properties and Thickness	
Resist Properties	
Exposure Dose	
Development Simulator	
Resist Development Properties	Resist Slope
	Resist Linewidth
Development Time	Resist Line-Edge Profile

Figure 2–17: SAMPLE Input and Output Parameters [1]

Measurement of CD

Each simulation package offers the ability to measure linewidth dimensions on developed features. However the presence of standing wave ripples on the edge profiles makes the measurement difficult, since the dimension is highly dependent on the measurement location.

To overcome this problem the simulators define linewidth dimensions as the width of the developed resist profile measured at the "waist" of the standing wave pattern nearest the substrate. [74] This convention makes comparison of linewidth dimensions from different simulation packages possible. (See Fig. 2–18).

2.5.3 Simulation of Exposure

For simulation purposes, lithographic exposure is separated into two component parts: determination of the image of the mask at the surface of the structure, and exposure of the photoresist layers.[74] [75] The intensity of the exposing radiation within the resist I(z,t) at any depth z and exposure time t, can therefore be written as:

$$I(z,t) = I_{incident} I_{sw}(z,t) \tag{2.20}$$

where $I_{incident}$ is the incident image intensity and I_{sw} is standing wave intensity.[76]

Determination of $I_{incident}$ is implemented using the theory of imaging with partially coherent illumination developed by Hopkins [77] [78]. The simulation programs define an optical projection system in terms of the following parameters: i) the wavelength of the illumination ii) the power density of the source iii) the numerical aperture of the objective lens iv) the degree of coherence.[79]

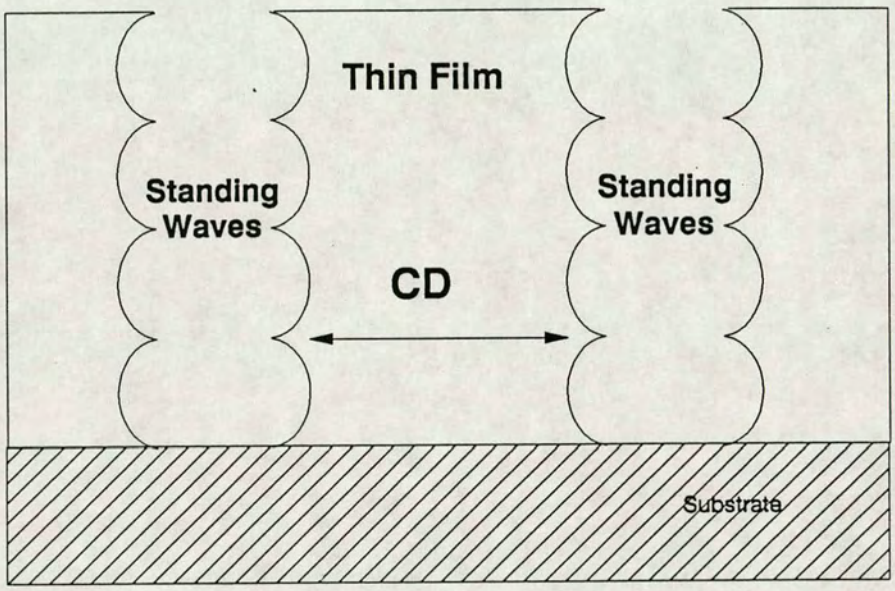

Figure 2–18: Definition of CD

Determination of $I_{sw}(z,t)$ is implemented using a method proposed by Berning [80]. The approach consists of partitioning the photoresist film into a large number of thin parallel layers and assuming that each layer is essentially isotropic. The bleaching model proposed by Dill *et al.* [81] is then used to predict the changes in optical absorption for each sub-layer as the resist undergoes photochemical changes during uv illumination. The absorption constant α is given by the equations:

$$\alpha = AM(z,t) + B \tag{2.21}$$

$$\frac{\partial I(z,t)}{\partial z} = -I(z,t)\,[AM(z,t) + B] \tag{2.22}$$

$$\frac{\partial M(z,t)}{\partial t} = -I(z,t)M(z,t)C \tag{2.23}$$

where M(z,t) is the relative amount of photobleachable dye (PAC) at any depth z in the resist and at exposure t, and I(z,t) is the light intensity. As is evident from these equations, parameter A relates to the absorption coefficient of the resist before exposure (M=1). Parameter B corresponds to the final absorption coefficient of the completely bleached resist (M=0). Parameter C signifies the bleaching rate for the resist.

2.5.4 Simulation of Development

Development simulation consists of modeling the mechanism of photoresist dissolution by a developer solution and calculating the resulting resist cross-sectional profiles. The simulation programs offer a choice of four models to simulate the development process: the Dill model [81] [82], the Berkley model proposed by Kim [83] [84], the Mack model [85] [86] [87] or the user's own model.

The default model for each simulator is the Dill model based on the three parameter equation:

$$r(M) = \exp(E_1 + E_2 M + E_3 M^2) \tag{2.24}$$

where r is the local resist development rate, M is the localized PAC concentration, and E_1, E_2 and E_3 are three parameters obtained using least-square fit to experimental data.

Commercial simulation packages can only model tank develop processes, which have relatively simple chemical and physical mechanisms. A track develop system is more complex to model because there are many more parameters to consider, such as type of dispense, spin speed and acceleration.[88] Research is currently being carried out in the EMF to design a develop rate monitor capable of modeling the behaviour of resist during development on a track system [89].

2.6 Lithography Control

Having reviewed the lithographic process it is evident that there is a large number of parameters which may affect linewidth uniformity. Identification of the key factors is the first step towards a characterization of their behaviour in terms of process control. [90] If their behaviour can be confidently predicted, then processing conditions may be optimised in order to achieve tighter tolerances on CD. [91] [92] [93] [94]

Lauchlan [95] has identified the ten most significant process variable affecting lithography. These are listed below: (not in any order of significance)

- Relative humidity
- Developer concentration and temperature
- Prebake temperature and time
- Underlying film thickness
- Substrate reflectance
- Fabrication temperature
- Photoresist thickness
- Time between processing steps

- Exposure time
- Development time

Consideration of these ten parameters would suggest that seven are easily controllable: the three exceptions being substrate reflectance, and the thicknesses of the underlying film and photoresist.

Substrate reflectance is easily measurable since it involves a simple optical measurement of spectral response at a particular wavelength using a photodetector.

Film thickness is not directly measurable, but can be extracted from the measured reflectivity. There is a wide variety of techniques and algorithms to extract thickness in common use. However, not all are suited for the fast acquisition of data required in a production environment. If the mapping of film thickness slows down production, there is an economic motivation to minimise measurement routines. This may be a false economy if film thickness uniformity is of fundamental importance to the yield of correctly functioning chips.

It would be useful to investigate experimentally the effect of film thickness variations on CD. If the experiments show that film thickness and photoresist thickness have a significant effect on CD, then a review of film thickness measurement techniques would be in order.

Initially however, it will be necessary to ensure that the CD measuring system in the EMF is sufficiently sensitive to detect small variations in dimensions. The following Chapter outlines various CD metrology techniques, and the theory on which they are based. The second half of the Chapter describes the tests done to measure the resolution and repeatability of the EMF's "Quaestor" and "Nanolab" metrology systems.

Bibliography

[1] J.T.M.Stevenson and A.M.Gundlach. The application of photolithography to the fabrication of microcircuits. *J. Phys. E:Sci. Instrum.*, pages 654–667, 1986.

[2] K.D.Bowers. Lithography - why go further? In *INTERFACE 85*, pages 4–11. Kodak Microelectronics Seminar, 1985.

[3] SERC School on Microfabrication, Edinburgh Microfabrication Facility, University of Edinburgh. *Optical Lithography - Exposure Tools*, June 1990.

[4] B.Allsop. Projection aligners in production. In *INTERFACE 85*, pages 20–27. Kodak Microelectronics Seminar, 1985.

[5] B.J.Lin. A comparison of projection and proximity printings: From uv to x-ray. In *Proceedings of Microcircuit Engineering*, pages 137–145, 1989.

[6] M.Hatzakis. Lithographic materials and processes for VLSI. In *International Conference on VLSI and CAD*, pages 542–544, 1989.

[7] K.Suwa and K.Ushida. The optical stepper with a high numerical aperture i-line lens and a field-by-field levelling system. In *Laser Microlithography*, pages 270–276. SPIE Vol. 922, 1988.

[8] S.Slonaker, S.McNamara, and K.Konno. Enhanced global alignment for production optical lithography. In *Laser Microlithography*, pages 73–81. SPIE Vol. 922, 1988.

[9] W.H.Arnold. Overlay simulator for wafer steppers. In *Laser Microlithography*, pages 94–105. SPIE Vol. 922, 1988.

[10] S.Sugiyama, T.Tawa, and Y.Oshida. New 5x i-line projection aligner forVLSI fabrication. In *Laser Microlithography*, pages 318–326. SPIE Vol. 922, 1988.

[11] H.M.Nishimoto, E.Tai, and R.J.Naber. Submicron imaging capabilites of a 0.40 NA broadband optical system. In *Laser Microlithography*, pages 309–317. SPIE Vol. 922, 1988.

[12] P.DiSessa. IC wafer fab economics and lithography equipment selection: The inextricable link. *Solid State Technology*, (12):155–161, 1983.

[13] A.N.Broers. The submicron lithography labyrinth. *Solid State Technology*, (6):119–126, 1985.

[14] G.van der Looij, V.Nagaswami, and P.Baltussen. A submicron lithography process using Phillips i-line stepper. In *Laser Microlithography*, pages 344–356. SPIE Vol. 922, 1988.

[15] S.Wittekoek. Optical lithography for microcircuits. In *Microcicuit Engineering*, pages 155–170, 1980.

[16] K.Hale and P.Luermann. Consistent image quality in a high performance stepper environment. In *INTERFACE 86*, pages 29–46, 1986.

[17] A.Goel. Analysis of a submicron i-line pilot process. In *Laser Microlithography*, pages 357–364. SPIE Vol. 922, 1988.

[18] C.Nolscher, L.Mader, and S.Guttenberger. Search for the optimum numerical aperture. In *Proceedings of Microcircuit Engineering*, pages 161–166, 1989.

[19] K.Eguchi, S.Miyazaki, and C.Takai. Half-micrometer lithography using a g-line stepper with a 0.6 numerical aperture lens. In *Laser Microlithography*, pages 335–343. SPIE Vol. 922, 1988.

[20] V.Miller and H.L.Stover. Submicron optical lithography: i-line wafer stepper and photoresist technology. *Solid State Technology*, (1):127–136, 1985.

[21] H.Sewell and A.R.Reinberg. Resolution in microlithography. In *Proceedings of Microcircuit Engineering*, pages 153–159, 1989.

[22] SERC School on Microfabrication, Edinburgh Microfabrication Facility, University of Edinburgh. *Resists and their Exposure Characteristics*, June 1990.

[23] B.J.Lin. Where is the lost resolution? *Solid State Technology*, (1):63–68, 1987.

[24] R.J.Holwill and J.T.M.Stevenson. Optical lithography and dry etching. In *Advanced Technologies and Processes in Communication and Power Systems*, pages 25–29. EUROCON 86, 1986.

[25] V.Nagaswami. Focus and overlay optimization for submicron i-line production lithography. In *KTI Microelectronics Seminar*, pages 301–314, 1988.

[26] M.Nakase. Potential of optical lithography. *Optical Engineering*, 26(4):319–324, 1987.

[27] C.A.Mack. Understanding focus effects in submicron optical lithography. In *Laser Microlithography*, pages 135–148. SPIE Vol. 922, 1988.

[28] B.Martin. 0.6 micron controlled optical lithography on a 0.35 NA g-line stepper using surface imaging and dry development by reactive ion etching. In *Proceedings of Microcircuit Engineering*, pages 197–200, 1989.

[29] R.M.Cogley. Measuring photoresist spectral response with a spectrosensitometer. In *Laser Microlithography*, pages 212–216, 1988.

[30] M.Ohta, T.Kojima, and C.Sato. The future of projection lenses and the new g-line lens for 0.7 micron lithography. In *Laser Microlithography*, pages 291–299. SPIE Vol. 922, 1988.

[31] S.G.Olson and J.H.Bruning. Routes to half-micron lithography. In *Laser Microlithography*, pages 300–308. SPIE Vol. 922, 1988.

[32] C.Lyons, D.Long, and S.Miura. i-line, 0.5 micron lithography with a 0.45 NA stepper and high performance resist. *Solid State Technology*, (11):95–100, 1990.

[33] J.D.Buckley. An advanced h-line stepper. *Solid State Technology*, (1):87–93, 1987.

[34] J.Greeneich and B.Katz. i-line stepper technology for 16 Mbit DRAMs. *Solid State Technology*, (3):63–68, 1990.

[35] G.Fuller. Optical lithography status. *Solid State Technology*, (9):113–118, 1987.

[36] B.Ruckle, P.Lockai, and H.Rosenkranz. Computerized wavelength stabilized 248.8 nm excimer laser for stepper. In *Laser Microlithography*, pages 450–453. SPIE Vol. 922, 1988.

[37] V.Pol. High resolution optical lithography: A deep ultraviolet laser-based wafer stepper. *Solid State Technology*, (1):71–76, 1987.

[38] T.A.Znotins, T.J.McKee, and S.L.Gutz. The design of excimer lasers for use in microlithography. In *Laser Microlithography*, pages 454–460. SPIE Vol. 922, 1988.

[39] D.J.Elliott and D.C.Ferranti. Sub-micron lithography at 248 nm and 193 nm excimer laser wavelengths. In *Laser Microlithography*, pages 476–482. SPIE Vol. 922, 1988.

[40] R.W.McCleary and P.J Tompkins. Performance of a KrF excimer laser stepper. In *Laser Microlithography*, pages 396–399. SPIE Vol. 922, 1988.

[41] H.Nakagawa, M.Sasago, and M.Endo. An advanced KrF stepper for production of 16Mbit DRAMs. In *Laser Microlithography*, pages 400–409. SPIE Vol. 922, 1988.

[42] D.A.Markle. The future and potential of optical scanning systems. *Solid State Technology*, (9):159–166, 1984.

[43] M.Rothschild and D.J.Ehrlich. Excimer projection lithography at 193 nm wavelength. In *Laser Microlithography*, pages 466–470. SPIE Vol. 922, 1988.

[44] D.Meyerhofer. Resolution and proximity effects in optical lithography. In *Laser Microlithography*, pages 174–187. SPIE Vol. 922, 1988.

[45] P.Trefonas, B.K.Daniels, and R.L.Fisher. Photoresist design for submicron optical lithography: Application of polyphotolysis. *Solid State Technology*, (8):131–137, 1987.

[46] F.P.Alvarez. Improved Novolak-based photoresist system for very large scale integration (VLSI) lithography. In *Micron and Submicron Integrated Metrology*, pages 152–161. SPIE Vol. 565, 1985.

[47] L.E.Stillwagon. Chromatography as a tool in the characterization and quality control of resist materials. *Solid State Technology*, (5):113–118, 1985.

[48] H.Sewell and I.Friedman. High resolution imagery: The matching of optical and resist systems in the mid-uv. In *Laser Microlithography*, pages 328–334. SPIE Vol. 922, 1988.

[49] K.Monahan, J.Hightower, and D.Bernard. In search of the ultimate photoresist. In *INTERFACE 86*, pages 17–28. Kodak Microelectronics Seminar, 1986.

[50] A.P.Weill, J.M.Francou, and J.P.Panabiere. Subhalfmicronic contact printing lithography using a microwave powered deep uv source. In *Laser Microlithography*, pages 236–240. SPIE Vol. 922, 1988.

[51] J.Austin, G.Keller, and G.Witting. A submicron optical lithography process. In *INTERFACE 86*, pages 95–105. Kodak Microelectronics Seminar, 1986.

[52] L.P.Mcdonnell, L.V.Gregor, and C.F.Lyons. Multilayer resist lithography: A perspective. In *INTERFACE 85*, pages 59–65. Kodak Microelectronics Seminar, 1985.

[53] K.Bartlett. A two-layer photoresist process in a production environment. In *Micron and Submicron Integrated Metrology*, pages 49–51. SPIE Vol. 565, 1985.

[54] A.Marsh. Printing sub-micron features beyond the normal optical resolution limit using a multi-level resist technique. In *Micron and Submicron Integrated Metrology*, pages 28–32. SPIE Vol. 565, 1985.

[55] P.R.West and B.F.Griffing. Contrast enhancement - a route to submicron optical lithography. In *Proc. SPIE*, volume 394, pages 33–38, 1983.

[56] M.C.King. The characterization of optical lithography. In *Microcircuit Engineering*, pages 239–265, 1980.

[57] J.D.Cuthbert. Optical projection printing. *Solid State Technology*, (8):59–69, 1977.

[58] R.S.Longhurst. *Geometrical and Physical Optics*, chapter 21. Longman, 1967.

[59] F.W.Sears, M.W.Zemansky, and H.D.Young. *University Physics*, chapter 22. Addison-Wesley, 1982.

[60] F.A.Jenkins and H.E.White. *Fundamentals of Optics*, chapter 14. McGraw-Hill, 1957.

[61] E.Hecht and A.Zajac. *Optics*, chapter 9. Addison-Wesley, 1974.

[62] F.Rodriguez, P.D.Krasicky, and R.J.Groele. Dissolution rate measurements. *Solid State Technology*, (5):125–131, 1985.

[63] V.Marriott. High resolution positive resist developers: A technique for functional evaluation and process optimization. In *Micron and Submicron Integrated Metrology*, pages 144–151. SPIE Vol. 565, 1985.

[64] W.Henke and G.Czech. Simulation of lithographic images and resist profiles. In *Proceedings of Microcircuit Engineering*, pages 629–633, 1989.

[65] B.J.Lin. The paths to subhalf-micrometer optical lithography. In *Laser Microlithography*, pages 256–269. SPIE Vol. 922, 1988.

[66] T.Ito, K.Kadota, and H.Fukuji. Submicrometer pattern correction for optical lithography. In *Laser Microlithography*, pages 9–17. SPIE Vol. 922, 1988.

[67] F.H.Dill, A.R.Neureuther, and J.A.Tuttle. Modeling projection printing of positive photoresists. *IEEE Transaction on Electron Devices*, ED-22(7):456–464, 1975.

[68] TMA Inc. *DEPICT: A 2-D Process Simulation Programme for Photolithography and Deposition*, 1987.

[69] R.Oldham. A general simulator for VLSI lithography and etching processes: Application to projection lithography. *IEEE Transactions on Electron Devices*, ED-26(4):717–722, 1979.

[70] A.R.Neureuther and W.G.Oldham. Resist modeling and profile simulation. *Solid State Technology*, (5):139–144, 1985.

[71] University of California, Berkley. *Using SAMPLE on a PC: User Guide*, February 1985.

[72] O.D.Crisalle, S.R.Keifling, and D.E.Seborg. A comparison of the optical projection lithography simulators in SAMPLE and PROLITH. Submitted for publication in IEEE Transactions on Semiconductor Manufacturing.

[73] SERC School on Microfabrication, Edinburgh Microfabrication Facility, University of Edinburgh. *Process Simulation*, June 1990.

[74] M.S.Yeung. Modeling aerial images in two and three dimensions. In *INTERFACE 85*, pages 115–126. Kodak Microelectronics Seminar, 1985.

[75] M.S.Yeung. Modeling high numerical aperture optical lithography. In *Optical/Laser Microlithography*, pages 149–167. SPIE Vol. 922, 1988.

[76] E.Kintner. Method for the calculation of partially coherent imagery. *Applied Optics*, 17(9):2747–2753, 1978.

[77] H.H.Hopkins. On the diffraction theory of optical images. In *Proceedings of the Royal Society*, pages 408–432, 1953.

[78] M.Born and E.Wolf. *Principles of Optics*, pages 491–555. Pergamon Press, 1984.

[79] S.Subramanian. Rapid calculation of defocused partially coherent images. *Applied Optics*, 20(5):1854–1857, 1981.

[80] P.H.Berning. *Physics of Thin Films*, pages 69–121. Academic Press, 1963.

[81] F.H.Dill. Optical lithography. *IEEE Transactions on Electron Devices*, ED-22(7):440–444, 1975.

[82] F.H.Dill, W.P.Hornberger, and P.S.Hauge. Characterization of positive photoresist. *IEEE Transaction on Electron Devices*, ED-22(7):445–445–452, 1975.

[83] D.J.Kim, W.G.Oldham, and A.R.Neureuther. Development of positive photoresist. *IEEE Transactions on Electron Devices*, ED-31(12), 1984.

[84] D.J.Kim, W.G.Oldham, and A.R.Neureuther. Characterization and modeling of a resist with a built-in induction effect. In *INTERFACE 83*. Kodak Microelectronics Seminar, 1983.

[85] C.A.Mack. Lumped parameter model of the photolithographic process. In *INTERFACE 86*, pages 228–238. Kodak Microelectronics Seminar, 1986.

[86] C.A.Mack. Development of positive photoresists. *Journal of the Electrochemical Society*, 134(1):148–152, 1987.

[87] C.A.Mack. PROLITH: A comprehensive optical lithography model. In *Optical Microlithography IV*, pages 207–220. SPIE Vol. 538, 1985.

[88] W.F.Cordes. The use of DRM methods to establish wafer fab procedures requiring dyed positive photoresists. In *Optical/Laser Microlithography*, pages 203–211. SPIE Vol. 922, 1988.

[89] S.Robertson. Modeling of positive photoresist and developer interactions. Technical report, Edinburgh Microfabrication Facility, University of Edinburgh, April 1990.

[90] S.A.Lis. Processing issues and solutions to conjugate lithography. In *INTERFACE 86*, pages 117–136. Kodak Microelectronics Seminar, 1986.

[91] G.Elmendorff, M.Staples, and T.Dejong. Process optimization using modified photoresist processing. In *INTERFACE 86*, pages 239–248. Kodak Microelectronics Seminar, 1986.

[92] J.Hughes and D.Fehrs. Reflective bleaching as a line width control technique. In *INTERFACE 86*, pages 209–248. Kodak Microelectronics Seminar, 1986.

[93] C.Flory and J.Valez. Critical dimension control for a positive photoresist process. In *INTERFACE 85*, pages 159–162. Kodak Microelectronics Seminar, 1985.

[94] L.Liauw, A.Murray, and M.Chen. Impact of wafer flatness on submicron optical lithography. In *Proc. SPIE*, volume 772, pages 232–238, 1987.

[95] L.Lauchlan, K.Sautter, and T.Batchelder. Automatic process control for VLSI linewidth. *Solid State Technology*, (4):333–337, 1985.

Chapter 3

Metrology

3.1 Introduction

As circuit geometries approach the wavelength of visible light, semiconductor metrology is challenged to provide critical dimension measurements of wafers. [1] Ideally, measurements of CD made during processing should be fast and automatic, while at the same time giving precise and reliable results. In reality, differences in linewidth measurement often exist between different types of linewidth measurement systems, between different systems of the same type, between different operators on the same system, and between measurements made by the same operator at different times of the day. [2]

The two factors which govern the reliability of linewidth measurements are repeatability and accuracy.[3] Repeatability is determined by the variance between measurements made from day to day, and from machine to machine. Accuracy is how the measurement obtained correlates to an absolute (or "accurate") measurement.[4] For example, a line may be measured repeatedly at $1 \pm 0.02\mu$m day after day, but the line may actually be 1.5μm. These measurements have a good repeatability but poor accuracy.

The choice of measurement tool depends on its function within the process:

1. Characterization of the tool/process [5]

2. In-situ measurements for control of equipment and processes

3. Product measurements

The first of these demands high accuracy; the second and third focus on repeatable results. The most economic way of controlling a lithography system is to provide the in-situ measurements and control capability. [6] Therefore most manufacturers in the semiconductor industry are more concerned with repeatability than accuracy when making linewidth measurements. [7] [8] A line edge specimen which has proven to work well in the process may be used to calibrate all the in-house instruments to the same arbitrary value. [9]

3.1.1 CD Measurement

There are three different types of linewidth measurement systems currently available: optical, electrical and based on a scanning electron beam (SEM). Optical techniques are currently accurate down to about 1μm feature size, although it is predicted that confocal and coherent imaging techniques will become increasingly important in the range $0.5 - 1\mu$m. [10][11] As CDs drop below 0.5μm, the large depth of focus, small sample width and inherently high resolution of SEM beams will become increasingly necessary, particularly if the measurements can be made at low beam energy to avoid radiation damage.[12] Electrical probing methods are a viable alternative in this range, and are particularly suited to mapping linewidth uniformity due to the speed of the measurements.[13] [14] However, this technique, as with the others, has limitations which will be discussed in the following sections.

This first half of this chapter reviews the various techniques for measuring linewidth, and discusses the sources of error common to each type of measurement system.[15] The second half of the chapter introduces the metrology tools used in the Edinburgh Microfabrication Facility (EMF). It describes the tests carried out to assess the capabilities of the Vickers "Quaestor" optical system and the "Nanolab" SEM in terms of accuracy and repeatability. The final section describes the correlation of the Quaestor with the Prometrix "Lithomap" (LM20) which is based on the electrical probing of sheet resistance. The Lithomap is at the heart of the metrology system at Plessey Semiconductors, Roborough. Their cooperation in allowing test wafers to be probed on the Lithomap was greatly appreciated.

3.2 Optical Techniques

3.2.1 Determination of Threshold

SEM and optical metrology have one problem in common, and that is, there is no universal definition of the meaning of the term "linewidth". One problem with defining the measurement location has already been encountered in Chapter 2 as a result of standing wave patterns in the resist sidewall. Another difficulty arises due to sidewall angles. An idealised resist image (Fig. 3–1c) has vertical sidewalls, and it does not matter whether the measurement is made at the top or bottom of the image. However, profiles may be positively sloped (Fig. 3–1a) or undercut (Fig. 3–1b) in which case the linewidth measurement depends on which edge is chosen [16]

Both optical and SEM linewidth measurements are made via a line profile which is generated due to the interaction of the probe beam with the sample.[17] As shown in Fig. 3–2, even with an ideal vertical material edge the optical image contains a gradual transition from light to dark at the line edge due to diffraction. [18][19] This diffraction results in a dark or fuzzy region at the line edge, which makes it difficult to determine where the line actually is.[20]

An optical threshold technique is used to overcome this problem. The profile is analysed by algorithms to determine the line edge.[21] The most common algorithm is the single threshold method, in which linewidth is defined as the distance across the signal when cut at a given percentage of the maximum signal. [22]

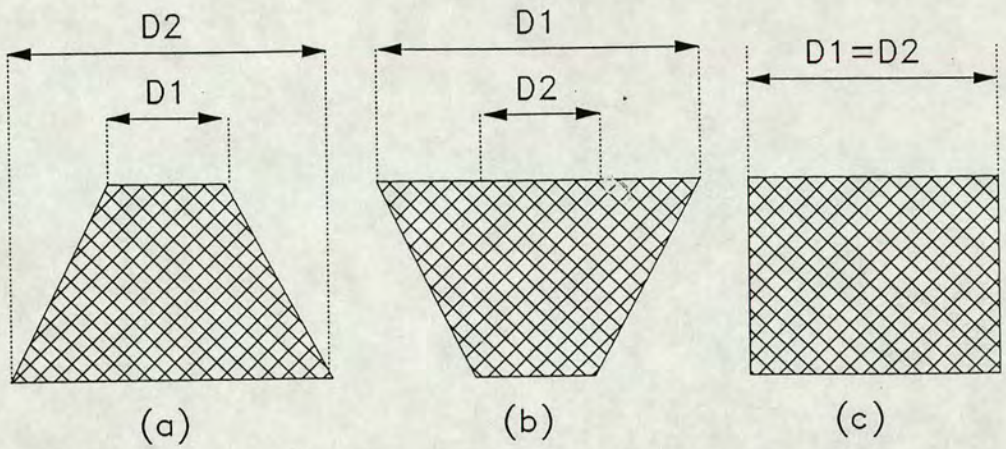

Figure 3–1: Line Structure Viewed in Cross Section. (a) Upper Width D1 is Smaller than the Base Width D2; (b) Undercut Structure where D1 is Larger than D2; (c) Structure with Vertical Sidewalls where D1 and D2 are Approximately Equal [16]

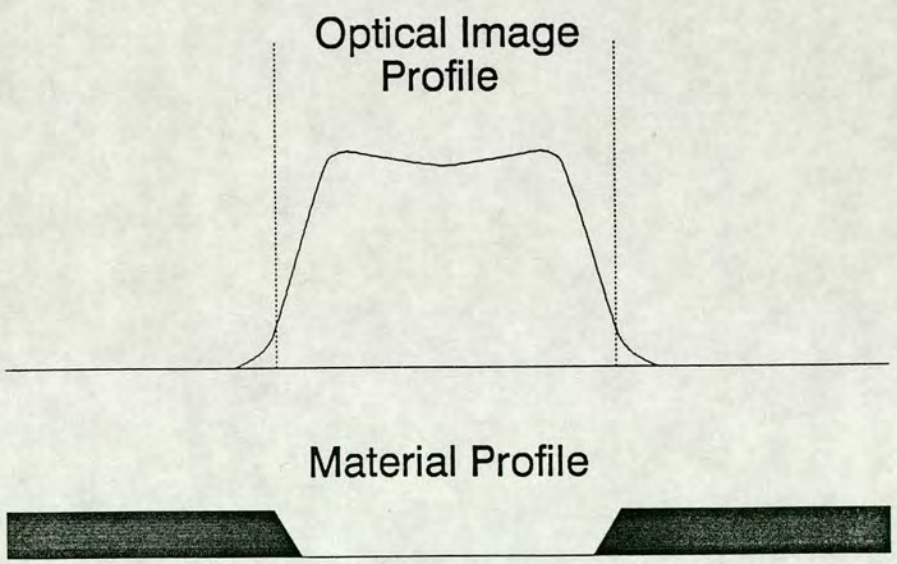

Figure 3–2: Sloping Sidewalls on the Sample Profile Create Sloping Sidewalls on the Image Profile, Resulting in the Need for Threshold Determination Techniques [18]

3.2.2 Measurement Systems

The majority of optical linewidth measurements in use are based on optical microscopy, [23][24] using the microscope as the basic building block to which any one of a variety of measurement attachments may be added. [25]

Filar Eyepiece

The oldest of the linewidth attachments is the filar or micrometer eyepiece. The filar technique is relatively inexpensive, but it is limited in terms of precision and flexibility. Typical filar eyepieces show a precision or repeatability of $\pm 0.2\mu$m. [18]

Image-Shearing

The superiority of image-splitting techniques to a filar eyepiece has been recognized by the IC industry for a number of years.[26] The improvement in precision achieved with an image-splitting eyepiece is principally due to the use of a more repeatable edge-detection criterion, corresponding to the use of a 50% optical threshold.

Vickers Instruments have developed an optical technique "Shearscan" based on image shearing. Two identical images of a feature are superimposed, but the outer sections of one image and the centre section of the other are suppressed. This creates one complete image. By shearing the centre image through its full width, the line on one side of the image aligns with the line on the opposite side of the second image, resulting in a measurement of the structure. Vickers claim a precision of 0.01μm on 2μm linewidths, although some operator judgement to determine the line edge is needed. [27]

Image-shearing offers high precision and low cost, but it requires manual operation.[28]

Scanning Slit

In an image scanning system, the visual eyepiece is replaced with a magnifying relay lens which projects the image onto a scanning slit. [29] Either the scanning

slit may be moved across the image or the sample moved while the scanning slit remains fixed. A scanning slit system basically consists of a microscope, a photomultiplier tube, a mechanically moved slit (about 1μm wide) and appropriate support electronics (Fig. 3–3). This system has the advantage over image-shearing in that it is possible to vary the edge detection threshold to accommodate differing materials, thereby reducing systematic errors. The slit scan technique may have some vibrational problems, but is cost effective and precise. [30]

Video Scan

Video scanning systems use a video camera which captures and stores the profile of the structure to be measured. This data is then utilised as the basis for the dimensional measurement.

A video scanning optical measurement system is typically composed of a microscope, a video camera, data analysis electronics, monitor and wafer handling capabilities [31] (See Fig. 3–4).

The main advantages of video systems are their higher throughput and increased flexibility. Video systems are frequently added to linewidth measurement systems because of the greater operator comfort associated with viewing a TV monitor for many hours as compared to looking through a microscope.[32] A video system does not however improve the quality of the measurement system, since degradation usually occurs. Problems are encountered on very small geometries, because current photoprocessing does not define them as acutely as it does larger geometries. It is generally accepted that this type of system can measure down to about 1μm with sufficient accuracy, although manufacturers claim they can go lower, often down to 0.5μm. [33]

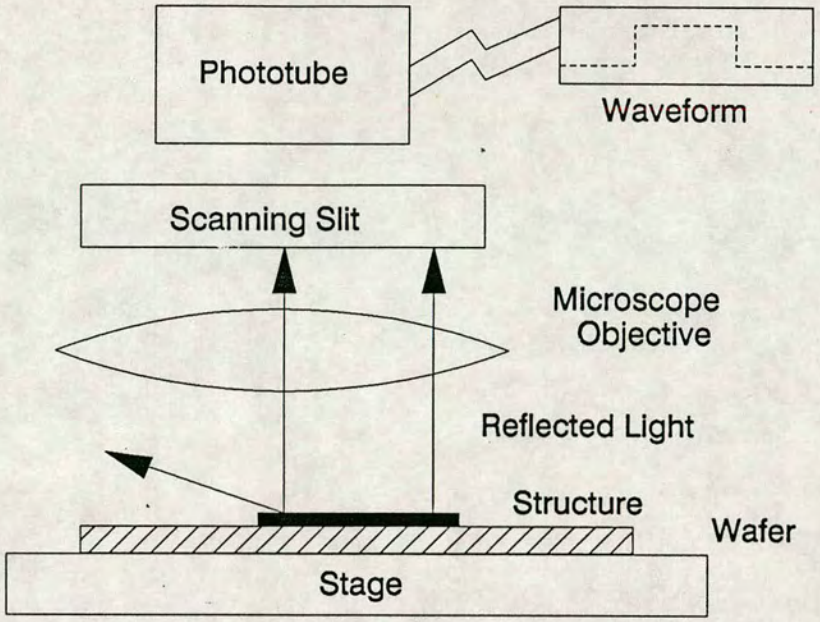

Figure 3–3: A Scanning Slit System [33]

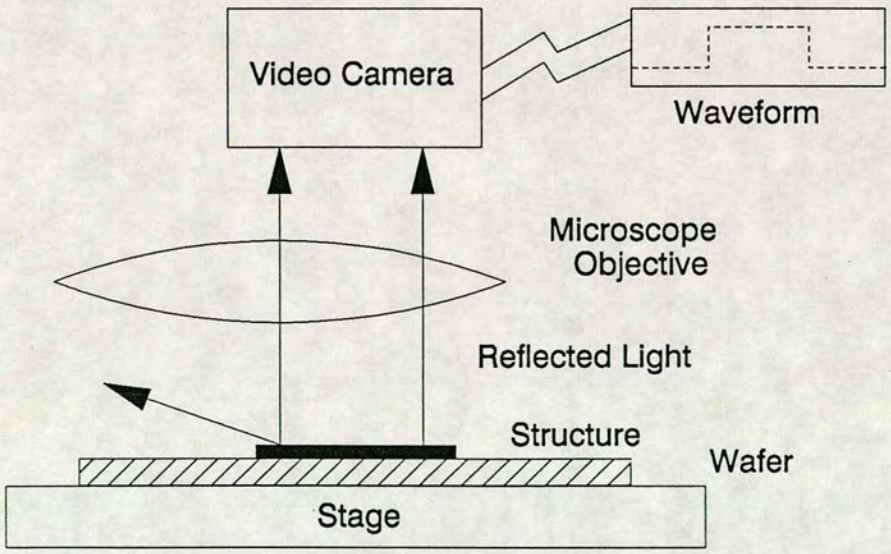

Figure 3–4: A Video Scan System [70]

Scanning Laser

In addition to video and slit scanning techniques, several other procedures have been developed that are capable of measuring linewidths on today's devices.[34][35] The scanning laser system (Fig. 3–5) combines an edge detection unit that determines pattern edges by directly scanning them with a precisely focused laser beam, a high resolution laser interferometer that can measure the travel of the laser beam spot between pattern edges, a programable image rotator and computer analysis of edge detection signals. Laser interferometric systems have very high precision but are also high in cost.

3.3 Scanning Electron Microscope

The capabilities of the optical based systems are limited by the resolution of the microscope as well as by the wavelength of light itself. Although new optical techniques are being developed that can push the optical limit down to the range of 0.3μm [33] it is predicted that the industry will eventually have to turn to scanning electron microscopes for linewidth measurement applications.[36] Among the advantages provided by the SEM for CD control are: [37][16]

- Very high resolution. When using the SEM for non-destructive wafer inspection (up to 2 keV accelerating voltage) the typical resolution is of the order of 20 nm (0.02μm). This provides improvement by a factor of at least 30 over optical resolution. Linewidth measurement accuracy is therefore increased for use well below sub-micron levels.

- High depth of focus. The SEM is not governed by the equation limitation that applies to optical depth of field (Δs) [38]

$$\Delta s = \pm \frac{\lambda}{2(NA)^2} \tag{3.1}$$

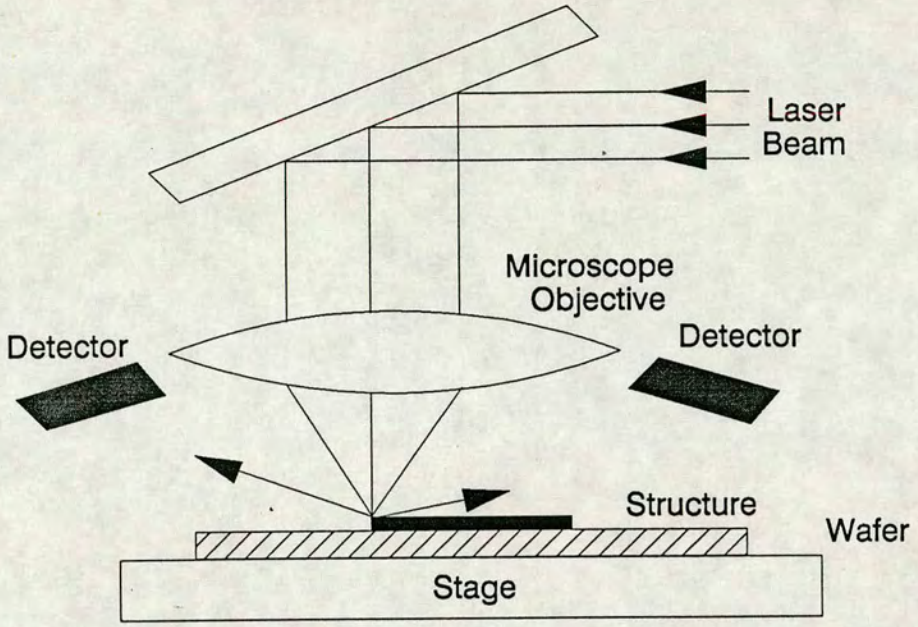

Figure 3–5: A Scanning Laser System [33]

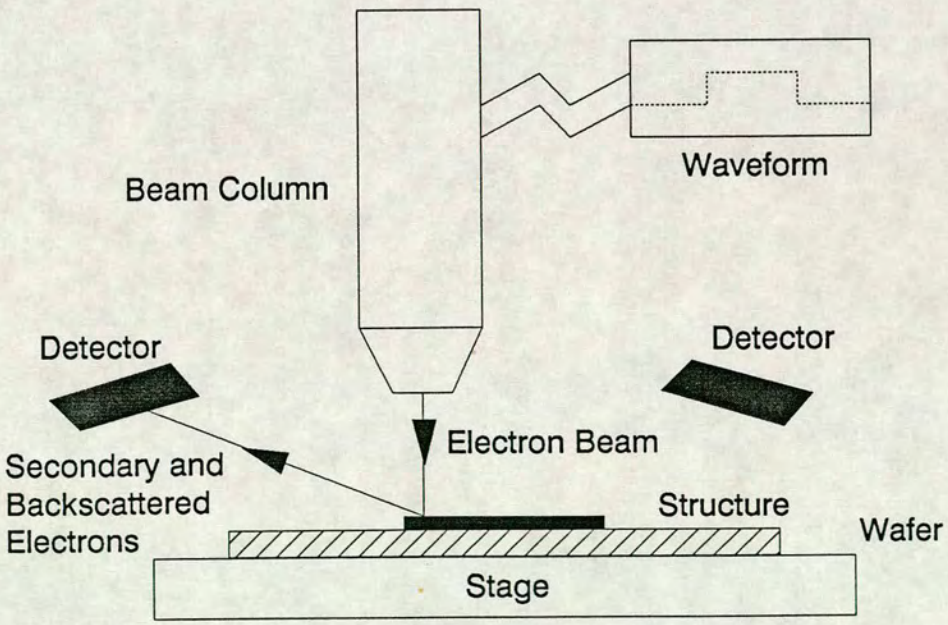

Figure 3–6: A Scanning Electron Microscope [33]

> By contrast, the SEM provides depth of field of the order of several tens of microns. This permits the inspection and measurement of tilted samples while maintaining focus over the entire field of view.[39]

An SEM operates by scanning a single electron beam across the surface of the object under observation.[40] Secondary and backscattered electrons are produced by this beam and sensed by a detector above the surface. The degree and intensity of the backscattered electrons indicates the geometry being bombarded.[41] This information is processed as a video signal, producing the image on a display screen. Since a video image already exists, it is a relatively simple matter to add electronics to allow CD measurement. Measurements are made by linear regression or threshold analysis of the secondary electron profiles. Thresholds are normally set at 50%, approximately corresponding to a maximum in the absolute first derivative of the secondary electron profile and a minimum in its sensitivity to defocus [42].

SEMs have not been widely employed in production processes to date, due to their relatively low throughput. More recently, dedicated SEM linewidth measurement systems have been developed featuring a higher throughput than research systems.[42] Concerns about damage to sensitive devices due to electron irradiation have kindled significant interest in low voltage SEMs.[43] In order to nondestructively measure a silicon wafer, the voltage of the accelerated electron beam must be around 1 to 2 keV.[44]

SEMs offer higher resolution than optical systems, but are more complicated to maintain and operate, and much more expensive to buy. [45] As repeatable as the SEM appears to be, it does not guarantee accurate measurements. On the contrary, there appear to be as many sources of error in obtaining accurate linewidth measurements using SEMs as with optical based systems.[46][47] These sources of error will be discussed in Section 3.5.

3.4 Electrical Techniques

Linewidth measurements may also be made using an electrical probe. This technique relies on the proportionality of the width W of a line defined in a conducting film, to its electrical conductance G [48]

$$W = \rho LG \tag{3.2}$$

The constant of proportionality is the product of the known length of the line L, and the sheet resistance of the film ρ. If these values are measured, the width can then be calculated.[49]

Sheet resistance (R_s) is measured using a van der Pauw resistor (also known as a Greek Cross) [50]

$$R_s = \frac{\pi}{ln2}\left(\frac{R_{34,12} + R_{13,24}}{2}\right) \tag{3.3}$$

where the resistance values are defined by $R_{34,12} = \frac{V_{34}}{I_{12}}$ and $R_{13,24} = \frac{V_{13}}{I_{24}}$, the subscripts denoting the test pad numbers as shown in Fig. 3–7

The most commonly used test structure for determining linewidth electrically combines a van der Pauw resistor with a bridge structure (See Fig. 3–8) [51] [52]

The width of the bridge structure *(W)* is calculated from measurements of its resistance (R') along with knowledge of the length between the voltage taps *(L)* and the sheet resistance (R_s) obtained from the van der Pauw structure [53]

$$W = \frac{R_s L}{R'} \tag{3.4}$$

This technique is mainly used for linewidth uniformity mapping, since the measurements can be made very quickly using standard probing techniques.[54][55] Tests have shown that electrical width measurements are sensitive to width changes of $\pm 0.1\mu$m. [56] A conducting film is required however, so the probing may only be done on metal or polysilicon layers. [57]

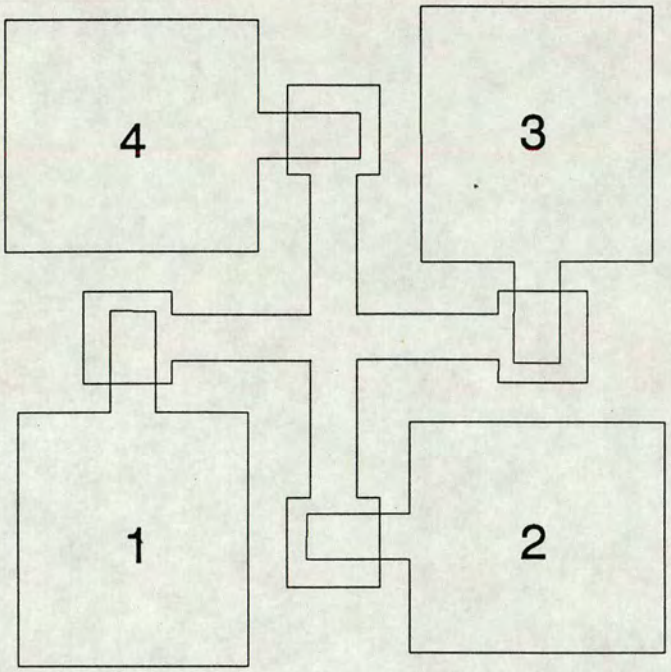

Figure 3–7: A van der Pauw Resistor [51]

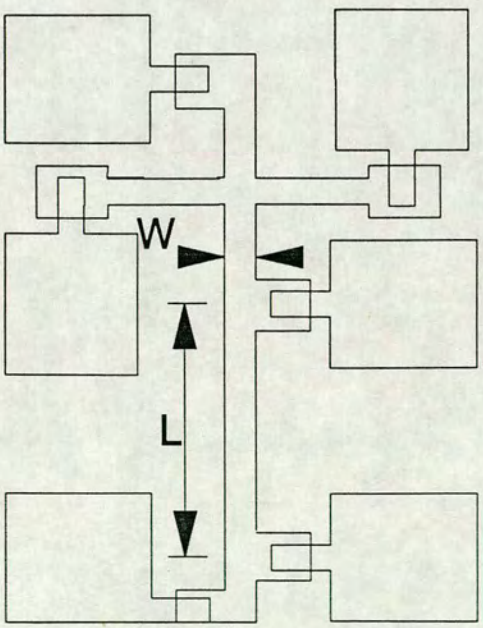

Figure 3–8: A Crossbridge Sheet Resistor Test Structure [51]

3.5 Reliability

3.5.1 Error Sources

There are a number of factors which can affect the reliability and accuracy of a linewidth measurement. This is true for both optical and SEM based systems, although the factors are very different in each case. [58]

With SEMs, for example, the image can be affected by operating parameters such as accelerating beam voltage, scan speed and tilt. In addition, surface charging can occur, being most severe at beam energies greater than 3 keV, resulting in image distortion or even damage to the IC.

In optical systems errors in linewidth values can originate from:

1. The properties of the microscope, including contrast and resolution of the optics, type of illumination and method of determining focus [59]

2. The way in which the measurement is made from the image produced by the optics [60]

3. The way in which the structure reflects the incident light. [61]

With optical systems in general, the structure is not measured directly, but an optical image of that structure. Therefore the quality of the optical system is very important. The characteristics of the optical image are determined by diffraction, stray light, aberrations in the optics, focus position, spectral bandwidth of the illumination, and the coherence parameter σ, which is defined as the ratio of illumination to objective numerical aperture (NA) [18]. These factors are generally well understood and can be compensated for.

The second source of problems in obtaining an accurate and repeatable measurement is dependent on the way in which the measurement is made from the optical image. [62] [63] For example, most systems allow the user to select the

threshold level at which the measurement is to be made. This requires the user to know at what level the most accurate measurement can be found, which is dependent on film type and thickness. [64]

The third and most complex source of repeatability problems in optical systems is the wide variety of indexes of refraction of patterned layers and sublayers, and the thickness of these layers. [65] Both of these parameters have a direct effect on the quality of the reflected light, and therefore on the image. [66]

3.5.2 Photoresist

The measurement of resist features presents a particular problem for most CD systems.[67] Photoresist is a transparent material, and the edges of the features are hard to define, especially on a highly reflective substrate such as metal. [68] The profile step height can reach values of over 1μm, which makes it difficult for optical systems to keep the entire profile in focus.[69] Since photoresist is a non-conducting material, electrical probe techniques cannot be applied. Measurement of resist structures using optical techniques showed such poor correlation with those performed on the features after etching, that metrology engineers at some wafer fabrication plants have concluded that they cannot rely on their CD measurement systems for accurate measurements of resist dimensions. (See Fig. 3–9). This leaves them with no apriori means of predicting etch dimensions. [70] Further research into improving existing CD measurement systems is obviously required.[71][72] However research to develop new alternative techniques capable of overcoming the problems posed by resist features must also be initiated.[73]

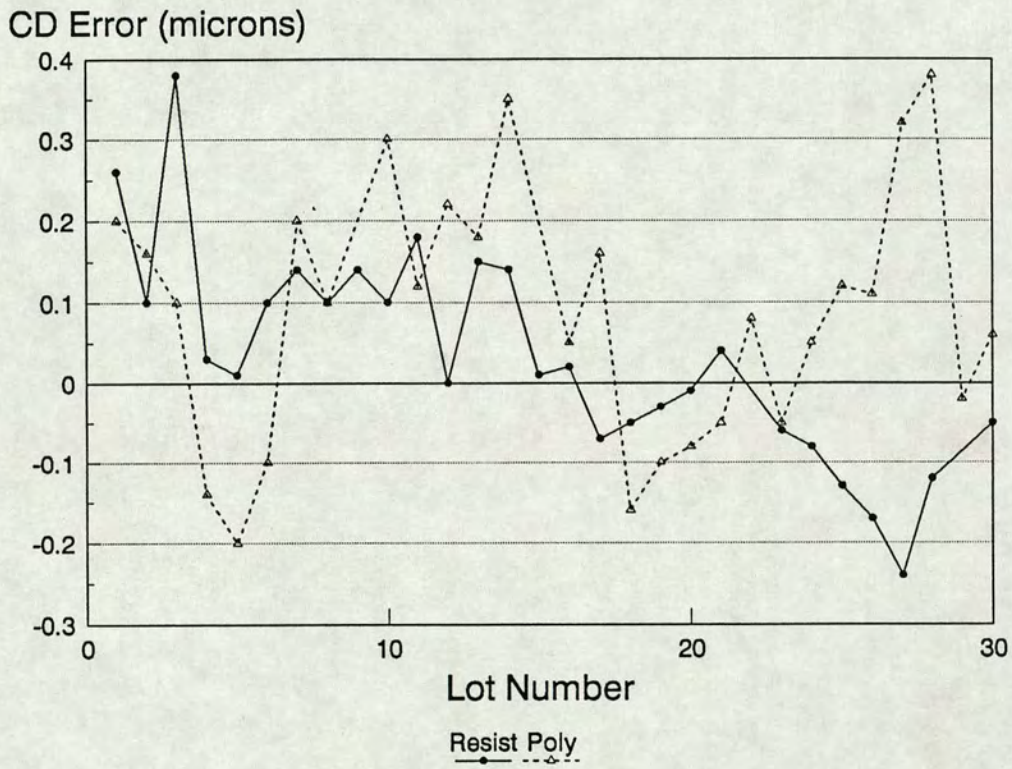

Figure 3–9: Errors in CD Measurement [33]

3.6 Linewidth Measurements at the EMF

Linewidth measurements at the Edinburgh Microfabrication Facility are presently carried out using each of the the three main techniques: optically, electrically and using a scanning electron microscope. [74] Optical measurements are carried out using a Vickers shearing microscope and a Quaestor automatic CD measurement system. The shearing microscope has no wafer handling capabilities and is therefore only suitable for taking a few spot checks of dimensions across a wafer. For a more comprehensive measurement of linewidth uniformity an automatic wafer mapping system is required. This need is fulfilled by the Quaestor.

The Quaestor's measurements are calibrated to an SEM. The SEM is a low voltage Nanolab Model D 3006 manufactured by Vickers.

The electrical test system is currently being upgraded. It is based on an HP 4062B Parametric Test System and will eventually use "Prometrix" type structures to measure and map linewidth uniformity (see Section 3.7). Since this system was not yet operative, the Prometrix "Lithomap" LM20 electrical probe system belonging to Plessey Semiconductors was used for experimental purposes. This instrument is described in the following section.

3.6.1 Nanolab SEM

The Nanolab D3006 is a scanning electron microscope designed by Vickers for non-destructive inspection and CD measurement of production wafers and masks. [75] The source is a single crystal lanthanum hexaboride (LaB_6) electron emitter which offers high image brightness, good resolution and long life compared to the more commonly used tungsten cathode. The specimen stage is fully automated, and can be rotated and tilted up to forty-five degrees from the horizontal.

By adding the Nanolab CD100F critical dimension measuring system to the D3006 instrument, a repeatability of better than 0.01μm (1 sigma) or one per cent of the line measured (whichever is greater) is claimed by the manufacturers.

The key to repeatability and transferability of the system lies in a semi-automatic calibration routine which refers the scanning of the beam to a built-in diffraction grating. The grating is mounted at the edge of the chuck in the same plane as the wafer and may be accessed at any time. The pitch of the grating is 833 nm and the system is calibrated against three pitches or 2.5μm, the operation taking about one minute to complete.

The CD100F is operated completely independently of all SEM parameters, including accelerating voltage, lens current, working distance and magnification. Because of this independence, these factors do not affect measurement accuracy when the CD100F is used. All measurements are performed automatically and programmable threshold settings, automatic scan alignment and automatic calibration reduce operator error. There is however, no automatic focusing system, and therefore some operator subjectivity is introduced.

3.6.2 Nanolab Repeatability Tests

Since the Nanolab is used as the calibration standard for the EMF, it is important to assess the repeatability of its CD measurement system. The stability and reproducibility were investigated by carrying out repeated measurements on two sample wafers, one having a resist pattern on 4000 A of polysilicon, the other having a resist pattern on 5200 A oxide. The resist was Hunt HPR204 spun at 6000 rpm, printed with an exposure matrix on an Optimetrix 10X stepper (436 nm, NA = 0.32) and track developed in Hunt HPRD428 using a spray-puddle process.

Resist on Polysilicon

Day-to-day stability is shown by measurements of a nominal 1.5μm line on consecutive days, without re-calibration and then after recalibration using the reference grating. (See Fig. 3–10).

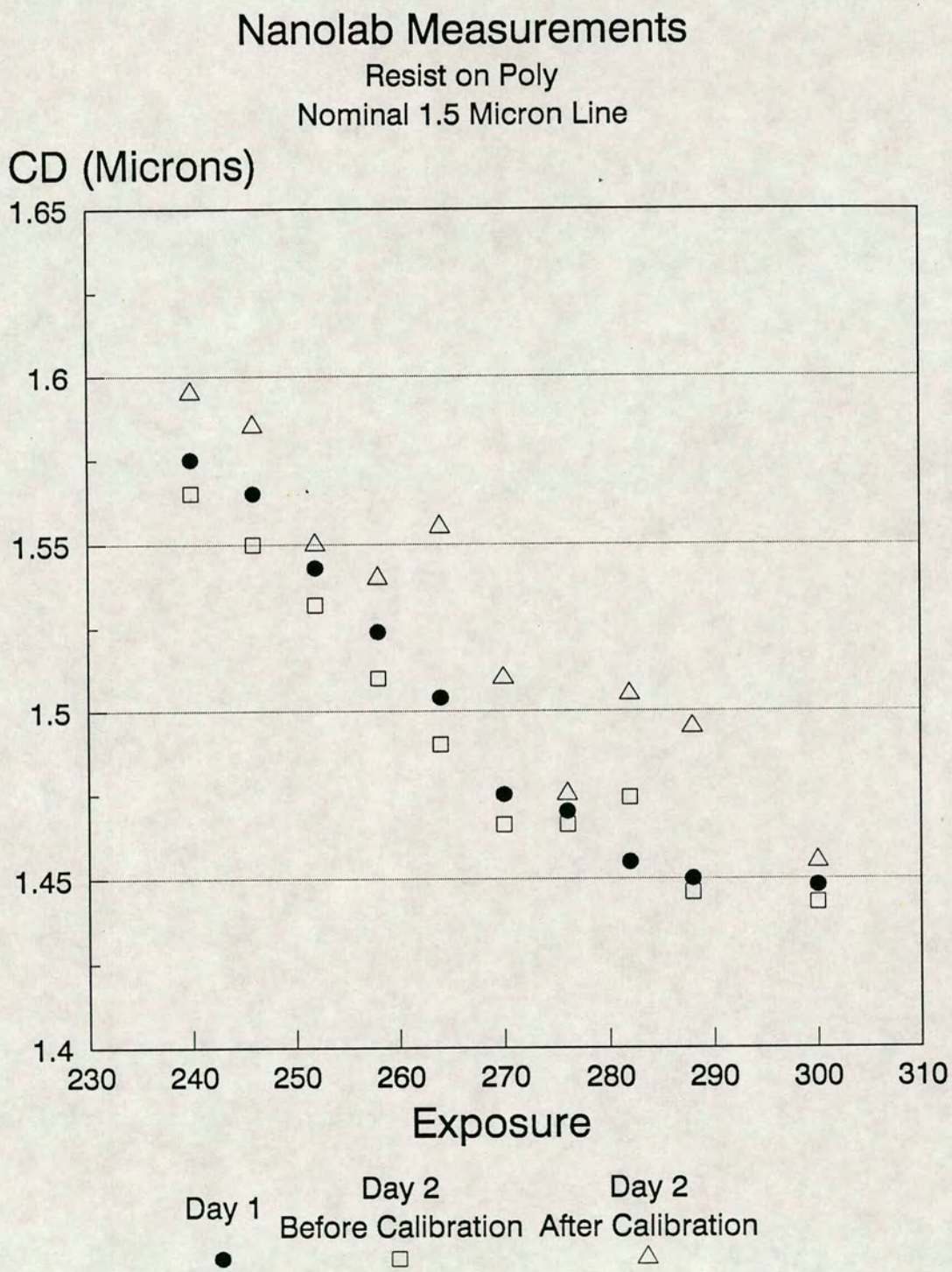

Figure 3–10: Nanolab Measurements of Resist on Polysilicon

Resist on Oxide

Surface charging on oxide is a major problem. Measurement of resist images on oxide requires considerable operator skill, judgement and patience. The above measurements were repeated on a nominal 1μm line, with different threshold algorithms. The results are shown in Fig. 3–11.

Results

1. The CD system can meet its specifications when measuring resist images on a conducting layer such as polysilicon.

2. Measurement of resist images on oxide is more problematic. There are many variables to be optimised, especially focus, and these have a direct bearing on the repeatability of results. Initial experience indicates a repeatability of about 20 nm, 1 sigma, when measuring resist lines on oxide.

3.6.3 Quaestor

The Quaestor CD07A is a critical dimension and registration measurement system designed by Vickers Instruments. [76] Wafer handling and feature measurement may be carried out fully automatically or placed under manual control. A visual inspection facility allows the quality of the wafers to be assessed and defect types to be logged.

Measurements are made using a video scan of the intensity profile. A "Shearscan" technique as described in the previous section is normally applied to the profile to determine CD. The operator specifies the measurement technique and optical threshold to give the most accurate results for the particular profile.

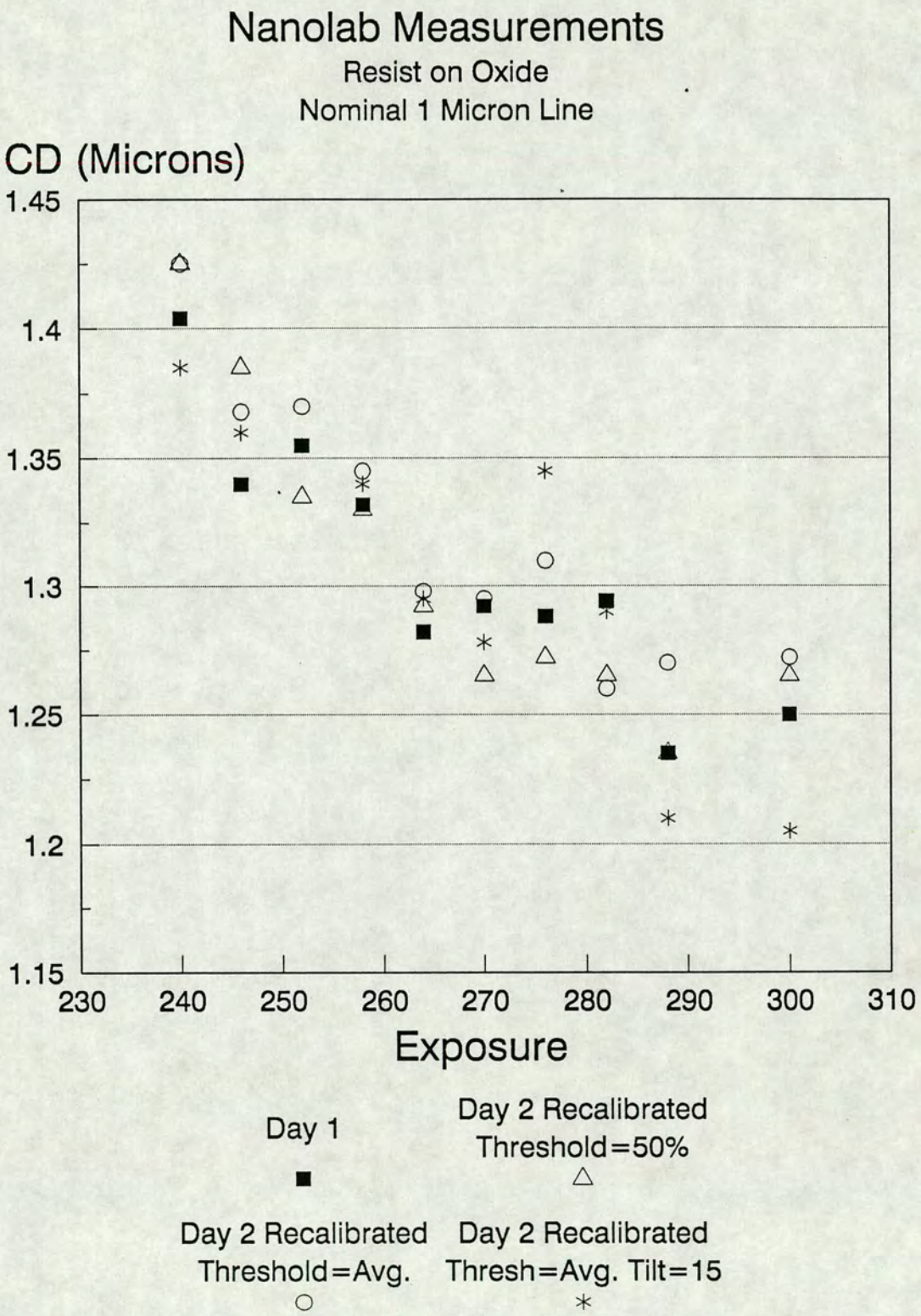

Figure 3–11: Nanolab Measurements of Resist on Oxide

The Quaestor uses pattern recognition to find and measure pre-selected features on the wafer. Feature location is taught during the measurement set up on the sample wafer, where precise X,Y positions are automatically stored. Pattern recognition steps are built into the program at each location to ensure that the correct feature has been found. Pattern recognition functions by correlating real-time images of the wafer with reference images logged in frame store.

Quaestor is programmed, at the engineer level, using a hierarchical menu structure which allows full set-up of system conditions, wafer handling, measurement sequences and results logging. Engineer written programs may be run by operators without requiring further access to the engineer programing facilities. Results may be downloaded to a host computer via a SECS II interface.

3.6.4 Quaestor/Nanolab Correlation

Very narrow resist lines can be produced by double exposure of a light field reticle with a sideways shift between exposures. For this experiment a pattern was printed in resist over 0.4 μm of polysilicon by double exposure. The resist was HPR204 spun at 6000 rpm and tank-developed for 60 seconds at 25 degrees Centigrade in AZ351 diluted 3.5:1. The unexposed resist thickness after development was 1.1 μm.

Quaestor measurements were recorded using the "Outside" technique with a 50% threshold, the measurements being averaged over 8 repeats per site. (See Fig. 3–12). An offset of +0.3 μm was introduced into Quaestor's automatic focus routine for a repeat of the measurements. Subsequently the experiment was repeated with a focus offset of -0.3μm. The results can be seen in Fig. 3–13.

The graph of Nanolab/Quaestor measurements shows a linear correlation between the two systems for all lines except those in the region 0.4 - 0.8 μm. Within this region, the Quaestor focus offsets create a wide spread in results. In the linear region of the graph, the spread of results due to the focus offset is much smaller.

This effect is shown in Fig. 3–14 which expresses the spread of Quaestor measurements (ΔQ) due to the $\pm 0.3\mu$m focus shift as a percentage $\frac{\Delta Q}{Q_0}$.

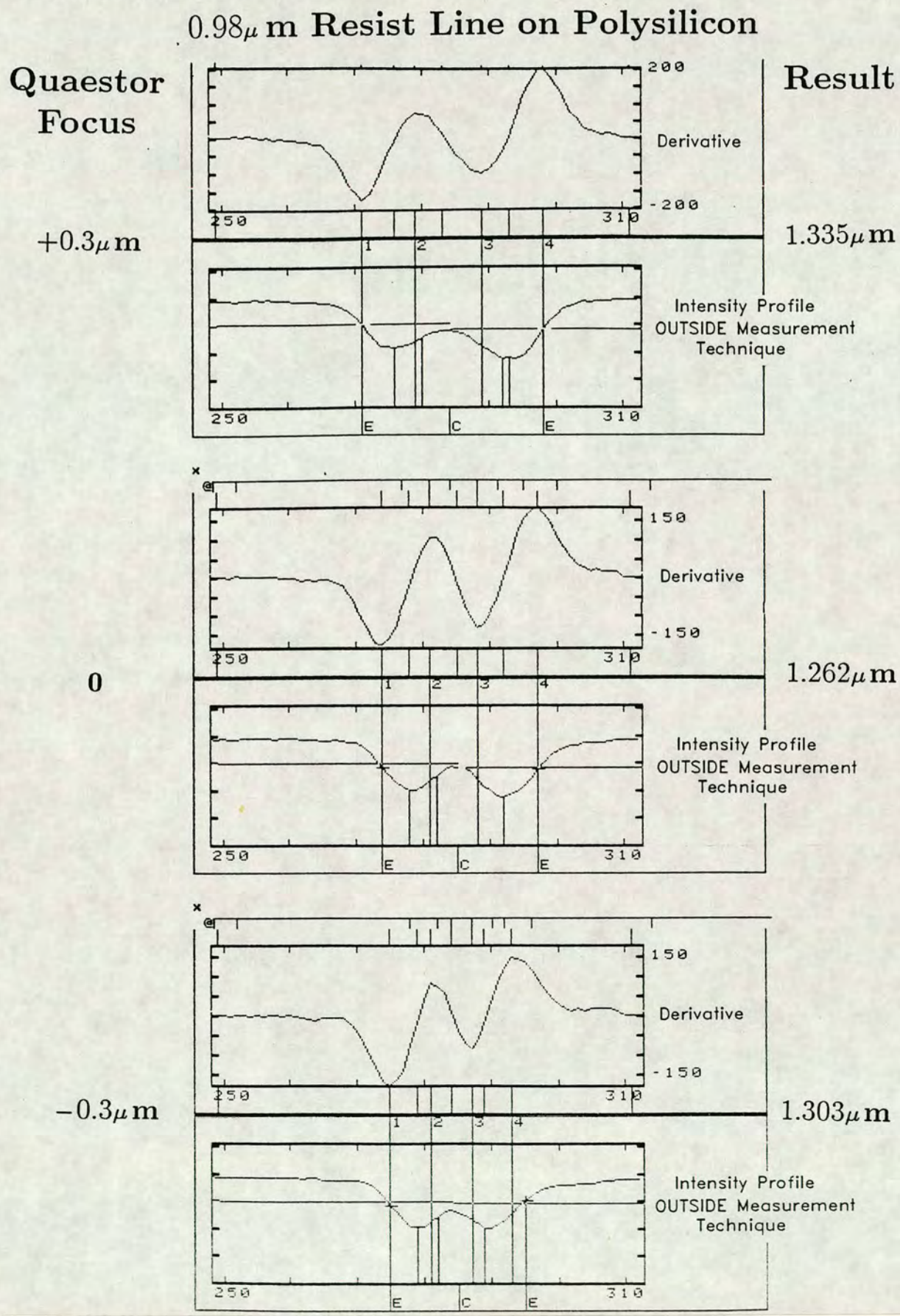

Figure 3–12: Quaestor Intensity and Derivative Profiles for Three Different Focus Settings. 0.98μm Resist Line on Polysilicon Measured Using the OUTSIDE Measurement Technique with a 50% Threshold [84]

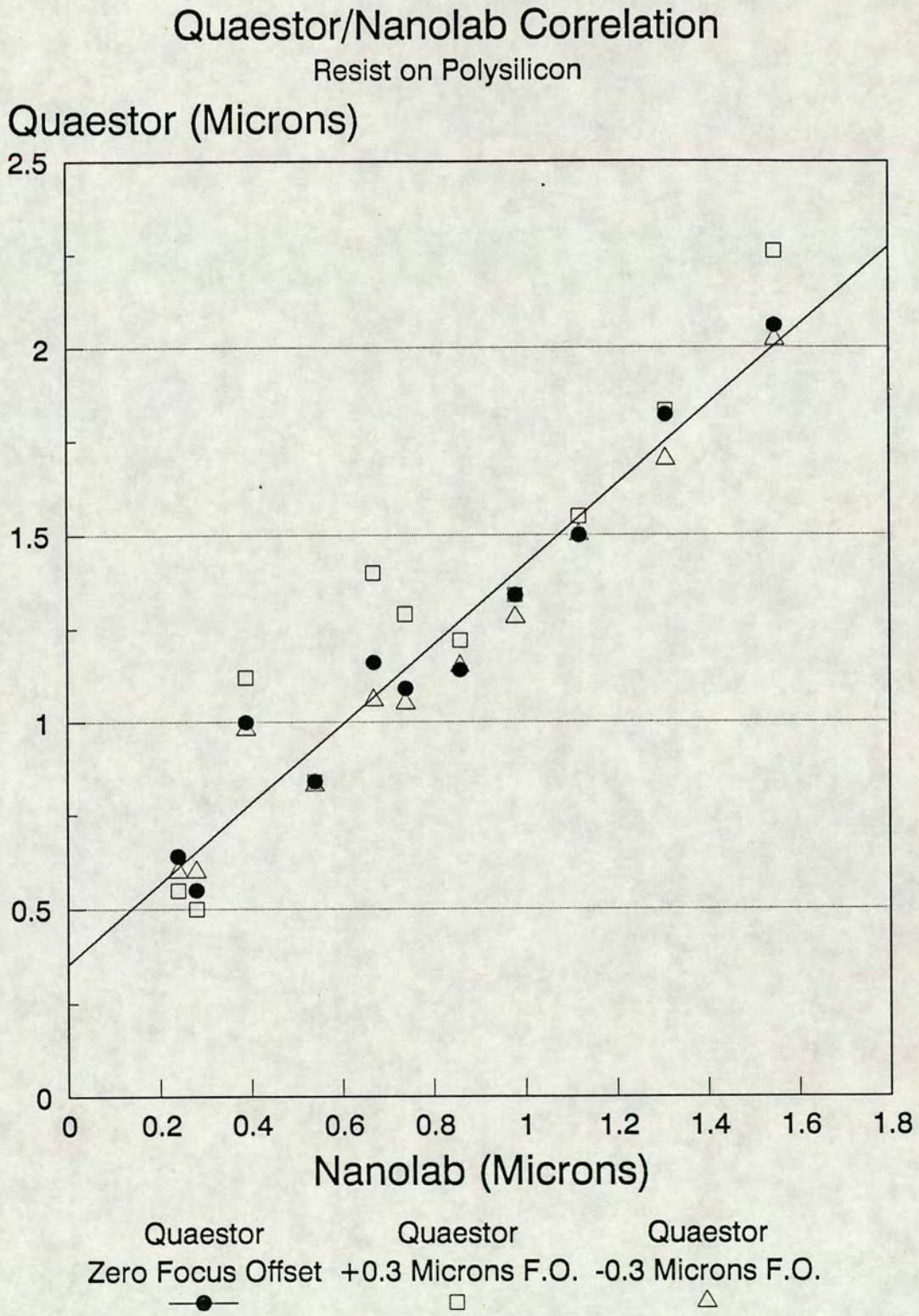

Figure 3–13: Quaestor/Nanolab Correlation of Linewidth Dimensions. Quaestor Measurements Taken Three Times: First with a Zero Focus Offset, Secondly with a Focus Offset of $+0.3\mu$m and Finally with an Offset of -0.3μm

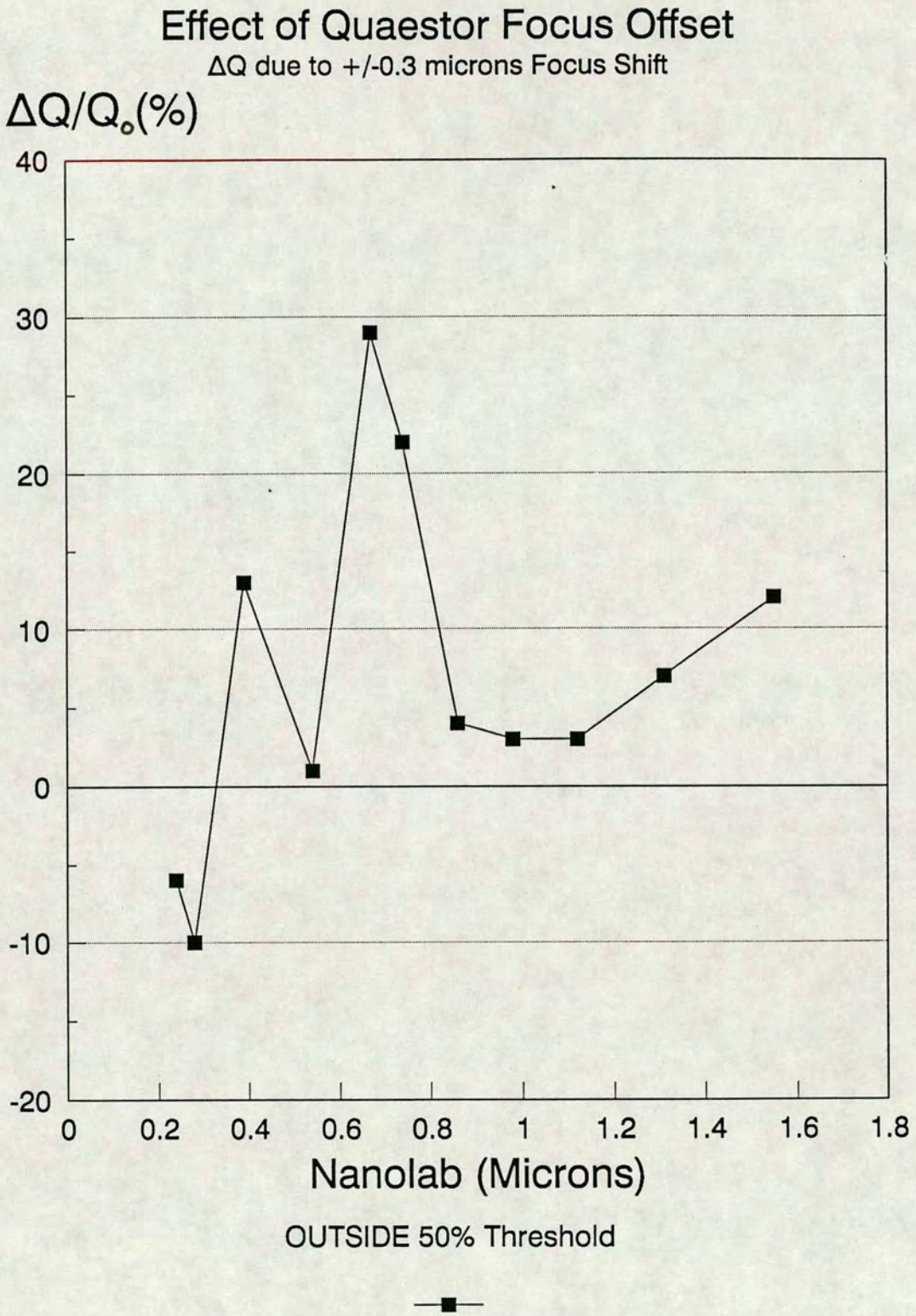

$$\frac{\Delta Q}{Q_0} = \frac{Q_{+0.3} - Q_{-0.3}}{Q_0}$$

where $Q_{+0.3}$ = Quaestor measurements with $+0.3\mu$m focus offset;

$Q_{-0.3}$ = Quaestor measurements with -0.3μm focus offset;

Q_0 = Quaestor measurements with 0 focus offset.

Figure 3–14: Effect of Quaestor Focus Offset

The data is plotted against the Nanolab measurements.

$$\frac{\Delta Q}{Q_0} = \frac{Q_{+0.3} - Q_{-0.3}}{Q_0} \tag{3.5}$$

where $Q_{+0.3}$ = Quaestor measurements with $+0.3\mu$m focus offset;

$Q_{-0.3}$ = Quaestor measurements with -0.3μm focus offset;

Q_0 = Quaestor measurements with 0 focus offset.

This graph has a peak value for the 0.67μm linewidth, as measured by Nanolab. This line was remeasured on Quaestor with a range of focus offsets. Fig. 3–15 confirms there is a strong linear relationship between focus and Quaestor measurements for this particular linewidth. Fig.3–16 shows that this relationship does not hold strongly for other linewidth dimensions.

It transpired that this effect was an anomaly of the Quaestor autofocus routine and was not related to any physical properties of the resist profiles. When the manufacturers became aware of this measurement aberration, it was eradicated from subsequent versions of the system software.

3.7 The Plessey Metrology System

Working in collaboration with Plessey Semiconductors it was decided that it would be useful to compare their standard linewidth measurement system with that of the EMF.

Fab 3 at Roborough near Plymouth, was opened in November 1986 at a cost of £50 million, processing six inch wafers of two micron CMOS chips. Over 70% of Plessey semiconductors are exported as application-specific devices made for commercial, professional and defence markets. The fabrication process from raw

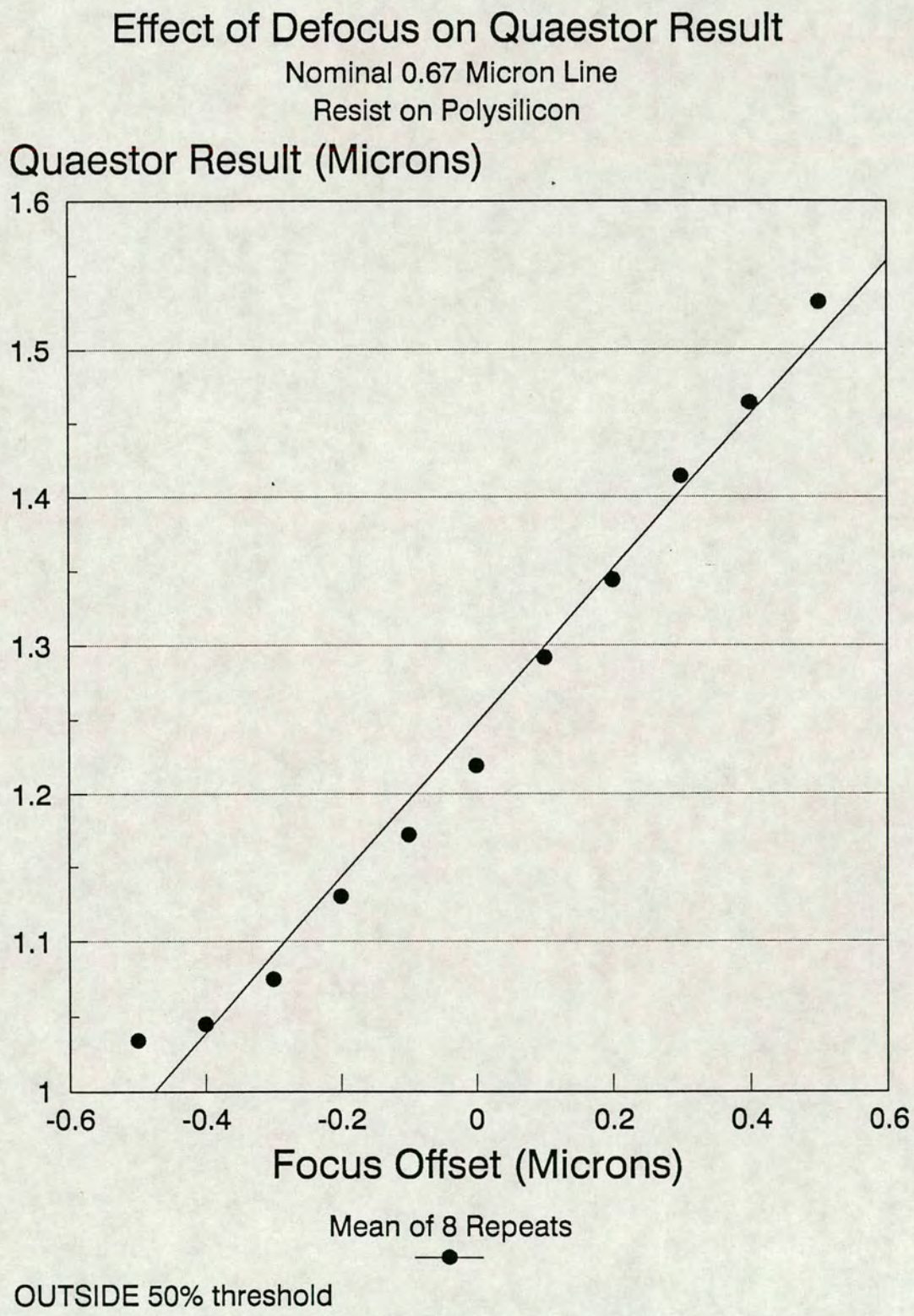

Figure 3–15: Effect of Defocus on Quaestor Result

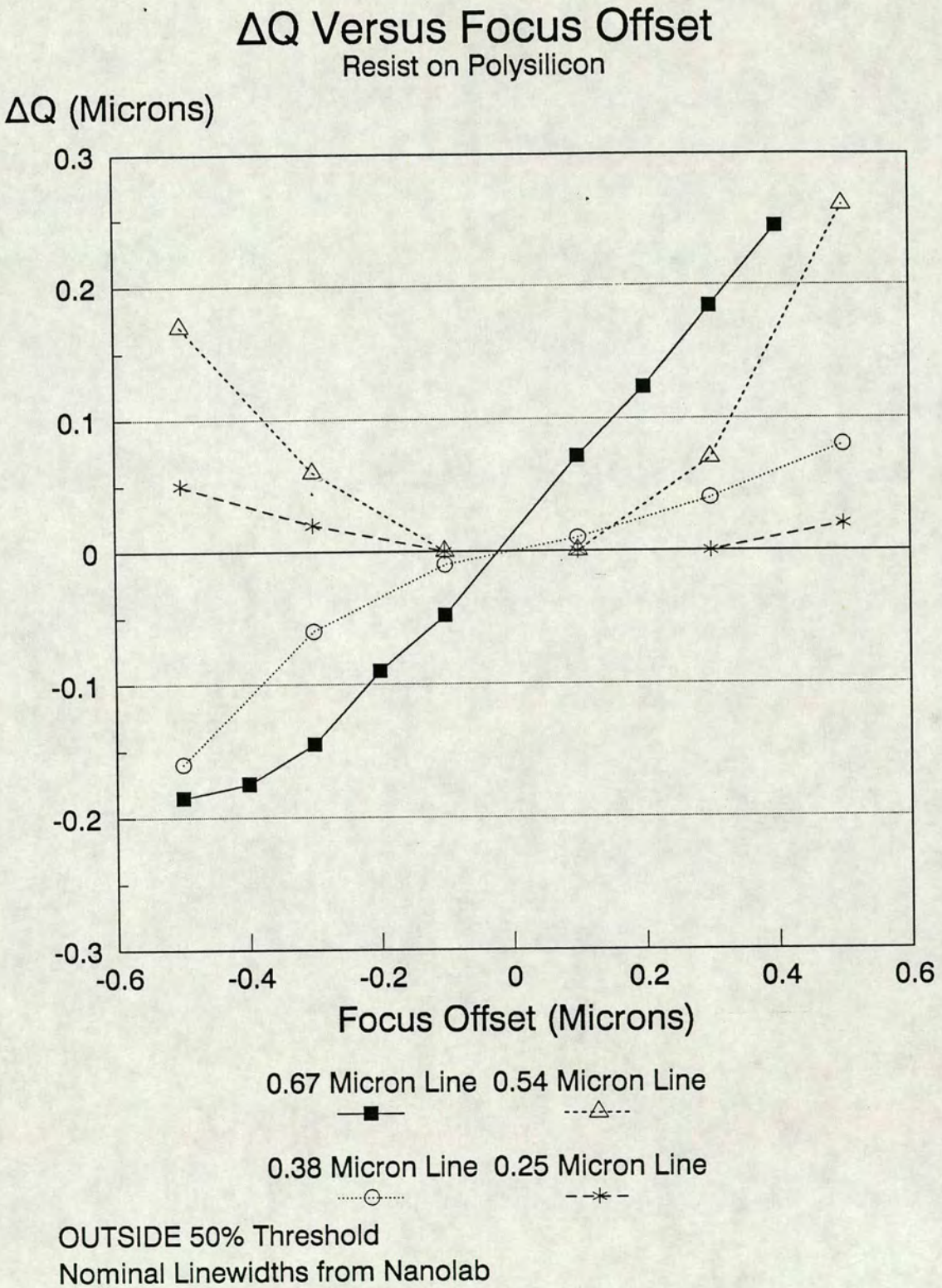

Figure 3–16: Delta Q versus Focus Offset

silicon to completed chip takes about thirteen weeks, although prototype semi-custom arrays in sizes up to 10 000 gates are offered in six weeks from completion of design.

Roborough's metrology system is based on the Prometrix Lithomap LM20, an electrical probing system which automatically produces linewidth uniformity maps of wafers. [77] CD data are taken by measuring the resistance of Bridge resistors of known length and then calculating the linewidths based on the sheet resistance, as determined from adjacent van der Pauw structures. [78] [79] (See Fig. 3–17).

In operation, for a typical wafer with sixty test sites, linewidth or vector maps can be produced in two minutes. The system can test up to 225 sites on a wafer using special probe cards. The manufacturers claim dimensions as small as 0.1μm can be measured with a precision of 0.01μm.[80]

The disadvantages of this system are two-fold. Firstly it cannot be used to measure non-conducting features on non-conducting substrates, and is therefore unsuitable for some of the most critical applications, such as measuring photoresist.

Secondly, it requires a probe card to contact the test structures, and some skill is required from the operator to align the probe points accurately onto the pads without scratching the wafer.

Plessey Semiconductors use this system because it gives a direct electrical measurement of linewidth, as opposed to an optical approximation of the intensity profile. However, since the Lithomap cannot measure non-conducting layers, an OSI video-scanning system is required for taking resist image dimensions. The OSI is calibrated to the Lithomap to minimise the dimensional offset between the two measurement systems.

An SEM is available for experimental and inspection purposes, but since it is not used in routine processing, it is not calibrated to the Lithomap.

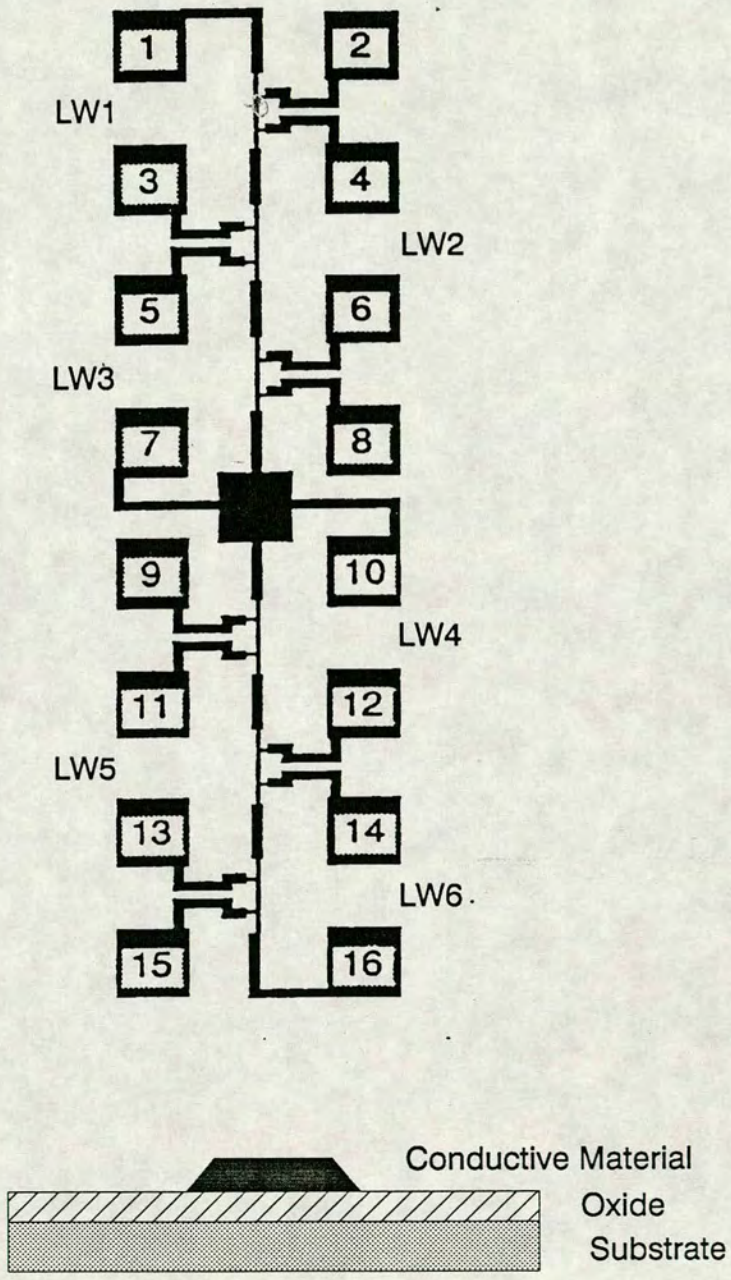

Figure 3–17: Prometrix Linewidth Module: Van Der Pauw and Six Bridge Resistors [77]

3.8 Quaestor/Prometrix Correlation

It is important to understand the relationship between photoresist and etched dimensions in order to specify process tolerances for linewidth variations. The purpose of these tests was two-fold. Firstly, to assess the relationship between resist and etch dimensions as measured on Quaestor; and secondly to derive the correlation curve between Prometrix and Quaestor measurements on etched lines.

3.8.1 Test Pattern

In order to compare results from Quaestor and Prometrix it was necessary to design a test reticle. Although Quaestor can be programmed to measure any feature in any position on a wafer, Prometrix requires special test structures to probe CD across the wafer. Plessey Semiconductors provided the dimensional data required to design the reticle. A software file was created for the pattern generator using a PC-based design tool developed within the department. [81]

The test pattern consisted of Prometrix structures of linewidth dimensions 0.8, 1.0, 1.4, 2.0, 2.5 and 3.0 μm. The 1μm line was of particular interest to Plessey since it was currently their minimum resolvable feature size. The reticle also included gratings of the same dimensions as the Prometrix lines. These served as a visual aid to assess lithographic performance.

3.8.2 Test Procedure

The testing was carried out on three inch wafers processed in the EMF. Prometrix structures must be printed on a conducting material above an insulating substrate. The samples prepared consisted of a thin layer of polysilicon deposited onto a layer of oxide a few hundred Angstroms thick. (See Fig. 3–17).

	Nominal	0.8	1.0	1.4	2.0	2.5	3.0
RESIST	mean	0.642	0.795	1.16	1.91	2.36	3.01
	SD	0.100	0.047	0.080	0.084	0.105	0.156
ETCHED	mean	0.734	0.924	1.28	1.88	2.44	3.06
	SD	0.031	0.031	0.035	0.050	0.056	0.052

Table 3–1 Comparison of Quaestor Data Before and After Etch

The wafers were coated with approximately 1.1μm of Hunt photoresist, spun on at 6000 rpm. They were printed at optimum focus and exposure with the test reticle, and developed with Hunt HPRD428. Resist dimensions were measured on Quaestor at 50 sites across the wafer. The Quaestor was calibrated initially to the Nanolab using the "Outside " measurement technique with a 50% threshold.

The wafers were then etched and remeasured on Quaestor in order to assess the relationship between photo and etch dimensions. Having collected this data, the etched wafers were taken to Plymouth and measured on Plessey's Lithomap. The results of these tests can be seen in the following section.

3.8.3 Comparison of Quaestor Before and After Etch

Figs. 3–18 to 3–24 are the correlation curves relating to this data. Fig. 3–18 shows that a linear relationship exists between resist and etched dimensions. The correlation coefficient r is a measure of the degree of linearity between two variables. Its value lies between -1 and $+1$, and largely refers to the deviation from the line of regression through the scatter points [82]. The correlation coefficient between Quaestor photo and etch measurements is calculated to be r = 0.94, indicating a strong degree of positive correlation.

Figs. 3–19 to 3–24 are the scatter plots showing the spread of results for each individual linewidth. They show that, with the exception of the 0.8μm line, the spread in resist measurements is approximately double that of the etched measurements.

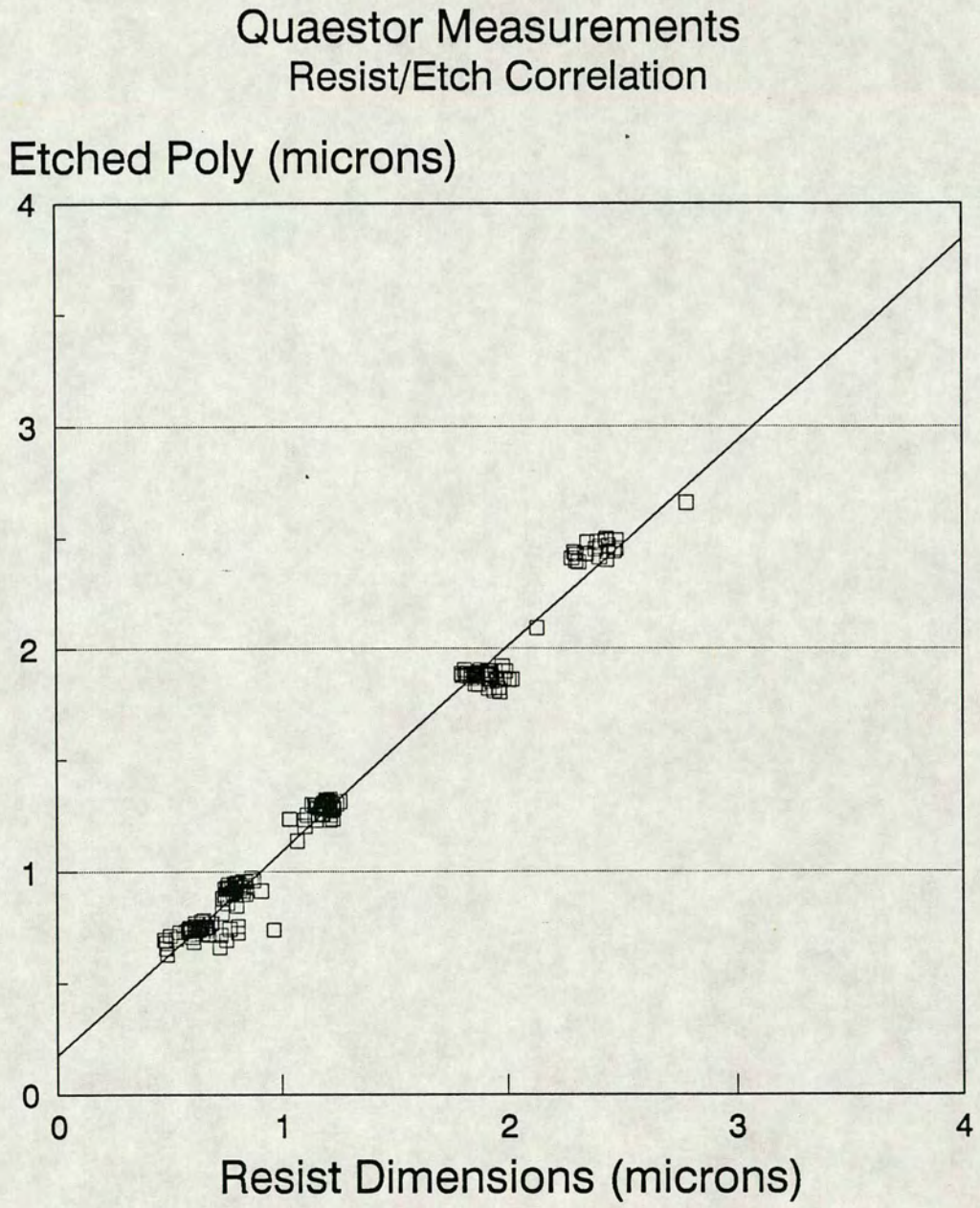

Figure 3–18: Quaestor Etched versus Resist Dimensions - All Lines

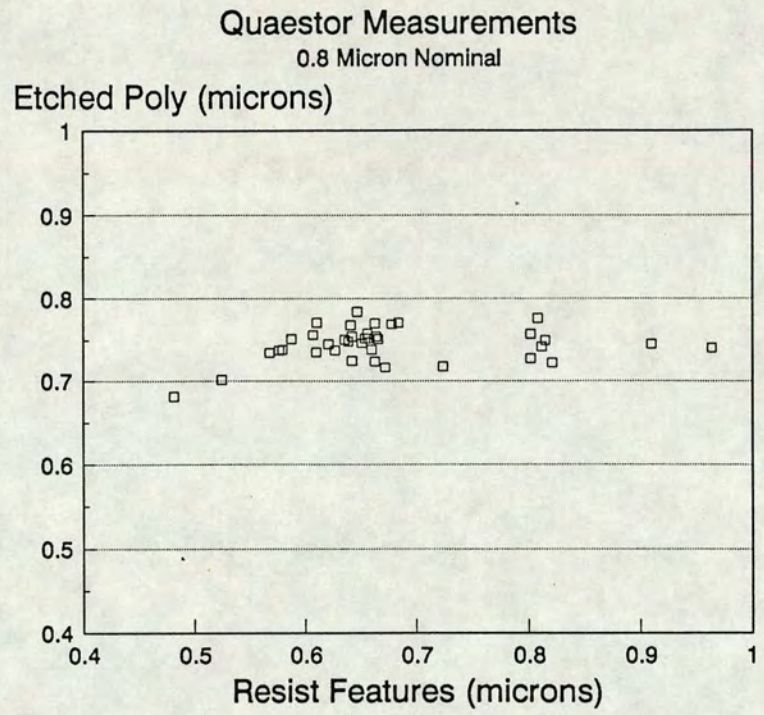

Figure 3–19: Quaestor Etched versus Resist Dimensions - 0.8 Micron Line

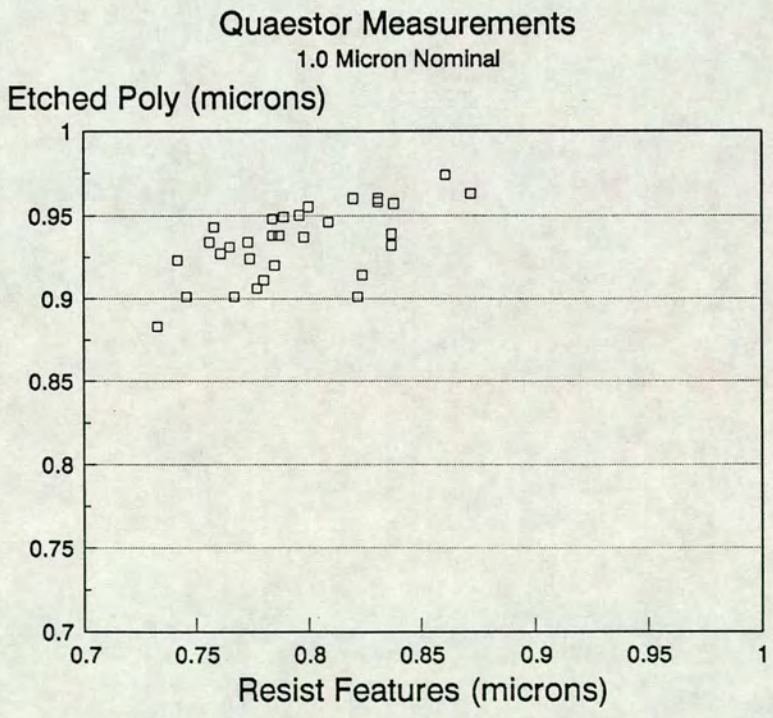

Figure 3–20: Quaestor Etched versus Resist Dimensions - 1.0 Micron Line

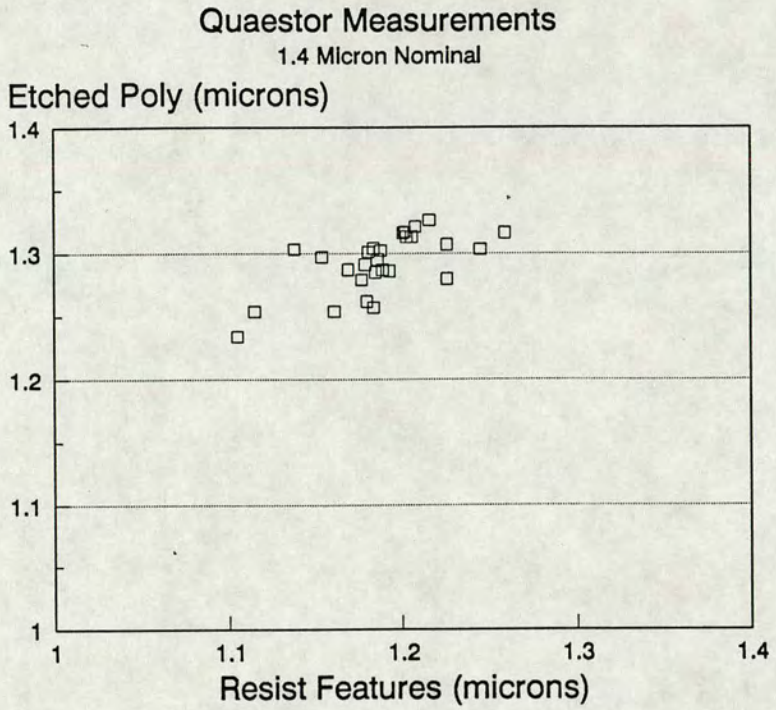

Figure 3–21: Quaestor Etched versus Resist Dimensions - 1.4 Micron Line

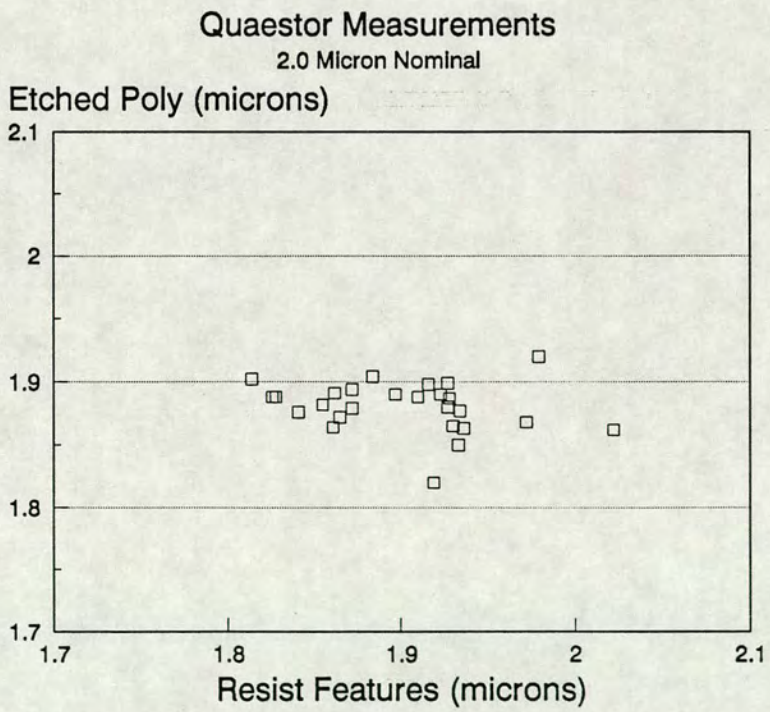

Figure 3–22: Quaestor Etched versus Resist Dimensions - 2.0 Micron Line

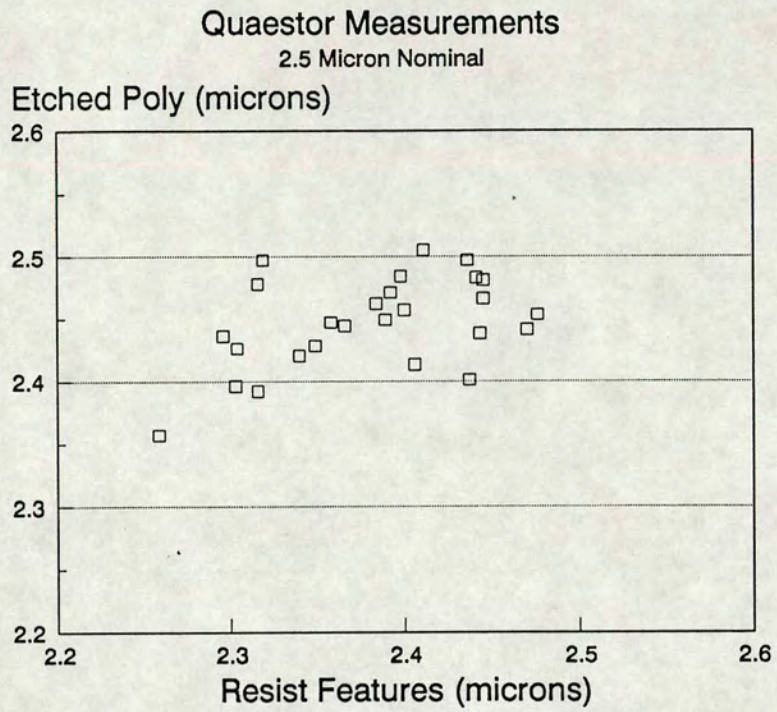

Figure 3–23: Quaestor Etched versus Resist Dimensions - 2.5 Micron Line

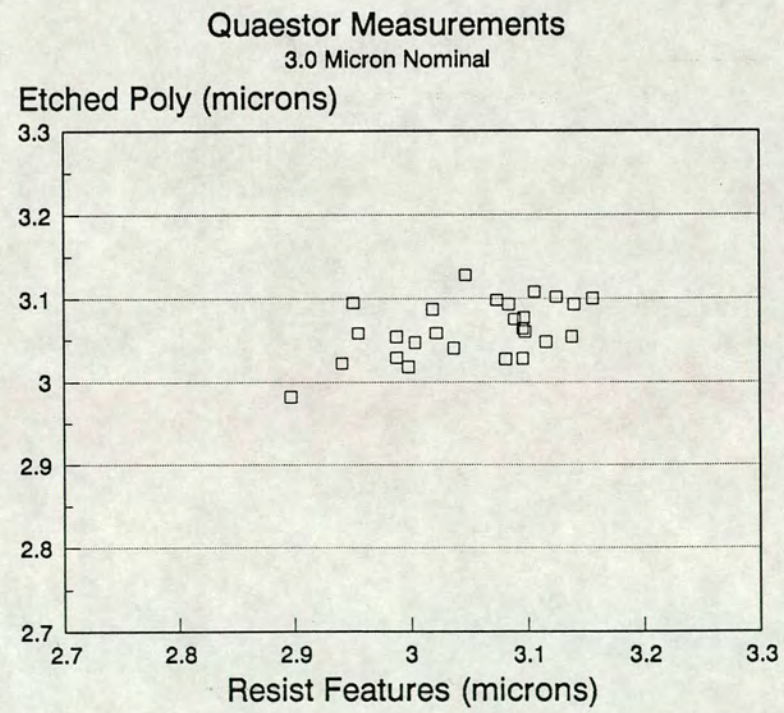

Figure 3–24: Quaestor Etched versus Resist Dimensions - 3.0 Micron Line

This is as expected, since resist is inherently difficult to measure, especially on a reflective substrate. The 0.8μm line shows an even greater spread in resist dimensions due to the difficulty in focusing on submicron features.

Table 3–1 confirms that the standard deviation (SD) of the resist measurements are greater than the standard deviation of the etched measurements. However, despite the apparent difficulty in obtaining accurate resist measurements, the mean etched dimensions vary between 2-8% of the target linewidth, which indicates that the lithography of the wafers has been well controlled.

Table 3–1 also shows that there is an apparent increase of size on etching. This is probably a result of the etch being not fully anisotropic and creating a sloping sidewall on the etched profile.

3.8.4 Comparison of Prometrix and Quaestor

Figs. 3–25 to 3–31 are the scatter plots relating to this data. Fig. 3–25 shows that the relationship between Quaestor and Prometrix measurements is not perfectly linear. In this case, the correlation coefficient r = 0.70, which implies that if one machine were to be calibrated to the other, the calibration would only be accurate over a narrow range of linewidths. Separate calibration curves should be generated for each target linewidth.

A line drawn through the graph data intercepts the X-axis at 0.1μm. This indicates an offset in the measurements such that Quaestor results are approximately 0.1μm greater than Prometrix results. This prediction is confirmed by Table 3–2.

Table 3–2 shows that, although the Quaestor has successfully measured more sites than the Prometrix, the Quaestor standard deviation of results is consistently smaller than that of the Prometrix. The Prometrix has failed to measure 16% of

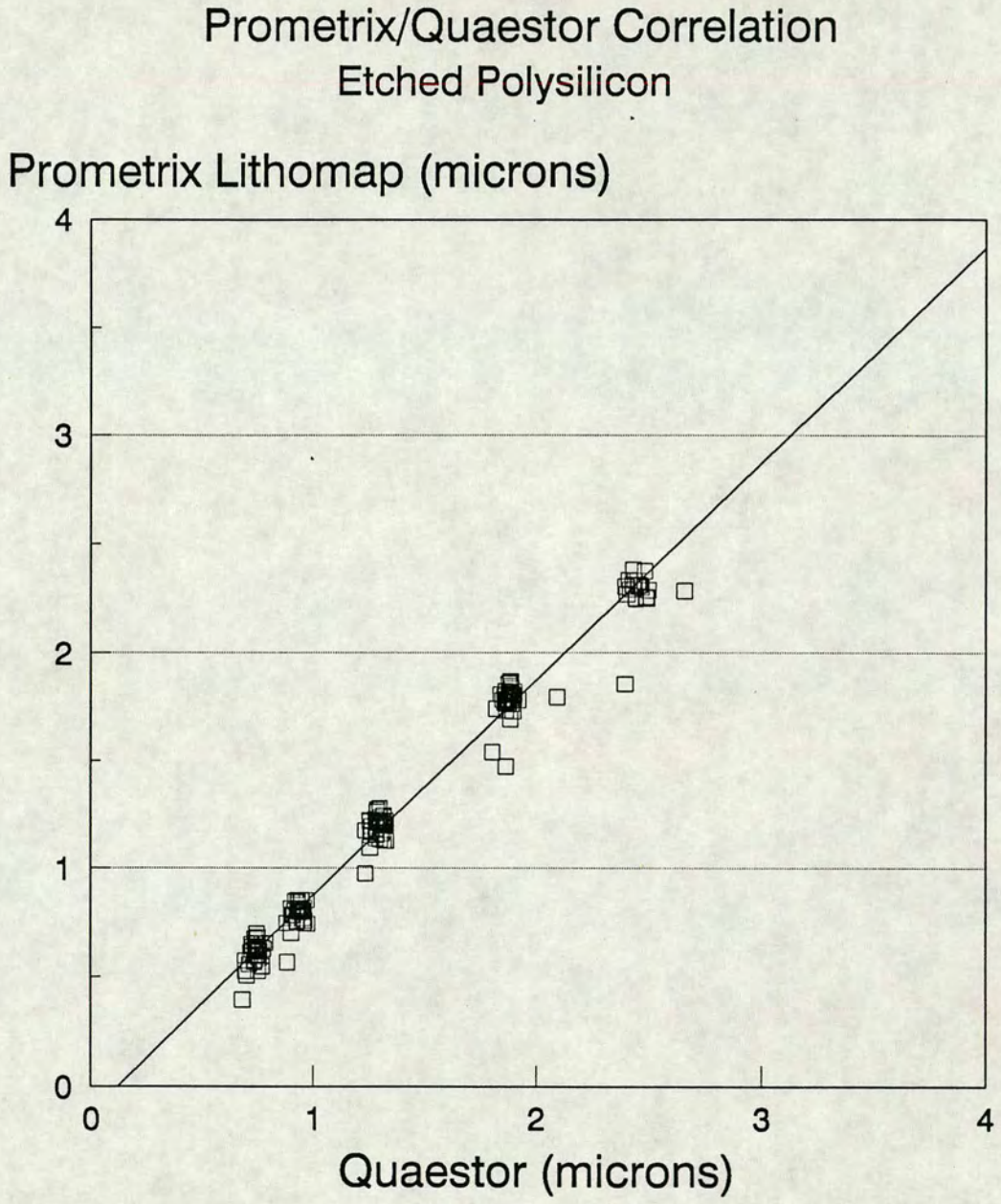

Figure 3–25: Prometrix/Quaestor Correlation - All Lines

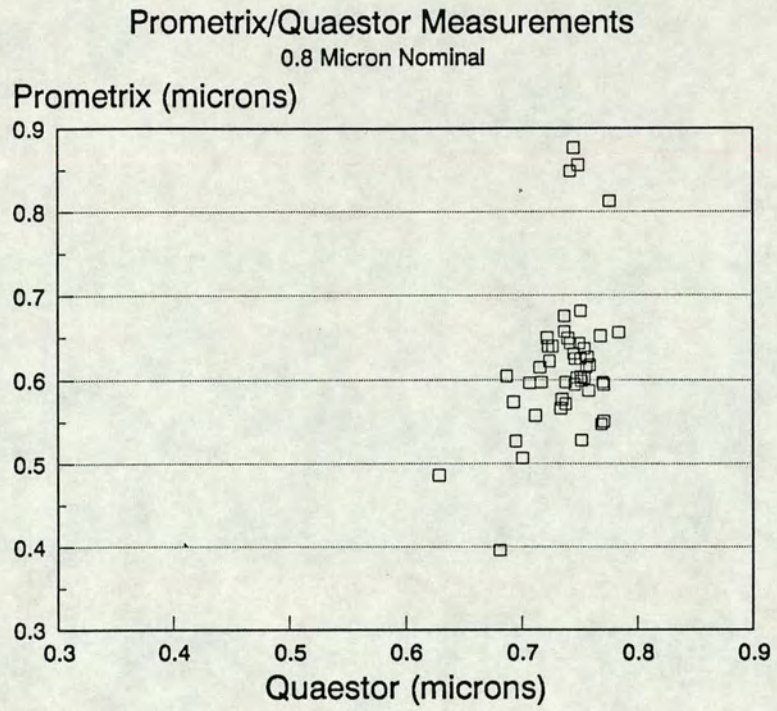

Figure 3–26: Prometrix/Quaestor Correlation - 0.8 Micron Line

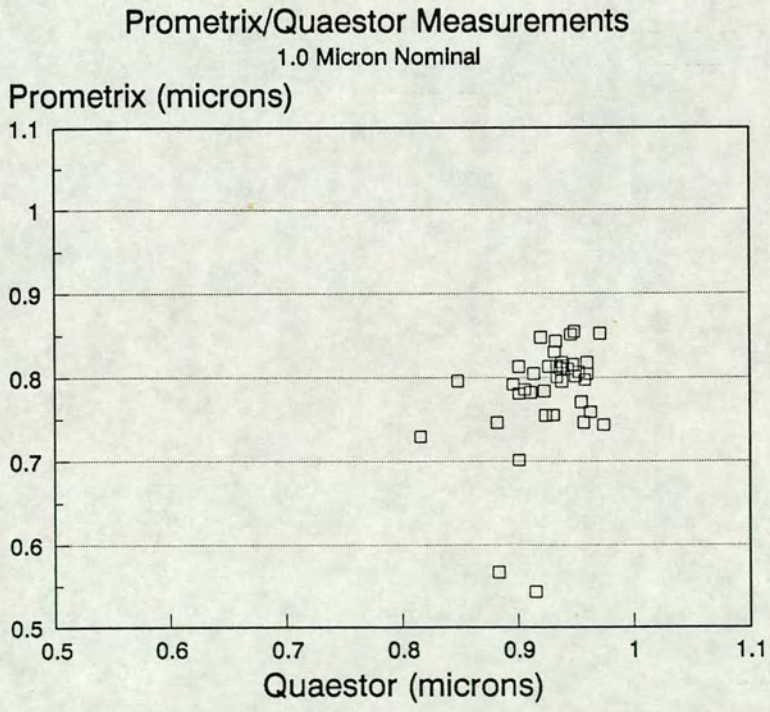

Figure 3–27: Prometrix/Quaestor Correlation - 1.0 Micron Line

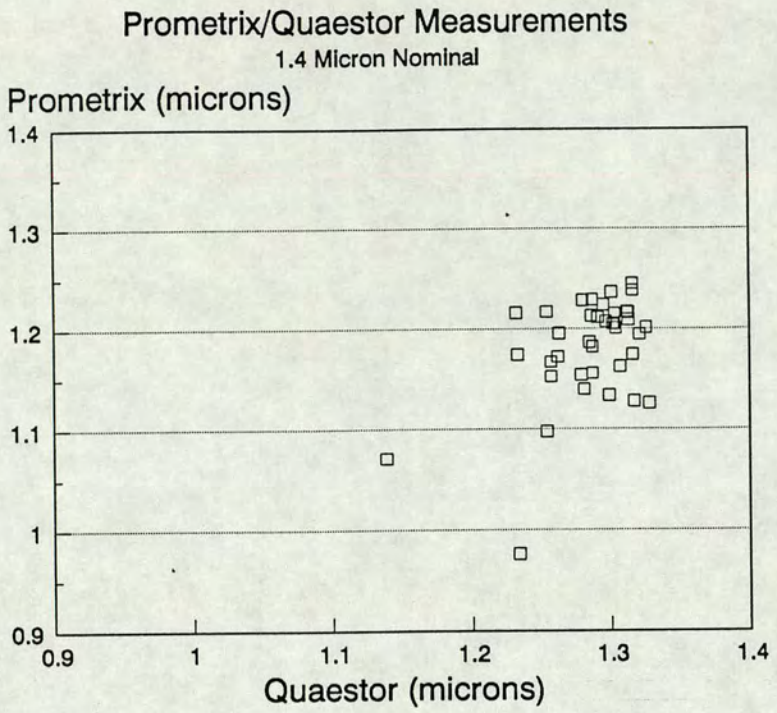

Figure 3–28: Prometrix/Quaestor Correlation - 1.4 Micron Line

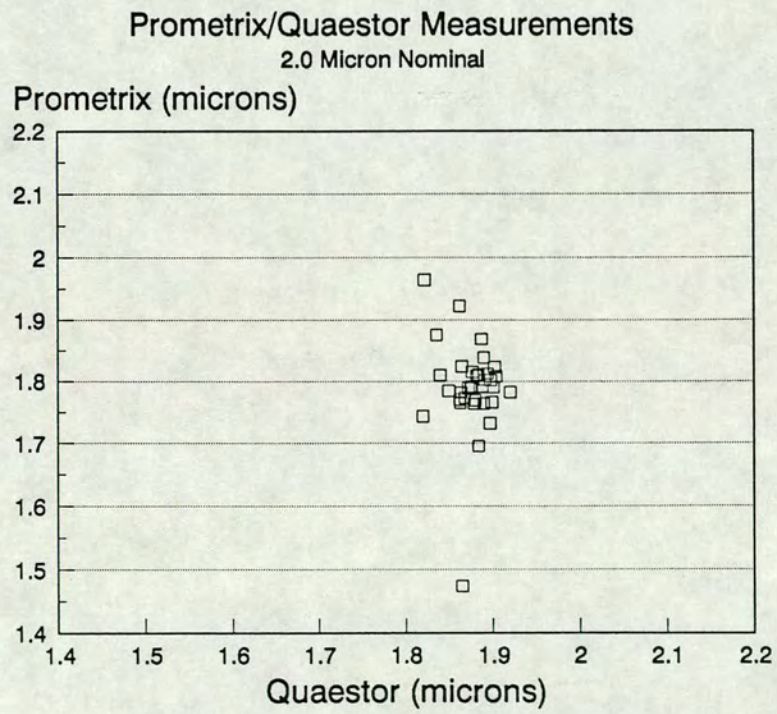

Figure 3–29: Prometrix/Quaestor Correlation - 2.0 Micron Line

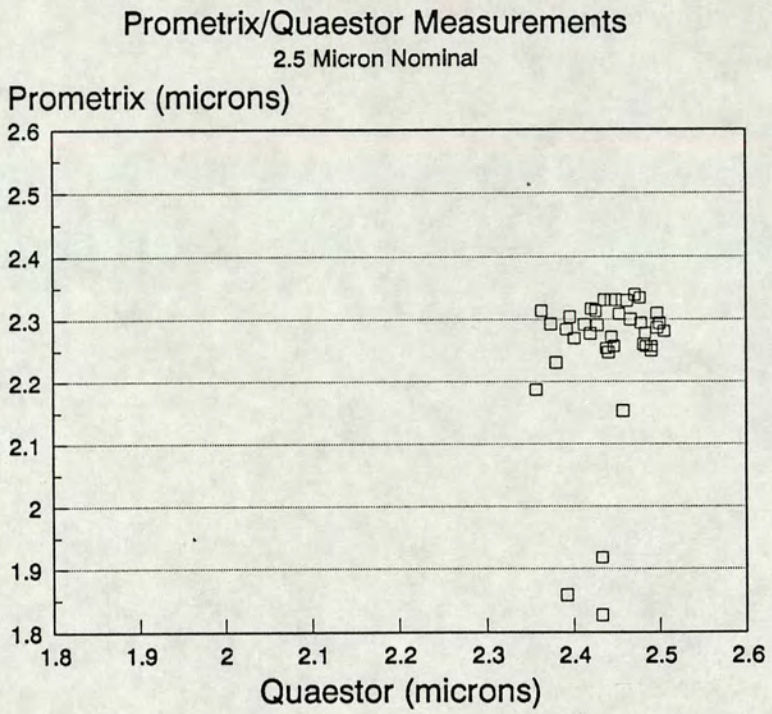

Figure 3–30: Prometrix/Quaestor Correlation - 2.5 Micron Line

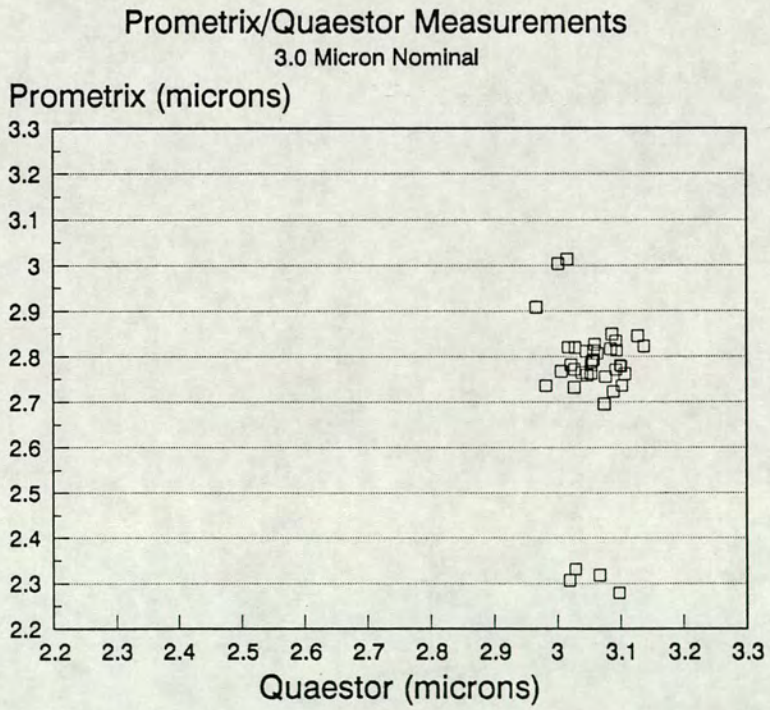

Figure 3–31: Prometrix/Quaestor Correlation - 3.0 Micron Line

all possible sites. The Lithomap checks its measurements during the probing routine, forcing current first one way through the line and then forcing it in the opposite direction. If the two results fail to match the site is discarded and the prober moves on to the next test structure. In this case poor probing has been detected, perhaps due to scratches on the wafer.

3.8.5 Comparison of Prometrix Statistics and Full Data Set

Table 3–3 has been generated by comparing the mean and standard deviation values displayed in the Lithomap contour maps with those calculated from the full data set.

The discrepancy between these values is due to the Lithomap discarding data which is more than three standard deviations from the mean. The implication of this data sort is that while the mean value is not much affected, the standard deviation displayed in the wafer statistics may be significantly smaller than the actual spread of results in the raw data.

The justification for removing outlying points from the data, according to Prometrix philosophy, is that isolated random defects, for example particles of dust, should not be allowed to distort the statistics of linewidth uniformity across the wafer. There is a danger however that process-induced local defects will be dismissed by the system as random defects, and that a true representation of wafer non-uniformities is partially hidden by removing outlying data.

	Nominal	0.8	1.0	1.4	2.0	2.5	3.0
PROMETRIX	mean	0.605	0.797	1.19	1.78	2.27	2.76
	SD	0.052	0.052	0.056	0.069	0.088	0.117
	sites	44	39	40	46	43	44
QUAESTOR	mean	0.734	0.924	1.28	1.88	2.44	3.06
	SD	0.031	0.031	0.035	0.050	0.056	0.052
	sites	51	49	51	51	51	50

Table 3–2 Comparison of Prometrix and Quaestor Measurements: 51 Possible Sites

	Nominal	0.8	1.0	1.4	2.0	2.5	3.0
RAW DATA	mean	0.605	0.797	1.19	1.78	2.27	2.76
	SD	0.052	0.052	0.056	0.069	0.088	0.117
	minimum	0.4	0.57	0.98	1.47	2.02	2.53
	maximum	0.7	0.88	1.28	1.87	2.38	2.87
PROMETRIX STATISTICS	mean	0.61	0.800	1.19	1.79	2.38	2.79
	SD	0.050	0.050	0.050	0.070	0.060	0.060
	minimum	0.52	0.744	0.976	1.47	1.86	2.31
	maximum	0.681	0.876	1.28	1.87	2.38	2.87

Table 3–3 Comparison of Prometrix Statistics and Full Data Set

3.8.6 Preliminary Conclusions

There are a number of conclusions to be drawn from consideration of these experiments.

1. The linear relationship that has been shown to exist between photo and etch measurements on Quaestor implies that final etch dimensions may be predicted from measurement of the resist image if the etch is well controlled.

2. The Prometrix data is presented in a much more useful form than that of the Quaestor. The Lithomap produces contour plots, vector maps and focus/exposure curves as well as simple statistical data. (See Figs. 3–32 and 3–33.) The Quaestor prints out raw data which must be transferred onto a personal computer for further analysis. This seems to be the greatest drawback of using Quaestor.

3. The Prometrix data file handling and system software is better structured and simpler to use than Quaestor. However, Quaestor is the more flexible instrument, since it can be programed to measure any feature and any number of sites on the wafer.

4. There is reasonable correlation between measurements on the two systems. Prometrix statistics displayed on the contour maps have an artificially low standard deviation due to a data sort which removes outlying data.

5. Quaestor and Prometrix have different wafer coordinate systems. This makes it difficult to compare data, since results have to be extracted from each data set and matched site by site. The only viable means of overcoming this problem would be for manufacturers of all metrology tools to agree on a standard wafer coordinate system. This seems unlikely, since there is no incentive for manufacturers to compare their systems with others commercially available.

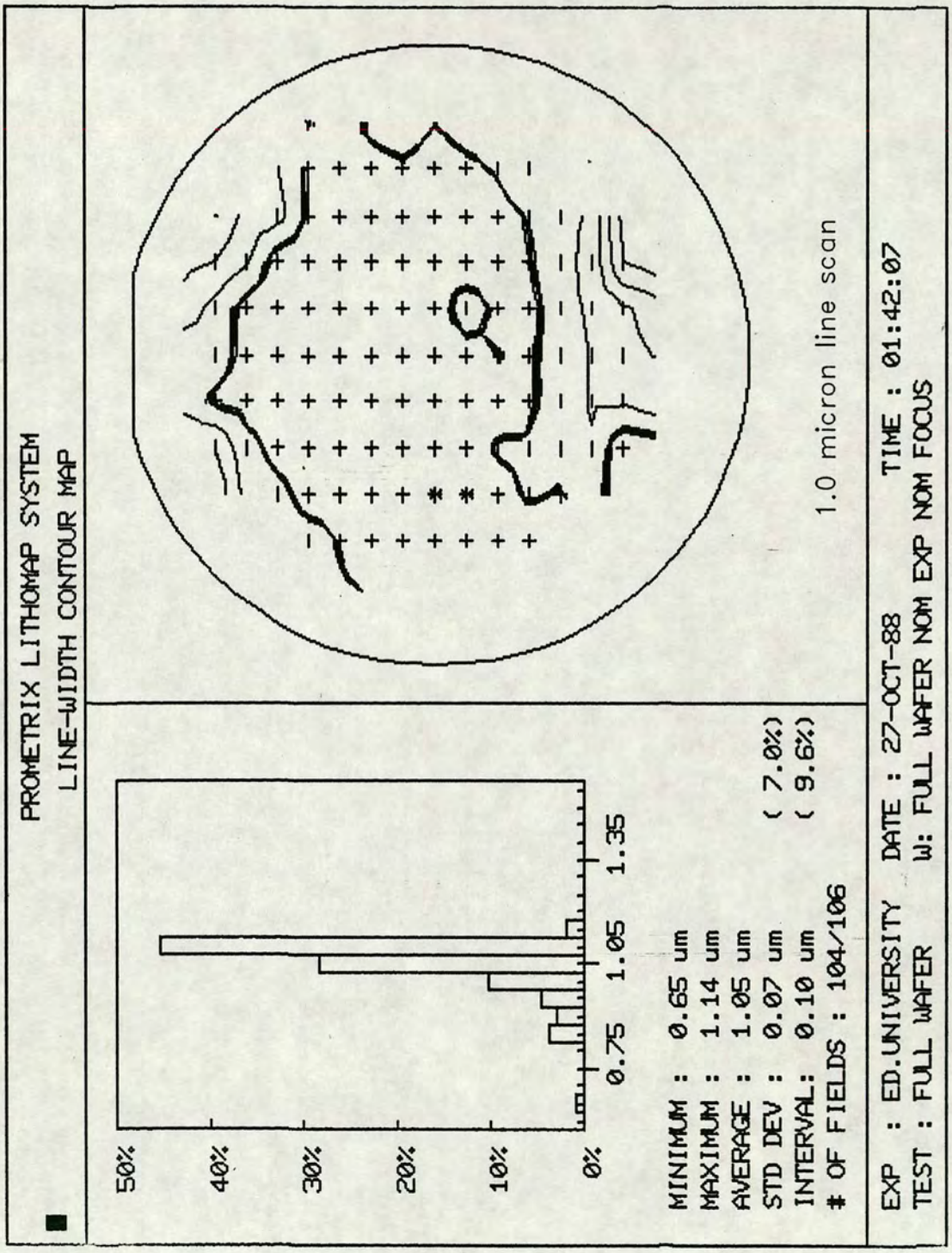

Figure 3–32: Prometrix Contour Map

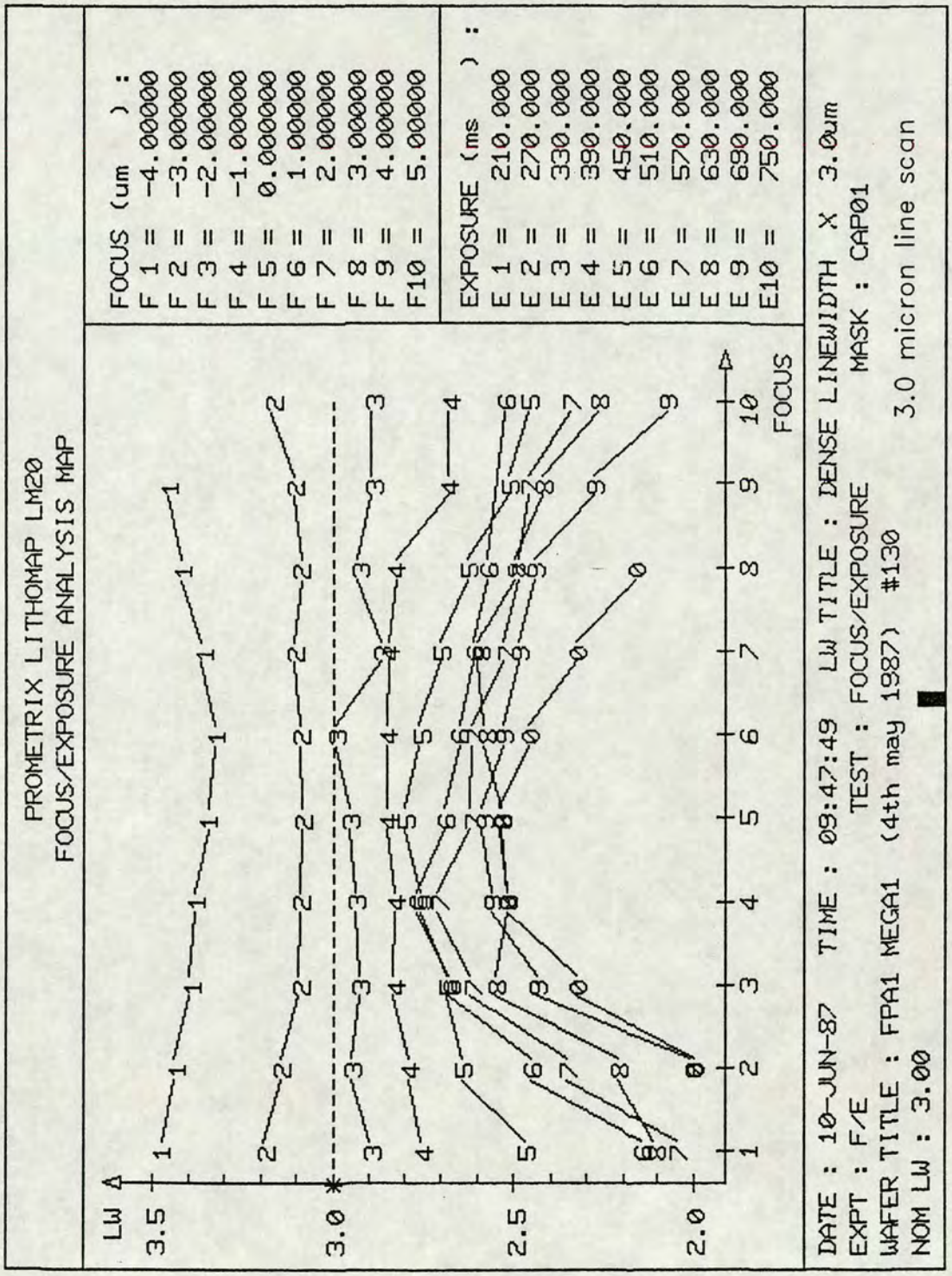

Figure 3–33: Prometrix Focus/Exposure Curves

3.9 System Limitations

Having made an experimental assessment of Nanolab, Quaestor and Prometrix linewidth measuring systems, it is possible to determine their most pertinent role in semiconductor metrology. This section draws together the main features of each system.

3.9.1 Nanolab

The ability to analyse the profiles of features with greatly enhanced depth of field is the main advantage of the Nanolab as a metrology tool.

However on difficult layers such as resist on oxide, the signal is noisy and the measurement is critically dependent on the quality of the secondary electron profile i.e. machine set-up. [83] As a result, the use of this instrument for routine measurements on a semiconductor process line would place high demands on the operator. Although the capability is there, the degree of automation necessary to realise it with semi-skilled operators is a daunting task and a long way off. [84]

3.9.2 Quaestor

The Quaestor is a powerful tool for measuring specific feature dimensions. It is also a highly complex machine, and needs a trained and experienced operator to obtain the best results. The pattern recognition capability is the main source of the system's complexities. Quaestor has the ability to find, recognise and measure features as small as one micron in size on a six inch wafer. If the test pattern were larger and easier to locate, the pattern recognition, the optical system and the stage mechanics could all be considerably simplified. There is of course appreciable resistance to printing large area test patterns within valuable chip design area. However, there are still large areas of the wafer unused in the scribe channels

between chips. If test patterns were printed in the scribe channels, it would be possible to scan linewidth uniformity continuously across the wafer surface.

Quaestor linewidth dimensions are highly dependent on the exact measurement location on the feature. Small bumps and scratches occurring at the measurement site are likely to cause a misrepresentation of the actual linewidth. An integrated measurement over a localized area would give a more accurate picture of linewidth dimensions at each site. However this is not a practical solution for Quaestor since it would result in a measurement routine that is too slow for production purposes.

3.9.3 Lithomap

This system gives good resolution and repeatability with rapid results in the form of wafer maps. The disadvantage of having to use a pattern etched in a conducting film such as polysilicon is twofold; firstly it means that the process cannot be characterized on other layers, and secondly, it introduces a delay which can be significant when trying to assess stepper matching. [85]

Another limitation associated with electrical probing techniques is that the result can be affected by the grain size of the polysilicon and other factors such as current crowding. [83].

3.10 Conclusions

Each of the systems described above has its own particular strengths and weaknesses. Quaestor's main advantage is that it can be used to predict etched dimensions from measurements of resist. However, both Quaestor and Nanolab are too slow for production purposes and too complex to automate. The Lithomap is a fully automated system, but is restricted to measuring conducting layers, and cannot measure resist. Therefore, none of the systems are ideal in terms of mapping linewidth uniformity across wafers for routine processing.

Linewidth measurements for process monitoring purposes have traditionally been based on electrical probing of test structures on process control chips. [86] [87] However there is no reason why the use of test structures should not be extended to include optical techniques, providing they are suited for automation.

The experiments in this chapter have served two purposes:

1. To show there is a need for a non-destructive fast-scan system for monitoring linewidth uniformity across wafers. If this system is to be implemented, it should be based on the use of large-scale optical test patterns.

2. To demonstrate that Quaestor is sufficiently sensitive to measure linewidth dimensions due to film thickness variations. The following chapter describes the experiments carried out to determine this relationship empirically.

Bibliography

[1] C.VanLeeuwen. What's ahead in test and measurement. *Semiconductor International*, (1):72–76, 1989.

[2] G.M.Oleszek. Analysis of photoprocess-induced non-linear linewidth variations. In *Microelectronics Measurement Technology Seminar*, pages 267–272, 1979.

[3] D.Nyyssonen and J.M.Jerke. Linewidth measurement: From fine art to science. In *Int. Electron Device Meeting*, pages 437–440, 1978.

[4] C.P.Kirk. A study of the instrumental errors made in linewidth and registration measurements made with an optical microscope. In *Integrated Circuit Metrology, Inpsection and Process Control*, pages 51–59. SPIE Vol. 775, 1987.

[5] S.P.Billat. Metrology: No longer an afterthought. *Solid State Technology*, (1):99, 1989.

[6] A.L.Flamholz and R.S.Charsky. Automatic width and overlay measurement. In *Developments in Semiconductor Microlithography*, pages 120–127. SPIE Vol. 135, 1978.

[7] D.Nyyssonen. Optical linewidth measurements on wafers. In *Developments in Semiconductor Microlithography*, pages 115–119. SPIE Vol. 135, 1978.

[8] H.Levinson and R.Rice. Overlay tolerances for VLSI using wafer steppers. In *Laser Microlithography*, pages 82–93. SPIE Vol. 922, 1988.

[9] G.Torolira and R.Melen. Critical dimension control in the late eighties - part 1. *Microelectronic Manufacturing and Testing*, 8(1):8–12, 1985.

[10] R.D.Larrabee. Submicrometer optical linewidth metrology. In *Integrated Circuit Metrology, Inspection, and Process Control*, pages 46–50. SPIE Vol. 775, 1987.

[11] M.Davidson, K.Kaufman, and I.Mazor. The coherence probe microscope. *Solid State Technology*, (9):57–59, 1987.

[12] N.K.L.Raja and K.J.Rangra. A SEM-image processing method for recognition and fast location of IC registration marks. In *Proceedings of Microcircuit Engineering*, pages 681–685, 1989.

[13] W.E.Ham. Accurate efficient LSI process answers from nominally identical closely spaced test structures. In *Microelectronics Measurement Technology Seminar*, pages 1–16, 1979.

[14] T.J.Russell, D.B.Maxwell, and M.G.Buehler. A microelectronic test pattern for measuring uniformity of an integrated circuit fabrication technology. *Solid State Technology*, (2):71–74, 1979.

[15] A.Brown, A.Minvielle, and A.Salugsugan. Automated product test wafer procedure. In *Integrated Circuit Metrology, Inpsection and Process Control*, pages 226–232. SPIE Vol. 775, 1987.

[16] M.T.Postek and D.C.Joy. Microelectronics dimensional metrology in the scanning electron microscope - part 1. *Solid State Technology*, (12):77–85, 1986.

[17] D.Nyyssonen. Linewidth measurement with an optical microscope. *Applied Optics*, 16(8):2223–2230, 1977.

[18] D.Nyyssonen. Linewidth measurement spotlight. *Semiconductor International*, (3):39–56, 1980.

[19] H.S.Damar, F.P.Chan, and T.T.Wu. Diffraction characterization for process monitoring, linewidth measurement and alignment. In *Optical Microlithography: Technology for the Next Decade*, pages 157–163. SPIE Vol. 470, 1984.

[20] R.E.Swing. Theoretical basis of a new optical method for the accurate measurement of small linewidths. In *Developments in Semiconductor Microlithography*, pages 65–77. SPIE Vol. 80, 1976.

[21] V.J.Coates. Computerized optical system for precision linewidth measurement. In *Microelectronics Measurement Technology Seminar*, pages 273–287, 1979.

[22] D.Nyyssonen. Optical linewidth measurements on wafers. In *Proc. SPIE*, volume 135, page 115, 1978.

[23] M.Davidson, K.Kaufman, and I.Mazor. An application of interference microscopy to integrated circuit inpection and metrology. In *Integrated Circuit Metrology, Inpsection, and Process Control*, pages 233–247. SPIE Vol. 775, 1987.

[24] N.S.Levine, T.R.Corle, and R.T.Mumaw. Multilevel CD/overlay metrology using a real-time confocal scanning optical microscope. In *Proceedings of Microcircuit Engineering*, pages 669–674, 1989.

[25] D.Nyyssonen, J.M.Jerke, and A.W.Hartman. Comparison of linewidth measurements on an SEM/interferometer system and an optical linewidth-measuring microscope. In *Semiconductor Microlithography*, pages 37–45. SPIE Vol. 100, 1977.

[26] J.M.Jerke, A.W.Hartman, and D.Nyyssonen. Accurate linewidth measurements at the National Bureau of Standards. In *INTERFACE 76*, pages 51–59. Kodak Microelectronics Seminar, 1976.

[27] C.P.Kirk and D.S.Moore. Analysis of linewidth measurements for the purpose of automation. In *Integrated Circuit Metrology*, pages 33–39. SPIE Vol. 480, 1984.

[28] G.Torlira and R.Melen. Critical dimensional control in the late eighties. *Microelectronic Manufacture and Testing*, 8(2):19–22, 1985.

[29] H.R.Rottmann. Small patterns in photolithography - problems and solutions. *Journal of Applied Photographic Engineering*, (3):119–127, 1978.

[30] P.H.Singer. Linewidth measurement: Approaching the submicron dimension. *Semiconductor International*, (3):48–54, 1983.

[31] D.Nyyssonen and J.M.Jerke. Optical linewidth measurement - a basic understanding. In *Microelectronics Measurement Technology Seminar*, pages 251–266, 1979.

[32] M.E.Guillaume, N.M.Noailly, and J.C.Reynaud. Fourier transform method for optical linewidth measurement. In *Integrated Circuit Metrology*, pages 71–77. SPIE Vol. 480, 1984.

[33] P.H.Singer. Linewidth measurement aids process control. *Semiconductor International*, (2):66–73, 1985.

[34] J.J.Chisholm. A new technique for linewidth measurement on one micron geometry process wafers using fluorescence. In *Integrated Circuit Metrology*, pages 49–56. SPIE Vol. 480, 1984.

[35] S.J.Erasmus, M.L.Reed, and U.Kaempf. A fluorescence linewidth measurement system for VLSI fabrication. In *Integrated Circuit Metrology*, pages 57–64. SPIE Vol. 480, 1984.

[36] M.G.Rosenfield. Analysis of linewidth measurement techniques using a low voltage SEM. In *Integrated Circuit Metrology, Inspection and Process Control*, pages 70–79. SPIE Vol. 775, 1987.

[37] M.Postek and D.C.Joy. Microelectronics dimensional metrology in the scanning electron microscope - part 2. *Solid State Technology*, (11):145–150, 1986.

[38] M.Postek. Submicrometer dimensional metrology in the scanning electron microscope. In *Integrated Circuit Metrology, Inspection and Process Control*, pages 166–171. SPIE Vol. 775, 1987.

[39] B.Stallard. Use of a confocal laser microscope for the measurement of submicrometer critical dimensions. In *Integrated Circuit Metrology, Inspection and Process Control*, pages 60–67. SPIE Vol. 775, 1987.

[40] S.Jensen, G.Hembree, and J.Marchiando. Quantitative sub-micrometer linewidth determination using electron microscopy. In *Semiconductor Microlithography*, pages 100–109. SPIE Vol. 275, 1981.

[41] D.G.Seiler and D.V.Sulway. Precision linewidth measurement using a scanning electron microscope. In *Integrated Circuit Metrology*, pages 86–92. SPIE Vol. 480, 1984.

[42] K.M.Monahan and D.S.Lim. Nanometer-resolution SEM metrology in a hostile laboratory experiment. In *Micron and Submicron Integrated Metrology*, pages 173–179. SPIE Vol. 565, 1985.

[43] E.Trautman. Accuracy of electron-optical measurements of critical dimensions. In *Integrated Circuit Metrology, Inspection and Process Control*, pages 140–152. SPIE Vol. 775, 1987.

[44] T.Ohtaka, S.Saito, and T.Furuya. Hitachi S-6000 field emission CD-measurement SEM. In *Micron and Submicron Integrated Metrology*, pages 205–208. SPIE Vol. 565, 1985.

[45] T.Ahmed, S.R.Chen, and H.M.Naguib. Low voltage SEM metrology for pilot line applications. In *Integrated Circuit Metrology, Inspection and Process Control*, pages 80–88. SPIE Vol. 775, 1987.

[46] W.Malkusch and T.Pioch. A method to test the accuracy of critical dimension measurement systems (CDMS). In *Proceedings of Microcircuit Engineering*, pages 675–679, 1989.

[47] J.L.Bataillon, D.Burlet, and H.Martin. New calibration method for IC dimensional measurements. In *Proceedings of Microcircuit Engineering*, pages 661–664, 1989.

[48] C.P.Auschnitt. Submicron measurements for lithographic evaluation. Technical report, Perkin-Elmer Corp., 1982.

[49] D.Yen, L.W.Linholm, and M.G.Buehler. A cross-bridge test structure for evaluating the linewidth uniformity of an integrated circuit lithography system. *Journal of the Electrochemical Society: Solid State Science and Technology*, (10):2313–2318, 1982.

[50] F.E.Wahl and D.S.Perloff. Techniques for the evaluation and display of VLSI process uniformity. In *Microelectronics Measurement Technology Seminar*, pages 17–26, 1979.

[51] M.G.Buehler, S.D.Grant, and W.R.Thurber. Bridge and van der Pauw sheet resistors for characterizing the linewidth of conducting layers. *Journal of the Electrochemical Society: Solid State Science and Technology*, (4):650–654, 1978.

[52] H.Neves and J.Robertson. *Experimental Assessment of Process.* COMETT 643D - A VLSI Teaching Package, Edinburgh Microfabrication Facility, University of Edinburgh, 1989.

[53] T.F.Hasan, S.U.Katzman, and D.S.Perloff. Automated electrical measurements of registration errors in step-and-repeat optical lithography systems. *IEEE Transactions on Electron Devices*, ED-27(12):2304–2312, 1980.

[54] R.Mumaw. Electrical characterization of hidden defects. *Solid State Technology*, (8):47–48, 1988.

[55] A.Marmiroli, E.Baracchi, and G.Vento. Step and repeat evaluation and control by automatic optical measurements. In *INTERFACE 86*, pages 220–227. Kodak Microelectronics Seminar, 1986.

[56] D.S.Perloff, A.K.Smith, and L.V.Lybeck. Advances in the use of resistivity measurements for on-line process control. *Solid State Technology*, (5):159–163, 1987.

[57] R.R.Allen and T.Hasan. Implementation of automatic alignment utilizing electrical wafer probe techniques. In *Optical Microlithography: Technology for the Next Decade*, pages 111–121. SPIE Vol. 470, 1984.

[58] G.F.Mendes, L.Cescato, and J.Frejich. Gratings for metrology and process control. *Applied Optics*, (2):571–575, 1984.

[59] K.Harris, I.Nadler-Niv, and D.Levy. Innate accuracy of a novel E-beam system. In *INTERFACE 86*, pages 149–163. Kodak Microelectronics Seminar, 1985.

[60] W.A.Bosenberg and H.P.Kleinknecht. Linewidth measurement on IC wafers from grating test patterns. *Solid State Technology*, (7):79–85, 1983.

[61] R.H.Jones. A method for verifying IC structures and masks. In *Proceedings of Microcircuit Engineering*, pages 665–668, 1989.

[62] KLA Instruments Corp. *KLA 5000 Coherence Probe Measurement System*, January 1988.

[63] L.J.Uhler. Automatic linewidth control systems. In *Integrated Circuit Metrology, Inspection and Process Control*, pages 2–7. SPIE Vol. 775, 1987.

[64] L.R.Baker. Semiconductor wafer inspection. In *Integrated Circuit Metrology*, pages 14–19. SPIE Vol. 480, 1984.

[65] K.M.Monahan. Submicrometer metrology patterns in resist. *Solid State Technology*, (9):141–146, 1987.

[66] C.Murray. Measurement tools for overlay registration. *Solid State Technology*, (2):62–68, 1987.

[67] W.H.Arnold, B.Singh, and K.Phan. Linewidth metrology requirements for submicron lithography. *Solid State Technology*, (4):139–145, 1989.

[68] D.W.Widmann and H.Binder. Linewidth variations in photoresist on profiled surfaces. *IEEE Transactions on Electron Devices*, ED-22(7):467–471, 1975.

[69] D.A.McGillis and D.L.Fehrs. Photolithographic linewidth control. *IEEE Transactions on Electron Devices*, ED-22(7):471–477, 1975.

[70] P.H.Singer. Life on the edge: Measuring critical dimensions. *Semiconductor International*, (12):84–87, 1988.

[71] J.Hightower, M.Blanco, and K.Monahan. An application of statistical experimental design: Comparison of process latitudes for photoresist and CEL. In *Microelectronics Measurement Technology Seminar*, pages 39–49, 1979.

[72] S.D.Bennett, E.A.Peltzer, and I.R.Smith. Ultra-violet confocal metrology. In *Scanning Microscopy Technologies and Applications*, pages 75–82. SPIE Vol. 897, 1988.

[73] S.D.Bennett, E.A.Peltzer, and J.McCall. Confocal optical metrology at 325 nm. In *Integrated Circuit Metrology, Inpection, and Process Control*, pages 85–90. SPIE Vol. 921, 1988.

[74] W.Gammie. Linewidth measurement systems in the EMF. Technical report, Edinburgh Microfabrication Facility, University of Edinburgh, 1988.

[75] Vickers Instruments (Canada) Inc. *D3006 SEM Operators Manual*, June 1984.

[76] Vickers Instruments Inc. *Quaestor CD07A Operating Manual*, 1988.

[77] Prometrix Corp. *Lithomap (LM20) Operators Manual*, 1987.

[78] R.Patrick. Plasma etch characterization using electrical linewidth measuring techniques. In *Integrated Circuit Metrology, Inspection, and Process Control*, pages 210–216. SPIE Vol. 775, 1987.

[79] A.J.Walton. *Process Monitoring and Control.* COMETT 643D - A VLSI Teaching Package, Edinburgh Microfabrication Facility, University of Edinburgh, 1989.

[80] Prometrix Corp. *Lithomap (LM20) Training Manual*, 1987.

[81] A.Snell and A.Ward. BBC mask design software. Technical report, Edinburgh Microfabrication Facility, University of Edinburgh, 1988.

[82] F.Caswell. *Success in Statistics*, chapter 9. J.Murray, 1982.

[83] SERC School on Microfabrication, Edinburgh Microfabrication Facility, University of Edinburgh. *Lithography Verification*, June 1990.

[84] J.T.M.Stevenson. CD measurement. Technical report, Edinburgh Microfabrication Facility, University of Edinburgh, 1988.

[85] R.Wetzel. Metrology for steppers. *Solid State Technology*, (1):106, 1989.

[86] SERC School on Microfabrication, Edinburgh Microfabrication Facility, University of Edinburgh. *Whole Process Verification*, June 1990.

[87] N.N.Kundu, K.I Arshak, and B.Lane. A new test structure for misregistration evaluation. In *Proceedings of Microcircuit Engineering*, pages 687–691, 1989.

Chapter 4

Film Thickness Effects on CD

4.1 Introduction

In Chapter 2 it was shown that although there is a wide variety of processing parameters which affect linewidth dimensions, only two present significant difficulties in terms of control: film thickness and photoresist thickness. [1] This Chapter will investigate experimentally the effect of film thickness variations on CD.

The simulation programs introduced in Chapter 2, DEPICT, SAMPLE and PROLITH are used to establish a theory for both single and double layer films. This theory uses standing wave patterns to predict the reflectance and exposure threshold of the films, as well as the dimensions of the developed resist images.

In the final section of the Chapter the theory is tested against measured linewidths on wafers for a range of film thicknesses, using the Nanolab SEM.

4.2 Simulation: Single Layer Films

As an initial step, it was decided to simulate various thicknesses of resist on bare silicon. The simulation plots reveal the standing wave patterns on the resist profiles. This should provide a key to understanding the effect of standing waves on resist dimensions.

4.2.1 Choice of Film Thickness

Consider a film of photoresist on a silicon substrate. If monochromatic light is projected onto the film, a standing wave pattern is created as the reflected light from the substrate interferes with the incident light. In Chapter 2 it was shown that the positions of the maxima (antinodes) and minima (nodes) of the standing wave within the film can be predicted from the following equations: (See Eqns. 2.13 and 2.14)

For antinodes (maxima)

$$(d-x) = \frac{\lambda}{4n}, \frac{3\lambda}{4n} \ldots (2N_1+1)\frac{\lambda}{4n}$$
$$(Odd\ multiples\ of\ \frac{\lambda}{4n})$$

For nodes (minima)

$$(d-x) = \frac{\lambda}{2n}, \frac{\lambda}{n} \ldots N_1\frac{\lambda}{2n}$$
$$(Even\ multiples\ of\ \frac{\lambda}{4n})$$

where $N_1 = 0, 1, 2 \ldots$; (d-x) is the distance from the substrate and λ is the wavelength of illumination.

These equations indicate that film thicknesses which differ by a factor of $\frac{\lambda}{2n}$ should exhibit similar optical characteristics, ignoring absorption effects. However, a change in film thickness of one-quarter wavelength will change a standing wave maximum in the standing wave at the surface of the film to a standing wave minimum, and vice versa.

Therefore the thicknesses of the resist films for simulation and experimentation were carefully selected to represent both even and odd multiples of $\frac{\lambda}{4n}$. These films offer optimum conditions for observing variations in linewidth.

For resist,

$$\frac{\lambda}{4n_{res}} = \frac{4358\ A}{4 \times 1.68} = 650 \text{ Angstroms} \qquad (4.1)$$

where n_{res} is the refractive index of photoresist and $\lambda = 4358$ A is the wavelength of the 10X Optimetrix stepper in the EMF. The standard resist coating technique

Wafer No.	$\frac{\lambda}{4n}$ Multiple (650 A)	Resist Thickness (A)
1	16	10400
2	17	11050
3	18	11700
4	19	12350
5	20	13000

Table 4–1 Simulated Resist Thicknesses

in the EMF consists of a 6000 rpm spin of Hunt HPR204 which coats the wafers with approximately 1.1μm of resist. The simulated resist films were chosen to be close to standard thickness, but multiples of 650 A, as shown in Table 4–1.

4.2.2 Standing Wave Profiles

Fig. 4–1 is the simulated standing wave profile for a photoresist film representing an odd multiple of $\frac{\lambda}{4n}$ (650 A) in thickness. Fig. 4–2 is the corresponding profile for an even multiple of $\frac{\lambda}{4n}$ printed at the same exposure. Both plots show a node (minimum) in the standing wave profile at the silicon substrate due to the π phase change occurring at reflection.

The implication of this node at the base of the film is that the thickness of the resist determines the standing wave profile at the surface. For example, if the film accommodates a whole number of standing waves, then there is a node at the surface, mirroring that at the substrate. If however the resist thickness corresponds to an odd number of quarter wavelengths, the node at the substrate results in a standing wave antinode (maximum) at the resist surface, as shown in Fig. 4–3.

At first glance the DEPICT simulated profiles (Figs. 4–1 and 4–2) do not seem to corroborate the theoretical profiles of Fig. 4–3, in terms of the standing waves at the surface of the film. The discrepancy arises due to the resist thickness loss

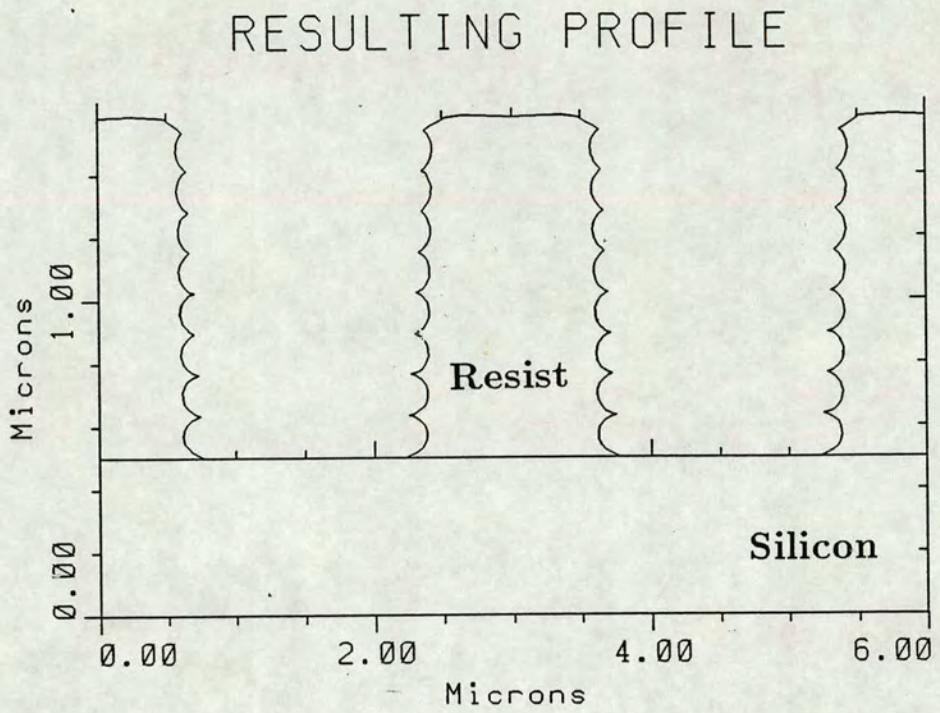

Figure 4–1: DEPICT Simulation Plot of a Single Film of Photoresist $17 \times \frac{\lambda}{4n}$ Thick

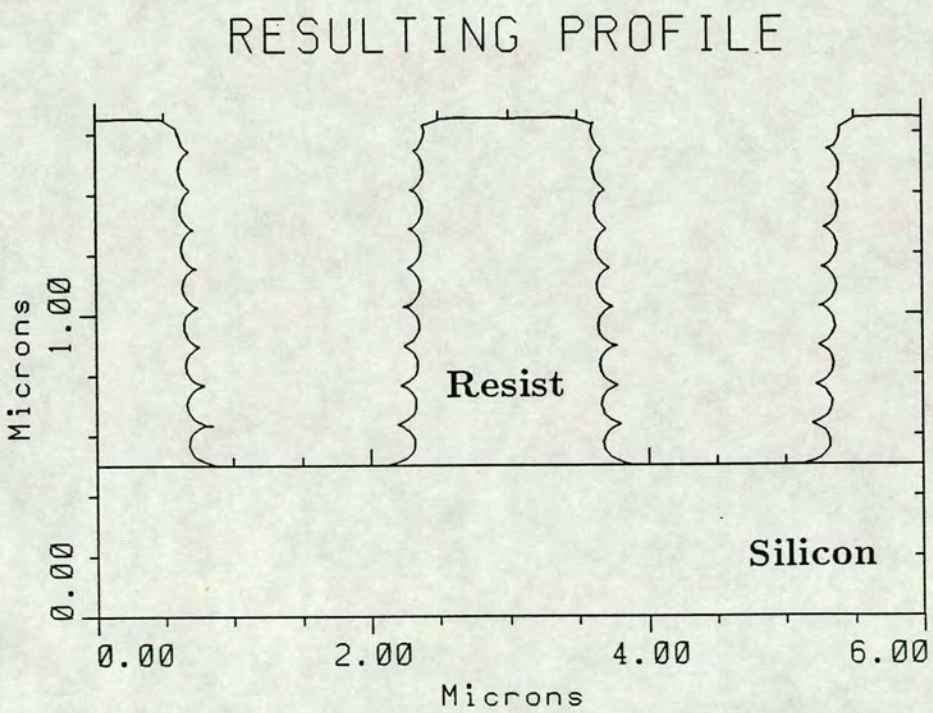

Figure 4–2: DEPICT Simulation Plot of a Single Film of Photoresist $18 \times \frac{\lambda}{4n}$ Thick

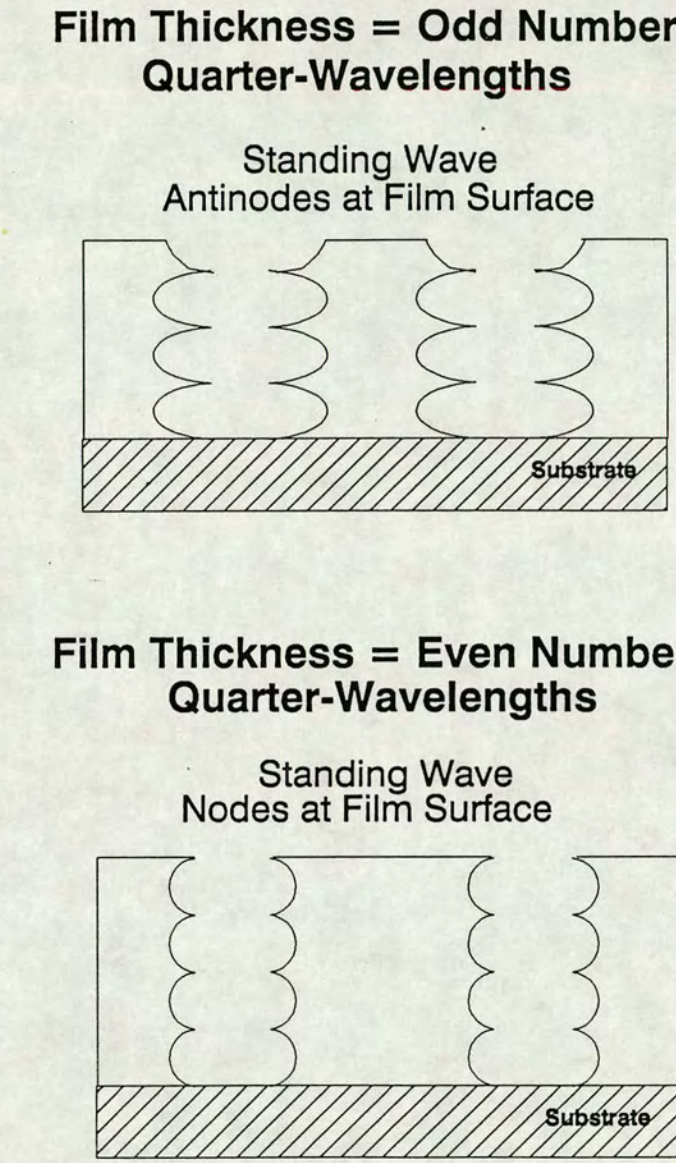

Figure 4–3: Standing Wave Patterns Within Thin Films

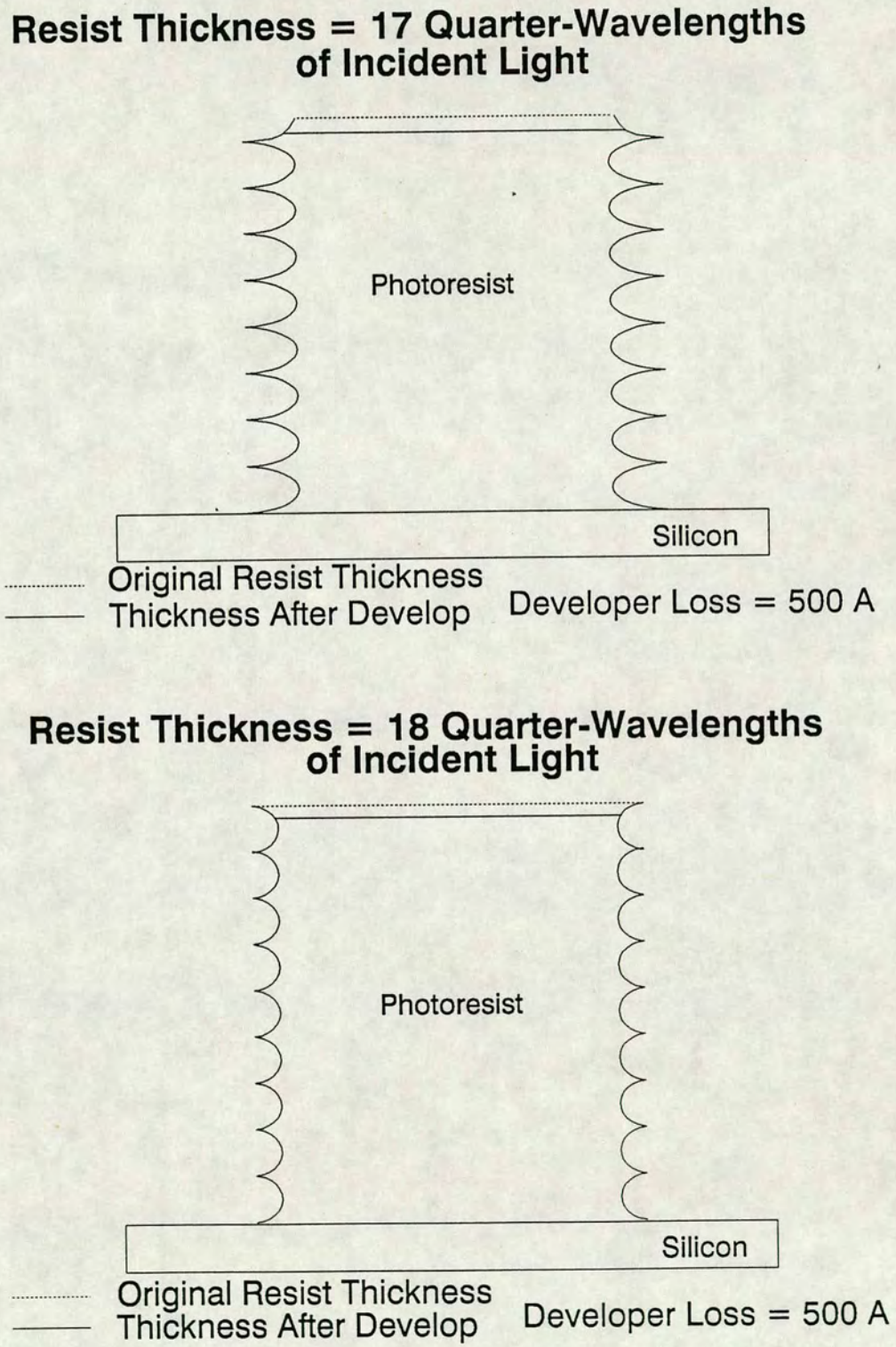

Figure 4–4: Resist Thickness Loss During Development - Single Layer

on the unexposed areas during development. Measurement of the DEPICT profiles reveal that the features have lost approximately 50 nm of resist from the top of the stack. If this loss is taken into consideration then the simulated profiles match the predicted profiles. (See Fig. 4–4).

The resist "developer loss" was measured experimentally to test whether a loss of 50 nm was feasible. Measurements on test wafers of resist thickness before and after develop indicated a loss of 45 nm, confirming that the figure generated by DEPICT was reasonable.

4.2.3 Standing Wave Intensity

Consider again Equation 2.12 which characterizes the *amplitude* of standing waves within thin films:

$$E_{23}(x) = 2E_2 \sin k(d-x) \cos(wt - kd + \phi) \tag{4.2}$$

The envelope function for the *intensity* of the standing wave is:

$$I_{23} = 4I_2 \sin^2 k(d-x) \tag{4.3}$$

Cuthbert [2] has shown mathematically the dependence of the intensity of the standing wave on film thickness. The maximum intensity envelope is given by :

$$I_{\max} = 4I_2(1-r)^{-2} \sin^2 k(d-x) \tag{4.4}$$

when $\mathrm{d} = (2\mathrm{N}_2 + 1)\frac{\lambda}{4\mathrm{n}}$

The minimum intensity envelope is given by:

$$I_{\min} = 4I_2(1+r)^{-2} \sin^2 k(d-x) \tag{4.5}$$

when $\mathrm{d} = \mathrm{N}_2\frac{\lambda}{2\mathrm{n}}$

where $\mathrm{r} = \frac{\mathrm{n}-1}{\mathrm{n}+1}$ is the reflection coefficient at the air/film interface and $\mathrm{N}_2 = 0, 1, 2 \ldots$ for both equations 4.4 and 4.5. These equations stipulate that films of an odd multiple of quarter wavelengths in thickness have a maximum standing wave intensity. Intensity is minimized for films comprising even multiples of $\frac{\lambda}{4\mathrm{n}}$.

4.2.4 Reflectance

Having mathematically determined the relationship between film thickness and standing wave intensity, the next step was to assess the relationship between thickness and reflectance.

It was predicted that films of thickness d = $(2N_2 + 1)\frac{\lambda}{4n}$ which have a maximum standing wave intensity, should have a minimum reflectance, due to a high coupling of energy within the film during exposure. Films of thickness d = $(2N_2)\frac{\lambda}{4n}$ should have a maximum reflectance. Further simulation tests were carried out to test this theory experimentally.

The reflectivity of each resist thickness was checked by creating PC software based on the thin film reflectance algorithm proposed by Fränz and Langheinrich (See Chapter 5, Section 5.2.2). [3]

$$R(\lambda) = \frac{A + X\cos\phi}{B + X\cos\phi} \tag{4.6}$$

$$\phi = \frac{4\pi nd}{\lambda} \tag{4.7}$$

where R(λ) is measured reflectivity at wavelength λ; A,B and X are functions of Fresnel coefficients and are functions of λ; n is refractive index and d is film thickness.

Figs. 4–5 and 4–6 confirm that when λ = 435.8 nm there is a minimum reflectance for films of optical thickness equal to an odd number of quarter wavelengths, and a maximum reflectance for films equal to an even number of quarter wavelengths.

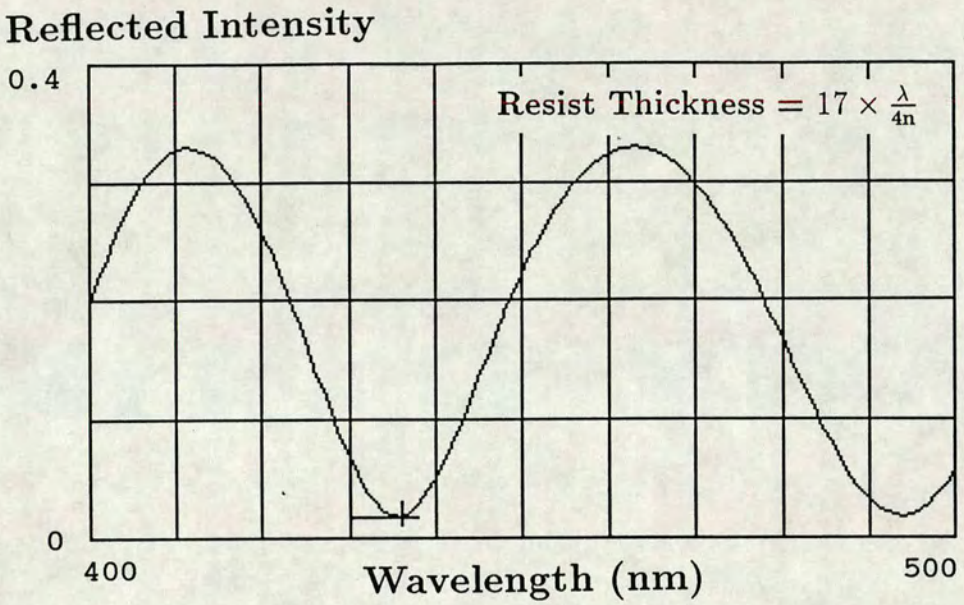

Figure 4–5: Reflectance of a Resist Film $17 \times \frac{\lambda}{4n}$ Thick

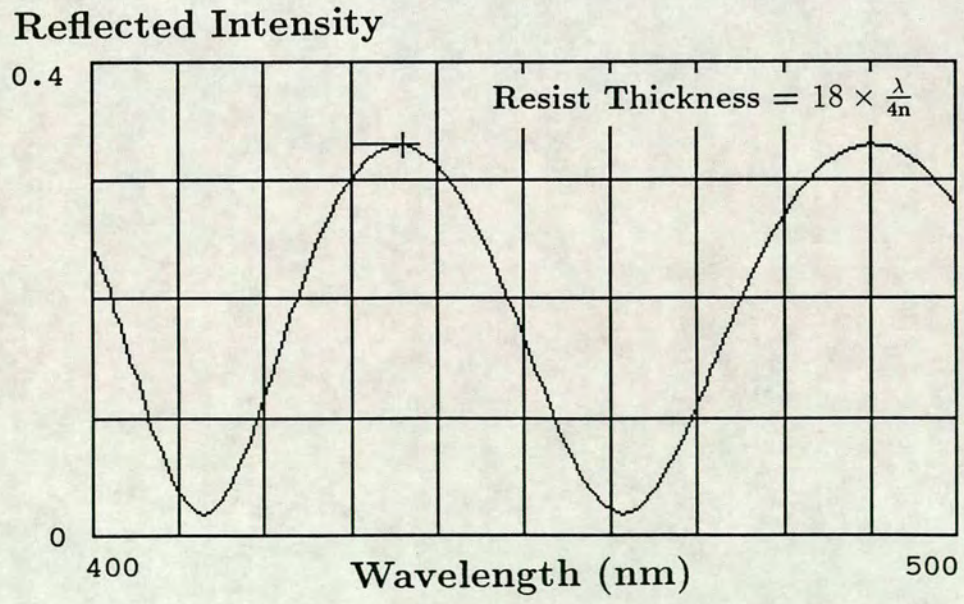

Figure 4–6: Reflectance of a Resist Film $18 \times \frac{\lambda}{4n}$ Thick

4.2.5 Threshold Exposure

The threshold dose is established by increasing the exposure dose until the resist profiles break through to the underlying substrate (See Fig. 4–7). A graph of exposure times required to clear the resist versus thickness (a "swing curve") shows that the minimum exposure times correspond to resist films with minimum reflectivity, whereas maximum times are required for highly reflective films. (See Fig. 4–8) The upward overall trend of the graph indicates that higher exposure doses are needed to clear the resist as the thickness of the film increases.

In industry, resist thicknesses are often chosen which represent the turning values of the "swing curve". The threshold exposure of these films is least sensitive to variations in resist thickness. In addition, positive and negative excursions in thickness have the same effect on E_0.

4.2.6 Linewidth

CD was measured from the simulated resist images by measuring the width of the profile at the "waist" of the standing wave pattern nearest the substrate, as described in Chapter 2 (Section 2.5).

The results show that, since all the films were exposed with the same dose, there is a periodic variation of linewidth as resist thickness is varied, with $\Delta CD \approx 0.15\mu m$. (See Fig. 4–9) As expected, the minimum linewidths occur for resist thicknesses that have minimum exposure threshold, whereas maximum linewidths correspond to thicknesses which require maximum exposure times to clear the resist.

CD should be less sensitive to variations in resist thickness at the turning values of this curve.

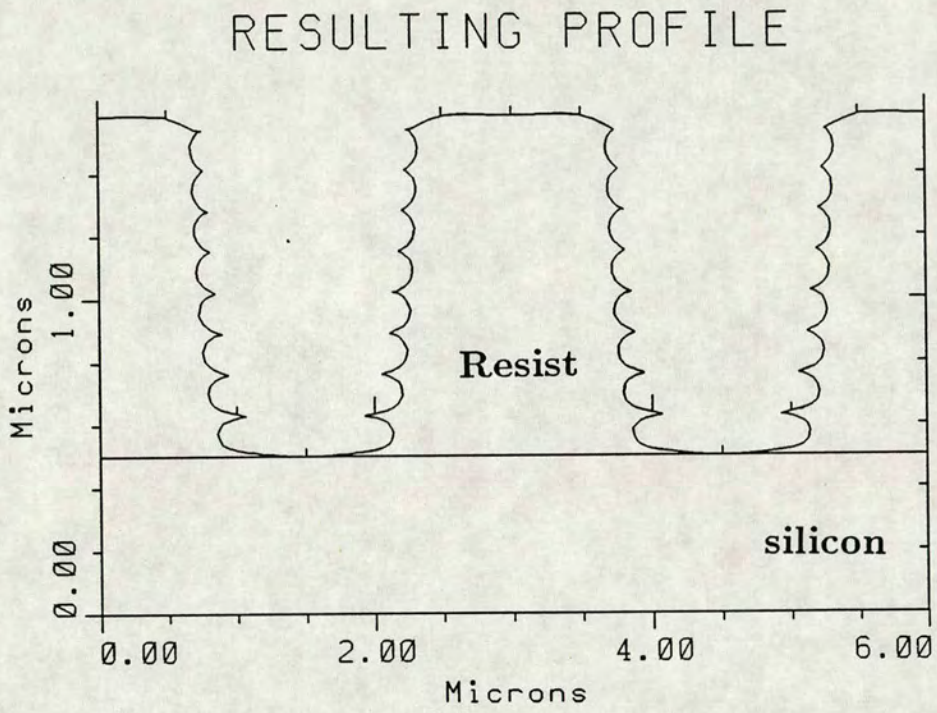

Figure 4–7: Determination of Threshold Exposure

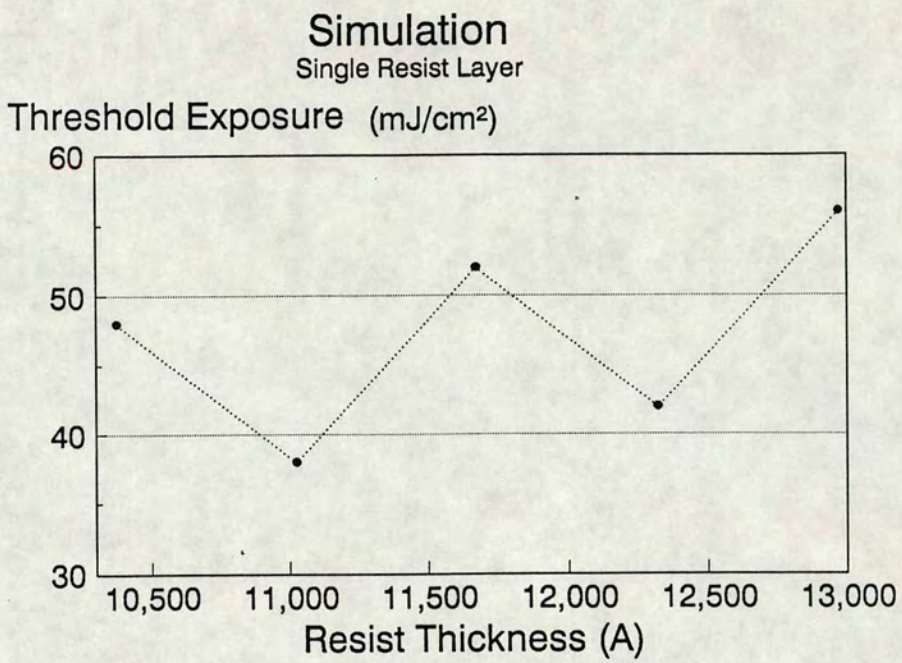

Figure 4–8: Threshold Exposure Versus Resist Thickness ("Swing Curve")

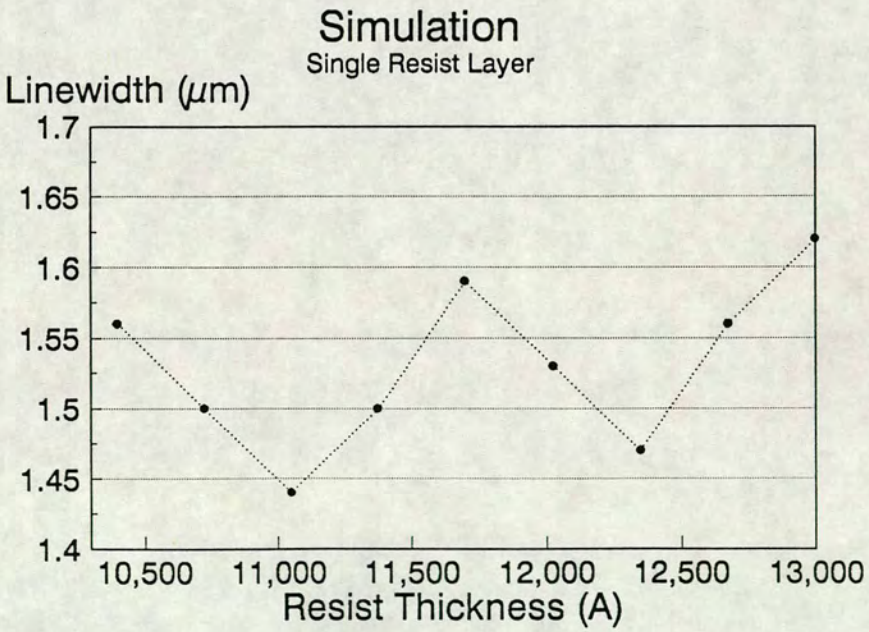

Figure 4–9: CD Versus Resist Thickness

4.2.7 Summary: Single Layer Films

These observations for single layer films can be summarized in the following manner: (See Fig. 4–10).

- Standing wave minimum at substrate due to π phase change
- Resist thickness determines standing wave profile at surface of resist and the intensity of the standing wave within the film
- Standing wave antinode at surface (odd number of quarter wavelengths thickness $d = (2N_2 + 1)\frac{\lambda}{4n}$)

  $\Rightarrow$ Maximum energy coupled into resist
  $\Rightarrow$ Maximum standing wave intensity
  $\Rightarrow$ Minimum reflectance
  $\Rightarrow$ Low exposure times (minimum turning values on E_0 "swing curve")
  $\Rightarrow$ Decreased linewidth

- Standing wave node at surface (even number of quarter wavelengths thickness $d = (2N_2)\frac{\lambda}{4n}$)

  $\Rightarrow$ Minimum energy coupling
  $\Rightarrow$ Minimum standing wave intensity
  $\Rightarrow$ Maximum reflectance
  $\Rightarrow$ High exposure times (maximum turning values on E_0 "swing curve")
  $\Rightarrow$ Increased linewidth

Consideration of these results suggests that single layer resist thicknesses should be chosen which represent either a maximum or a minimum in the threhold exposure "swing curve". Linewidth control is optimized for these films, since small variations in thickness cause minimal variations in the energy required to expose the resist. Ideally a minimum turning value should be selected $d = (2N_2 + 1)\frac{\lambda}{4n}$ since exposure time is minimized for these films.

Film Thickness = 7 Quarter-Wavelengths

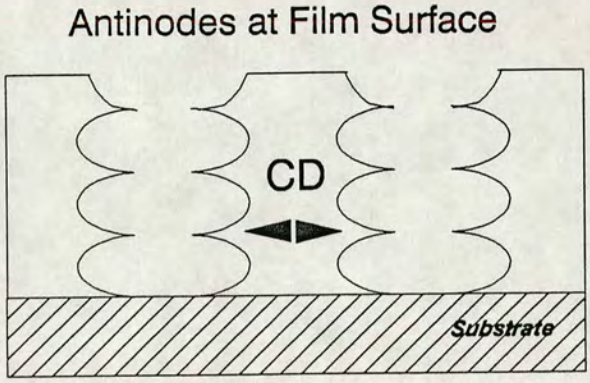

Max. Standing Wave Intensity
Max. Energy Coupling
Min. Reflectance
Low Exposure Times
Decreased Linewidth

Film Thickness = 8 Quarter-Wavelengths

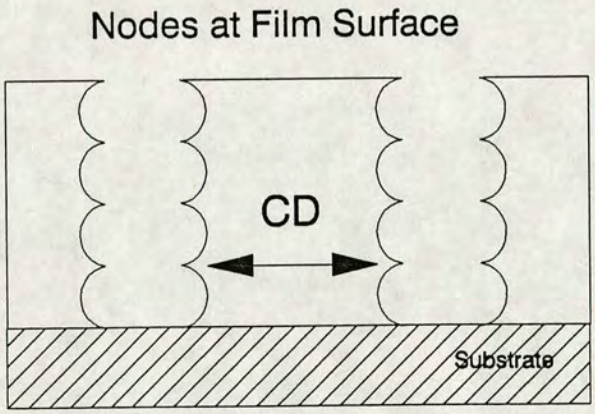

Min. Standing Wave Intensity
Min. Energy Coupling
Max. Reflectance
High Exposure Times
Increased Linewidth

Standing Wave Period = Half the Wavelength of Incident Light in the Photoresist

Figure 4–10: Optical Characteristics of Single Layer Films

Wafer No.	$\frac{\lambda}{4n}$ Multiple (750 A)	Oxide Thickness (A)
1	8	6000
2	9	6750
3	10	7500
4	11	8250
5	12	9000

Table 4–2 Oxide Film Thicknesses

Having developed this theory for single films the next step was to adapt it to multiple film stacks.

4.3 Simulation: Double Layer Films

A two-layer film consisting of photoresist on oxide was chosen for simulation. Oxide films were used because they represent the most commonly used dielectric in semiconductor processing. Oxide films are also easily grown, which facilitates later experiments on test wafers.

The film thickness multiple $\frac{\lambda}{4n_{ox}}$ for oxide is:

$$\frac{\lambda}{4n_{ox}} = \frac{4358\ A}{4 \times 1.45} = 750 \text{ Angstroms} \tag{4.8}$$

where n_{ox} is the refractive index of silicon dioxide.

Five oxide films representing odd and even multiples of 750 A were selected for simulation. These were combined with five different resist coatings, multiples of 650 A. (See Tables 4–1 and 4–2).

Fig. 4–11 shows the major reflections inside a two-layer film on a silicon substrate. The refractive indices of common resists ($n_{res} = 1.68$) are very close to that of silicon dioxide ($n_{ox} = 1.45$). This means that the reflections which occur at the resist/oxide interface are very weak, and to a good approximation can be ignored.

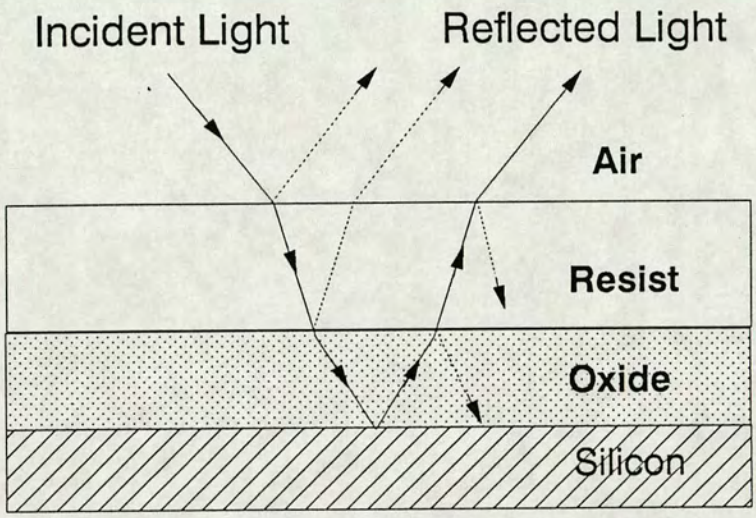

Figure 4–11: Double Layer Film Physics Showing the Reflectance at Each Film Interface. The Major Rays are Shown as Unbroken Lines, the Lesser Rays are Dotted

Oxide Thickness (A)	No. standing Waves In Oxide Film	Resist/Oxide Interface	
		Predicted Profile	Simulated Profile
6000	4	node	node
6750	$4\frac{1}{2}$	antinode	antinode
7500	5	node	node
8250	$5\frac{1}{2}$	antinode	antinode
9000	6	node	node

Table 4–3 Standing Wave Profiles at the Resist/Oxide Interface

4.3.1 Standing Wave Profiles

Oxide Film

In order to apply the theory developed for single layer films, it is most convenient to consider this stack beginning at the substrate and working upwards. In the previous section it was shown that there is always a standing wave minimum (node) at the silicon substrate due to the π phase change occurring at reflection. This enables a prediction of the intensity profile at the resist/oxide interface, providing the oxide thickness is known. The period of the standing wave within the oxide film is:

$$T_{sw}(oxide) = \frac{\lambda}{2n_{ox}} = \frac{4358 \text{ A}}{2 \times 1.45} = 1500 \text{ Angstroms}$$

Figs. 4–12 and 4–13 are the simulation plots for a resist film $17 \times \frac{\lambda}{4n}$ thick with underlying oxide films ranging in thickness from 6000 A to 9000 A. Table 4–3 shows the agreement between predicted intensity profiles at the resist/oxide interface with those simulated by DEPICT. This result confirms that, although the standing wave profile at the base of the oxide film cannot be seen in the DEPICT plot, it must be a node in each case, as predicted.

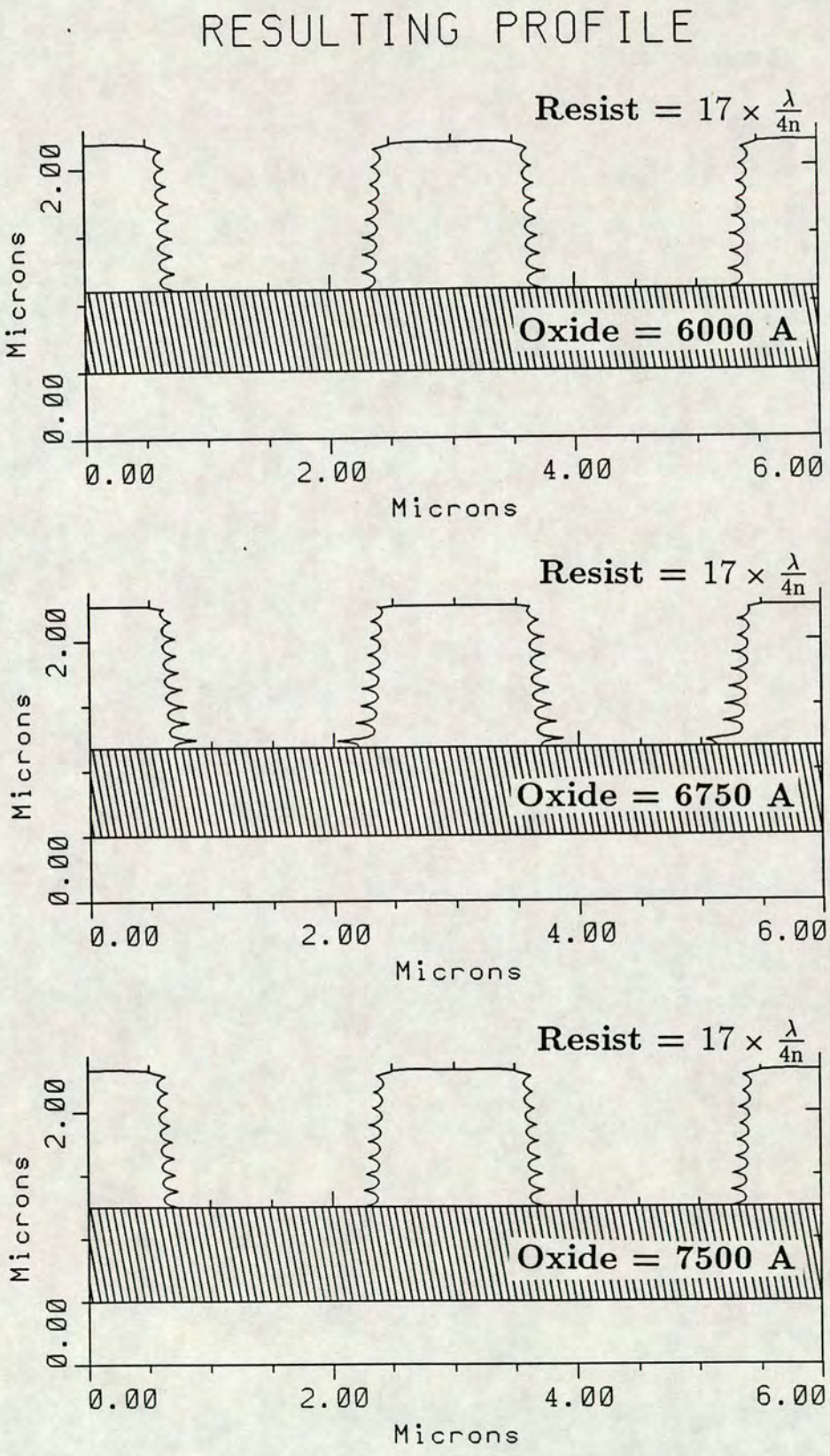

Figure 4–12: DEPICT Simulation Plot for Resist on Oxide Film Stacks: Resist Thickness = $17 \times \frac{\lambda}{4n}$, Oxide Thickness Range = 6000 - 7500 A

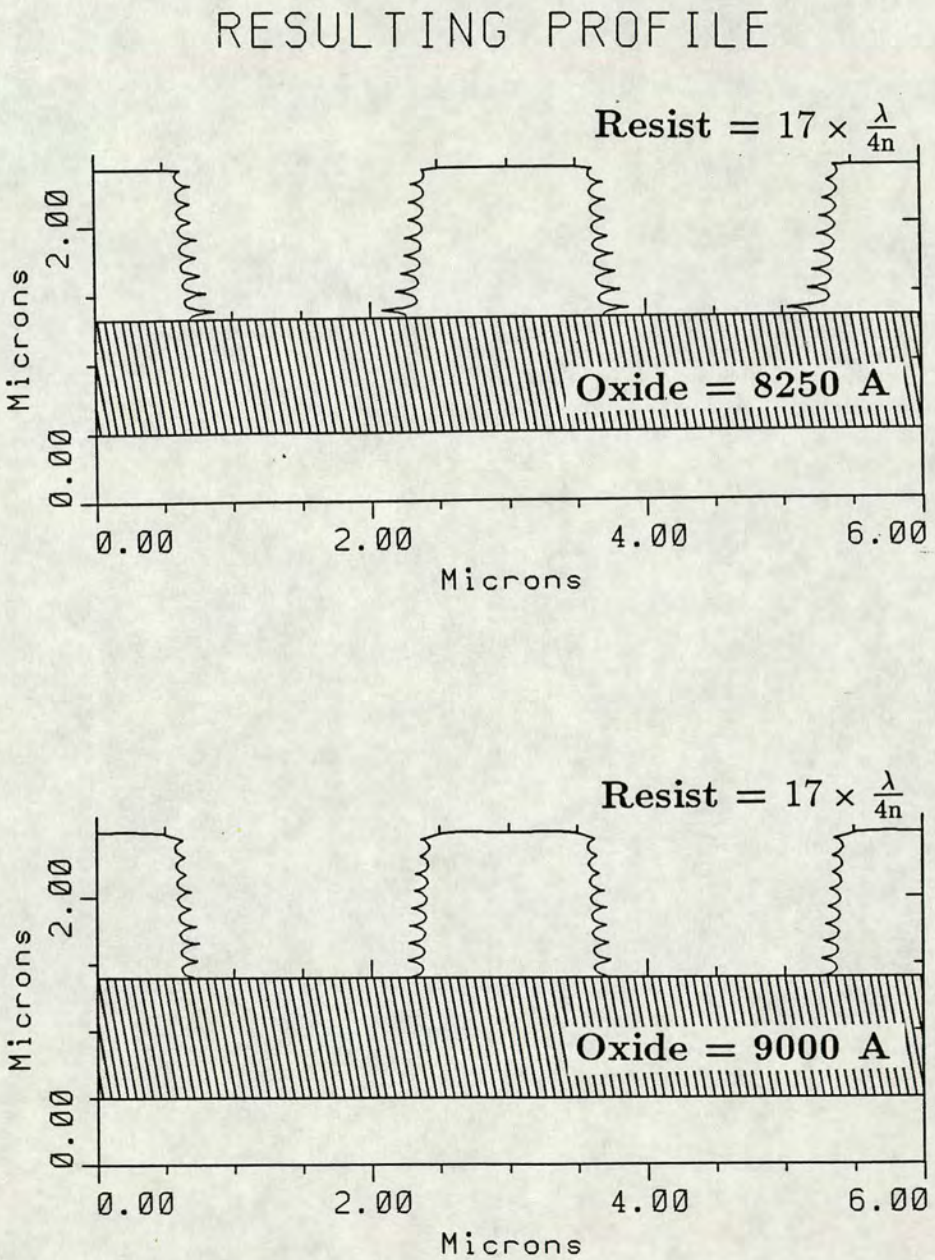

Figure 4–13: DEPICT Simulation Plot for Resist on Oxide Film Stacks: Resist Thickness = $17 \times \frac{\lambda}{4n}$, Oxide Thickness Range = 8250 - 9000 A

Figs. 4–14 and 4–15 are the corresponding simulations for the oxide films with a resist coating $18 \times \frac{\lambda}{4n}$. These plots have identical intensity profiles at the resist/oxide interface as the previous plots with the thinner resist coating. This suggests that the standing wave at the resist/oxide interface is determined by the oxide thickness.

Resist Film

A similar investigation was carried out on the standing waves in the resist film i.e. to predict the intensity profile at the resist/air interface knowing the profile at the oxide/resist interface. The period of the standing wave within resist is:

$$T_{sw}(resist) = \frac{\lambda}{2n_{res}} = \frac{4358 \text{ A}}{2 \times 1.68} = 1300 \text{ Angstroms}$$

The resist thicknesses chosen represent even and odd multiples of quarter wavelengths. In the former case $d = (2N_2)\frac{\lambda}{4n}$ the film accommodates a whole number of standing waves; therefore the profile at the top of the film should be the same as at the bottom. In the latter case $d = (2N_2 + 1)\frac{\lambda}{4n}$ the film does not represent a whole number of standing waves; in this case a node at the base of the film should translate to an antinode at the surface (and vice versa).

These results are corroborated by the DEPICT simulations if, as before, the "developer loss" of approximately 50 nm from the surface of the unexposed resist is taken into consideration. Fig. 4–16 shows the effects of the reduction in resist thickness caused by the develop process. The first film is $17 \times \frac{\lambda}{4n}$ thick. As predicted, if before development there is a standing wave minimum at the oxide/resist interface, there is a maximum at the resist surface. The second film is $18 \times \frac{\lambda}{4n}$ thick, and as expected, a node at the resist/oxide interface translates to a node at the resist/air interface. Table 4–4 compares the predicted intensity profiles with those generated by DEPICT.

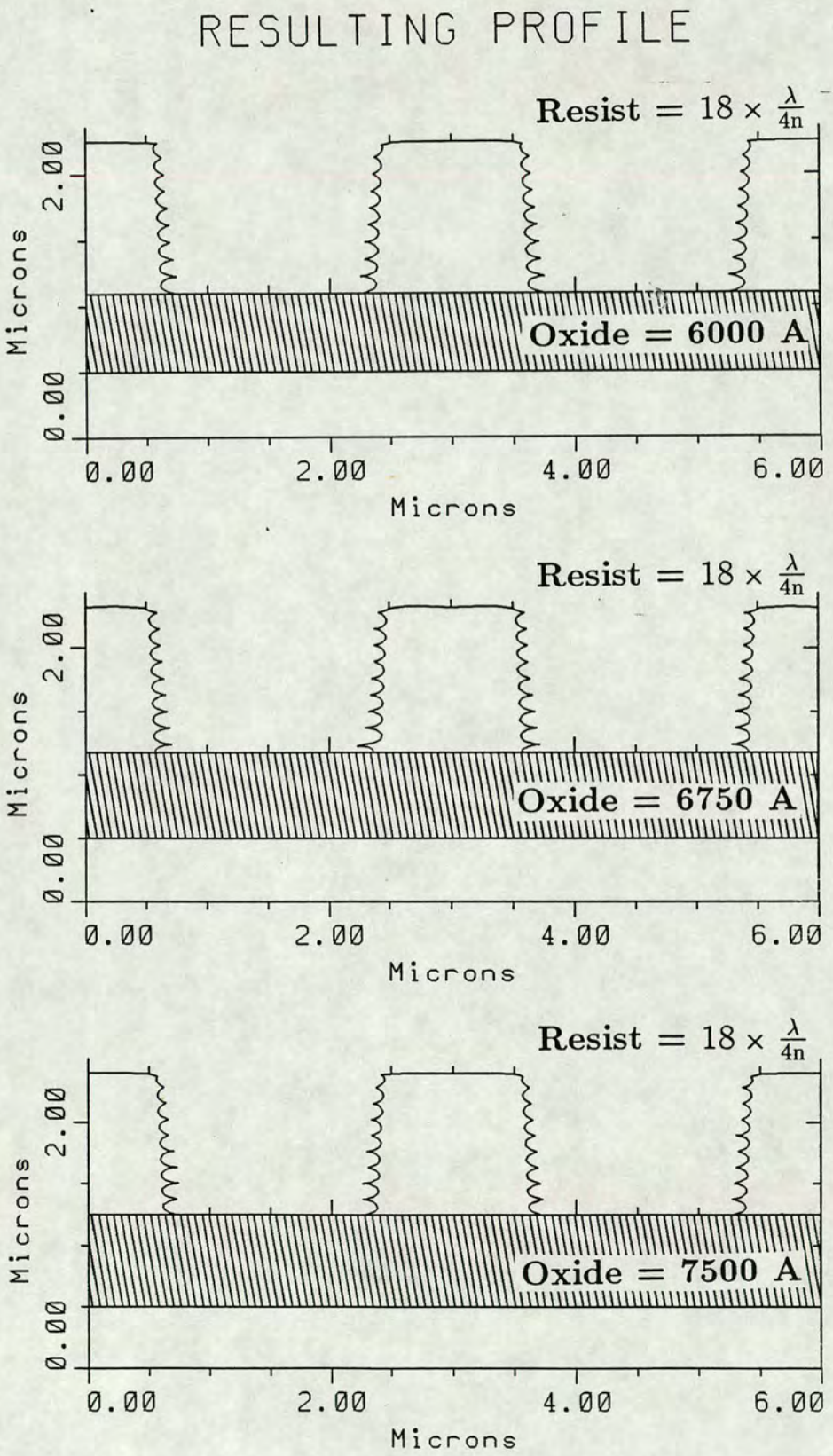

Figure 4–14: DEPICT Simulation Plot for Resist on Oxide Film Stacks: Resist Thickness = $18 \times \frac{\lambda}{4n}$, Oxide Thickness Range = 6000 - 7500 A

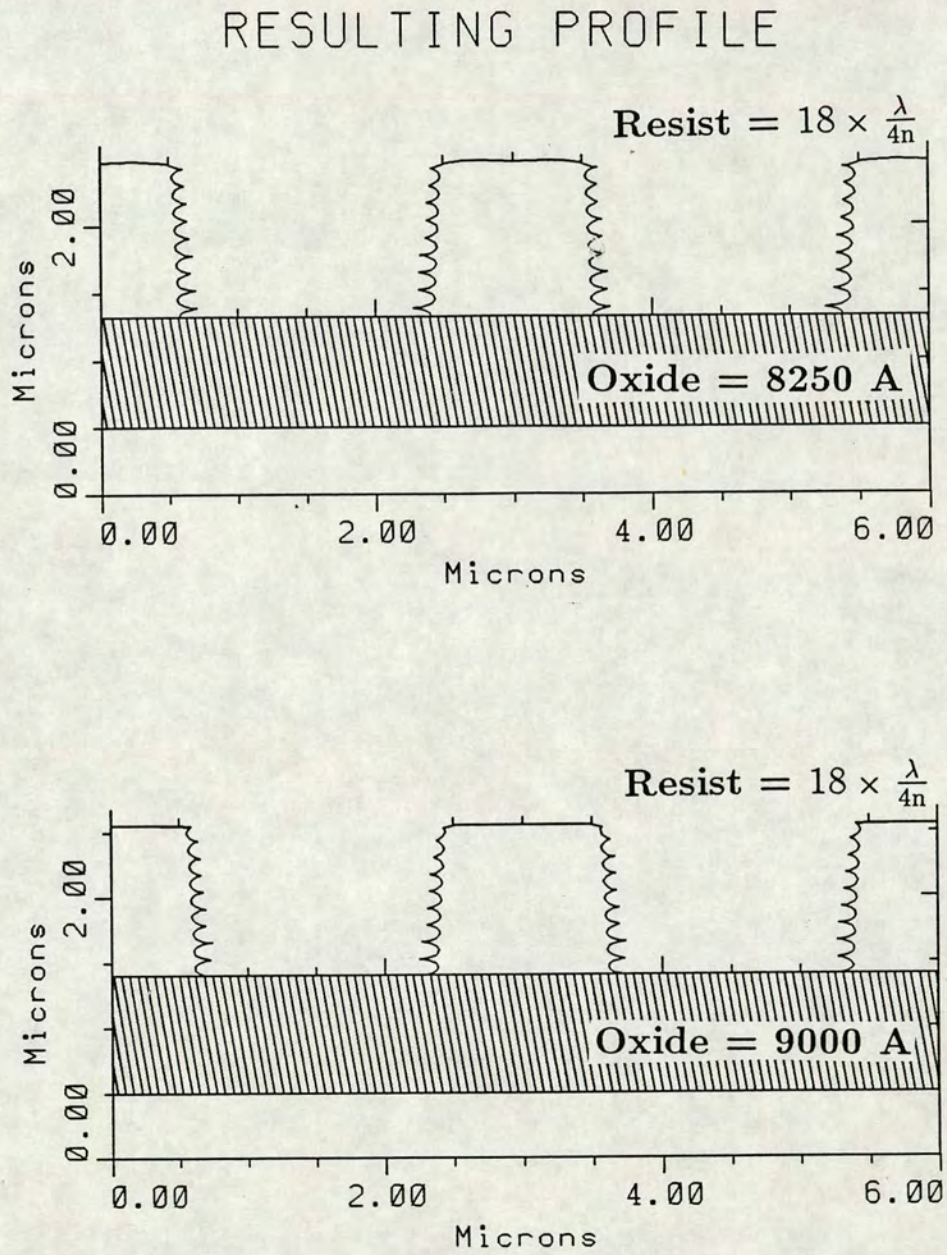

Figure 4–15: DEPICT Simulation Plot for Resist on Oxide Film Stacks: Resist Thickness = $18 \times \frac{\lambda}{4n}$, Oxide Thickness Range = 8250 - 9000 A

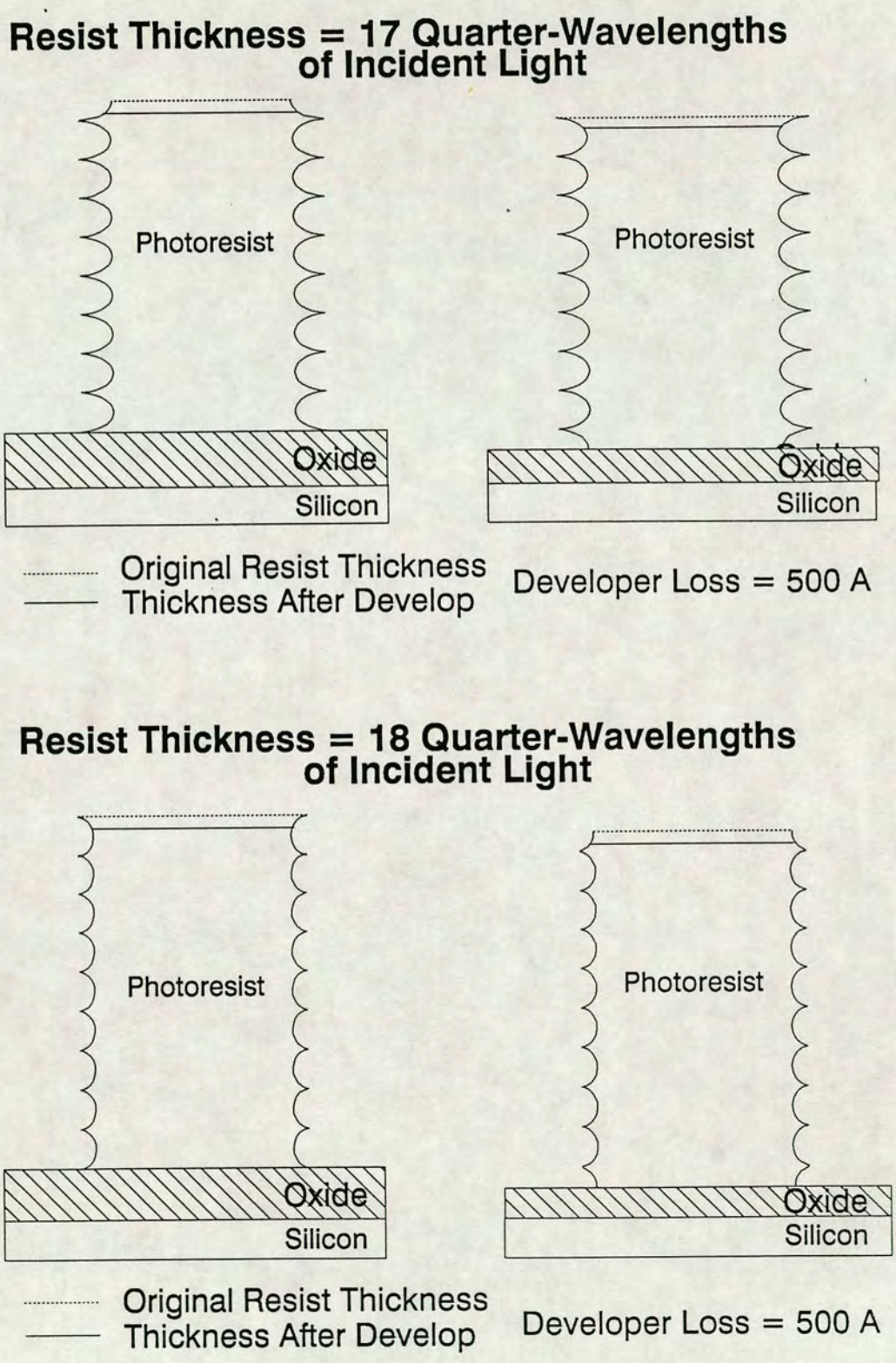

Figure 4–16: Resist Thickness Loss During Development - Double Layer

Resist Thickness Multiple ($\frac{\lambda}{4n}$)	Oxide/Resist Interface	Resist/Air Interface	
		Predicted Profile	Simulated Profile
17	node	antinode	antinode
	antinode	node	node
18	node	node	node
	antinode	antinode	antinode

Table 4–4 Standing Wave Profiles at the Resist/Air Interface

4.3.2 Reflectance

Having ascertained the standing wave profiles throughout the film stack, the next stage was to establish the relationship between film thickness and the overall reflectance of the stack. The simple reflectivity algorithms used for single layer films cannot be applied to multiple layers. However, a mathematical model which predicts reflectance for multilayer thin-film stacks was found and implemented [4]. The model is based upon a matrix formulation of the boundary conditions of the E and H fields at each thin-film interface. The elements of each "characteristic" matrix (M_i) are a function of the film thicknesses, refractive indices and the angle of incidence of the incoming light. The intensity reflectance coefficient *(R)* of a film stack consisting of n layers is then expressed in terms of the elements of the product matrix $M = M_1 \times M_2 \ldots M_n$.

Software based on this algorithm was written for a two-layer, resist-on-oxide stack. Figs. 4–17 and 4–18 show how reflectance varies with oxide thickness for five different oxide films. Fig. 4–17 was generated for a resist thickness of $17 \times \frac{\lambda}{4n}$. Fig. 4–18 corresponds to a resist coating of $18 \times \frac{\lambda}{4n}$. In each case the peak reflectances on the graphs correspond to DEPICT simulations which have a composite film thickness comprising an even number of quarter wavelengths. Film stacks which have a total thickness equal to an odd multiple of $\frac{\lambda}{4n}$ have a minimum reflectance.

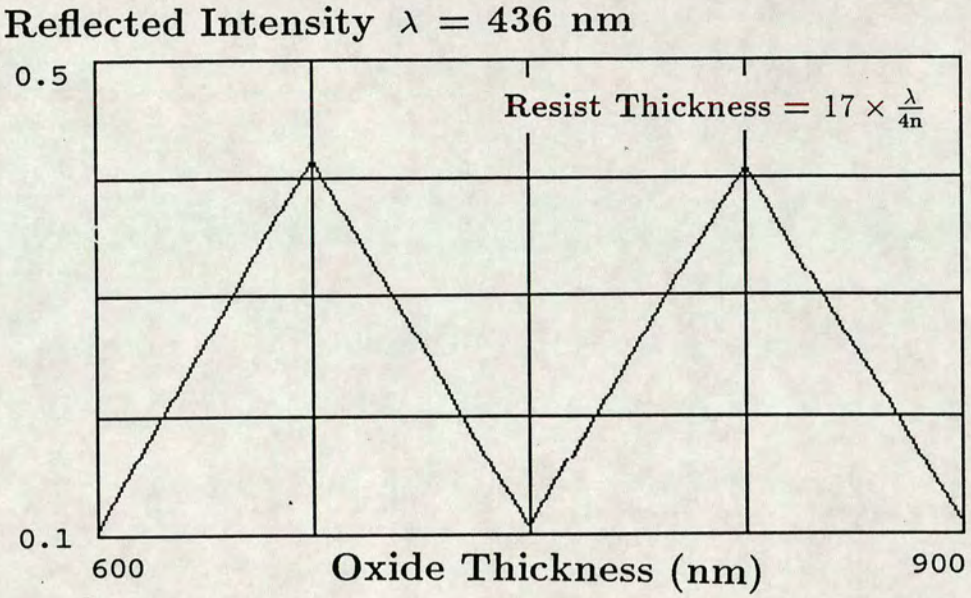

Figure 4–17: Reflectance Versus Oxide Thickness for Resist Film $17 \times \frac{\lambda}{4n}$ Thick

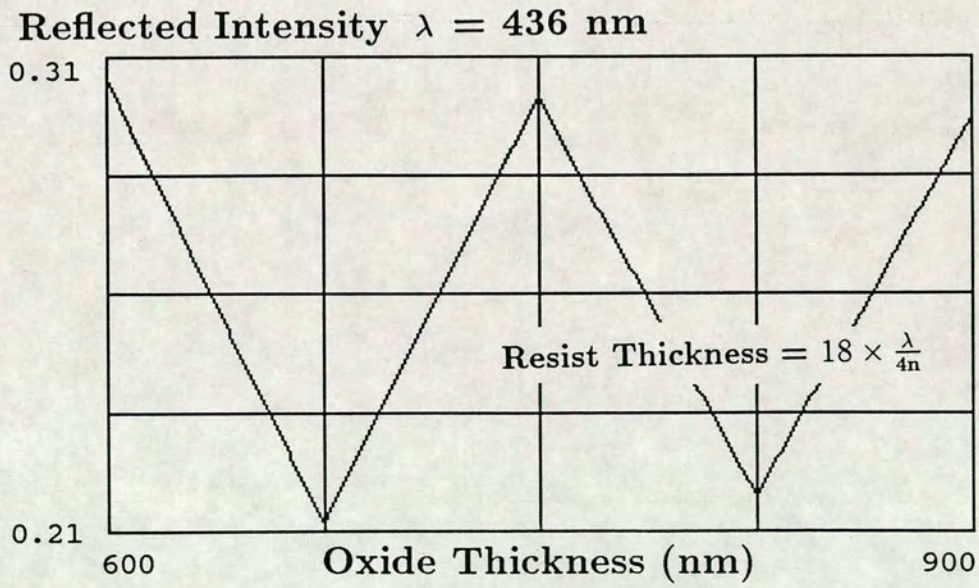

Figure 4–18: Reflectance Versus Oxide Thickness for Resist Film $18 \times \frac{\lambda}{4n}$ Thick

4.3.3 Threshold Exposure

The threshold exposure of each resist/oxide film was simulated using DEPICT. Fig. 4–19 shows the variation in threshold exposure with oxide thickness for several different resist layers. Comparison of this result with Figs. 4–17 and 4–18 reveals that there is a direct relationship between threshold exposure and reflectance. As expected, films that are highly reflective require higher exposure times to clear the resist.

Both resist films $d_r = (17 \times \frac{\lambda}{4n})$ and $d_r = (18 \times \frac{\lambda}{4n})$ experience a significant change in threshold exposure as the thickness of the underlying oxide is varied. A resist film $d_r = (17\frac{1}{2} \times \frac{\lambda}{4n})$ is significantly less sensitive to variations in oxide thickness.

4.3.4 Linewidth

The effect of differences in threshold exposure for each film stack on the linewidth dimensions can be seen in Fig. 4–20. As shown in the previous section, film stacks that are highly reflective have a high threshold exposure; whereas low reflectance films require lower exposure times to clear the resist. Therefore if films of varying reflectance are exposed at equal dose, the resulting features will vary in size. Highly reflective films produce comparatively large linewidth dimensions; films that are less reflective produce smaller linewidths.

Comparison with Fig. 4–19 confirms that resist films of thickness $d_r = (17 \times \frac{\lambda}{4n})$ and $d_r = (18 \times \frac{\lambda}{4n})$ produce a greater variation in linewidth than the intermediate resist thickness $d_r = (17\frac{1}{2} \times \frac{\lambda}{4n})$.

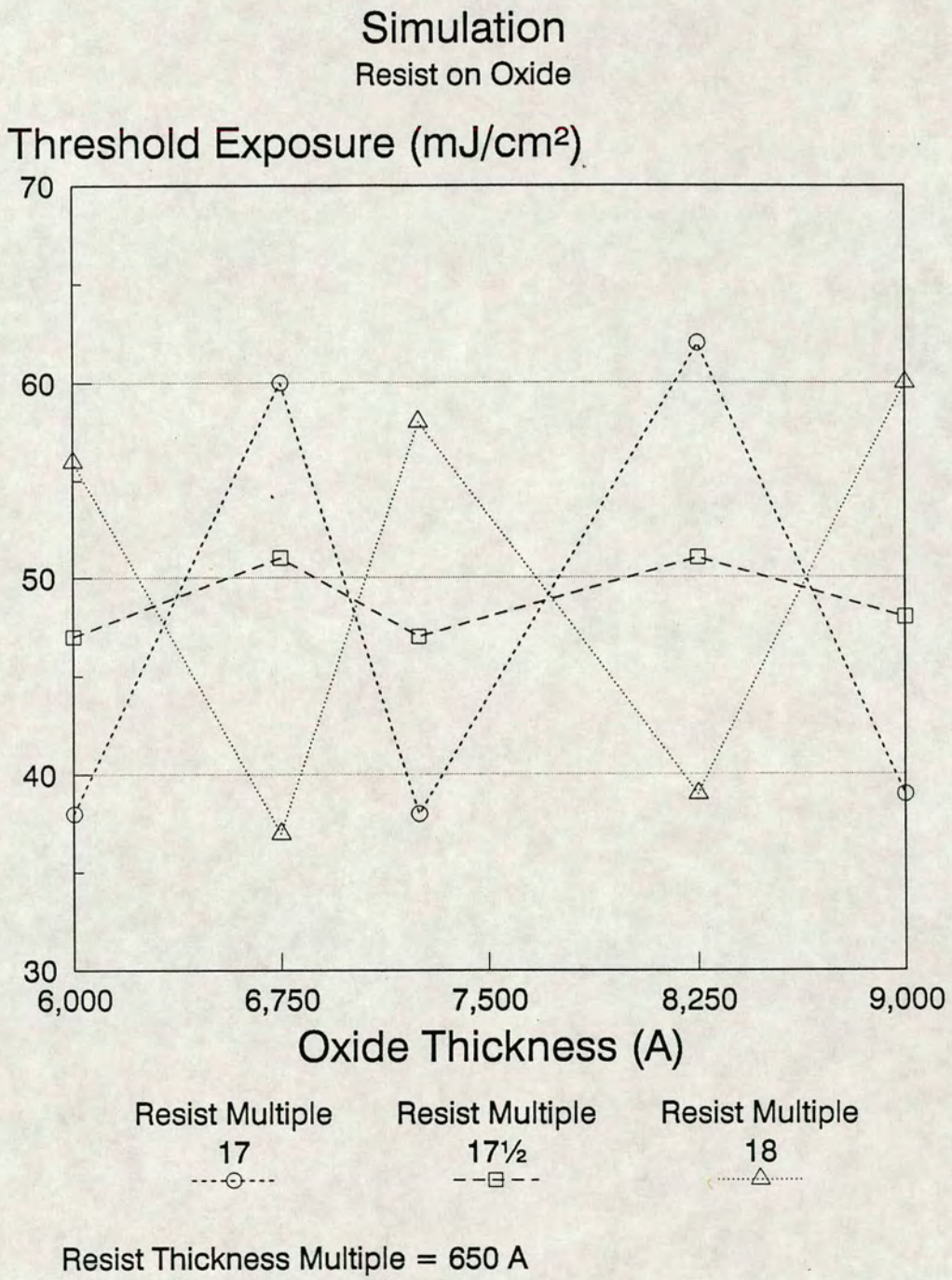

Figure 4–19: Threshold Exposure Versus Oxide Thickness

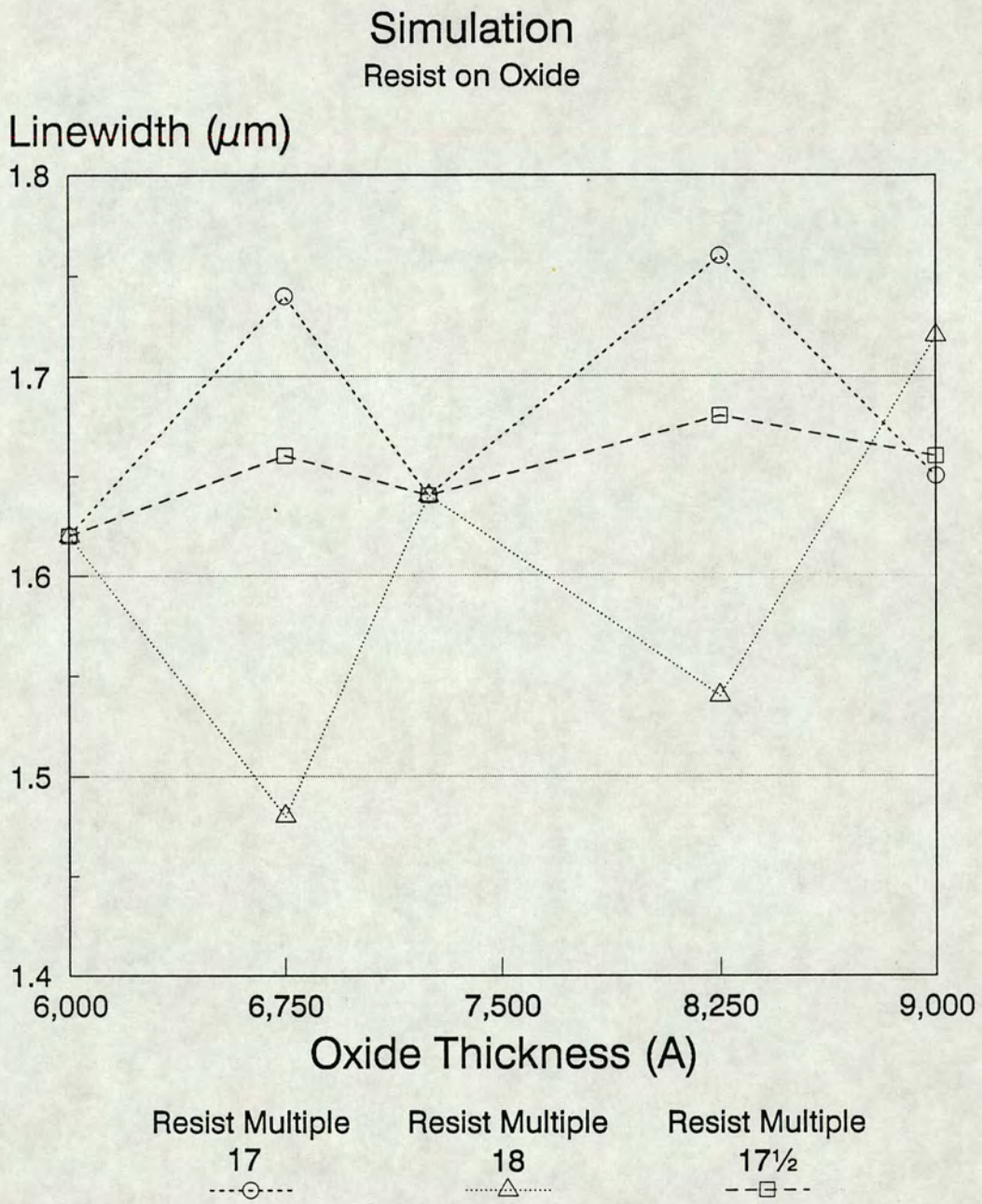

Figure 4–20: CD Versus Oxide Thickness

4.3.5 Summary: Double Layer Films

The results from the simulation experiments on double layer films can be summarized as follows:

- A π phase change occurs at reflection from the silicon surface, creating a node in the standing wave pattern at the base of the oxide layer
- The thickness of the oxide film determines the standing wave profile at the resist/oxide interface.
- The composite thickness of the stack determines the intensity of the standing waves within the stack:

  Total thickness equal to odd multiple $\frac{\lambda}{4n}$ $\rightarrow$ Maximum standing wave intensity
  Total thickness equal to even multiple $\frac{\lambda}{4n}$ $\rightarrow$ Minimum standing wave intensity

- Reflectance of the stack is affected by the standing wave profile at the surface of the film

  Standing wave antinode $\rightarrow$ Low reflectance
  Standing wave node $\rightarrow$ High reflectance

- Threshold exposure is dependent on reflectivity:

  Low reflectance $\rightarrow$ Maximal coupling of energy into film
  $\rightarrow$ Low exposure times to clear resist
  High reflectance $\rightarrow$ Minimal coupling of energy into film
  $\rightarrow$ High exposure times to clear resist

- Linewidth is affected by threshold exposure levels:

  Low threshold exposure $\rightarrow$ Decreased linewidth
  High threshold exposure $\rightarrow$ Increased linewidth

4.4 Experimentation

Having investigated the theoretical relationship between film thickness and CD, it was necessary to confirm the results by experimental means. Resist on oxide film stacks identical to those simulated in the previous section were fabricated for testing.

Five different thicknesses of oxide were grown onto bare silicon wafers. These thicknesses were multiples of 750 A, corresponding to the quarter wavelength of light travelling through an oxide film. (See Table 4–2).

A spinspeed curve was generated to find the speeds required to coat the wafers with the target photoresist thicknesses. These films were approximately 1μm thick, but multiples of 650 A.

1. Experiment 1 involved coating the five oxidized wafers with a resist film of thickness ($17 \times \frac{\lambda}{4n}$). These wafers were printed with the EMF resolution test pattern, which consists of a series of gratings and line/space modules, and the 1.0, 1.2, 1.4, 1.5 and 1.6 μm lines within a centrally located die were measured in the Nanolab SEM.

2. Having extracted linewidth data for each wafer, the wafers were stripped of resist and recoated with ($18 \times \frac{\lambda}{4n}$) for the second experiment in the series.

3. For the third experiment a resist coating of ($17.5 \times \frac{\lambda}{4n}$) was used.

4.4.1 Results

1. Fig. 4–21 shows the results for Experiment 1 (resist thickness $= 17 \times \frac{\lambda}{4n}$). There is a variation in linewidth of approximately 0.1μm for each photoresist line as the underlying oxide film changes. This corresponds to a 6% variation in linewidth for the 1.6μm line and 10% for the 1.0μm feature.

2. Fig. 4–22 is the corresponding graph of results for Experiment 2 when the resist coating was $18 \times \frac{\lambda}{4n}$ thick. Once again the variation in dimensions (ΔCD) for all lines is approximately 0.1μm. However in this case, the variations are in the opposite sense to the previous graph: where Fig. 4–21 indicates a positive swing in ΔCD, Fig. 4–22 indicates a negative swing and vice versa.

3. Fig. 4–23 shows the results for Experiment 3 (nominal 1.0μm line) with an intermediate resist thickness of $17.5 \times \frac{\lambda}{4n}$. The variation in linewidth is approximately half that of the previous cases, with $\Delta\text{CD} \approx 0.05\mu$m.

4.4.2 Discussion

From these results it can be seen that the theory developed for single and double films has been shown to work on test wafers. Fig. 4–20, which simulates the effect of variations in resist and oxide thicknesses on linewidth, matches the results obtained experimentally on the SEM (See Figs. 4–21 and 4–22). Evidently the combined thicknesses of the oxide and resist films have a direct influence on CD.

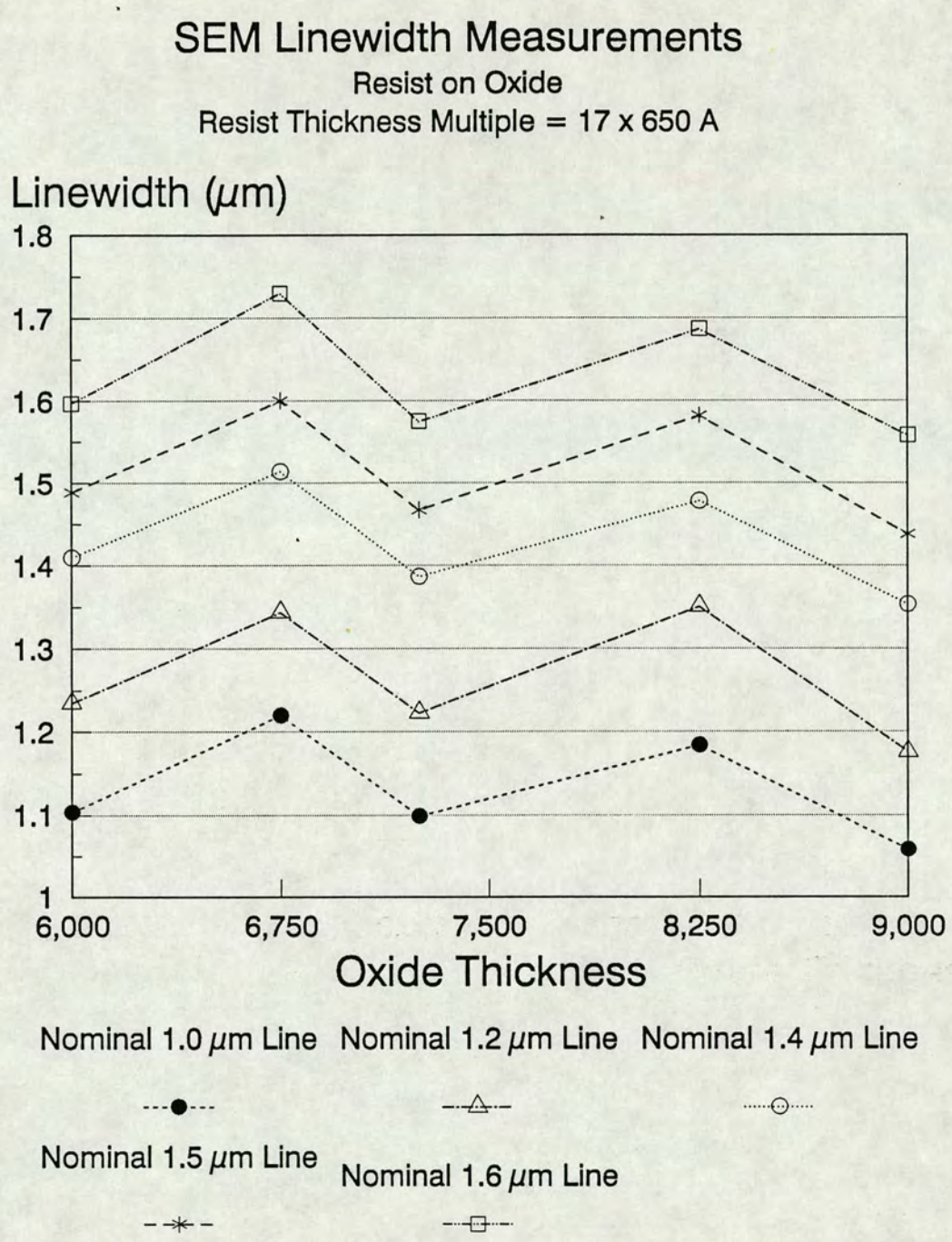

Figure 4–21: SEM CD vs Oxide Thickness: Resist Thickness = $17 \times \frac{\lambda}{4n}$

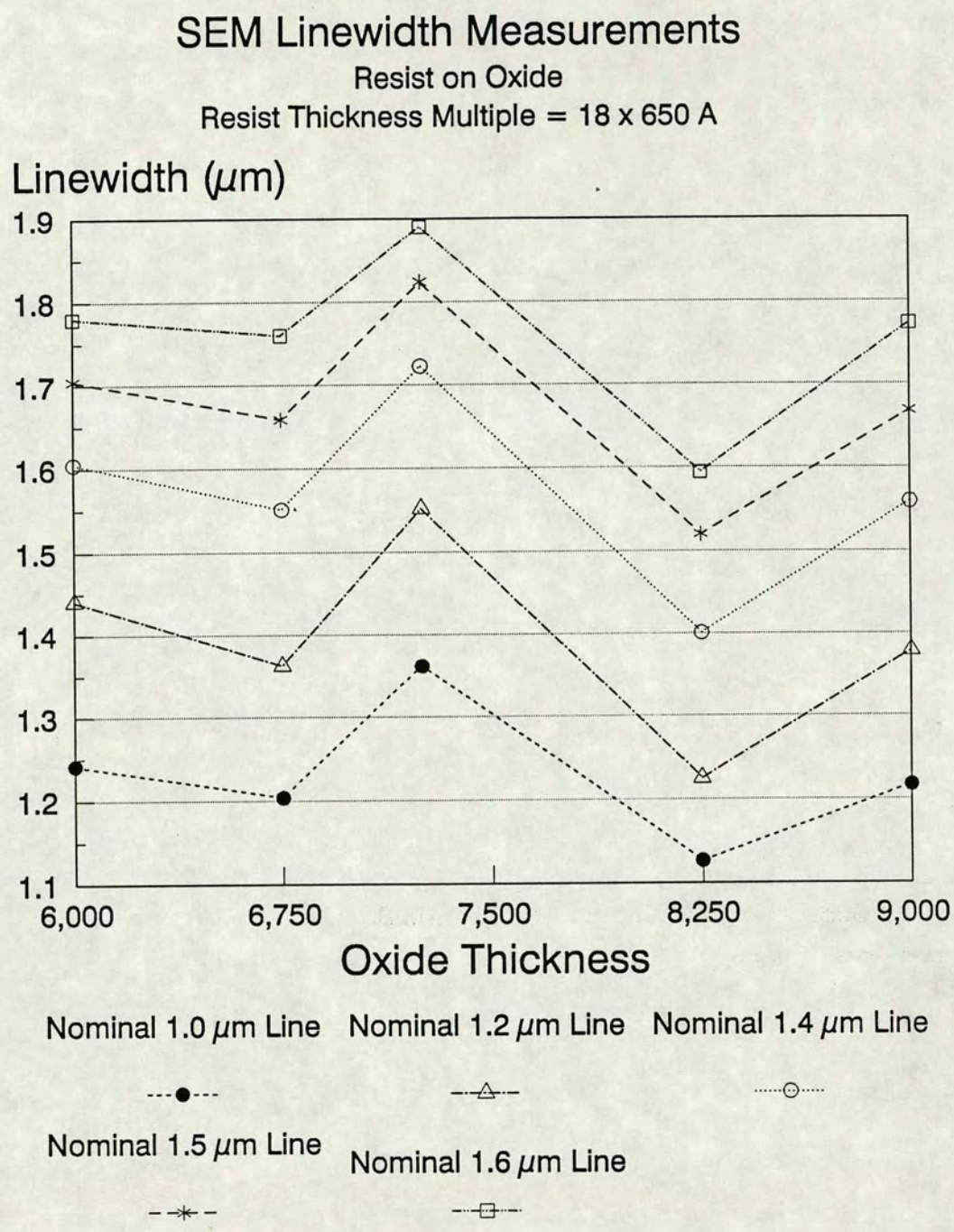

Figure 4–22: SEM CD vs Oxide Thickness: Resist Thickness = $18 \times \frac{\lambda}{4n}$

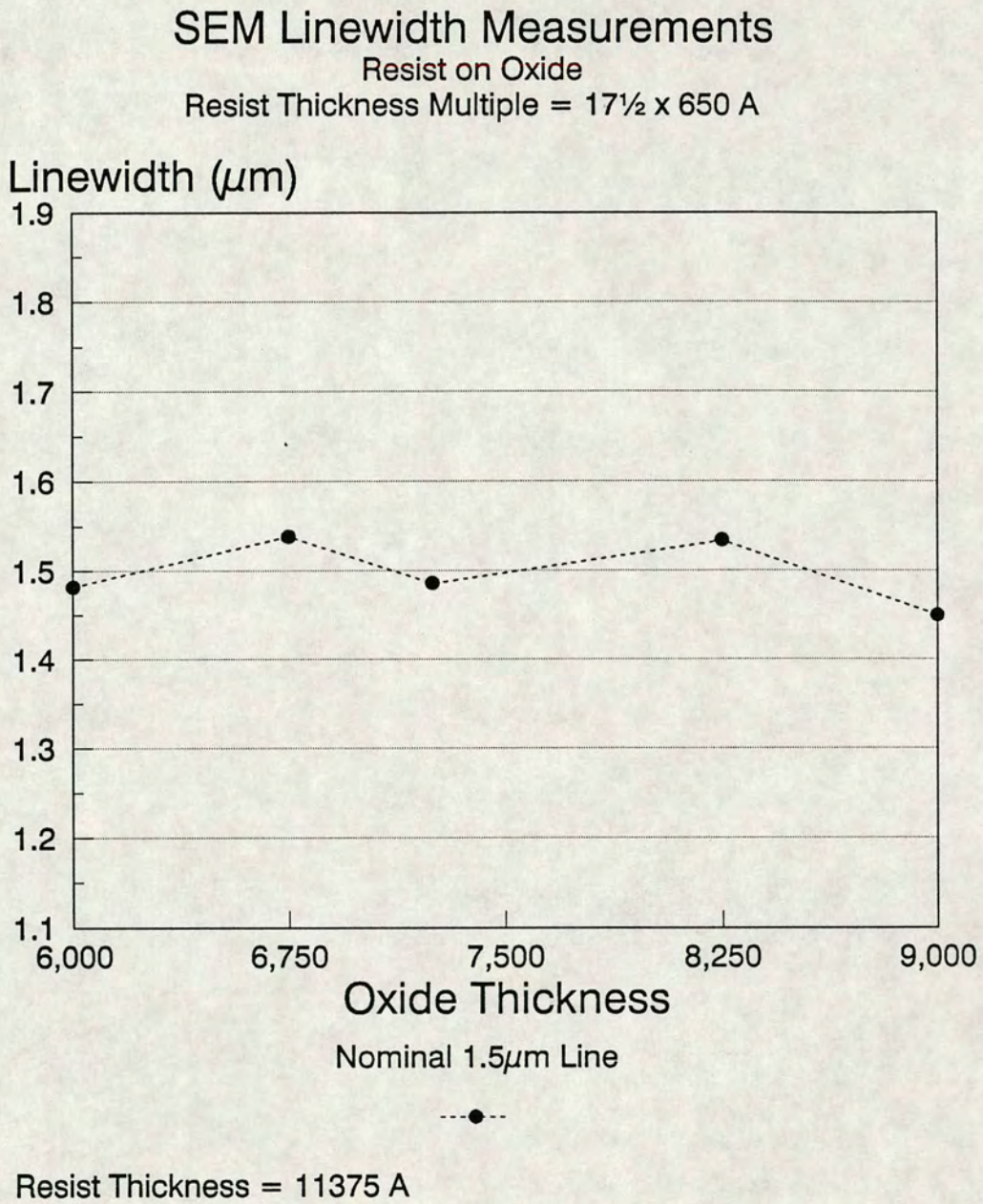

Figure 4–23: SEM CD vs Oxide Thickness: Resist Thickness = $17.5 \times \frac{\lambda}{4n}$

This relationship can be summarized by stating that odd multiples of a quarter-wavelength in total optical thickness of resist plus dielectric layer result in a minimum reflectivity at the resist surface and maximum energy coupling into the resist, whereas even quarter-wavelength multiples maximize reflectance and minimize energy absorbed in the resist. This can result in changes in the exposure required to produce a given size line of up to a factor of two, which can mean the difference between creating the correct size opening or having no opening at all.

4.4.3 Linewidth Control

These tests show that the optimum choice of resist thickness in terms of linewidth control may be governed by the uniformity of the underlying film. For single resist layers it was shown that resist thicknesses should be chosen which represent the extrema of the threshold exposure "swing curve" (e.g. $d_r = 17 \times \frac{\lambda}{4n}$ and $d_r = 18 \times \frac{\lambda}{4n}$). The exposure threshold (and hence CD) of these films is relatively insensitive to small variations in resist thickness. This is the strategy for the selection of resist thickness most commonly used in industry.

However it has been shown for double layer stacks that these resist films are particularly sensitive to variations in the thickness of the underlying layer. (See Figs. 4–21 and 4–22). Intermediate values of resist thickness (e.g. $d_r = 17\frac{1}{2} \times \frac{\lambda}{4n}$) are less sensitive to variation in oxide thickness (See Fig. 4–23) and these values should ideally be used for film stacks with a non-uniform oxide layer.

4.4.4 Reducing Standing Waves

This critical sensitivity to layer thickness is due to the monochromatic illumination of the projection system. The results seen here do not generalize to polychromatic illumination as is commonly used for contact printing.[5] Resist exposure with polychromatic illumination will have a small dependence on the film thickness, particularly for thick resist films.

For thick resist ($> 3\mu$m) standing waves are negligible because the resist absorbs so much of the light propagating downwards that little is reflected from the bottom layers. [6]

Dyed resists may also be used to reduce the intensity of the reflected light. However they require higher exposure doses than undyed resists, and sloping sidewalls often occur since the top of the resist receives more exposure than the bottom.

In industry, a "post-exposure bake" is generally used to remove standing waves from resist profiles. This promotes diffusion of PAC towards areas of lower concentration; thus areas containing local concentration maxima lose inhibitor, and as a direct consequence, the peaks of the standing wave are reduced.[7]

In the EMF the develop process is longer than is commonly used in industry, which effectively removes standing waves from resist sidewalls. This technique is only feasible in a research establishment, where throughput is not of primary concern.

Whatever technique is used, it is obvious that resist profiles must be routinely inspected during processing, and standing waves eradicated in order to minimize CD variations.

4.5 Conclusions

1. These experiments demonstrate the need to control film thickness uniformity in order to maintain control of CD. Whereas some resist thicknesses are sensitive to variations in the underlying film, other resist coatings apparently mask the effect on CD.

2. Simulation programs such as DEPICT and SAMPLE are shown to be a valuable tool for predicting lithographic performance. To prevent misinterpretation of results, an understanding of the models on which they are based is thoroughly recommended.

3. An important implication of these experiments is that it is shown to be possible to predict the effect of film thickness changes on linewidth, according to the "Double Layer Theory".

4. This prediction is only valid however if film thickness can be accurately measured. The next stage is therefore to investigate the techniques commonly used in industry for measuring thickness uniformity. The following chapter discusses the theory and operation of film thickness measurement systems, and the limitations associated with each of them.

Bibliography

[1] G.D.Maxwell, A.J.W.Tol, F.A.Vollenbroek, and Y.F.Rody. The impact of thin fim interference effects on sub-micron lithography processing. In *Microcircuit Engineering 89*, pages 213–218, 1989.

[2] J.D.Cuthbert. Optical projection printing. *Solid State Technology*, (8):59–69, 1977.

[3] I.Fränz and W.Langheinrich. A simple non-destructive method of measuring the thickness of transparent thin films between 10 and 600 nm. *Solid State Electronics*, 11:59–64, 1968.

[4] S.Cosentino, J.Schaper, and J.H.Peavey. Application of thin film reflectance calculations to linewidth measurements for HMOS circuit fabrication. In *INTERFACE 83*, pages 34–39. Kodak Microelectronics Seminar, 1983.

[5] E.J.Walker. Optical interference effects on linewidth in positive photoresist films. In *The Electrochemical Society Spring Meeting*, April 1974.

[6] J.A.Bruce, B.J.Lin, and D.L.Sundling. Characterization of linewidth variation for single and multiple layer resist systems. In *INTERFACE 86*, pages 52–62, 1986.

[7] E.J.Walker. Reduction of photoresist standing wave effects by post exposure bake. *IEEE Transactions on Electron Devices*, ED-22(7):464–468, 1975.

Chapter 5

Film Thickness Measurements

5.1 Introduction

The experiments in Chapter 4 demonstrated the effect of film thickness variations on CD, and the need to measure and control film thickness uniformity. The first half of this Chapter reviews techniques commonly used for measuring film thickness in industry and introduces the systems used in the Edinburgh Microfabrication Facility. The limitations of these systems are discussed, and the need for an automated fast scan system for mapping film thickness uniformity becomes apparent.

The second half of the Chapter describes the design and construction of a new film thickness system based on an Optical Multichannel Analyser (OMA). Test wafers are used to correlate the OMA to the systems used for routine processing in the EMF.

The two principal optical measurement instruments for determining film thickness are:

1. Spectral analysis instruments, which employ polychromatic incident light and are based on determining the intensity as a function of wavelength of the reflected light [1]

2. Ellipsometers, which employ an incident beam of monochromatic light and depend on measurements of intensity and polarization of the reflected light. [2]

Spectral analysis instruments are widely used because of their ability to characterise transparent as well as absorbing films, and because of the speed (typically less than five seconds) with which accurate thickness values can be obtained. [3] [4]

In contrast, ellipsometers are useful for measuring thickness below about 10 nm and the index of refraction for films thicker than about 30 nm. However, they are slower (7 - 30 seconds/test) and generally require greater technical judgement on the part of the user.[5] Ellipsometers are therefore used primarily off-line, as a complement to spectral analysis instruments.

5.2 Spectral Analysis

There is a wide variety of techniques for film thickness based on spectral analysis. [6] [7] [8] [9] [10] Some of the tests are destructive or require special processing, for example to create steps in the film. [11] Colour comparison using the naked eye and a colour chart is perhaps the most simple technique, but requires judgement and is precise only in certain thickness ranges. [12] Many of the techniques are not suited to process control because of the skill required to make measurements. Interferometry however, is ideally suited to automation.

5.2.1 Interferometry (3000 A - 2μm)

Traditionally, interference techniques have been used to determine the extrema of reflected intensity versus wavelength. (See Fig. 5–1). The general condition for interference is expressed as:

$$d = \frac{N\lambda}{2n_2 cos\theta_2} \tag{5.1}$$

where d is the film thickness, λ is the wavelength of incident light,
N is the order of interference = $\frac{1}{2}, \frac{3}{2}, \frac{5}{2}$ for intensity minima, 1, 2, 3, for intensity

maxima,
n_2 is the index of refraction of the film at wavelength λ and θ_2 is the angle of refraction at wavelength λ. (See Fig. 5–2)

Pliskin [13] [14] modified Equation 5.1 to compensate for phase shift (Δt_ϕ) and reflectivity corrections (Δt_r),

$$d = \frac{N\lambda}{2n_2 cos\theta_2} + \Delta t_\phi + \Delta t_r \tag{5.2}$$

When phase shift and reflectivity corrections are accounted for, accuracies of better than 50 A can be obtained. [15]

Experimentally, this technique may be based on either a spectrophotometer or a monochromator. If a spectrophotometer is used, the wavelength of the radiation is varied while the angle of incidence is fixed; whereas with the monochromator, the wavelength is fixed and the angle of incidence is varied.

The main disadvantages of interferometry are that the optical properties of the film must be known, and if Equation 5.1 is to be applied, the film must be thick enough for a number of fringes to occur. For films whose optical thickness is less than $\frac{\lambda}{4}$ no extrema occur, and interferometry techniques cannot be used. This imposes a minimum thickness limit for SiO_2 films on Si of about 700 A.[16] In practice, these limits are often higher due to the fact that the extrema at low orders tend to be broad, making accurate determination difficult. [17]

5.2.2 Thin Films (100 - 6000 A)

The method used to determine the thickness of films whose optical thickness is less than $\frac{\lambda}{4}$ was initially suggested by Lukes and Schmidt [18]. Additional work using the same method has been done by Fränz and Langheinrich [19]

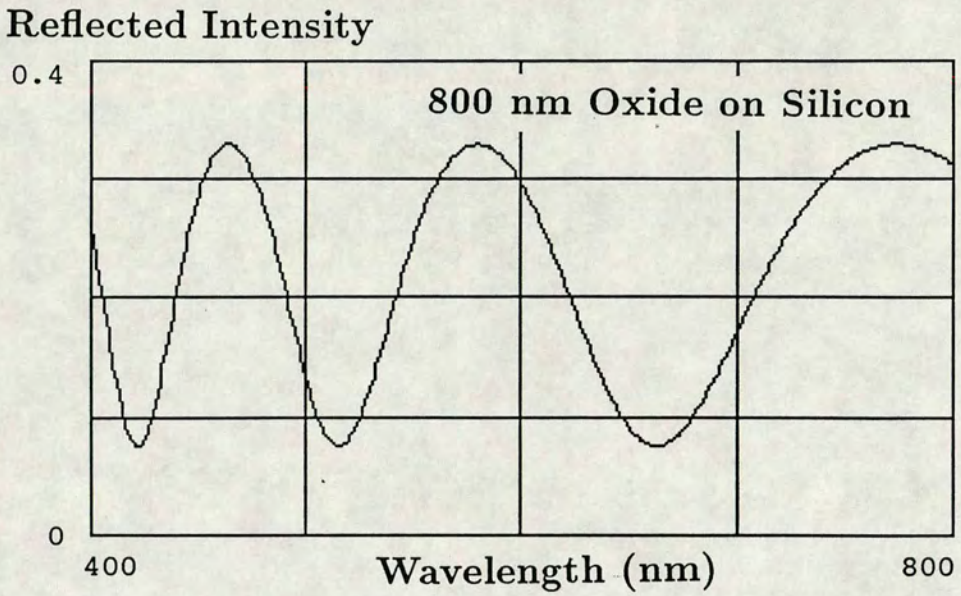

Figure 5–1: Reflectivity Curve Generated from an Oxide Film 800 nm Thick and Normalised to the Spectrum from Bare Silicon

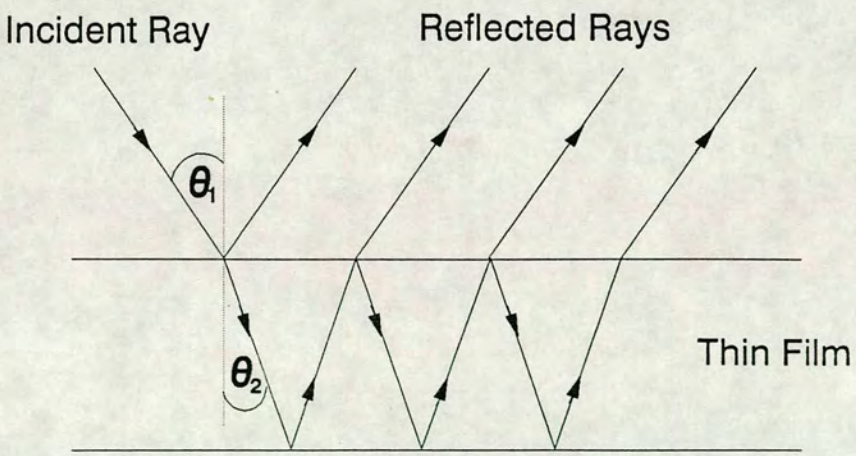

Figure 5–2: Reflections Occurring in a Thin Film [6]

This technique uses the theoretical relationship for the reflectivity of a transparent film on an absorbing substrate to give

$$R = \frac{A + F}{B + F} \tag{5.3}$$

with

$$A = \frac{(n_1 n_3 - n_2)^2}{(n_2^2 - n_1^2)(n_3^2 - n_2^2)}$$

$$B = \frac{(n_1 n_3 + n_2)^2}{(n_2^2 + n_1^2)(n_3^2 + n_2^2)}$$

$$F = \frac{1}{2}(1 + cos\phi)$$

$$\phi = \frac{4\pi n_2 d}{\lambda}$$

where R is the intensity of reflected light; n_1 is the refractive index of air; n_2 is the refractive index of the film; n_3 is the real part of the substrate dielectric constant $\tilde{n_3} = n_3 - jK_3$; K_3 is the extinction coefficient of the substrate; λ is the wavelength of light used and d is film thickness .

For substrate materials with little absorption, in other words with negligible K, the reflected intensity becomes at its maximum equal to the intensity of the light reflected directly from the substrate. The quantity R_0 is used as a reference in the measurements

$$R_{max} = R_0 = \frac{A + 1}{B + 1} = \left(\frac{n_3 - n_1}{n_3 + n_1}\right)^2$$

Therefore, knowing the optical constants of the film and silicon, the ratio $\frac{R}{R_0}$ can be expressed as a function of the thickness of the film, assuming normal incidence.

Fig. 5–3 illustrates the relationship of $\frac{R}{R_0}$ as a function of d at wavelengths of 5000 A and 6000 A [20]. It should be noted that it is possible to have the same value of $\frac{R}{R_0}$ for different thicknesses. Therefore more than one wavelength should be used.

In practice $\frac{R}{R_0}$ is determined by measuring the reflected intensity from a coated wafer, and dividing this by the reflected intensity from a bare silicon wafer at

the same wavelengths. It has been established that equally good results can be obtained either by measuring R_0 on the same wafer (prior to depositing film) on which R was measured, or by measuring R_0 on another bare silicon wafer.[19]

5.3 Ellipsometry

Ellipsometers measure changes in the state of polarization of monochromatic light, caused by reflection from the surfaces of substances. Fig. 5–4 shows a schematic of an ellipsometer. [21] The laser is typically He-Ne with a power in the 2 mW region. The technique depends upon finding two extinction positions by varying the angle of polarization of the incident wave and altering the angle of the analyzer. This enables two parameters Psi (Ψ) and Delta (Δ) to be calculated using the following equations:

$$\Psi = \frac{180 - A_2 + A_1}{2} \tag{5.4}$$

$$\Delta = P_1 + P_2 \tag{5.5}$$

where A and P are the angles of the analyzer and polarizer. These parameters can be used to interpret the thickness and refractive index of the film from a chart or "nomograph".

The advantages that ellipsometry has over other techniques of measuring film thickness are as follows:

1. It can measure thickness of films at least an order of magnitude smaller than can be measured by other methods such as interferometry [22]

2. It permits determination of the index of refraction of thin films of unknown thickness [23]

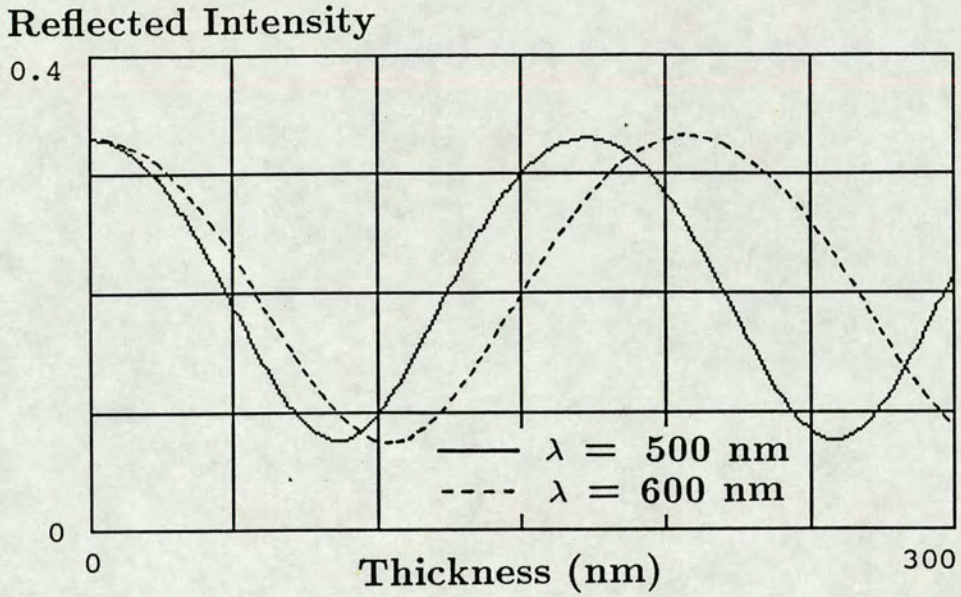

Figure 5–3: Reflectivity as a Function of Film Thickness

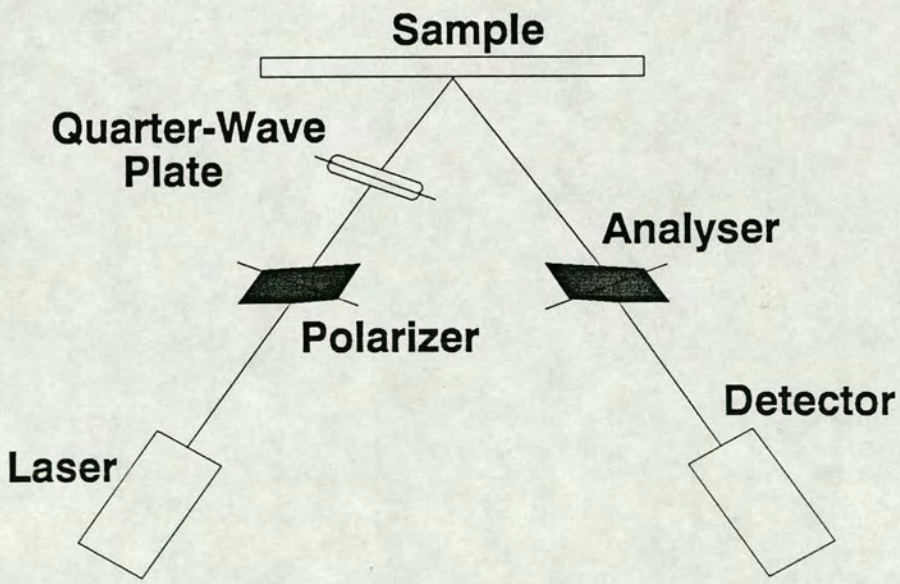

Figure 5–4: Ellipsometer [21]

5.4 Film Thickness Measurements at the EMF

The EMF has two principal systems for film thickness measurements, the Nanospec designed by Nanometrics and an ellipsometer from Applied Materials. A Monolight Spectrum Analyser has recently been purchased by the EMF to study film thickness changes during the development of photoresist.

5.4.1 Nanospec

The Nanospec is based on an interferometric technique and is used routinely during processing. It can be programmed to measure the thickness of a range of films and combinations of films, including oxide, nitride, photoresist and polysilicon. Simple statistical data, for example the maximum, minimum and standard deviation of accumulated measurements may be displayed. [24]

The accuracy of the measurement is dependent upon both the film composition and the program used. The program which measures SiO_2 thickness in the range 500 A to 3μm range sweeps between wavelengths of 480 and 800 nm and produces a film thickness accurate to within $\pm 2\%$. For SiO_2 films thinner than 500 A a different technique is used. The reflectance of the film is measured at a single wavelength (520 nm) and this is compared with the reflectance of a bare silicon wafer (See Section 5.2.2). Erroneous readings will result if this program is used on films thicker than 500 A.

The disadvantages of the Nanospec are as follows:

1. It has no wafer handling capability, and the measurement position on the wafer has to be judged by eye

2. It requires manual focusing and is tedious to use for large numbers of measurements

3. It is prone to vibration. Calibration checks are carried out routinely, but nevertheless, the repeatability of the measurements is not implicitly trusted.

5.4.2 Ellipsometer II

The EMF has until recently, relied upon a traditional ellipsometry system, the Ellipsometer II, which requires a nomograph for calculation of Psi and Delta parameters. [25] Although this system has better repeatability and accuracy than the Nanospec, it is slow and complex to use, and is therefore used primarily for measurement of refractive index.

A new computer-controlled ellipsometer with wafer handling and scanning facilities has been acquired by the department, and is currently undergoing validation checks. This system has excellent data management and presentation facilities. Fig. 5–5 is a sample two dimensional contour map showing the thickness uniformity of an oxide film. Fig. 5–6 includes a full print-out of the measurements taken at 69 points across the wafer.

However, despite the obvious superiority of this system to its predecessor, it is still too slow to be used for normal processing.

5.4.3 Monolight Spectrum Analyser

The Monolight system is currently undergoing a series of tests to determine whether it is capable of functioning as a track develop rate monitor.

The system is based on a COMPAQ 376 personal computer. [26] A scanning monochromator scans intensity versus wavelength in the range 200-900 nm and standard reflectometry techniques are used to generate film thickness data.

Initial results are encouraging [27], but the Monolight is dedicated to the develop track and is unavailable for routine film thickness measurements.

Figure 5–5: Scanning Ellipsometer 2-D Wafer Map

Figure 5–6: Scanning Ellipsometer Measurement Data

5.4.4 Preliminary Conclusions

It is evident that the EMF has need of an automated film thickness measurement system with wafer mapping facilities. Ideally, the machine should be simple to control, fast, accurate and reliable. The results should be easy to interpret and there should be a system of data storage to allow trend plots and wafer maps to be analysed off-line. Preliminary tests on the Monolight spectrum analyser show good results. An equivalent system attached to an XY stage would seem to be the most promising option.

5.5 Optical Multichannel Analyser

5.5.1 Introduction

Having determined to construct a film thickness measurement system, it was necessary to purchase a spectrophotometer on which to base the system. The Optical Multichannel Analyser (OMA) designed by Princeton Research Corporation was chosen because it incorporates spectral analysis capability with a powerful microcomputer. This machine is therefore able to function as the control centre for the entire system.

The other hardware components required for a film thickness measurement system based on the OMA include a spectrograph, a detector and a detector controller. (See Fig. 5–7). An automatic wafer stage has been added to give full wafer scanning facilities . A microscope with white light source has been mounted over the stage to focus the measurement spot beam onto the wafer.

The light is transmitted onto the wafer, and then reflected back along a fibre optic cable into the spectrograph where it is split into its component wavelengths.

The photodiode array detector, under direction from the detector controller takes the incoming spectral data from the spectrograph, converts it into electrical signals, and then transmits it to the detector controller via cable.

The detector controller translates the electrical signals from the detector into digital data and sends it to the 1460 System Processor.

This system effectively measures reflected intensity as a function of the pixel number of the photodiode array. Using lamps of a known spectrum, such as mercury or argon, the system can be calibrated to work in wavelengths (nanometers). Reflectivity curves may then be produced, and film thickness data generated by algorithmic means. The following sections describe the basic hardware and software components of this system .

5.5.2 System Controller

The OMA can be controlled either by means of its touch-activated screen menus, or its resident software, Hemenway BASIC. [28] This gives the user the option of writing applications programs capable of accessing and manipulating the experimental data generated by the system. The system has a twin $5\frac{1}{4}$ inch disk drive unit; the disk in Drive 0 contains system boot files and the BASIC system software; the disk in Drive 1 is used to store data and results files.

The BASIC software must incorporate four specific functions in order to scan a wafer map of film thickness:

1. Control of the wafer prober
2. Spectral data acquisition
3. Application of film thickness algorithm
4. Data storage and presentation

Calibration

The uncalibrated OMA screen displays intensity versus pixel number. Calibration of the X-axis allows the pixel number to be expressed in terms of wave-

length (nanometres). Calibration is achieved by obtaining the spectrum of a mercury/argon lamp on the screen, and teaching the instrument to recognise the wavelengths of well-defined peaks. (See Fig. 5–8). A cubic fit method is then used to determine the best curve that fits between four or more data points. [29] [30]

The vertical axis of the OMA data acquisition screen is normally scaled to the number of detected counts. The user has the option of calibrating the Y-axis to the intensity of a standard lamp. However, for this application, since all measurements are expressed relative to a plain substrate, it is not necessary to determine absolute values of intensity.

5.5.3 Wafer Prober

The AWP-1050 is an automatic wafer prober manufactured by Wentworth. [31] The mechanical design consists of two stepper motors which drive the stage along lead screws in X and Y directions with a resolution of ten microns in each direction. An initialisation routine is required to give the prober datum information when first powered on. Once the stage has established two reference positions, subsequent stage movements are issued in terms of incremental or absolute coordinates in X and Y directions.

The prober has an EPROM based command set which may be accessed by the OMA via an IEEE-488 interface. This interface allows a two-way flow of information, so that the prober can listen to commands from the controller and feedback a response once the command has been obeyed. The procedure can be monitored via a status register byte which indicates the current state of activity in the interchange. An interrogation, or serial poll of this register reveals when a command has been carried out and the prober is awaiting further instruction.

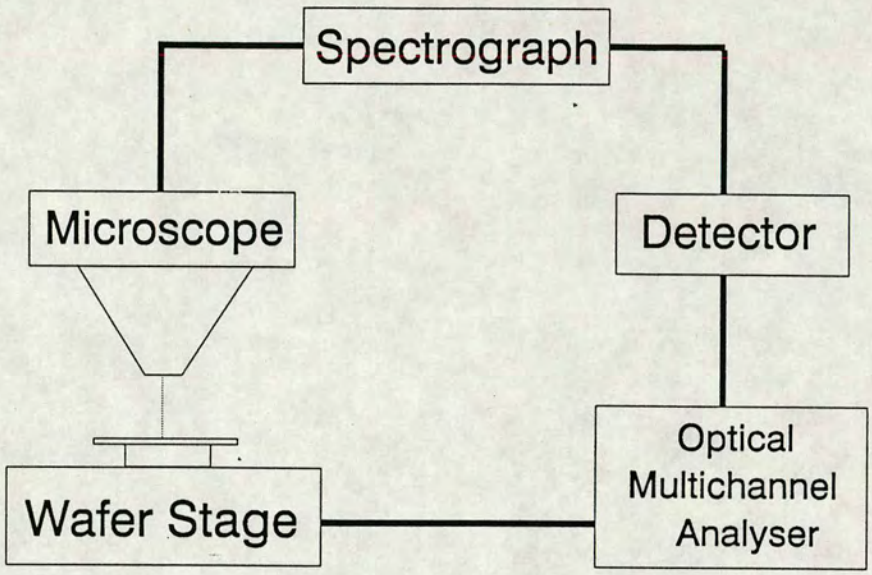

Figure 5–7: System Hardware

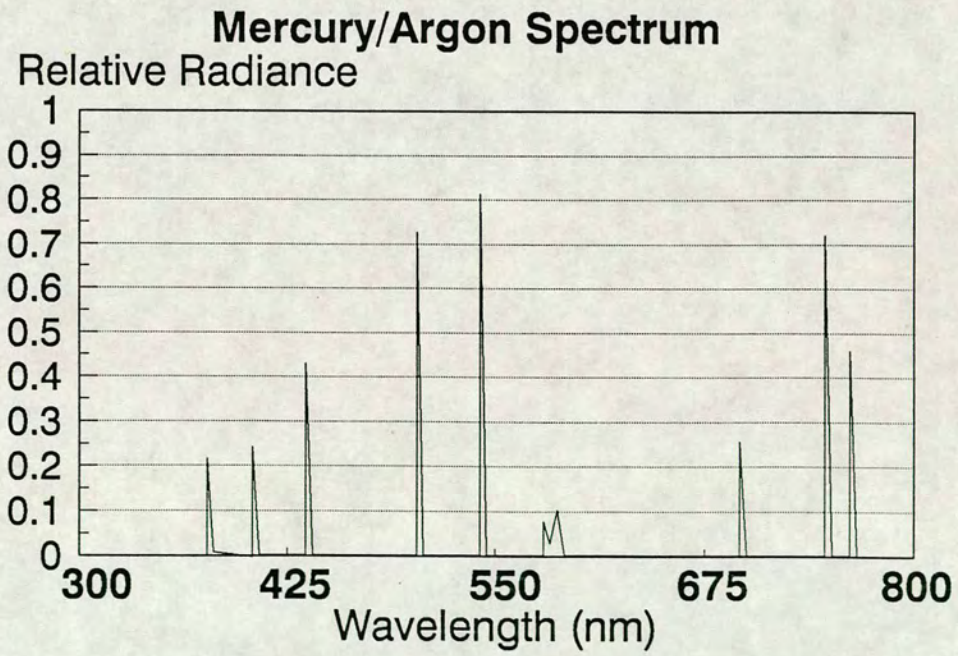

Figure 5–8: Mercury/Argon Spectrum [28]

5.5.4 Microscope

A frame has been built above the wafer stage to hold the microscope. The microscope has a trinocular head and a beam splitter which directs 20% of the light to the eyepieces, and 80% to the fibre optic cable linking the microscope to the spectrograph.

The light source is a high intensity halogen lamp. Focusing of the light beam onto the wafer is currently done manually. However the wafer stage is capable of travel in the Z-direction, and commands can be issued from the OMA to drive the stage up or down in order to achieve optimal focus. A small stepper motor has been attached to the wafer stage to mechanise this movement, and a control board to drive the stepper motor has been assembled. The focal position of the wafer stage could be established by monitoring the integrated intensity of light reflected from the wafer. However, further research to investigate this technique is required if automatic focusing is to be implemented.

5.5.5 Spectrograph

The Monospec 18 spectrograph employs the crossed Cszerny-Turner optical design. [32] (See Fig. 5–9). Light enters the instrument through the entrance slit and strikes the collimating mirror. The collimating mirror is aligned to reflect the light to the grating. The grating diffracts the light into its component wavelengths and directs the wavelengths to the focusing mirror. The focusing mirror reflects the light through an adjustable exit assembly and into the detector unit. A trickle of clean nitrogen gas is fed into the spectrograph chamber to keep the optical system dry and prevent condensation forming on the mirrors.

Since the OMA system is based on a white light source, a spectrograph grating of 300 grooves per mm, which has a wavelength range of 300-800 nm was chosen.

5.5.6 Photodiode Array Detector

The detector receives the optical signal from the spectrograph, quantifies the intensity of each wavelength by scanning a 1024-element photodiode array, and sends the electrical signal to the detector controller. The signal is then digitised before it returns to the OMA to be displayed on the screen as a scan of intensity versus wavelength. [33]

The detector scan rate may be varied until sufficient light levels are obtained on the screen. The minimum scan rate for this particular detector is 30 ms; in practice a rate of 960 ms per scan was used as standard. [34]

5.6 Software

5.6.1 Reflectivity Curve

A reflectivity curve is a measure of reflected intensity as a function of wavelength. It may be used in the calculation of film thickness by the application of an algorithm to the extrema of the curve. The initial step therefore towards a calculation of film thickness is to convert a scan of the photodiode array intensity function into a recognisable reflection spectrum.

This necessitates the data to be normalised to a standard substrate material. A plain silicon wafer is scanned and the data stored on disk. All subsequent measurements on coated wafers are ratioed to the reference wafer.

Background noise inherent in the system, and due to ambient light must also be considered. Noise levels are monitored during the measurement routine and subtracted from the measured data.

The reflection spectrum obtained in this way may be considered as:

$$R(\lambda) = \frac{D(\lambda) - B(\lambda)}{S(\lambda) - B(\lambda)} \tag{5.6}$$

where $R(\lambda)$ = Resultant reflectivity and is a function of wavelength; $D(\lambda)$ = Measured data; $B(\lambda)$ = Background noise; $S(\lambda)$ = Substrate reflectivity

A moving average routine has been incorporated into the software to remove noise. [35] [36] [37]

5.6.2 Turning values

Having obtained a reflection spectrum $R = f(\lambda)$, the next step towards the calculation of film thickness is to find the extrema of the reflectivity curve. The maxima and minima of a curve correspond to those points at which the slope of the tangent is equal to zero.

$$\frac{dR}{d\lambda} \equiv f'(\lambda) = 0 \tag{5.7}$$

By examining the slope of the tangent on either side of the turning point it can be established that the sign of the slope changes as the tangent moves through the turning value. (See Fig. 5–10). A fairly coarse scan stepped along the reflectivity curve finds the approximate positions of the turning values. Linear interpolation is then used to pinpoint the precise wavelength at which these turning functions occur.

5.6.3 Film Thickness Algorithm

Once the extrema of the reflectivity curve have been found, it is a relatively simple matter to apply an algorithm to these extrema in order to calculate film thickness. The algorithm selected for this purpose is the Ananthakrishnan algorithm [38], which is a refinement of the interferometric technique described in Section 5.2.1. The advantage of using this algorithm is that it does not require fore-knowledge of the order number of the film being measured. Other techniques more commonly used require either the order number or the approximate thickness of the film.

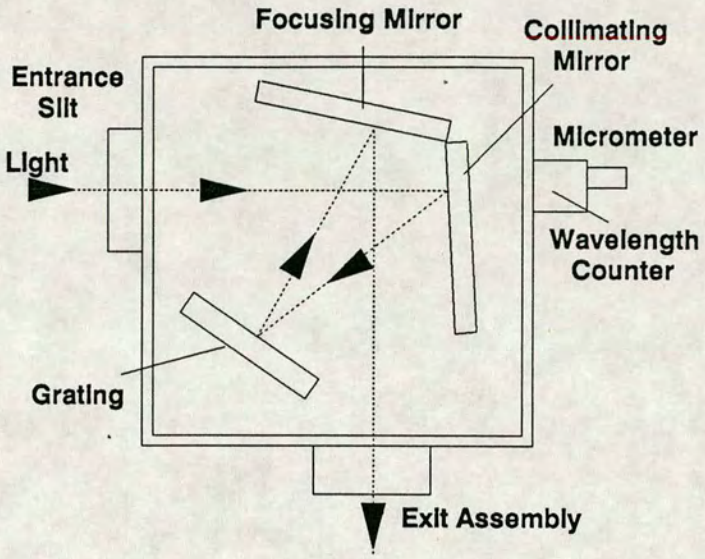

Figure 5–9: Spectrograph [32]

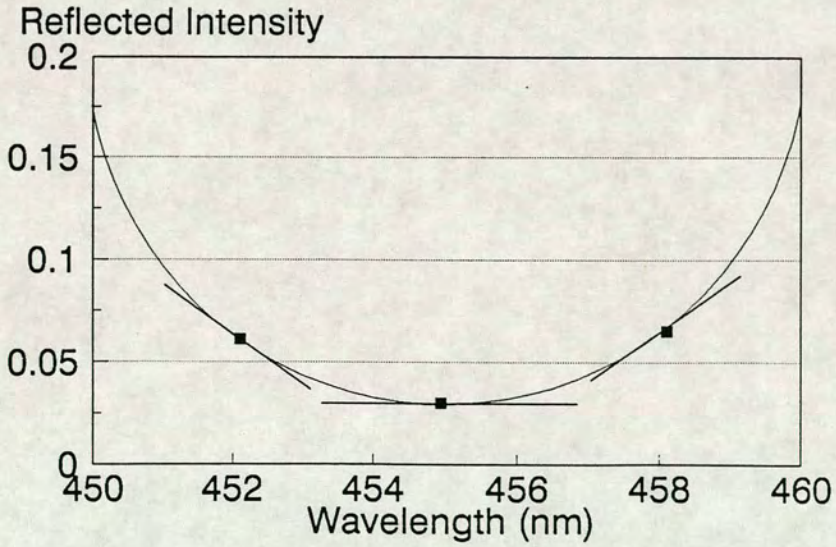

Figure 5–10: Tangents at the Turning Values of a Curve

This algorithm makes use of the fact that the order numbers at the extrema are integers, odd or even depending on whether the extrema is a minimum or a maximum. The wavelengths at which these extrema occur are arranged in ascending order as follows:

point (p):	1	2	.	.	.	t
wavelength:	λ_1	λ_2	.	.	.	λ_t
θ:	$\frac{n}{\lambda_1}$	$\frac{n}{\lambda_2}$	.	.	.	$\frac{n}{\lambda_t}$
θ_1:	$\frac{n}{\lambda_t}$	$\frac{n}{\lambda_{t-1}}$	.	.	.	$\frac{n}{\lambda_1}$

If $(\theta - \theta_1)$ is plotted against the point number p, then the film thickness d can be shown to be equal to $\frac{-1}{2m}$ where m is the gradient of the best fitting line through the points. (See Fig. 5–11).

The slope of the best fitting line is determined using a least mean square technique according to the equation below:

$$m = \frac{t\sum p(\theta - \theta_1) - \sum p \sum(\theta - \theta_1)}{t\sum p^2 - (\sum p)^2} \tag{5.8}$$

where t is the number of turning values.

A few simple scan patterns have been written for the prober. Future developments of the system would include the provision of a wider selection of scan routines. Once all sites have been scanned, mean ($\bar{d}$) and standard deviation (σ) values are calculated [39]:

$$\bar{d} = \frac{\sum d}{n} \tag{5.9}$$

$$\sigma = \sqrt{\frac{\sum(d - \bar{d})^2}{n}} \tag{5.10}$$

where n is the number of sites scanned.

A wafer map may then stored on floppy disk to enable film thickness results to be accessed and analysed at a later date. [40]

Ananthakrishnan Algorithm

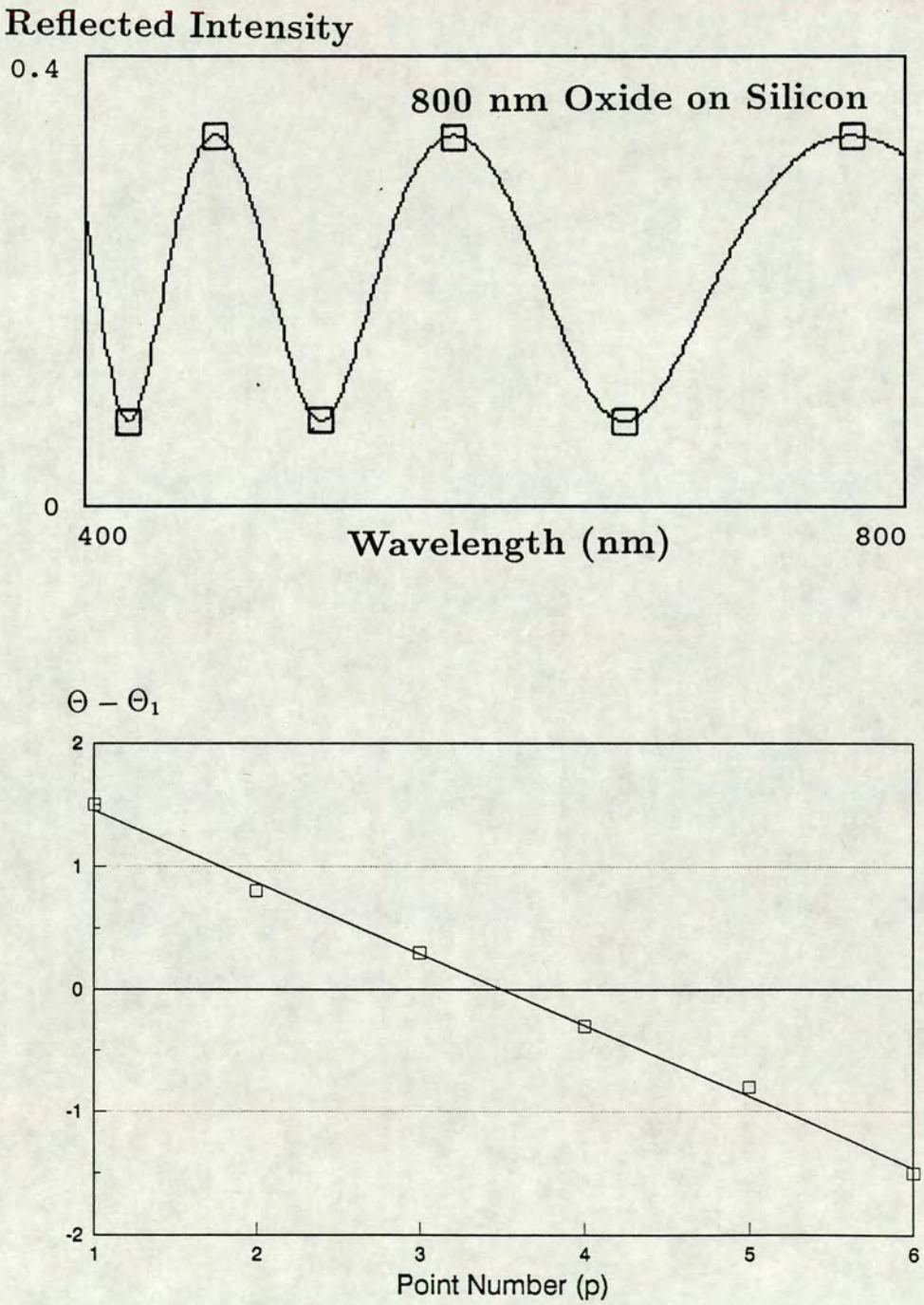

Figure 5–11: The Two Stages Involved in the Application of the Ananthakrishnan Film Thickness Algorithm [38]. i) Find the Turning Values of the Reflectivity Curve Generated by the Film ii) Find the Slope of the Best Fitting Line Plotted Through the Points Generated by Each Turning Value ($\theta = \frac{n}{\lambda}$)

5.7 Testing

Having built the OMA system, it was necessary to test it against the other film thickness systems in the EMF. Test wafers with various thicknesses of oxide and photoresist were prepared and analysed on: i) OMA ii) Scanning Ellipsometer iii) Monolight iv) Nanospec. The experiments and results are described in the following section.

5.7.1 Silicon Dioxide Thickness Tests

Five different thicknesses of oxide were chosen, covering a range of values commonly used in processing. Each oxide thickness was grown on two wafers, giving a total of ten wafers for testing. These wafers were measured at five sites on the OMA, Nanospec and Ellipsometer. The mean thicknesses of these measurements are shown in Table 5–1.

Fig. 5–12 shows the correlation of the OMA results with those of the Nanospec. The correlation coefficient r, which is a measure of the "Goodness of Fit" of the data to the line of regression, is computed to be 0.995.[41] Fig. 5–13 shows the correlation of the OMA with the scanning ellipsometer.

The data from which the mean values were calculated was also used to calculate the spread of results for each system. The data generated by the OMA and Nanospec can be seen in Figs. 5–14 and 5–15 respectively. Fig. 5–16 shows that the standard deviation of measurements from each system varies in a similar manner from wafer to wafer. A high value of standard deviation indicates a non-uniform oxide coating.

Nominal Thickness	OMA		Nanospec		Ellipsometer	
	Mean	Sigma	Mean	Sigma	Mean	Sigma
6000 A	6120	0.20	6100	0.22	6060	0.35
	6020	0.28	6050	0.15	6014	0.28
6750 A	6880	0.76	6878	0.76	6862	0.74
	(Broken)		6751	0.15	6661	0.13
7500 A	7620	0.26	7566	0.25	7565	0.14
	7540	0.27	7515	0.24	7532	0.17
8250 A	8260	0.31	8258	0.23	8241	0.26
	8330	0.16	8268	0.22	8253	0.22
9000 A	8990	0.45	9004	0.51	8959	0.47
	9070	0.20	9041	0.19	8983	0.23

Table 5–1 Mean Thicknesses of Oxide Coated Wafers

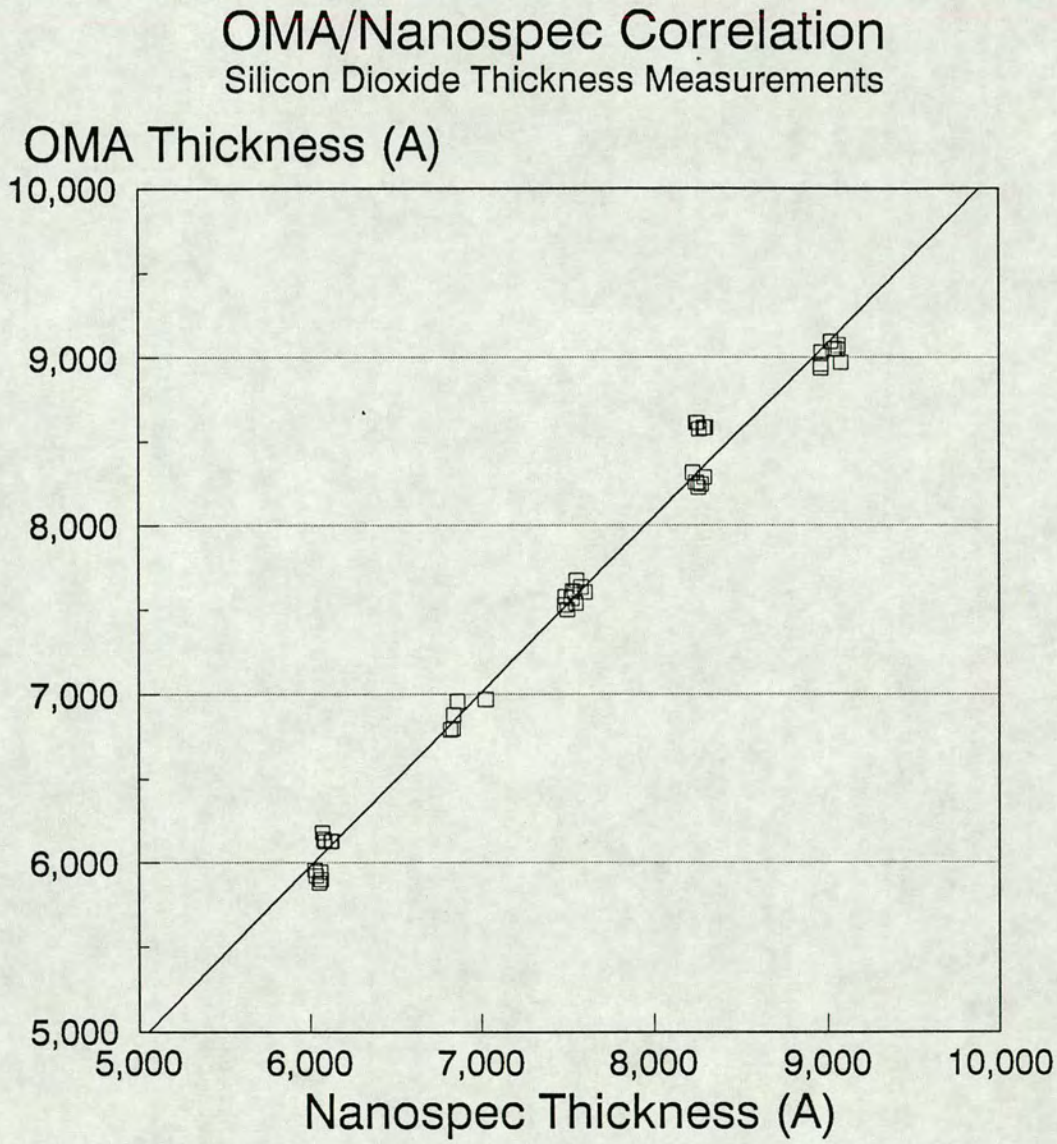

Figure 5–12: OMA/Nanospec Correlation

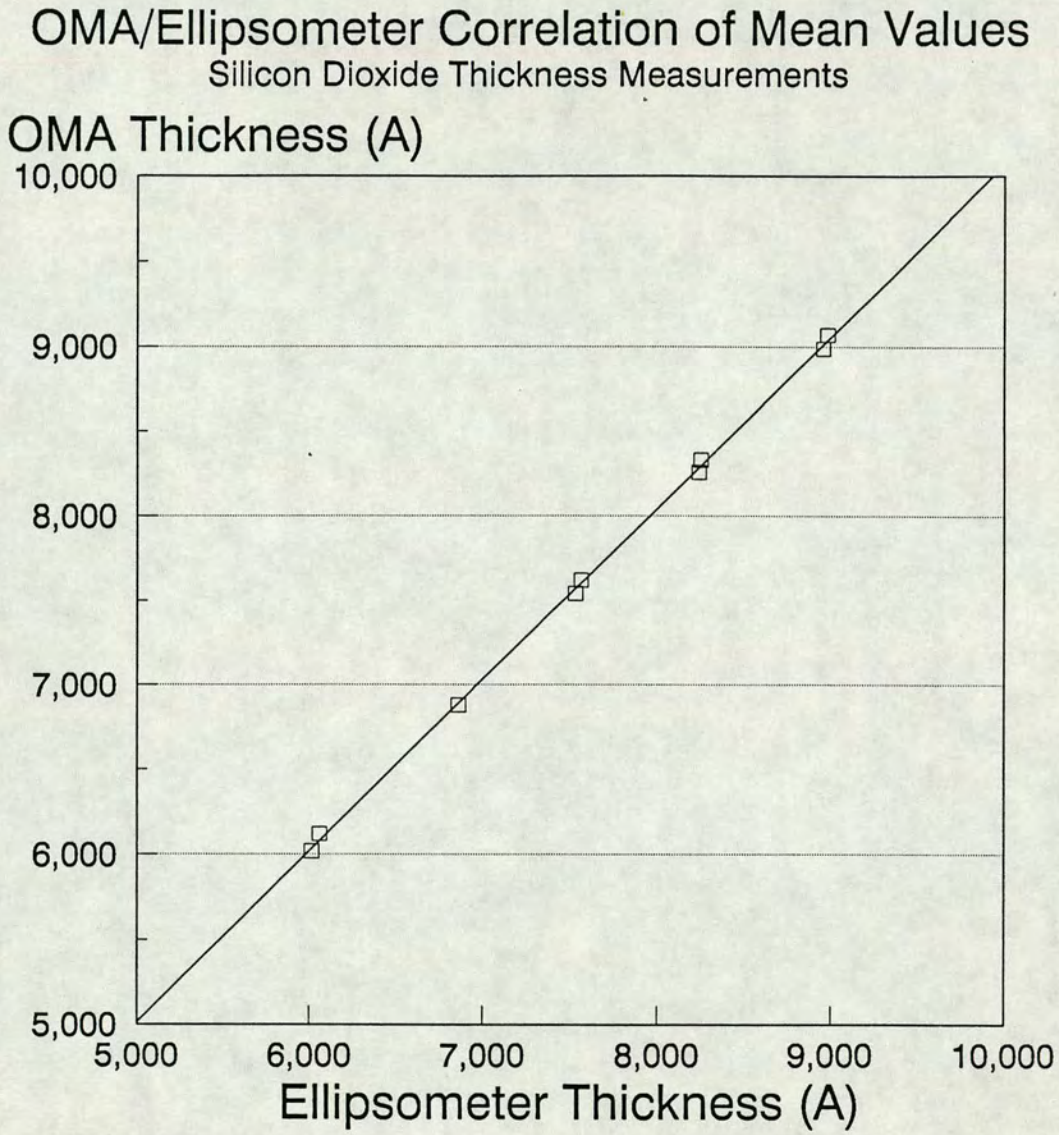

Figure 5–13: OMA/Ellipsometer Correlation

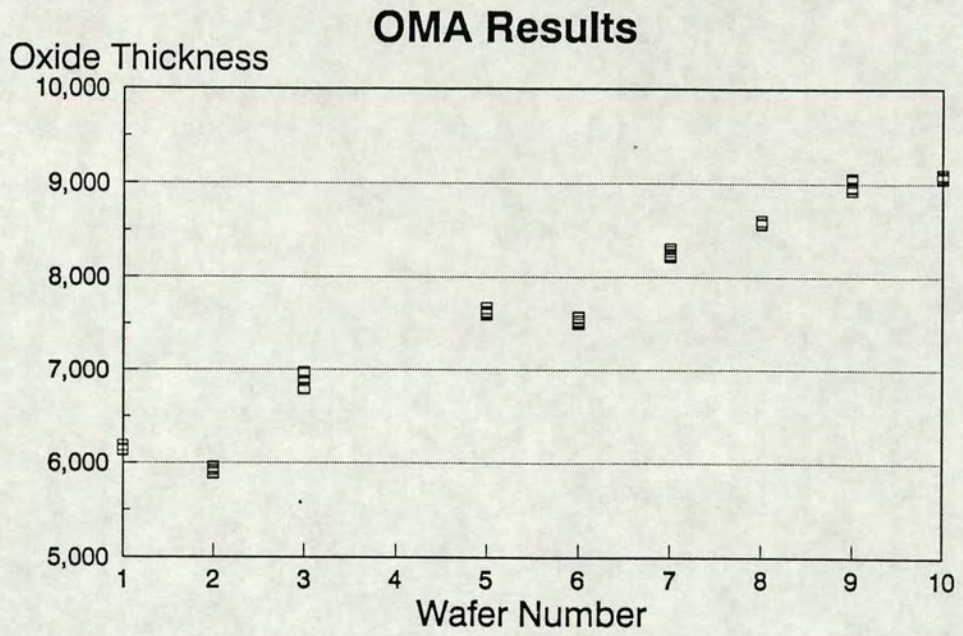

Figure 5–14: Oxide Thickness: OMA Results

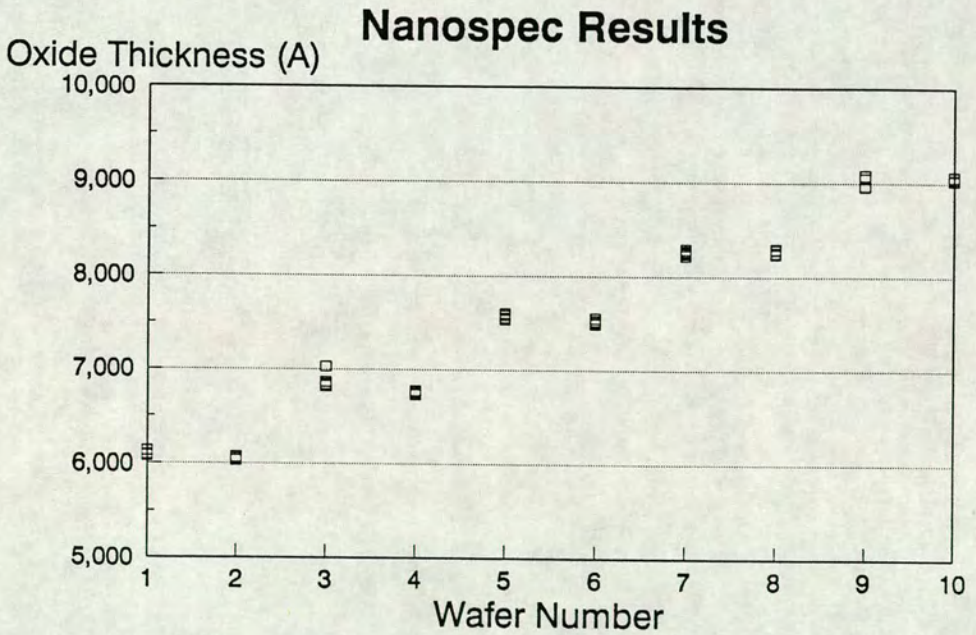

Figure 5–15: Oxide Thickness: Nanospec Results

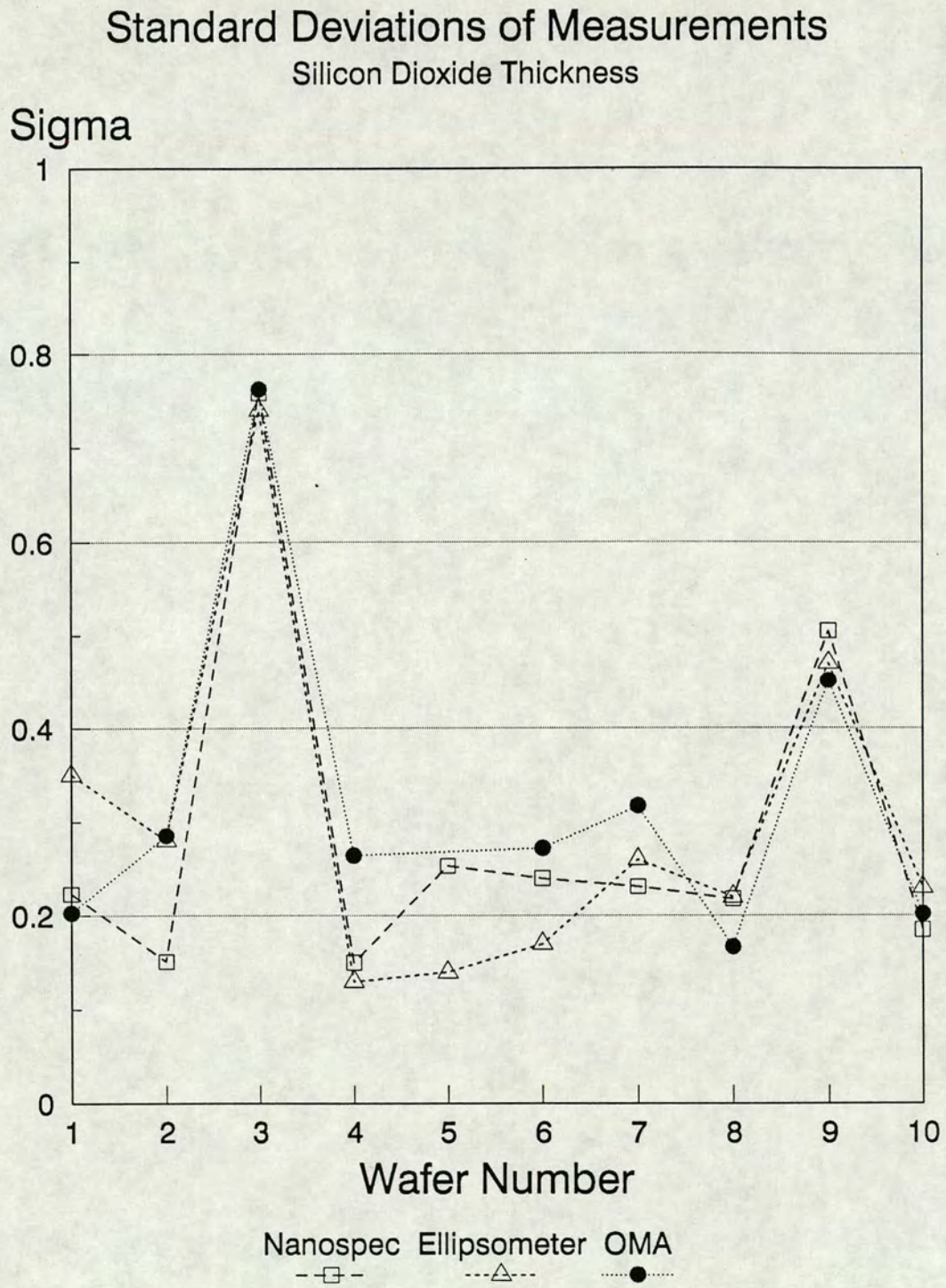

Figure 5–16: Oxide Thickness: Standard Deviations of Measurements

5.7.2 Resist Thickness Tests

This experiment involved the characterisation of an Olin Hunt photoresist HPR204. Resist thickness varies inversely with the spin speed of the resist track. Thirty six wafers were coated with resist at speeds varying from 3500 - 7000 rpm. The spin speed curves obtained from the OMA, Monolight and Nanospec are shown in Fig. 5–17. From these results it can be seen that the Monolight records the smoothest spin speed curve, while the Nanospec results deviate most from the ideal curve.

Having accumulated the data, it was possible to correlate the results between each instrument, as shown in Figs. 5–18 and 5–19. The correlation curves indicate that the OMA measurements agree more closely with the Monolight results than with those obtained from the Nanospec. This result is not surprising, since the OMA and the Monolight systems employ the same algorithm to calculate film thickness. The Monolight data was obtained using a measurement routine which took 1000 scans at each site in order to smooth out noise. Reducing the number of scans for the Monolight data acquisition routine causes a corresponding decrease in the correlation with the OMA results.

5.7.3 Repeatability

The repeatability of the OMA system was assessed by taking a single measurement of an oxide coated wafer every day for twenty days. The variation in thickness recorded over this period can be seen in Fig. 5–20. The standard deviation of these measurements is 0.05% which compares favourably with the repeatability of Nanospec measurements. (See Section 5.4.1).

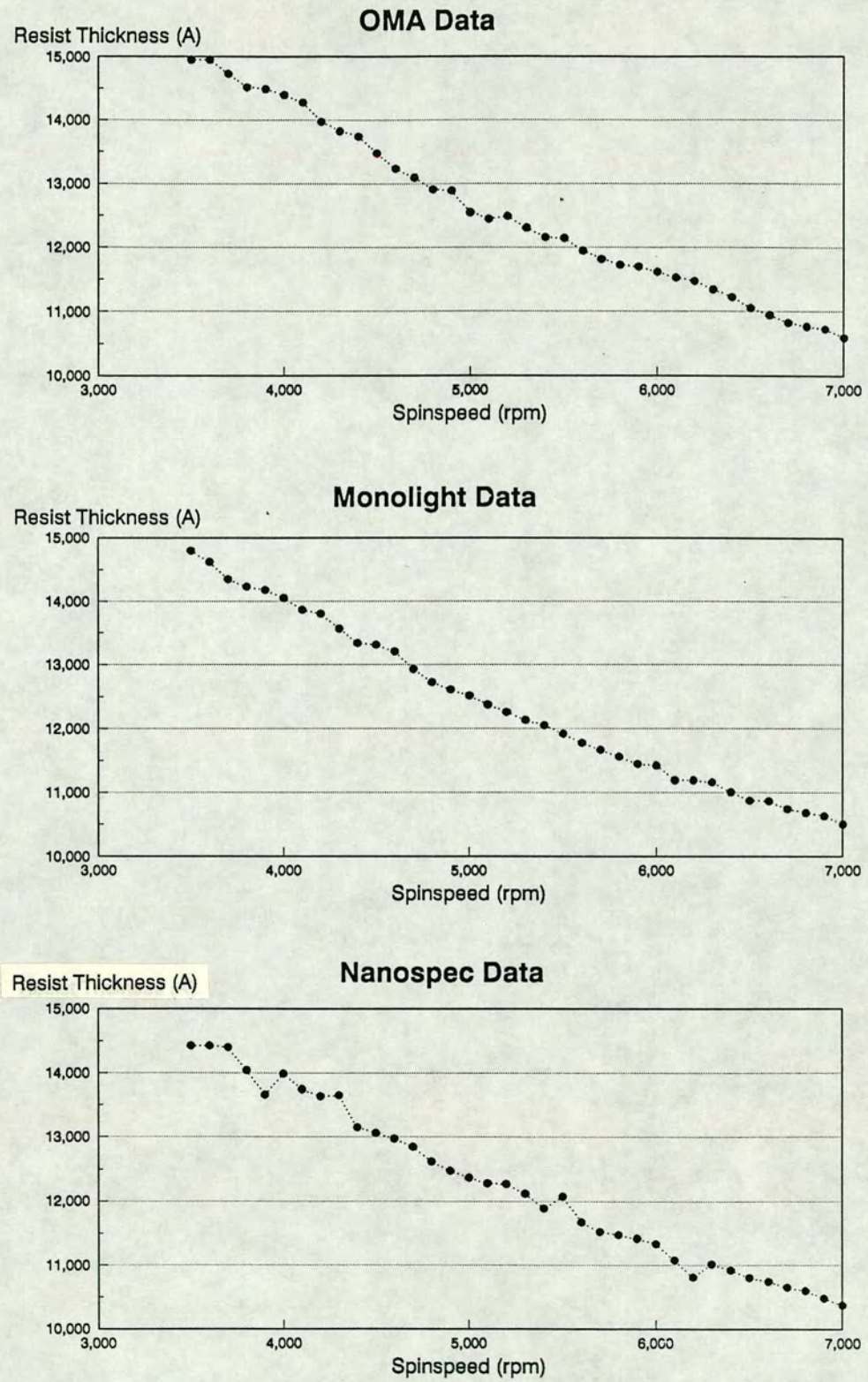

Figure 5–17: Spin Speed Curves

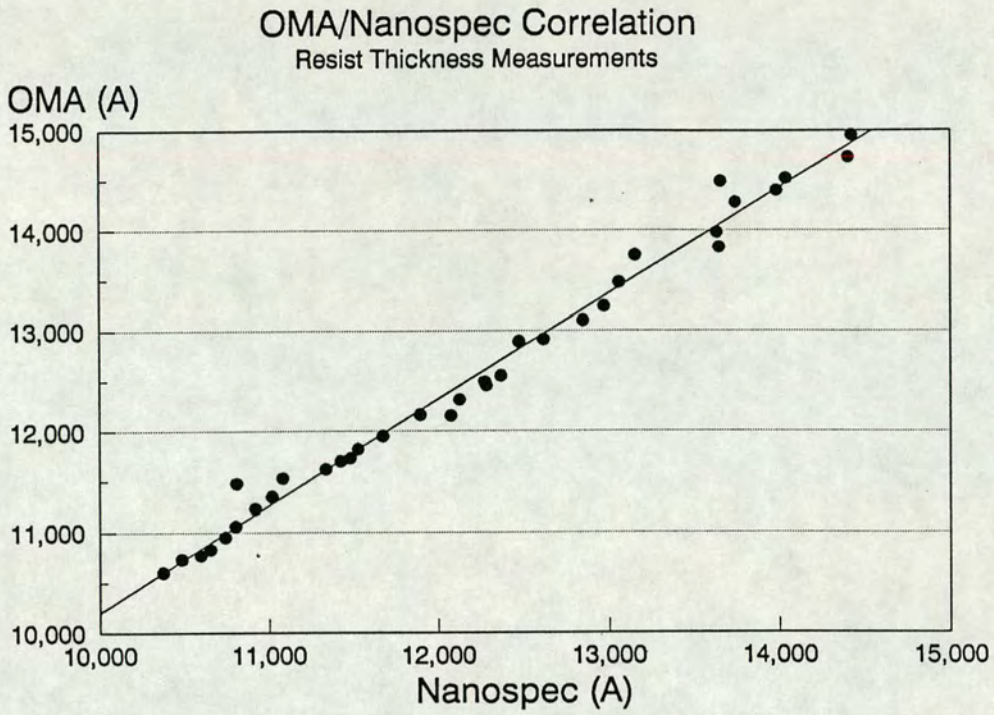

Figure 5–18: OMA/Nanospec Correlation Curve

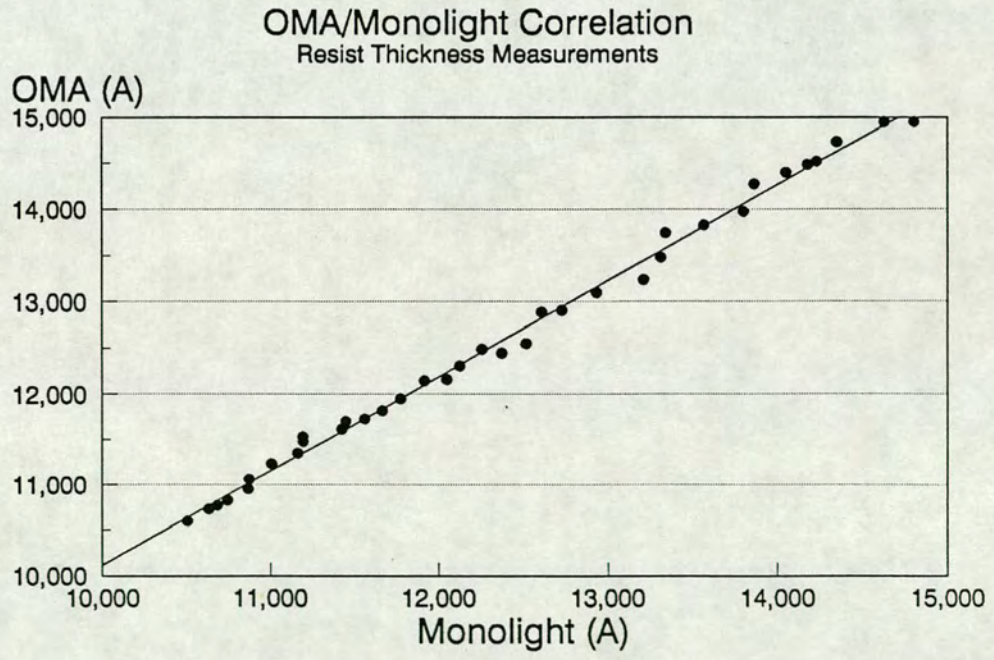

Figure 5–19: OMA/Monolight Correlation Curve

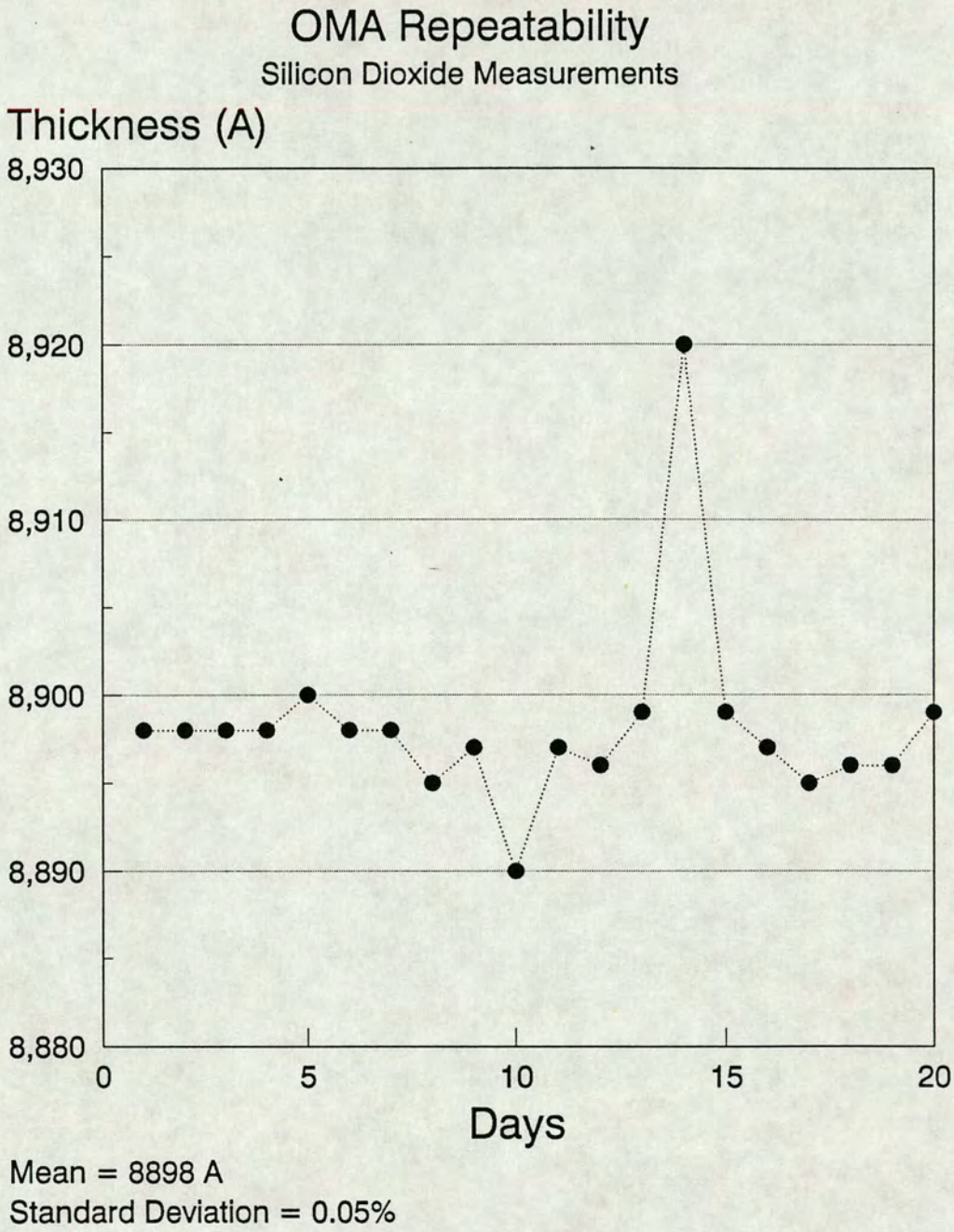

Figure 5–20: Repeatability Test

5.7.4 Discussion

From these tests it can be seen that the OMA results are comparable to those obtained from the Nanospec and Ellipsometer. Although further tests are required to confirm the accuracy of the OMA, its repeatability tests show promising results. These initial experiments are sufficient to justify the technique on which the prototype system is based. Further developments of the system, to refine its measurement capability and to broaden its potential application may now be considered.

1. The system can currently measure the thickness of any thin transparent film with a thickness greater than approximately 1000 A. Below this thickness there is an insufficient number of turning values in the reflectivity curve to apply the Ananthakrishnan algorithm with a reasonable degree of accuracy. Very thin films require an alternative technique for measurement, employing a single wavelength and data look-up tables to determine thickness. (See Section 5.2.2)

2. The OMA software is not optimised for high speed data processing. The determination of film thickness currently takes about 8 seconds per site. A refinement of the smoothing algorithms may improve this scan rate by approximately 0.5 seconds per site, but a maths co-processor is required for a faster scan rate.

3. An intensified detector could be used to improve noise levels.

4. Future modifications to the system may include the ability to measure double layer films. This could be implemented if the thickness and refractive index of the underlying film were known.

5.8 Conclusions

The provision of fast and accurate wafer maps is a valuable aid to process diagnosis and control. The OMA has demonstrated its potential for monitoring film thickness uniformity across wafers.

However the intrinsic value of this system would be considerably increased if it incorporated a linewidth measurement capability. This would enable a simultaneous measurement of two critical process parameters, and should lead to a better understanding of the relationship between them.

The linewidth measurement must be based on reflectivity techniques to be compatible with the existing OMA system. It should also be based on the use of optical test patterns to allow the system to be easily automated, as suggested in Chapter 3.

Initial investigations of a novel technique for determining linewidth uniformity from the optical characteristics of a large area test pattern showed such promising results that they merited further research. The technique is based on a chequerboard pattern of clear and opaque squares. The following chapter introduces the basic theory on which "Chequerboard" test patterns are based, and describes their implementation as a fast CD scan capability for the OMA system.

Bibliography

[1] J.S.Hill. Interferometric thickness measurements on transparent thin films. *Journal of Applied Physics*, 4:741–747, 1971.

[2] R.M.A.Azzam. Ellipsometric configurations and techniques. In *Proceedings of the Society of Photo-Electrical Instrumentation Engineers*, 1981.

[3] H.V.Pham, H.S.Dumar, C.L.Mallory, and D.S.Perloff. Shedding new light on multiple-layer film thickness measurements. *Microelectronic Manufacturing and Testing*, pages 18–20, 1987.

[4] Tencor Instruments. Thin film thickness monitor. *Solid State Technology*, (6):48–50, 1990.

[5] D.E.Aspnes. Studies of surface, thin film and interface properties by automatic spectroscopic ellipsometry. *Journal of Vacuum Science and Technology*, 18, 1981.

[6] E.A.Corl and H.Wimpfheimer. Thickness measurement of silicon dioxide layers by ultraviolet-visible interference method. *Solid State Electronics*, 7:755–761, 1964.

[7] N.Goldsmith and L.A.Murray. Determination of silicon oxide thickness. *Solid State Electronics*, 9:331–332, 1966.

[8] G.F.Mendes. Gratings for metrology and process control: Thin film thickness measurement. *Applied Optics*, 23(4):576–583, 1984.

[9] F.Reizman. Optical thickness measurement of thin transparent films on silicon. *Journal of Applied Physics*, 36(12):3804–3807, 1965.

[10] R.A.Wesson, R.P.Phillips, and W.A.Pliskin. Phase-shift-corrected thickness determination of silicon dioxide on silicon by ultraviolet interference. *Journal of Applied Physics*, 38:2455–2460, 1967.

[11] G.R.Booker and C.E.Benjamin. Measurement of thickness and refractive index of oxide films on silicon. *Journal of the Electrochemical Society*, pages 1206–1212, 1962.

[12] D.T.Larson, L.A.Lott, and D.L.Cash. Surface film thickness by reflectance measurements. *Applied Optics*, 12(6):1271–1275, 1973.

[13] W.A.Pliskin and R.A.Wesson. Reflectivity corrections for silicon dioxide films on silicon for VAMFO. *IBM Journal*, pages 192–194, 1968.

[14] W.A.Pliskin and E.E.Conrad. Nondestructive determination of thickness and refractive index of transparent films. *IBM Journal*, pages 43–51, 1964.

[15] G.W.Hopkins and A.Schwarz. An optical system for full-spectrum measurements. *Hewlett-Packard Journal*, (2):17–24, 1980.

[16] H.H.Hopkins. On the diffraction theory of optical images. In *Proceedings of the Royal Society*, pages 408–432, 1953.

[17] M.Ruiz-Urbieta, E.M.Sparrow, and E.R.G.Eckert. Methods for determining film thickness and optical constants of films and substrates. *Journal of the Optical Society of America*, 61(3):351–359, 1971.

[18] F.Lukes and E.Schmidt. Another method for the determination of silicon oxide thickness. *Solid State Electronics*, 10:264–266, 1967.

[19] I.Fränz and W.Langheinrich. A simple non-destructive method of measuring the thickness of transparent thin films between 10 and 600 nm. *Solid State Electronics*, 11:59–64, 1968.

[20] L.J.Fried and H.A.Froot. Thickness measurements of silicon dioxide over small geometries. *Journal of Applied Physics*, 39(12):5732–5735, 1968.

[21] A.J.Walton. *Process Monitoring and Control.* COMETT 643D - A VLSI Teaching Package, Edinburgh Microfabrication Facility, University of Edinburgh, 1989.

[22] K. Riedling. *Ellipsometry for Industrial Applications*, chapter 1. Basics of Ellipsometry, pages 1–79. Springer Verlag, 1987.

[23] K.Riedling. Error effects in the ellipsometric investigation of thin films. *Thin Solid Films*, 75, 1981.

[24] Nanometrics. *Nanospec/AFT Film Thickness System*, 1982.

[25] Applied Materials Inc. *Ellipsometer II*, 1976.

[26] Monolight Instruments Inc. *Monolight User Manual*, 1988.

[27] S.Robertson. Modeling of positive photoresist and developer interactions. Technical report, Edinburgh Microfabrication Facility, University of Edinburgh, April 1990.

[28] EGG Princeton Applied Research. *Optical Multichannel Analyser Operating Manual*, 1985.

[29] M.P.Watts. An analysis procedure for production linewidth data. In *Integrated Circuit Metrology, Inspection and Process Control*, pages 312–319. SPIE Vol. 775, 1987.

[30] R.Stein, D.Cummings, and J.Schaper. Calibrating microscopic linewidth measurement systems. *Semiconductor International*, (4):132–136, 1986.

[31] Wentworth Laboratories Ltd. *Automatic Wafer Prober Model AWP1050 Instruction Manual*, 1986.

[32] Jarrell Ash/Fisher Scientific Company. *Monospec 18 Service and Instruction Manual*, 1982.

[33] EGG Princeton Applied Research. *Model 1462 Detector Controller Operating and Service Manual*, 1985.

[34] EGG Princeton Applied Research. *Model 1453 Silicon Photodiode Detectors*, 1985.

[35] C.G.Enke. Signal-to-noise ratio enhancement by least squares polynomial smoothing. *Analytical Chemistry*, 48(8):705–712, 1976.

[36] F.R.Ruckdeschel. Data smoother. Dynacomp Inc., 1985.

[37] A.Savitzky and M.J.Golay. Smoothing and differentiation of data by simplified least squares procedure. *Analytical Chemistry*, 36(8):1627–1639, 1964.

[38] R.B.Ananthakrishnan and J.A.Tuttle. Algorithm for computing thin-film thickness. *IBM Technical Disclosure Bulletin*, 18(11):3618-3620, 1976.

[39] C.J.Spanos. Statistical significance of error-corrupted IC measurements. *IEEE Transactions on Semiconductor Manufacturing*, 2(1):23–28, 1989.

[40] A.K.Smith and E.F.Wang. The application of contour maps and statistical control charts in monitoring dielectric processes. In *Integrated Circuit Metrology, Inspection and Process Control*, pages 8–32. SPIE Vol. 775, 1987.

[41] C.Bissell and D.Chapman. Modelling applications of spreadsheets. *IEE Review*, (8):267–271, 1989.

Chapter 6

A Novel Metrology Technique

6.1 Introduction

In the final stages of this project it is useful to recall the original intentions of the research. To recap, the aim was to improve the understanding of CD control by investigating the sources of variations in linewidth dimensions. In Chapter 4 it was shown experimentally that film thickness variations have a profound effect on CD. Chapter 5 described the implementation of a film thickness uniformity measurement system based on the OMA. The next step towards improved process control is to monitor film thickness and linewidth simultaneously by incorporating a CD measurement capability into the OMA system. This Chapter introduces a novel metrology technique and assesses its effectiveness as a means of measuring linewidth uniformity across wafers.

6.2 Design Considerations

The objective was to design a metrology system that was simple to implement and suited to automation. Having worked with several CD measurement systems, it was possible to define a novel technique based on the following design considerations:

1. The assessment of linewidth uniformity across the wafer yields more useful information to the process engineer than spotchecks of absolute dimensions

at a few sites. Furthermore, the repeatability of a measurement instrument is of greater significance in terms of process control than the accuracy.

2. Ideally the addition of a linewidth measurement capability to the OMA system should require as few hardware modifications as possible. Therefore, the measurement must be based on reflectivity techniques.

3. The technique should be based on the use of an optical test pattern to allow for an automated fast scan of data across the wafer. The test pattern should be large-scale to remove the need for pattern-recognition which is complex to implement and slows down the scanning routine. A large-scale test pattern may be located within the scribe channels between chips to avoid using valuable chip design area.

The test pattern designed to fulfill these requirements is a chequerboard of clear and opaque squares. [1] (See Fig. 6–1) The optical characteristics of a chequerboard are sensitive to variations in the ratio of "clear" area to "opaque" area. Therefore the test pattern effectively enhances deviations in CD by translating changes in linewidth into an area change on the chequerboard.

The nominal size of the chequerboard is not critical as the measurement scales to any dimension. [2] For example, a 10% change in linewidth (ΔCD) results in a change in area of the chequerboard squares of nearly 20%, whether the nominal linewidth is 1μm or 5μm. Fig. 6–2 shows the relationship between variations in CD (ΔCD) and the chequerboard area (ΔA). The slope of the curve is greatest for small values of ΔCD, which indicates that this technique is most sensitive for variations in linewidth of up to 10%. This is the critical range in terms of process control for most wafer fabrication.

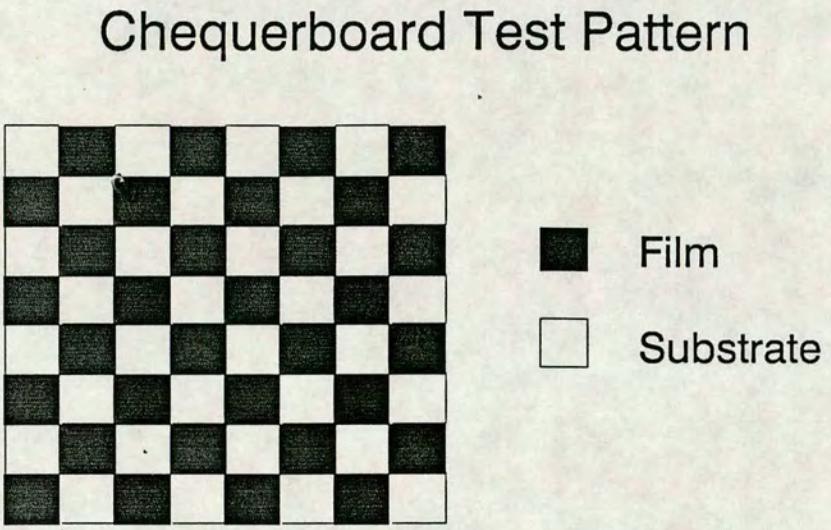

Figure 6–1: Chequerboard Test Pattern

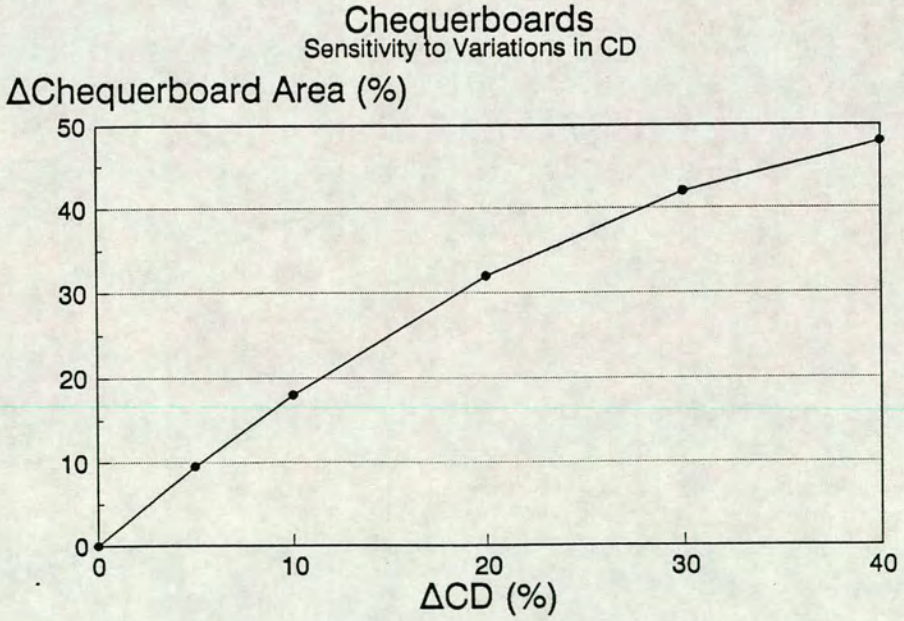

Figure 6–2: Chequerboard Sensitivity to Changes in CD

An optical test pattern based on chequerboards for measuring both CD and film thickness may be designed as shown in Fig. 6–3. The measurement beam spot size of the OMA system is approximately 2.5 mm in diameter. If chequerboards of nominal dimension 2.5μm are scanned on this system, the measurement is effectively integrated over 1×10^6 chequerboard elements. This makes the measurement less prone to error due to small-scale localized variations in CD at the measurement sites on the wafer.

6.3 Chequerboards in Transmission

The simplest means of studying chequerboards is to consider transmission through glass test wafers. (See Fig. 6–4) Transmission is directly proportional to the ratio of clear/opaque area within the chequerboard. Therefore an optimally exposed chequerboard has a transmission of 50%. Overexposure causes a marked increase in transmission (linewidth smaller than nominal) and underexposure causes a similar decrease in transmission (linewidth greater than nominal). (See Fig. 6–5)

The sensitivity of this technique can be demonstrated by printing an aluminium chequerboard over the entire surface of a glass wafer. The regularity of this pattern enhances hidden defects in the lithographic process. [3]

6.3.1 Glass Wafer 1

Fig. 6–6 shows a three-inch glass wafer which has been coated with a thin layer of aluminium and printed with a chequerboard of nominal size 2.5μm. Although the variation in linewidth across this wafer is only 10% it is clearly visible to the naked eye. [4] Furthermore, the causes of this non-uniformity in linewidth are revealed to be in the resist-spinning and exposure processes. For example:

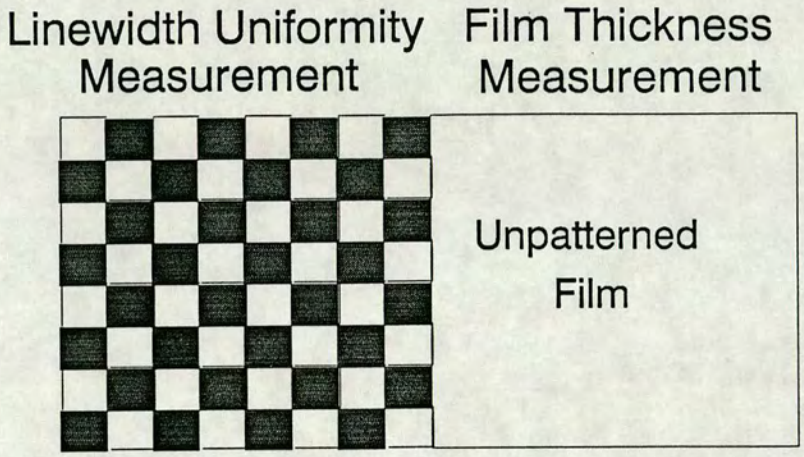

Figure 6–3: Combined Optical Test Pattern

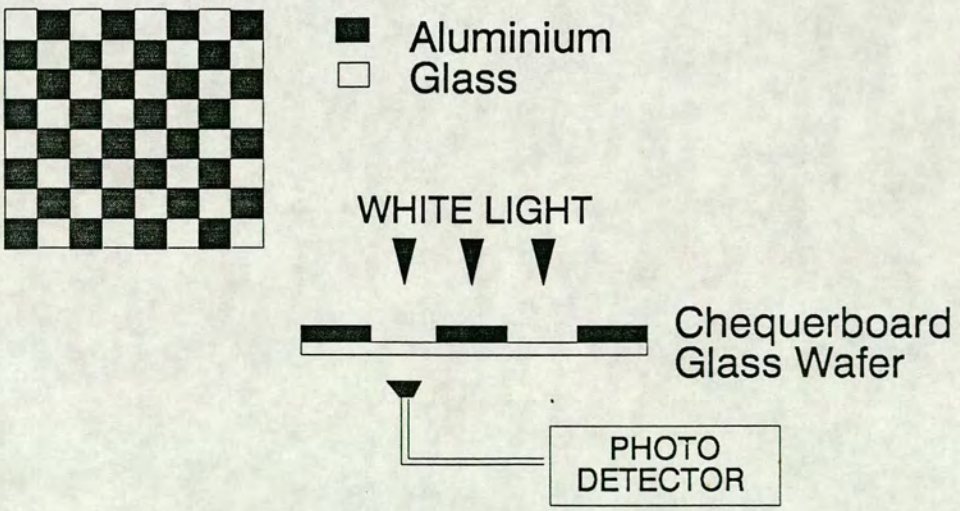

Figure 6–4: Chequerboard Test Patterns in Transmission

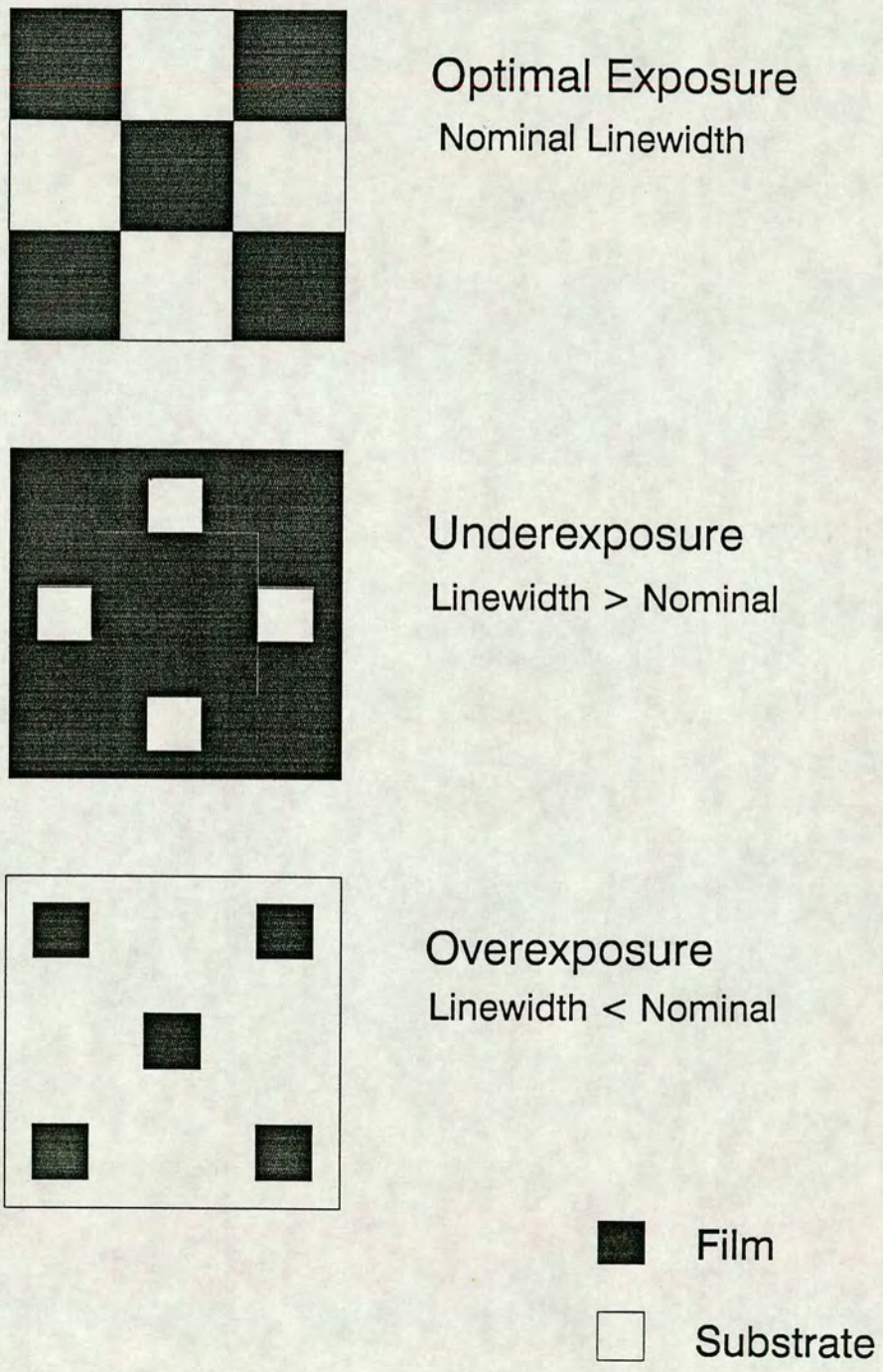

Figure 6–5: Effect of Variations in Exposure on Chequerboards

Chequerboards
Aluminium on Glass Wafer #1

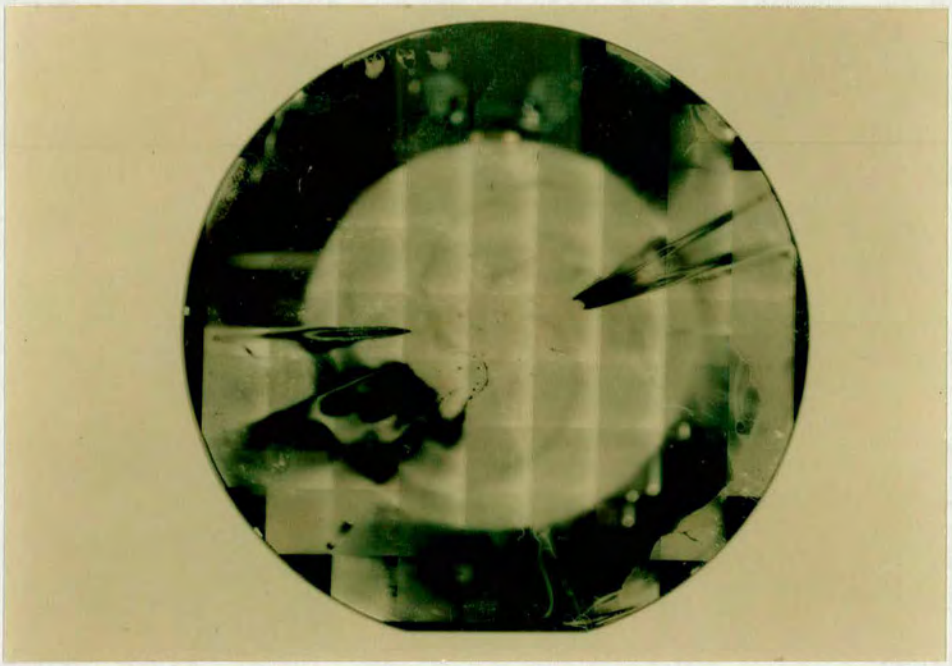

Figure 6–6: Chequerboards Printed On Glass Wafers Reveal the Inherent Non-uniformity of the Resist-Spinning and Exposure Processes

1. The indentation on the wafer created by the vacuum chuck on the resist track is immediately apparent.

2. The spirals radiating from the centre are caused by the grooves in the surface of the wafer chuck.

3. The "darts" are the result of droplets of resist flying off the wafer at high speed.

4. The non-uniformity of illumination in each exposure field may also be seen.

These seemingly dramatic variations in linewidth across the wafer are not entirely due to poor process control. It should be remembered that the actual variation in linewidth is only of the order of 10%. The effect is due to variations in the intensity of the standing wave profiles within the resist.

Aluminium is a highly reflective substrate and standing waves are set up in the resist during exposure. The standing waves are determined by the resist thickness, and a variation of only 650 A is sufficient to change the standing wave from a maximum to a minimum (or vice versa) at the resist/air interface. This is likely to affect the etched dimensions of the chequerboard, as described in Chapter 4. As a result, slight variations in resist thickness have a profound effect on metal linewidth. (See Fig. 6–7)

6.3.2 Glass Wafer 2

The results from the first test led to a revision of the set-up of the stepper. Later, after the installation of a new resist track, the test was repeated to see if the uniformity of the resist had improved significantly. A second glass wafer was coated and printed, and the results can be seen in Fig. 6–8.

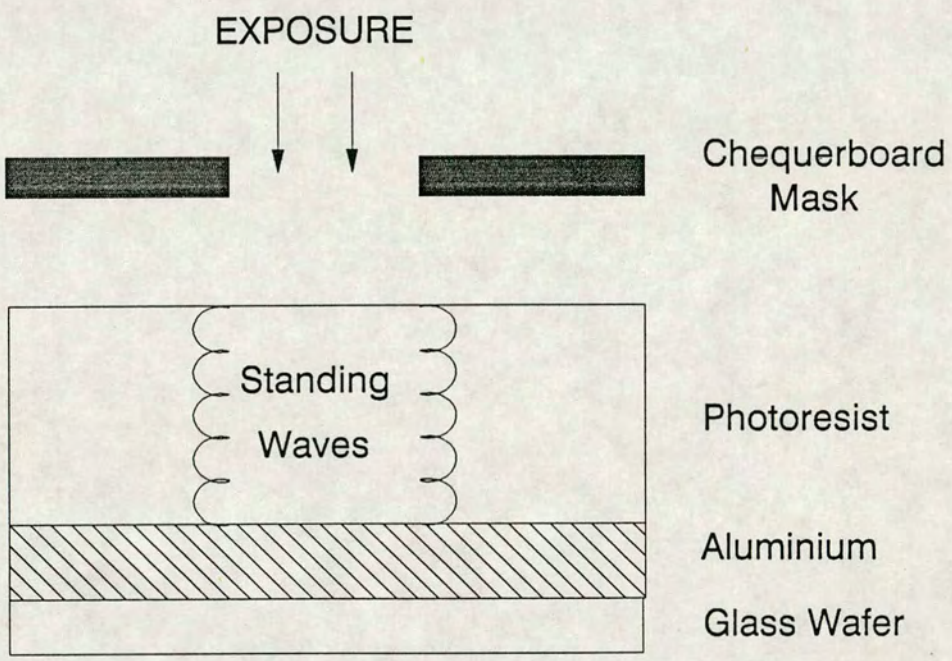

Figure 6–7: Standing Waves Patterns are Generated in the Resist During Exposure Due to Reflections from the Metal Substrate

Chequerboards
Aluminium on Glass Wafer #2

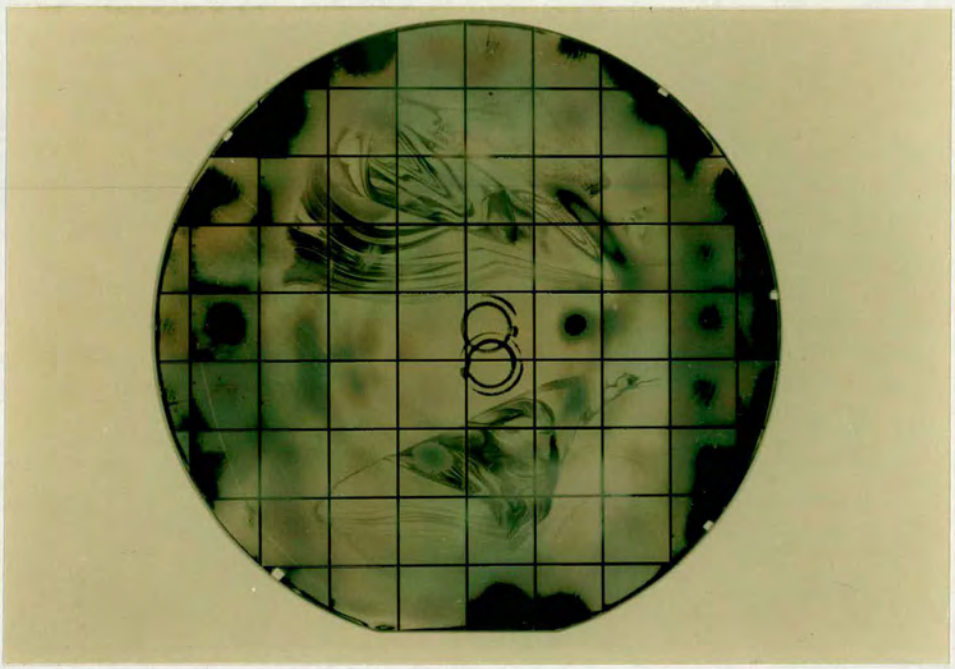

Figure 6–8: Chequerboards Confirm that Wafers Coated using the New Resist Track Exhibit Better Uniformity of Resist

The pattern on this wafer is quite different from the original. It is evident that the intra-field uniformity of illumination has improved. This time the circular pick-up marks from the wafer stepper can be seen, where the resist has been slightly damaged. It seems likely that the swirling patterns on this wafer were caused during the develop process, and as a result, a review of the develop program on the track was proposed.

6.3.3 Spray versus Ultrasonic Develop

The standard develop process in the EMF has traditionally been based on a spray dispense system. However, the lithography group had invested in a new ultrasonic dispense nozzle for the develop track. The reasons for buying this new dispense system were as follows:

1. It develops wafers faster

2. It uses approximately one third less chemicals than the spray dispense.

Chequerboard test wafers were used to compare developer activity. The first wafer was developed using standard spray dispense. Fig. 6–9 shows that there is poor uniformity across this wafer.

The second wafer was developed using ultrasonic dispense. This nozzle breaks the stream of developer into a fine mist which settles over the surface of the wafer. As can be seen in Fig. 6–9, the uniformity across this wafer is much improved. These results were sufficient to justify the capital outlay for the new dispense system.

Developer Activity

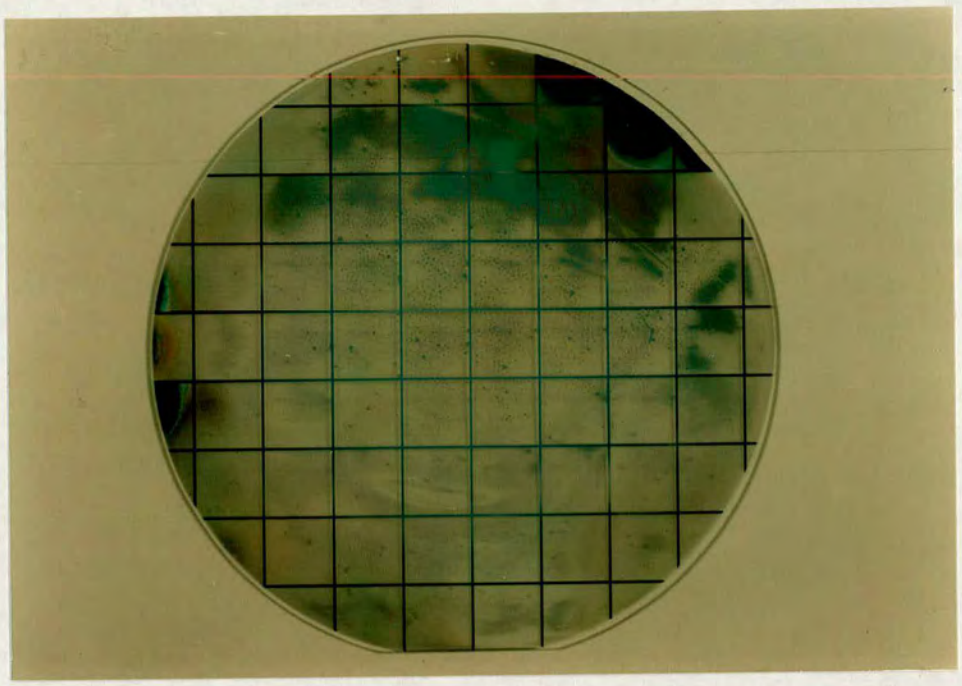

Spray Dispense

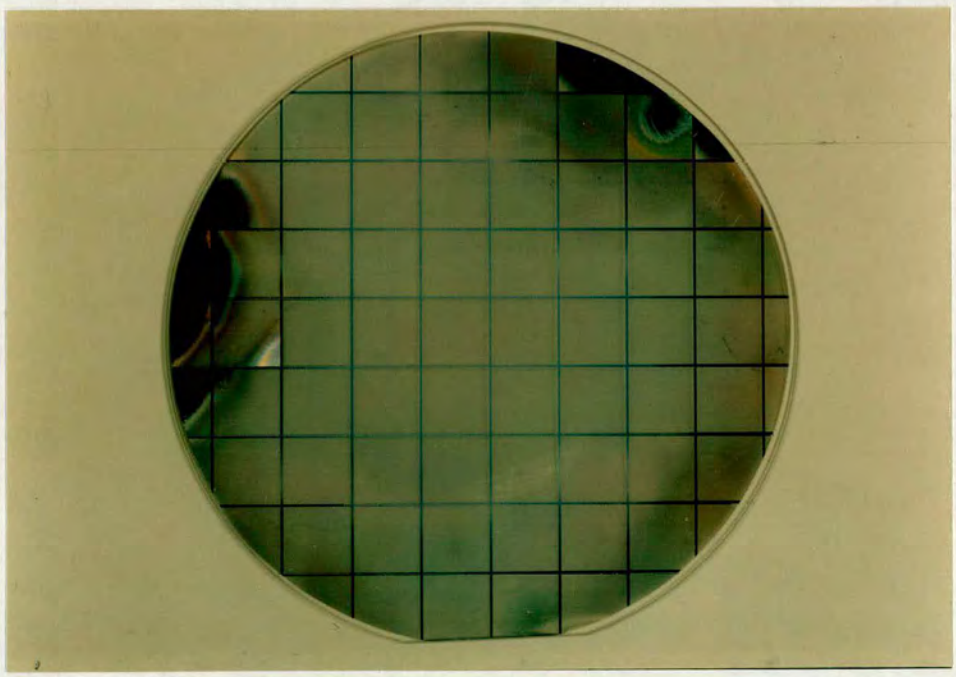

Ultrasonic Dispense

Figure 6–9: Developer Activity

6.3.4 Conclusions

These tests confirm a number of process control issues proposed earlier:

1. The wafers give an excellent visual representation of the effect of several lithographic factors on linewidth uniformity. Variations in resist coating, exposure and development parameters across the wafer are immediately apparent. However these parameters are, on the whole, easily controlled: having been identified they may be adjusted to minimise process non-uniformities.

2. The wafers demonstrate the inadequacy of spotchecks of linewidth dimensions for maintaining process control. Alternatively, linewidth uniformity measurements across the wafer may reveal information about the source of process variations.

However, although chequerboards printed on glass test wafers have been shown to be a useful diagnostic aid for assessing lithographic performance, the technique must be adapted to work in reflectivity if it is incorporated into the OMA system. This would enable chequerboards to be printed on product wafers and measured routinely during processing.

6.4 Chequerboards in Reflection

The interrogation of chequerboard patterns is more complex using reflectance techniques than it is when based on the measurement of transmission. The reflected intensity is dependent on the thickness and optical characteristics of the underlying film, and if chequerboards are to be used throughout processing, they may be printed above several layers which have been previously deposited.

To simplify matters, consider a chequerboard printed above a single transparent film. (See Fig. 6–10). Basically, the reflected light consists of three component parts:

1. Reflected light from the chequerboard elements (M). If for example, the chequerboard is of metal, then approximately 90% of incident light is reflected straight back from the metal surface.

2. Reflected light from the underlying film and substrate (F). This term is dependent on film type and thickness. However it is possible to predict a reflectivity curve for each film, as described in the previous Chapter.

3. Scattered light (S). This component includes light scattered from the metal edges and from the substrate. It also includes an interference loss because the chequerboard elements behave in much the same way as a diffraction grating.

According to these definitions, M and F are area-dependent terms. Therefore if,

$$a = \frac{\text{ChequerboardArea}}{\text{TotalArea}} \tag{6.1}$$

Then,

$$R = aM(I) + (1 - a)F(I) + S \tag{6.2}$$

where R = Reflected Intensity, and I = Incident Intensity. The task is to solve this equation for a. Having established the relative area of the chequerboard elements, it should be possible to determine linewidth dimensions.

6.4.1 Preliminary Testing

As a preliminary measure, it was necessary to test the sensitivity of the OMA, to confirm that it was able to detect variations in chequerboard reflectance caused by small changes in dimension.

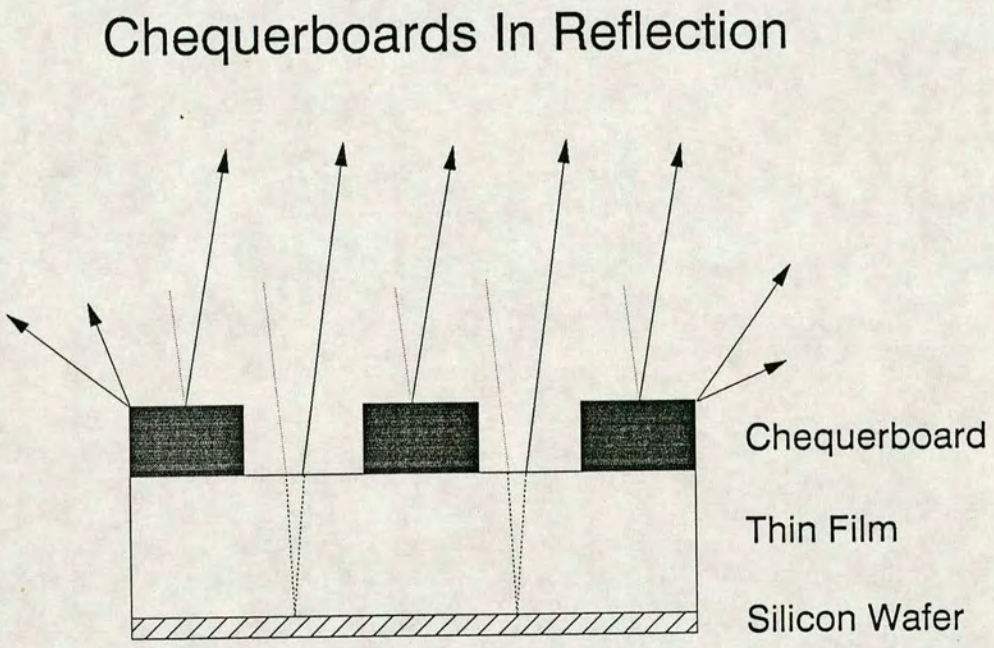

Figure 6–10: Reflected Light from the Chequerboard Film Stack Consists of Light Reflected from the Chequerboard Elements, from the Surface of the Film and from the Substrate. Scattering Losses Occur Since Light is Scattered from the Chequerboard Edges and from the Substrate

A test wafer consisting of a thin layer of aluminium on 2300 A oxide was prepared. A 2.5μm chequerboard pattern was printed on the wafer in such a way that each successive field received an increased exposure dose. The OMA was then used to measure the reflectance of each chequerboard pattern. The results are shown in Fig. 6–11

- Spectrum 1 refers to the unpatterned oxide film. This is the data which is normalised to the reflectivity spectrum of silicon in order to calculate film thickness.

- Spectra 2a, b and c were recorded from the chequerboard printed on top of the film. Their higher reflectivity is due to the aluminium.

  Spectrum 2a - Chequerboard was overexposed by 10%.

  Spectrum 2b - Chequerboard was printed at optimal exposure.

  Spectrum 2c - Chequerboard was underexposed by 10%.

These results confirm that the OMA is able to differentiate between patterns that have been given different exposure doses, and therefore have different linewidth dimensions. Having demonstrated the sensitivity of chequerboard reflectance to variations in linewidth, it is possible to proceed with a more detailed investigation of the relationship between these parameters. It is necessary to repeat the experiments described in Chapter 4 to determine whether the relationship established between reflectance and CD for unpatterned films holds true for chequerboard patterns.

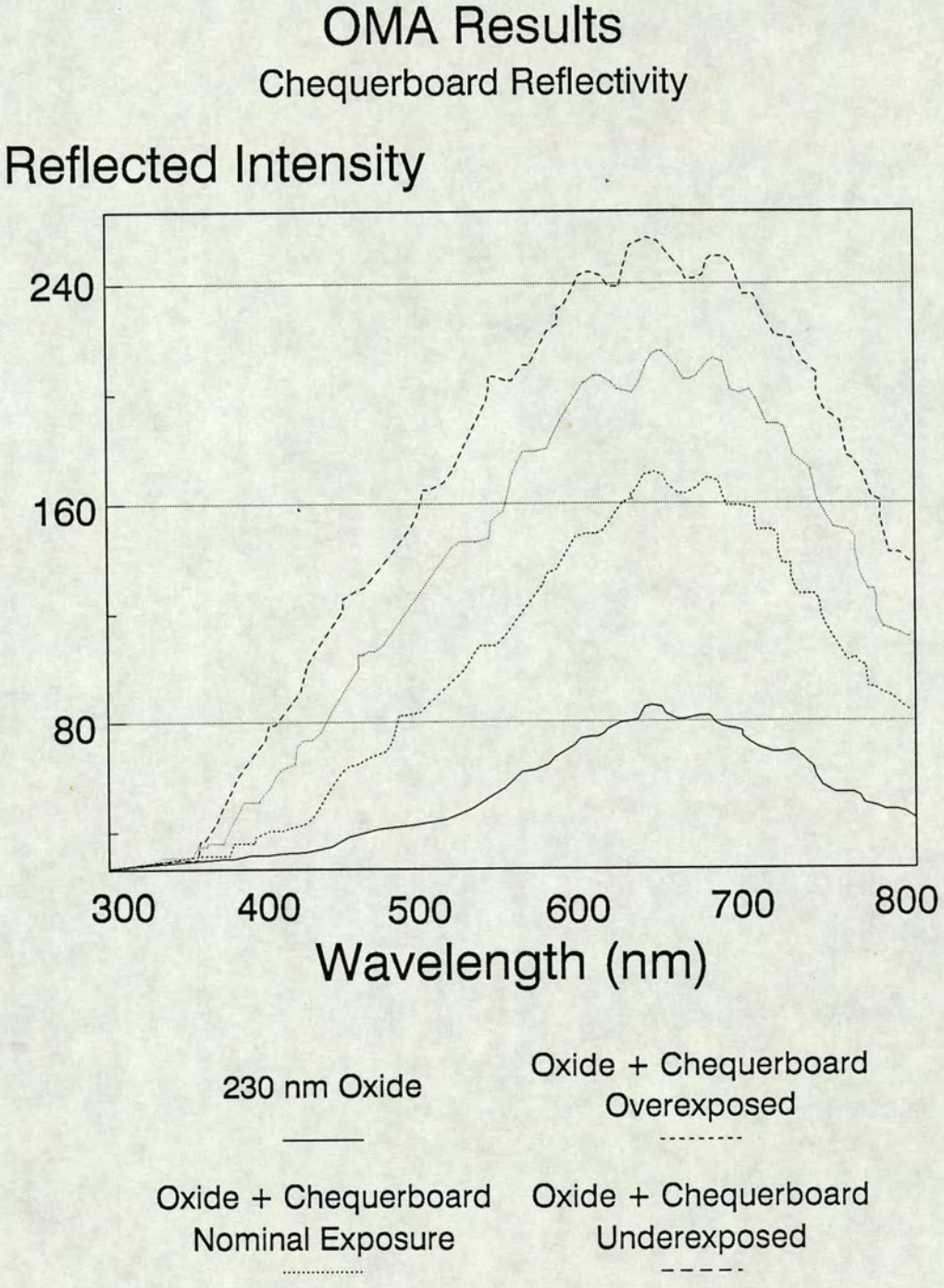

Figure 6–11: Effect of Variations in Exposure on Chequerboard Reflectivity

6.5 Experimental Assessment of Chequerboard Reflectance and CD

Consider a single layer of photoresist. In Chapter 4 it was shown that the thickness of the photoresist determines the standing wave profile at the surface. The standing wave at the resist/air interface determines the energy coupled into the resist, and hence the reflectance of the film. This chain of events has an influence on the final dimensions of the line, which can be summarized by stating (in simplified form):

High reflectivity → Increased linewidth
Low reflectivity → Decreased linewidth

An experiment was devised to test this relationship for chequerboard-printed wafers.

6.5.1 Procedure

Five bare wafers were coated with various thicknesses of resist. These thicknesses were the same as the values used previously in Chapter 4 (see Table 4-1), representing odd and even multiples of $\frac{\lambda}{4n}$ (650 A).

Each wafer was printed at constant focus and exposure, with a row of 2.5μm chequerboards, and a row of the EMF resolution test pattern. (See Fig. 6–12) The test pattern was included so that linewidth data from Quaestor could be evaluated and compared to chequerboard reflectance. The chequerboard elements were too small to be measured directly on Quaestor, but since the test pattern and chequerboard were printed in close proximity on the wafer, it was assumed that any variation in linewidth exhibited by the test pattern would be reflected in the chequerboard dimensions.

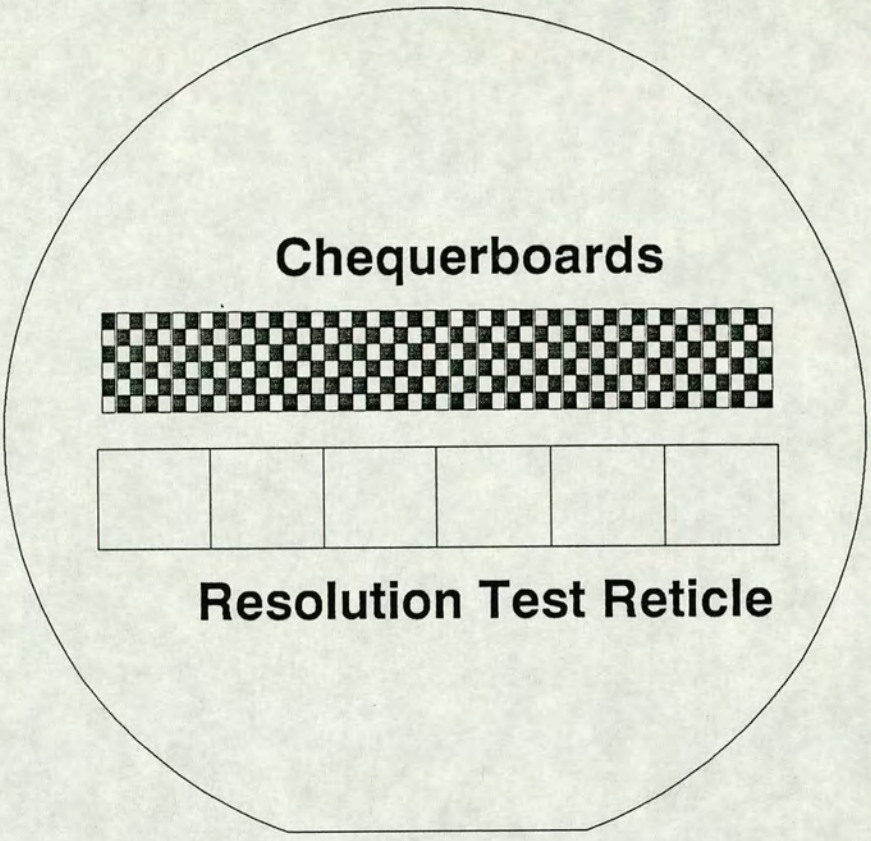

Figure 6–12: Chequerboard Test Wafer

The resist thicknesses were checked on Nanospec and OMA. The correlation of these results is shown in Fig. 6–13. Reflectivity curves for each wafer were generated by the OMA and compared to theoretical curves obtained from Equation 5.3 (see Chapter 5). For example, Fig. 6–14 shows the results for Wafer 4 which has a resist coating of approximately 1.25μm. It shows a close relationship between experimental and simulated data. Since each of the test wafers measured close to target thickness, and exhibited good uniformity of resist coating, it was possible to proceed with the next stage of the experiment.

6.5.2 CD versus Film Thickness

Results from previous experiments in Chapter 4 showed that films of an odd multiple of quarter-wavelengths thickness ($\frac{\lambda}{4n}$) correspond to linewidth dimensions that are smaller than nominal size, whereas films of even quarter-wavelength multiples correspond to increased linewidth dimensions.

Therefore, since the films in this experiment represent odd and even multiples of $\frac{\lambda}{4n}$, it was expected that identical features measured on each wafer would show a periodic variation in dimension from wafer to wafer.

Linewidth dimensions were measured on Quaestor. Mean data was calculated for each wafer and is displayed in Fig. 6–15. Evidently the results from this test corroborate the theory proposed in Chapter 4. (See Fig. 4-9).

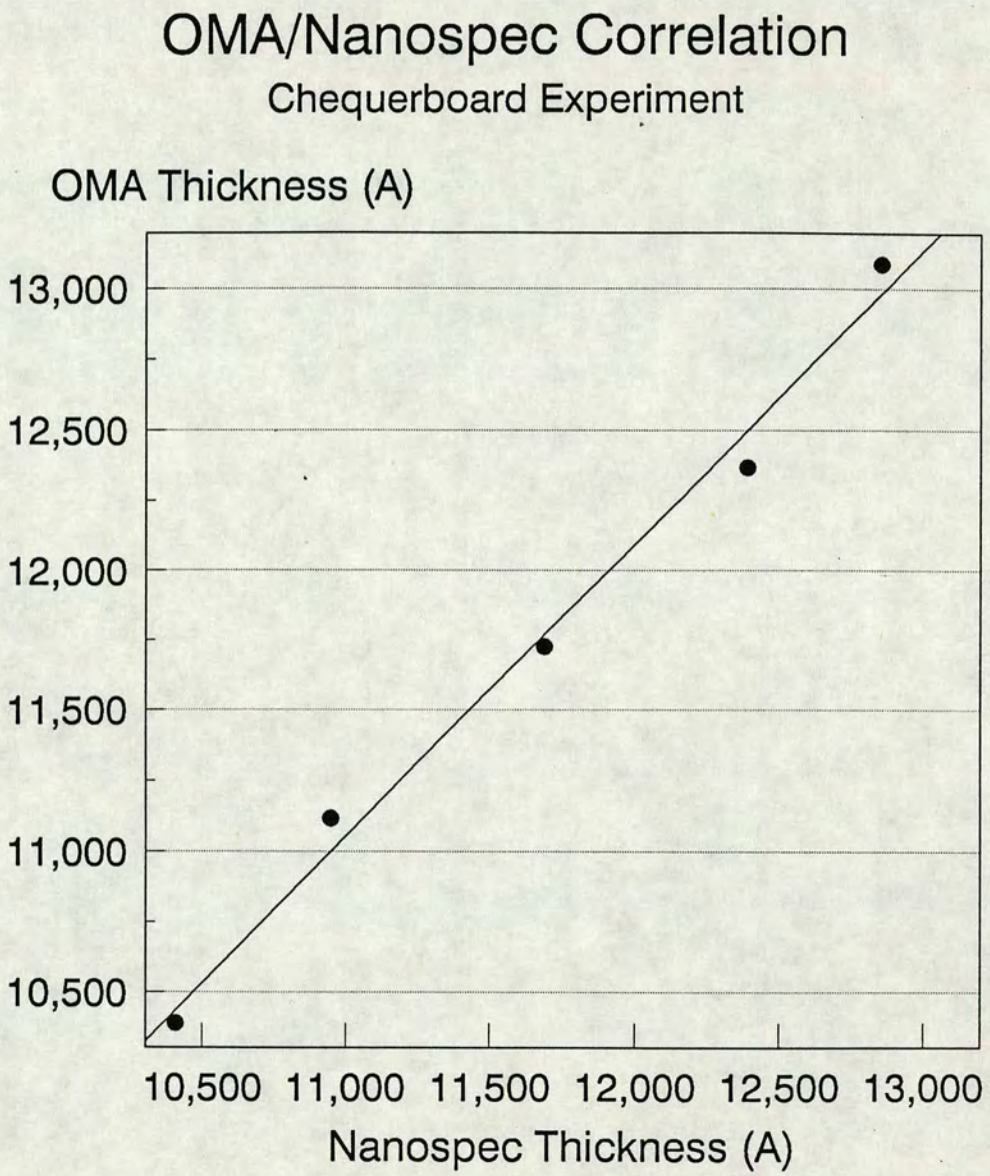

Figure 6–13: OMA/Nanospec Resist Thickness Correlation

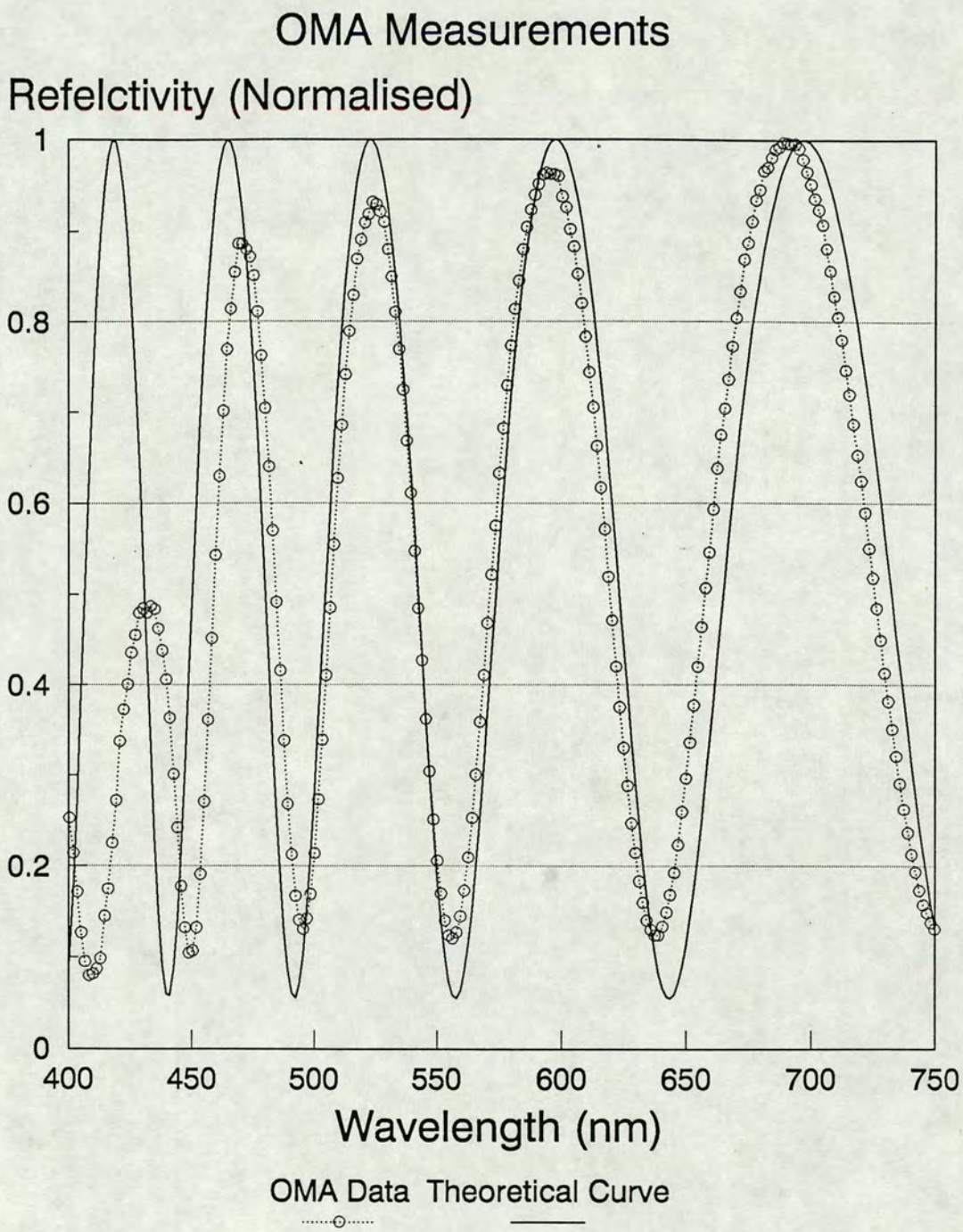

Figure 6–14: Reflectivity Curves: OMA Data and Simulated

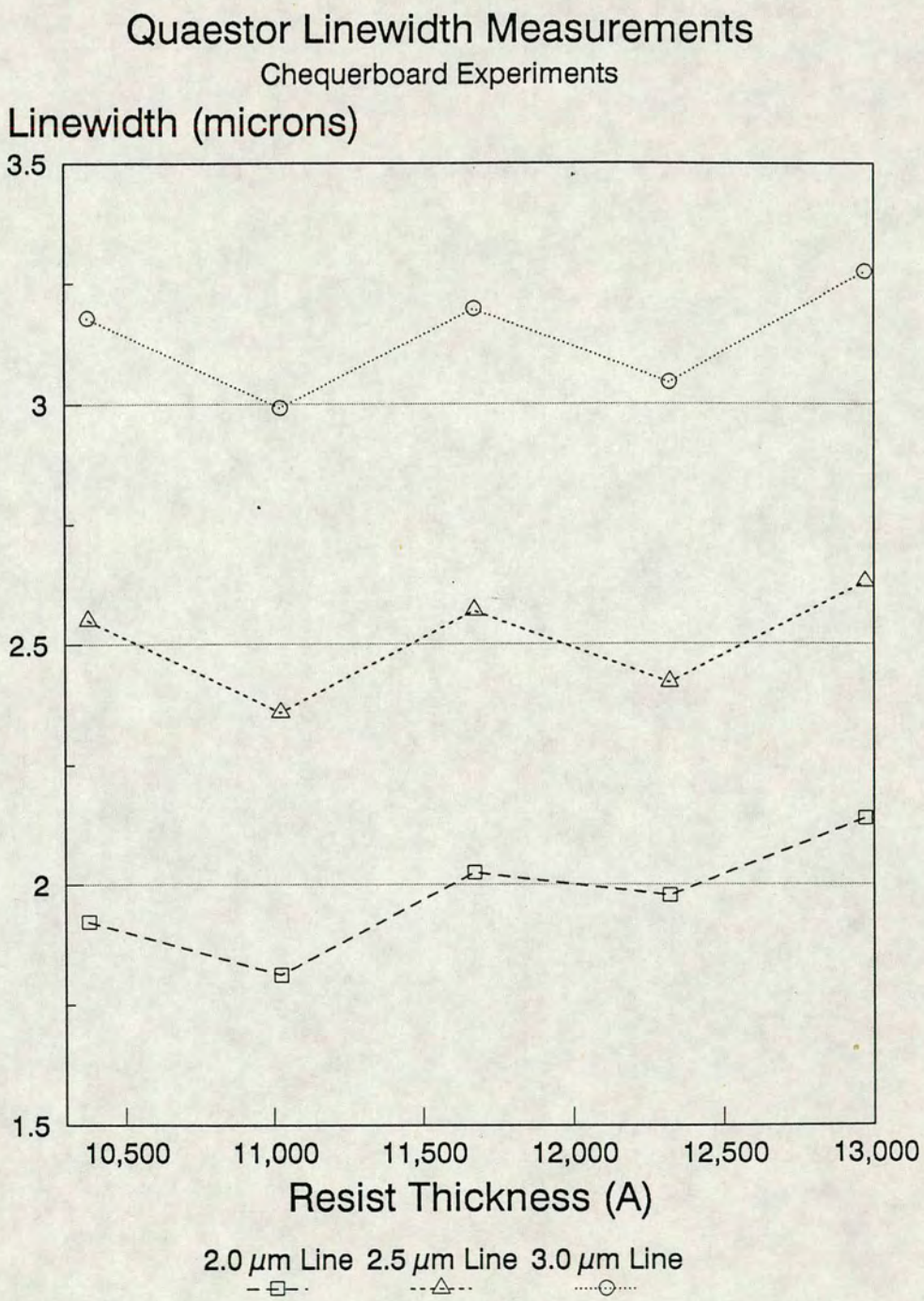

Figure 6–15: Quaestor CD versus Resist Thickness

6.5.3 Reflectance versus Thickness

Having confirmed that the wafers exhibit a variation in CD with resist thickness, the next task was to check that there was a corresponding variation in reflectance from wafer to wafer. Measurements were taken from both the chequerboard-printed areas on the wafer and the unpatterned resist film, at a wavelength $\lambda = 436$ nm, the exposure wavelength of the stepper.

Unpatterned Film

The reflectance of the unpatterned resist films was measured on the OMA and on the Monolight Spectrum Analyser. (See Figs. 6–16 and 6–17 respectively.) The Monolight results are displayed against the theoretical reflectance values generated from Equation 5.3. (Section 5.2.2) Both test results show a periodic variation in reflectance as predicted.

Chequerboard Reflectivity

The reflectance of the chequerboard patterns was measured for each wafer on the OMA. It was expected that the results would closely mirror those obtained from the unpatterned film. However, as can be seen in Fig. 6–18, although the chequerboards reveal a periodic variation in reflectance from wafer to wafer, the variation is in the opposite sense to the previous results from the unpatterned films (Fig. 6–16). This effect is caused by a combination of factors:

1. Resist thickness loss experienced by the unexposed chequerboard elements during development

2. Diffraction losses

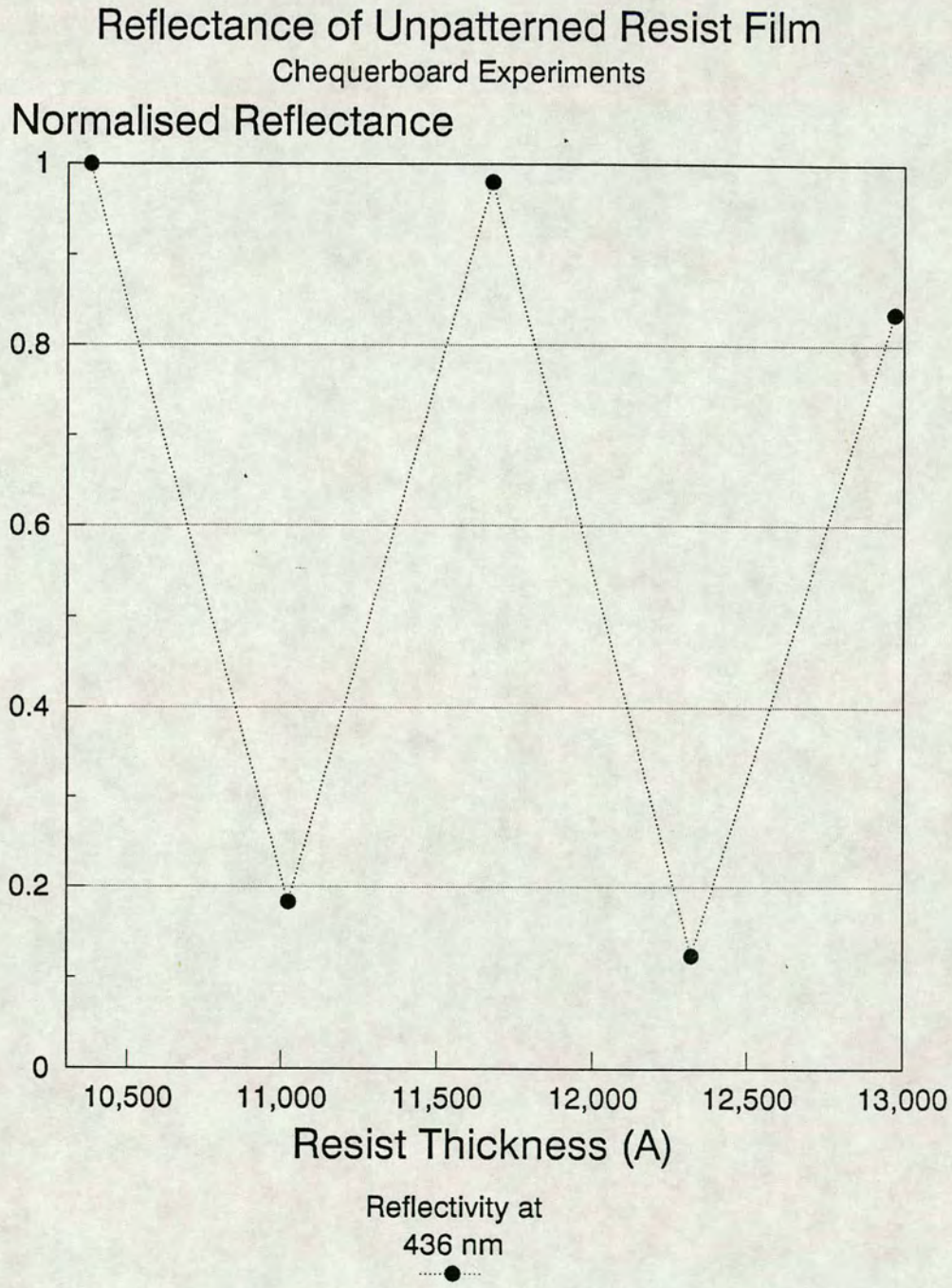

Figure 6–16: OMA Reflectance as a Function of Resist Thickness

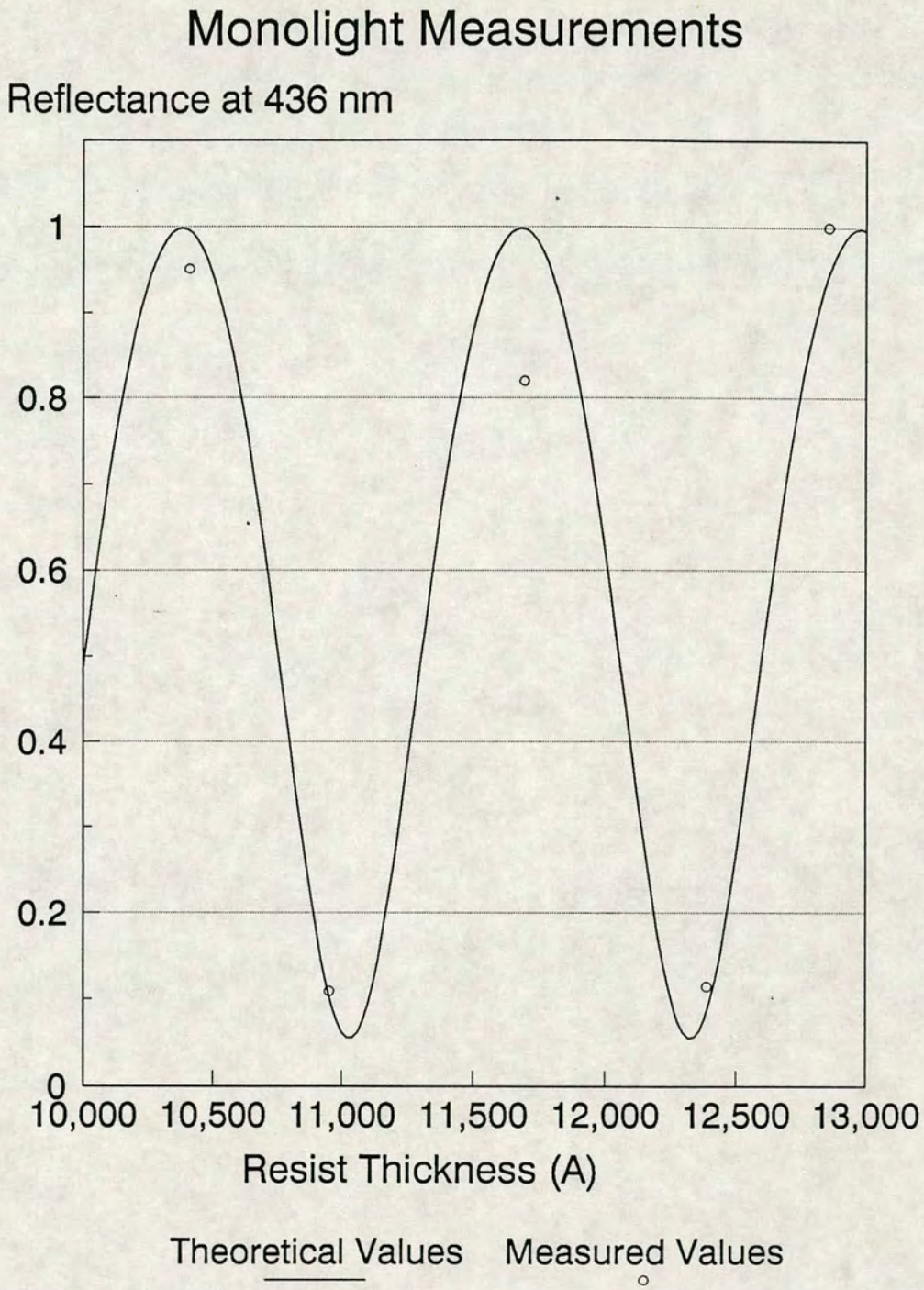

Figure 6–17: Monolight Reflectance as a Function of Resist Thickness

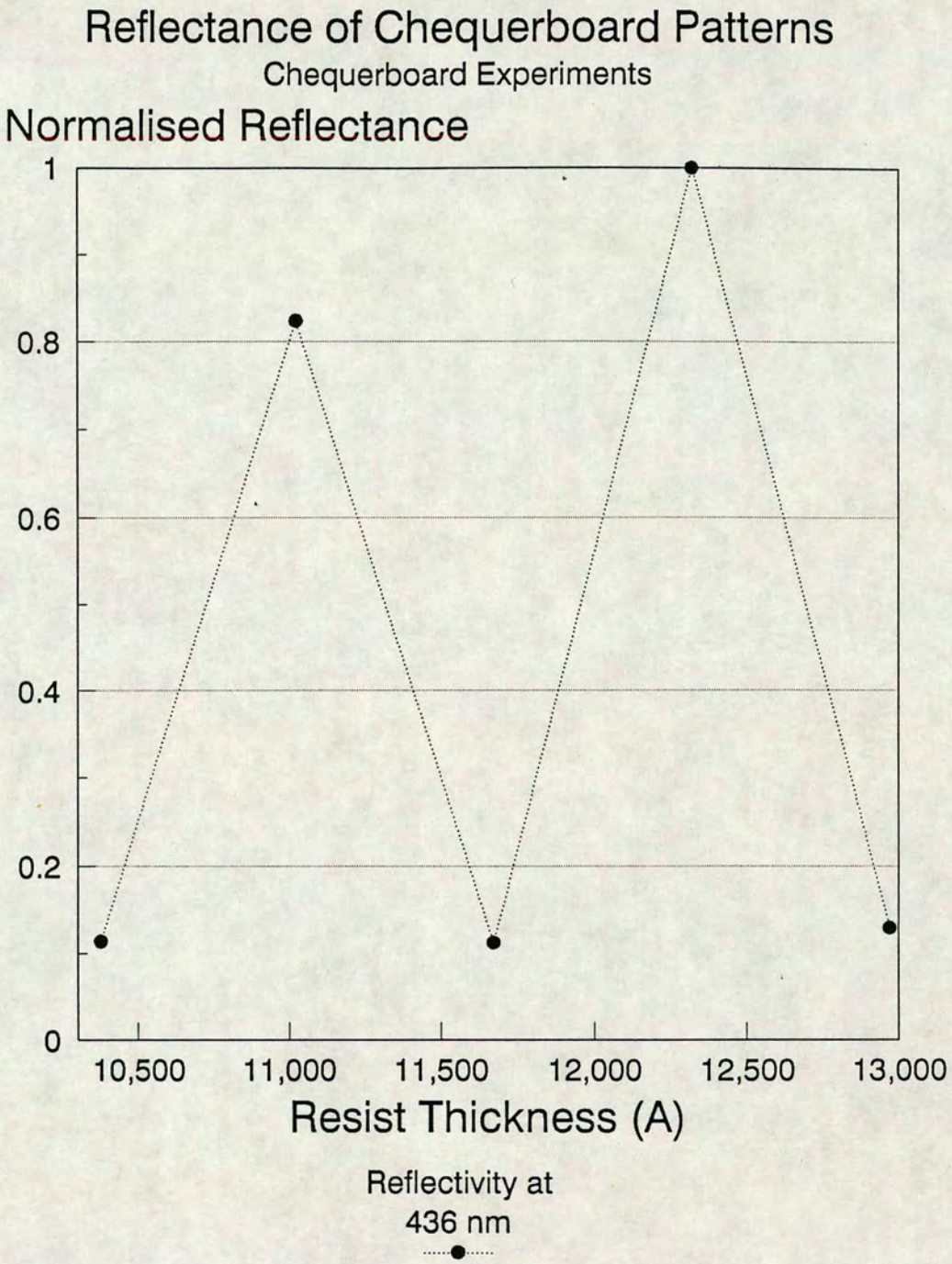

Figure 6–18: Chequerboard Reflectivity

In the first case, leakage of light occurs from the exposed to the unexposed areas of the chequerboard during exposure. This results in a difference in resist thickness between the developed profiles in the chequerboard-printed areas and the unpatterned film (See Fig. 6–19). This step height was measured experimentally using a Dectac surface profile recorder. Despite the inherent inaccuracy of this technique, a step height of approximately 500 A was recorded, which accounts for a shift in reflectivity in Fig. 6–18.

The second contributary factor towards this shift in reflectivity is that interference occurs between the light reflected from adjacent chequerboard elements, resulting in diffraction losses. These losses could be assessed using Fraunhofer diffraction techniques to measure the transmittance of chequerboards printed on a glass wafer.

The transmittance spectrum of a diffraction grating is a sinc squared function. The zeroth order of this function yields information on the intensity of the non-diffracted transmittance. The higher orders represent the diffracted transmittance of the grating. A sensitive photodetector may therefore be used to measure the relative intensities of the orders, in order to calculate diffraction losses. The same technique can be applied to chequerboards, which may be considered as similar to two-dimensional diffraction gratings.

6.5.4 Discussion

Having taken these losses into consideration, these experiments demonstrate nevertheless, that a strong relationship exists between chequerboard reflectance and chequerboard dimensions. Therefore, theoretically at least, it should be possible to use reflectivity as a means of monitoring CD uniformity.

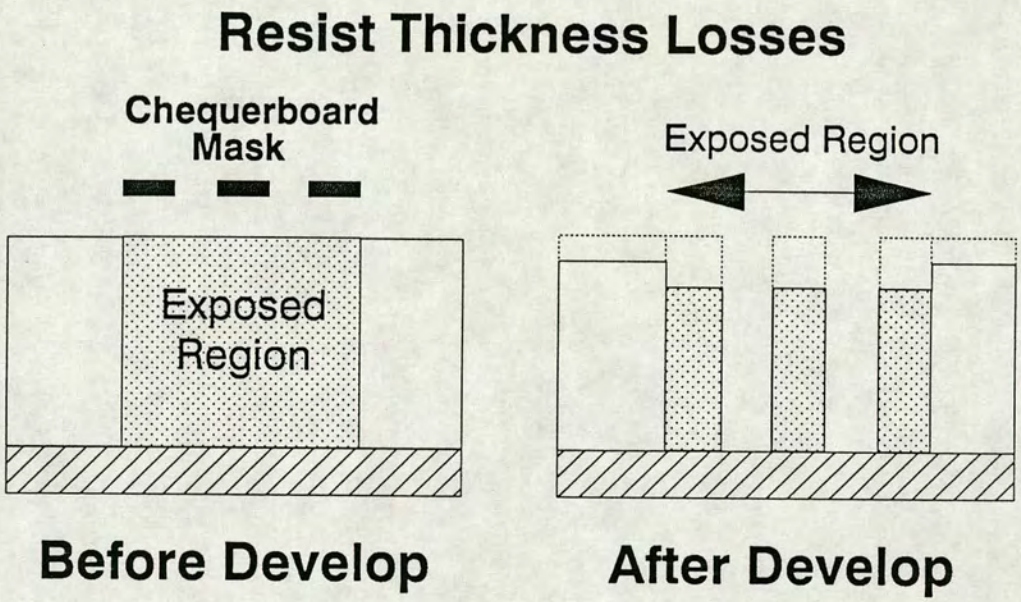

Figure 6–19: Developer Loss In Chequerboard Patterns

However, these experiments also emphasize the difficulty in obtaining a direct measurement of CD from chequerboards using reflectivity techniques. The difficulties arise from the phase changes occurring in reflected light since the optical characteristics of chequerboards are similar to those of a diffraction grating. This effect makes the determination of CD using reflectance techniques more complex and probably unrealistic. An alternative means of interrogating chequerboard may be appropriate, and one possible approach, based on laser diffraction, is currently being investigated. [5] [6] [7] [8] This is a topic for another PhD in the Edinburgh Microfabrication Facility, started in 1990.

6.6 Conclusions

The following conclusions may be drawn from this Chapter:

1. A novel CD metrology technique based on the use of optical test patterns has been introduced. The technique has been designed with the aim to achieve an automated fast scan of linewidth uniformity across wafers in conjunction with the OMA film thickness measurement system.

2. The development of the technique from working in transmission through glass test wafers to working in reflection from silicon wafers has been described.

3. The sensitivity of the technique to variations in CD has been demonstrated for both transmission and reflectance measurements.

4. The difficulty in obtaining accurate results using reflectance techniques has been highlighted. It is likely that a more feasible means of interrogating chequerboards is based on laser diffraction techniques.

Bibliography

[1] I.B.Binnie, R.J.Holwill, J.T.M.Stevenson, J.M.Robertson, and J.Burnie. Chequerboards: A novel technique to measure linewidth uniformity for process control. In *International Conference on VLSI and CAD*, pages 438–441, 1989.

[2] A.J.Walton R.J.Holwill, J.T.M.Stevenson and J.M.Robertson. Wafer scale etch assessment using single layer test patterns. In *VLSI Workshop on Test Structures*, pages 68–76. IEEE, 1986.

[3] E.Swinton. Wafer scale etch assessment. Technical report, Final Year Project, Edinburgh Microfabrication Facility, Universisty of Edinburgh, 1985.

[4] I.B.Binnie. Optical dosimetry as a process monitoring tool. Technical report, Final Year Project, Edinburgh Microfabrication Facility, Universisty of Edinburgh, 1986.

[5] H.P.Kleinknecht and H.Meier. Linewidth measurement on IC masks and wafers by grating test patterns. *Applied Optics*, 19(4):525–533, 1980.

[6] H.P.Kleinknecht and H.Meier. Optical monitoring of the etching of oxide and nitride on silicon by the use of grating test patterns. *Journal of the Electrochemical Society: Solid-State Science and Technology*, 125(5):798–803, 1978.

[7] H.P.Kleinknecht and W.A.Bosenberg. Linewidth measurement on IC masks by diffraction from grating test patterns. *Solid State Technology*, (10):110–115, 1982.

[8] H.P.Kleinknecht and W.A.Bosenberg. Linewidth measurement on IC wafers by diffraction from grating test patterns. *Solid State Technology*, (6):79–85, 1983.

Chapter 7

Conclusions

7.1 Metrology: No Longer an Afterthought

The philosophy on which this thesis is based may best be explained by a description of the evolution of the science of metrology, to demonstrate the importance of its role today within semiconductor manufacturing. Fifteen years ago, metrology tools were simple, straightforward and low cost. Each process engineer was, in general, responsible for monitoring a defined process-area. Linewidths were measured with filar eyepieces in the microscope. Film thicknesses were determined with a colour chart, or for sophisticated control, with an ellipsometer and a wall chart to decipher the data. Metrology was an afterthought for the process engineer, rarely an identified discipline.

Advancements were made with the introduction of computerized CD and film thickness measurement systems. Improved process equipment, for example scanning aligners, often had metrology improvements included, but these were viewed as secondary in importance. A radical change in the principle of metrology initiated in Japan. Rather than being viewed only as a means to an end, statistical process control became a key part of a philosophy aimed at assuring quality and manufacturability. Separate process control groups within process engineering departments were common. Visitors to Japan learned that a higher percentage of capital dollars were spent on metrology equipment than in comparable U.S. facilities, and that with tighter control came tighter yields.

As U.S. companies now strive for world-wide competitiveness, attention has been focused on improved process control. New approaches and methodologies are

being explored. Time-consuming stepper set-up procedures are being challenged by in-situ metrology. High-speed defect detection over full patterned wafers drives new equipment models for yield production. The continuing shrink of circuit feature sizes propels the need for even more complex analytical instrumentation. However, the cost of these analytical tools directly reflects their sophistication. Clearly, technical as well as budgetary considerations demand that metrology no longer be an afterthought.

7.2 Thesis Summary

The objective of this thesis has been to improve the understanding of lithographic metrology and control by studying the factors which influence CD. Optical lithography plays a central role in semiconductor manufacturing, but is only just beginning to become a quantitative engineering science.

In **Chapter 2** it was shown that, although there is a great number of factors which affect linewidth, most are easily controllable. The two significant exceptions to this general rule are underlying film thickness and photoresist thickness. It was therefore decided that film thickness effects on CD should be analysed experimentally.

Chapter 3 began with a review of CD measurement techniques commonly used in industry, and outlined the limitations of each system. A comparative study of the metrology systems within the Edinburgh Microfabrication Facility and Plessey Semiconductors at Roborough, was carried out. The EMF has a pilot process line which is used predominantly for research purposes, whereas Plessey Semiconductors has a commercial ASIC production line. It became apparent however that both facilities shared a common problem: they lacked a simple and fast optical measurement system for scanning linewidth uniformity on both resist and etched wafers. The findings of this study prompted research into developing a new metrology technique to overcome this shortfall.

Chapter 4 described an experimental assessment of film thickness effects on critical dimensions. Simulation programs were employed to establish a theory which uses standing wave patterns within the film to predict the effects of variations in reflectance and exposure threshold on the dimensions of the developed resist images. The theory was initially established for single layer films of photoresist; later it was developed for the more complex optical environment comprising double layer films.

The simulation experiments were subsequently corroborated by measurements of features on test wafers. The results confirm that odd multiples of a quarter-wavelength in total optical thickness of resist plus dielectric layer usually result in a minimum reflectivity at the resist surface and maximum energy coupling into the resist, whereas even quarter-wavelengths multiples maximize reflectance and minimize energy absorbed in the resist. This can result in changes in exposure required to produce a given size line of up to a factor of two.

Further investigation of this technique is required to quantify the parameters. However, it is evident that resist sidewalls should be routinely inspected during processing and standing waves eradicated by means of a "post-exposure bake".

Chapter 5 began with a review of film thickness measurement systems. An evaluation of the system within the EMF revealed the need for a new system with wafer mapping capability. The Optical Multichannel Analyser system, which uses standard reflectometry techniques to calculate film thickness, was developed to fulfill this need.

Test wafers were used to correlate OMA measurements with those from standard film thickness measurement systems. Results were sufficiently good to warrant further developments of the technique. Future modifications to the OMA will include the ability to measure double layer films and a wider range of thicknesses. An upgraded version of this system should use a host computer with a maths co-processor to allow for a faster thickness computation rate.

Chapter 6 described the implementation of a CD measurement capability for the OMA, to enable the simultaneous measurement of film thickness and linewidth

uniformity. The technique is novel, and is based on the optical characteristics of a "chequerboard" test pattern, consisting of clear and opaque squares. The chequerboard effectively enhances deviations in CD by translating variations in linewidth into an area change on the chequerboard.

The technique was originally investigated by printing aluminium chequerboards over the entire surface of a glass wafer. These wafers give an excellent visual representation of the effect of several lithographic factors on linewidth uniformity, and demonstrate the inadequacy of spotchecks of CD for maintaining process control.

The implementation of the technique using reflectance from silicon wafers was then described. Experiments on test wafers confirmed that a strong relationship exists between chequerboard reflectance and linewidth dimensions. However, the determination of accurate dimensions is a challenging task due to complex optical interference effects which occur in the light reflected from the chequerboards. These diffraction effects make the determination of CD using reflectance techniques more complex and probably unrealistic. A more plausible approach may be to employ laser diffraction techniques, and this is the subject for another PhD, which will continue investigations into chequerboard interrogation.

The research undertaken for this thesis is only a starting-point for future work. The need for continued improvements in process control strategies has been shown: the task is to deepen the understanding of the issues introduced here.

Appendix

The following paper was presented at the International Conference of VLSI and CAD (ICVC'89) in Seoul, South Korea, October 17-20 1989.

CHEQUERBOARDS: A NOVEL TECHNIQUE TO MEASURE LINEWIDTH UNIFORMITY FOR PROCESS CONTROL

*I.B.Binnie, R.J.Holwill, J.T.M. Stevenson, J.M.Robertson and J.Burnie**

EMF, Dept. of Electrical Engineering, University of Edinburgh.

*Plessey Semiconductors PLC, Roborough.

ABSTRACT

A novel technique for measuring linewidth uniformity across product wafers is described. The technique is based on the reflectivity of an optical test pattern which may be placed in the scribe channels between chips. The test pattern consists of a chequerboard array of clear and opaque squares. The regularity of this pattern enhances hidden defects in the lithographic process. The technique may be applied to poly and metal layers, and measurements can be taken of both resist and etched dimensions.

1. INTRODUCTION

The successful fabrication of VLSI circuits requires the capability not only to define and etch small features, but also to achieve good uniformity of feature size across each die area, and across the wafer as a whole. Measuring and maintaining process uniformity becomes increasingly difficult as lithography goes sub-micron, and it is evident that the metrology techniques currently used in industry cannot meet these more stringent demands. Furthermore, there is a growing need for an *apriori* means of predicting etched dimensions from a resist image. This is a need which electrical test measurement systems cannot fulfill.

To overcome this problem, a novel technique for measuring and mapping linewidth uniformity across wafers is currently being developed. It involves a simple optical measurement of a large area test pattern consisting of an array of alternate clear and opaque squares i.e. a chequerboard.

This paper will describe the development of this technique from the measurement of transmission of light through chequerboard patterns, to the measurement of their reflectivity.

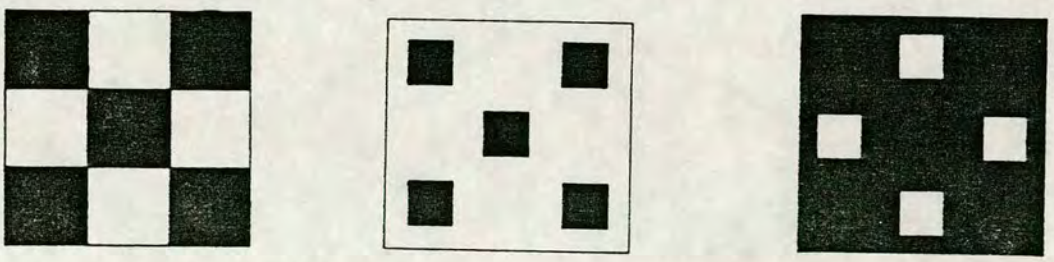

Optimal Exposure (Nominal Linewidth)

Overexposure (Linewidth < Nominal)

Underexposure (Linewidth > Nominal)

Fig 1. Effect of Overexposure and Underexposure on Chequerboards

KITE-ICVC/89/0000-438 © 1989 KITE

2. CHEQUERBOARDS IN TRANSMISSION

The technique was originally proven by measuring transmission of white light through an aluminium chequerboard printed on a glass test wafer. An optimally exposed chequerboard has a transmission of 50%. Overexposure causes a marked increase in transmisssion (linewidth smaller than nominal), and underexposure causes a similar decrease in transmission (linewidth greater than nominal).

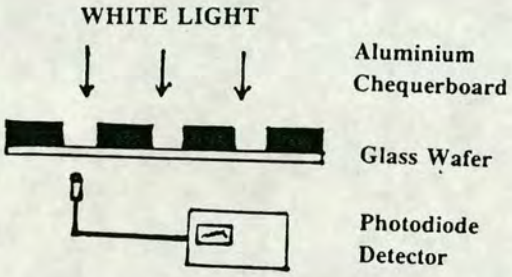

Fig 2. Chequerboards in Transmission

Effectively this structure enhances any deviation of a critical dimension by translating variations in linewidth into an area change on the chequerboard. The nominal size of the chequerboard is not critical as the measurement scales to any dimension, and as the measurement area is large in comparison to the size of each square, the linewidth measurement is effectively integrated over a large number of chequerboad elements, thus improving accuracy.

The sensitivity of this technique can be demonstated by printing an aluminium chequerboard of nominal size 2.5μm over the entire surface of a glass wafer (see fig.3). A variation of only 5% in linewidth across this wafer is clearly visible to the naked eye. Furthermore, the cause of this variation in linewidth is revealed, as details such as the distortion of the wafer by the vacuum chuck on the resist track, and the "darts" caused by droplets of resist flying off the wafer at high speed are immediately obvious.

3. CHEQUERBOARDS IN REFLECTION

This technique is currently being developed to work on reflection from process wafers. The ideal location for chequerboards is in the scribe channels between chips. In this case, linewidth uniformity can be monitored across the wafer without using valuable chip design area, and without disrupting the normal lithographic print sequence (c.f. drop-in chips).

If this technique is to be incorporated as a routine part of the process line, then the chequerboards will inevitably be printed on top of several layers of film which have been previously deposited. Overall reflectivity will consequently

Fig 3. A Metallised Glass Wafer Printed with a Chequerboard of Nominal Size 2.5μm Reveals the Inherent Non-Uniformity of Resist Spinning and DSW Exposure

comprise of three component parts: reflection from the chequerboard elements, reflection from the substate, and also reflection from the underlying film.

The initial objective has been to model the absoption of this underlying film in order to predict its effect on overall reflectivity. An algorithmic approach is taken to plot a wafer map of film thickness.

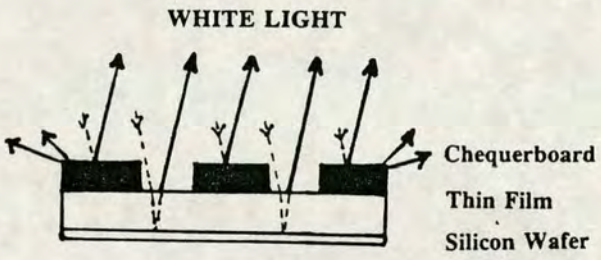

Fig 4. Chequerboards in Reflection

Thin Films

If light is directed upon a transparent film, interference occurs, according to the phase difference between the light reflected form the upper and rear sides of the film. Film thickness may be determined by applying an algorithm to the maxima and minima of the corresponding reflectivity curve. There are several standard techniques widely used for the computation of film thickness. The Ananthakrishnan algorithm [4] has been selected in this case since it does not require fore-knowledge of the order number of the film.

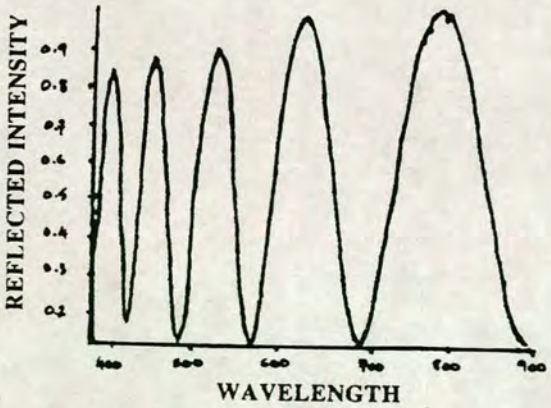

Fig 5. Reflectivity Curve for 100nm Resist on Silicon

4. SYSTEM HARDWARE

The system which has been developed is based upon an Optical Multichannel Analyser (OMA). The OMA is a microprocessor controlled instrument for storing and displaying spectral data. It has been calibrated to measure reflected intensity as a direct function of wavelength. This enables film thickness measurements to be taken, and the Ananthakrishnan algorithm has been written into the software.

The other major components of the system comprise the microscope, the spectrograph and the photodiode array detector. An automatic wafer stage is included to give full scanning and mapping facilities.

White light is projected onto the wafer surface, and the reflected light is transmitted back through the microscope and into the spectrograph, where it is split into its component wavelengths. The photodiode array detector measures the intensity of each wavelength, and this data is fed back into the OMA for further analysis.

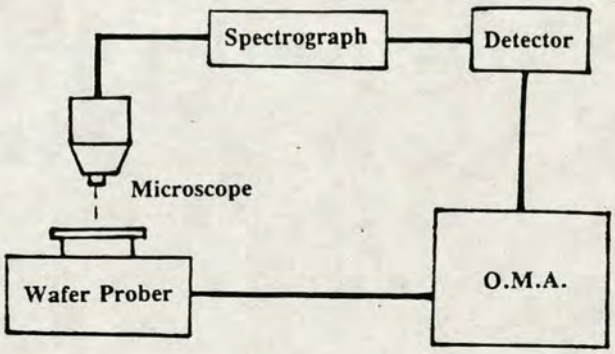

Fig 6. System Design

Further Work

The hardware setup described above is merely the prototype for testing the chequerboard technique. Eventually, the OMA will be transferred onto a Quaestor system, which has superior wafer-handling and optics. Quaestor is an automatic Critical Dimension (CD) measurement and inspection system. A video scan technique is used to obtain CD's from intensity profiles. It has in-built pattern recognition capability, which enables it to move to, find,

focus on and measure pre-selected features on the wafer. This makes it an ideal machine on which to test the chequerboard system.

Further resuslts will be presented at the conference.

5. CONCLUSIONS

A novel technique for measuring linewidth uniformity across wafers has been dicussed. Preliminary tests indicate that the technique is sufficiently sensitive to reveal the non-uniformities inherent in resist spinning and DSW esposure.

Further work is needed to assess this technique more fully, and the likely course of future developments in system design have been indicated.

6. ACKNOWLEDGEMENTS

This work has been supported by the Science and Engineering Research Council of Great Britain. Additionally, I.Binnie would like to acknowledge the technical and financial support of Plessey Semiconductors.

7. REFERENCES

[1] HOLWILL,R.; STEVENSON,J.; WALTON,A.; ROBERTSON,J.: "Wafer Scale Etch Assessments Using Single Layer Test Patterns", IEEE VLSI Workshop on Test Structures, Feb. 1986, pp68-76.

[2] OBERAI,A.: "Lithography - Challenges of the Future", Solid State Technology, Sept. 1987, pp123-128.

[3] BURNS,G.; GRENIER,J.; REAGAN,M.; WOOD,P.: "Wafer Fabrication Equipment Five-Year Forecast", Solid State Technology, Jan. 1989, pp35-38.

[4] ANANTHAKRISHNAN,R.: "Algorithm for Computing Thin-Film Thicknesses", IBM Technical Disclosure Bulletin, April 1976, pp3618-3520.